

THE UNIVERSITY OF SHEFFIELD

FACULTY OF ENGINEERING

DEPARTMENT OF CHEMICAL AND BIOLOGICAL
ENGINEERING

**Synthesis of Symmetrical Urea Derivatives
From CO₂ and Amines Over Copper-Based
Core-Shell Catalysts**

*A thesis submitted in fulfilment of the requirements for the degree of
Doctor of Philosophy*

by

CİHAD KARAÇAM

JUNE 2023



**University of
Sheffield**

Abstract

Urea derivatives are key intermediates in the synthesis of agrochemicals and pharmaceuticals and also have applications as additives in fuels and polymers. Traditional production routes require the use of highly toxic chemicals such as phosgene, isocyanates and carbon monoxide. Carbon dioxide is emerging as an alternative feedstock for the production of urea derivatives, avoiding the use of such hazardous materials. Previous studies, however, employed catalysts based on rare and expensive metals for long reaction times of up to 48 h. This work presented here shows the successful synthesis of urea derivatives from CO₂ and various amines using inexpensive and abundant copper and iron-based catalysts with reduced reaction times.

Urea derivatives synthesis was conducted using 20 mmol butylamine, 5 MPa CO₂, 4 ml organic solvent and 10 mol% catalyst at 463 K in an autoclave with a volume of 45 ml. The influence of solvent, temperature, reaction time, reactant amounts and different metal oxide catalysts on reaction yield was studied to optimise reaction conditions.

Results demonstrate that CuO can successfully catalyse the synthesis of urea derivatives from CO₂ with a reaction yield of up to 45% at 463 K in 2 h. While effective catalysts, these materials suffer from leaching of the active metal oxide during the reaction. This limits the recyclability of the catalyst. In order to address this while maintaining the benefits of the copper oxide catalyst, a novel CuO@SiO₂ core-shell catalyst has been prepared. In these materials the active phase is encapsulated by an inert outer shell, thereby avoiding catalyst deactivation because of migration, sintering or leaching. TEM, SEM, XRD, and FTIR have been used to characterise the catalysts and relate catalytic performance to catalyst structure. Experiments showed that mesoporous silica coating dramatically enhanced the reactivity of the catalyst as well as its stability against catalyst leaching. 20 mol% CuO@SiO₂ produced a similar yield compared to bulk CuO in 2 h with up to 95% less catalyst leaching. It demonstrated greater reactivity for longer reaction times and reached 56% yield in 4 h thanks to the interaction between core and shell species.

Acknowledgements

The author would like to express sincere gratitude to Dr James McGregor for their invaluable advice, continuous support and patience during the project. I would also thank the technical staff in the Chemical and Biological Engineering department. Many special thanks should also go to every member of the Catalysis group, especially Eleanor O’Doherty, Fatima Muhammad, Gareth Davies and Mariya Konstantinova for their friendships to make these tough days memorable with laughs.

I would also like to express my deepest gratitude to my little man, Mehmet Asaf and my much-loved wife, Şeyma Gül, without whom I could not have undertaken this journey without her endless support. I am also thankful to my parents for their unwavering support and belief in me. Many thanks to our family in Sheffield, particularly Dr İdris Tuğrul Gülenç and Dr Yunus Azaklı for their valued advice in every step of this journey.

Finally, I would like to extend my sincere thanks to the Ministry of National Education of the Republic of Türkiye for this opportunity and their generous support for my education.

Table of Contents

| | |
|--|-------------|
| Abstract | i |
| Acknowledgements | ii |
| Table of Contents | iii |
| List of Figures | vii |
| List of Tables | xi |
| List of Equations | xiii |
| Chapter 1: Introduction | 1 |
| 1.1. Project aim and objectives | 5 |
| Chapter 2: Literature Review | 7 |
| 2.1. Activation of CO ₂ | 9 |
| 2.2. Value-added product synthesis by CO ₂ utilisation..... | 10 |
| 2.2.1. Cyclic carbonates synthesis | 11 |
| 2.2.2. Dimethyl carbonate synthesis..... | 15 |
| 2.2.3. Methanol synthesis | 21 |
| 2.2.4. Methylamines synthesis..... | 25 |
| 2.2.5. Urea and its derivatives synthesis..... | 28 |
| 2.3. Core-shell catalysts | 36 |
| 2.4. Summary of literature review | 38 |

| | |
|---|-----------|
| Chapter 3: Materials and Methodology | 40 |
| 3.1. Materials | 41 |
| 3.2. Experimental method | 41 |
| 3.2.1 Set-up | 41 |
| 3.2.1. Core-shell catalysts preparation | 43 |
| 3.3. Analytical methods | 44 |
| 3.3.1. Analysis of urea derivatives by GC-MS | 44 |
| 3.3.2. Scanning electron microscopy | 46 |
| 3.3.3. X-ray diffraction | 46 |
| 3.3.4. Atomic absorption spectroscopy | 47 |
| 3.3.5. Fourier transform infrared spectroscopy | 48 |
| 3.3.6. Transmission electron microscopy | 48 |
| Chapter 4: Conversion of CO₂ Into Urea Derivatives Over Heterogeneous Metal Oxide Catalysts | 50 |
| 4.1. Results and discussion | 52 |
| 4.1.1. Optimisation of the reaction conditions for DBU production | 52 |
| 4.1.1.a. The influence of solvent | 54 |
| 4.1.1.b. The effect of reactant amounts | 58 |
| 4.1.1.c. The influence of temperature and time | 61 |
| 4.1.2. Catalytic performance on urea derivatives synthesis | 65 |
| 4.1.2.a. The effect of metal oxide catalysts | 65 |
| 4.1.2.b. Conversion of different amines into urea derivatives | 69 |
| 4.1.3. Catalyst leaching | 72 |
| 4.2. Conclusion | 76 |
| Chapter 5: Preparation of Silica-Coated Metal Oxide Core-Shell Catalysts | 79 |

| | |
|--|------------|
| 5.1. Experimental methods | 80 |
| 5.2. Results and discussion | 81 |
| 5.2.1. Core-shell catalyst preparation | 81 |
| 5.2.1.a. The effect of surfactant on shell formation..... | 81 |
| 5.2.1.b. Solvent influence on shell formation..... | 86 |
| 5.2.1.c. Effect of acetate amount on shell formation..... | 89 |
| 5.2.1.d. The influence of precipitation agent on mesoporous silica synthesis . | 92 |
| 5.2.1.e. Effect of synthesis and drying temperatures on silica shell formation | 94 |
| 5.2.1.f. The effect of calcination temperature increase rate on shell formation | 96 |
| 5.2.2. Analysis of core-shell nanoparticles | 100 |
| 5.2.2.a. Template removal assessment..... | 100 |
| 5.2.2.b. Compositional analysis of prepared core-shell catalysts..... | 101 |
| 5.2.2.c. Morphological analysis of core-shell catalysts | 103 |
| 5.2.2.d. The crystal composition of catalysts | 106 |
| 5.2.2.e. Synthesis of different metal oxide core nanoparticles | 107 |
| 5.3. Conclusion..... | 111 |
| Chapter 6: Urea Derivatives Synthesis Over Copper-Based Catalysts | 114 |
| 6.1. Results and discussion | 115 |
| 6.1.1. Optimisation of the reaction conditions for urea derivatives synthesis | 115 |
| 6.1.1.a. The influence of solvent | 116 |
| 6.1.1.b. The effect of substance amounts..... | 118 |
| 6.1.1.c. The influence of temperature and time..... | 124 |
| 6.1.2. Catalytic performance on urea derivatives synthesis | 128 |
| 6.1.2.a. The effect of solvent at optimised conditions..... | 129 |
| 6.1.2.b. The assessment on the reactivity of different metal oxide catalysts... | 131 |

| | |
|---|------------|
| 6.1.2.c. Catalytic conversion of different amines into urea derivatives | 134 |
| 6.1.3. DBU synthesis over CuO@SiO ₂ core-shell catalysts..... | 137 |
| 6.2. Conclusion..... | 141 |
| Chapter 7: Conclusions and Future Work | 144 |
| 7.1. Conclusions..... | 146 |
| 7.1.1. Conversion of CO ₂ into urea derivatives over heterogeneous metal oxide catalysts | 146 |
| 7.1.2. Preparation of silica-coated metal oxide core-shell catalysts | 147 |
| 7.1.3. Urea derivatives synthesis over copper-based catalysts | 148 |
| 7.2. Recommendations for future work..... | 149 |
| References | 152 |
| Chapter 8: Appendices | 171 |
| A. GC-MS CALIBRATION CURVES..... | 172 |
| B. AAS CALIBRATION CURVES..... | 176 |

List of Figures

| | |
|--|----|
| Figure 1.1 Innovative phases of technologies for CCS and CCU..... | 2 |
| Figure 2.1 The changes in CO ₂ level since 1958..... | 8 |
| Figure 2.2 Possible routes of CO ₂ utilisation in chemical production | 10 |
| Figure 3.1 The diagram of setup used for the synthesis of urea derivatives from CO ₂ and amines (1: Inlet valve; 2: Pressure gauge; 3: Outlet valve; 4: Pressure relief valve) | 42 |
| Figure 3.2 The schematic diagram of the reflux setup used for the preparation of core-shell catalysts | 44 |
| Figure 4.1 Dependence of CO ₂ pressure and butylamine concentration on the reaction rate using solvent-only experiments | 53 |
| Figure 4.2 Dependence of CO ₂ pressure and butylamine concentration on the reaction rate using CeO ₂ in THF | 53 |
| Figure 4.3 Influence of solvent on DBU synthesis and the correlation between DBU yield and dielectric constants of solvents..... | 55 |
| Figure 4.4 The effect of solvent amount on DBU synthesis from butylamine and CO ₂ using DMSO..... | 58 |
| Figure 4.5 Changes in DBU yield over increased CO ₂ pressure..... | 59 |
| Figure 4.6 Butylamine conversion at different concentrations and the effect of amine amount on DBU selectivity..... | 60 |
| Figure 4.7 The influence of temperature on butylamine conversion and DBU selectivity | 62 |
| Figure 4.8 Changes in butylamine conversion and DBU selectivity over reaction times | 64 |

| | |
|---|-----|
| Figure 4.9 Changes in butylamine conversion and DBU selectivity over Fe ₂ O ₃ amounts | 68 |
| Figure 4.10 The impact of temperature on the iron concentration detected after the reaction | 73 |
| Figure 4.11 Effect of amine amount on iron concentration leached after the reaction | 74 |
| Figure 5.1 SEM images of prepared CuO@SiO ₂ using different surfactants: a) No surfactant, b) 0.0063 g of CTAB, c) 0.25 g of CTAB, d) 1 g of CTAB, e) 2 g of CTAB, f) 2 g of Pluronic P123 | 84 |
| Figure 5.2 TEM images of prepared CuO@SiO ₂ using different surfactants: a) No surfactant, b) 0.25 g of CTAB, c) 2 g of CTAB, d) 2 g of Pluronic P123 | 85 |
| Figure 5.3 SEM images of core-shell catalysts prepared by different solvent amounts: a) 15 ml water, b) 60 ml water, c) 15 ml water:15 ml ethanol; TEM images of CuO@SiO ₂ prepared using 15 ml of water (d) and 60 ml of water (e) | 87 |
| Figure 5.4 SEM images of silica-coated nanoparticles at various ethyl acetate amounts: a) None, b) 7.5 ml, c) 15 ml | 90 |
| Figure 5.5 TEM images of prepared CuO@SiO ₂ particles at several acetate amounts: a) 7.5 ml, b) 15 ml | 91 |
| Figure 5.6 SEM images of prepared silica-coated copper (II) oxide nanoparticles using various ethanolamine amounts: a) 0.6 ml, b) 1.2 ml | 93 |
| Figure 5.7 The synthesis of CuO@SiO ₂ core-shell catalysts at room temperature (a) and 80 °C (b) | 94 |
| Figure 5.8 Samples morphology dried at room temperature (a) and 80 °C (b)..... | 96 |
| Figure 5.9 SEM images of catalysts before (a) and after the calcination with a ramp rate of 0.5 (b), 1 (c), 2 (d), 4 (e) and 8 °C/m (f) | 98 |
| Figure 5.10 TEM images of samples with a calcination temperature ramp rate of 1 °C/m (a) and 4 °C/m (b) | 99 |
| Figure 5.11 FT-IR spectrums of prepared core-shell catalysts before and after the calcination..... | 100 |
| Figure 5.12 SEM-EDS analysis of silica-coated copper (II) oxide catalysts: a) SEM image of particles, b-d) images for EDS mappings of particles..... | 102 |
| Figure 5.13 The morphological analysis of samples with several copper oxide loadings: a) 20 mol%, b) 40 mol%, c) 60 mol%..... | 104 |
| Figure 5.14 Particle size changes on mesoporous silica-coated copper oxide particles over TEOS amount: a) 9.7, b) 4.2, c) 1.4, and d) 0.47 ml..... | 105 |

| | |
|--|-----|
| Figure 5.15 XRD patterns of core-shell nanoparticles with different loadings | 106 |
| Figure 5.16 SEM images of core-shell catalysts with different metal oxides: a) CuO, b) ZnO | 107 |
| Figure 5.17 TEM images of different metal oxide cores coated with mesoporous silica: a) CuO, b) ZnO..... | 108 |
| Figure 5.18 XRD pattern of CuO@SiO ₂ and ZnO@SiO ₂ core-shell catalysts..... | 108 |
| Figure 5.19 TEM images of silica-coated CuO (a) and Fe ₂ O ₃ (b) with 40 mol% loadings..... | 109 |
| Figure 5.20 SEM-EDS analysis of the prepared CuO/Al ₂ O ₃ @SiO ₂ catalyst | 110 |
| Figure 6.1 The influence of different solvents on DBU synthesis and the correlation between DBU yield and dielectric constants of solvents | 116 |
| Figure 6.2 The effect of solvent amount on DBU synthesis from butylamine and CO ₂ using DMSO over copper (II) oxide | 118 |
| Figure 6.3 Butylamine conversion at different concentrations and the effect of amine amount on DBU selectivity..... | 119 |
| Figure 6.4 Changes in DBU yield over the increase of CO ₂ pressure..... | 120 |
| Figure 6.5 Changes in butylamine conversion and DBU selectivity over a range of CuO amounts | 122 |
| Figure 6.6 The catalyst leaching over copper (II) oxide amounts | 123 |
| Figure 6.7 Changes in the conversion and selectivity over temperature | 125 |
| Figure 6.8 The impact of temperature on the leaching of copper (II) oxide | 126 |
| Figure 6.9 The synthesis of DBU from butylamine and CO ₂ over copper oxide at different reaction times | 127 |
| Figure 6.10 The effect of time on the leached copper concentration after the reaction | 128 |
| Figure 6.11 Catalyst leaching in various solvents at two different temperatures ... | 130 |
| Figure 6.12 Changes in butylamine conversion and DBU selectivity over CuO@SiO ₂ with various loadings..... | 138 |
| Figure 0.1 1,3 dibutylurea calibration curve used in Chapter 4, obtained by GC-MS analysis of standard solution prepared from commercial DBU | 172 |
| Figure 0.2 Butylamine calibration curve used in Chapter 4, obtained by GC-MS analysis of standard solution prepared from commercial butylamine..... | 173 |

Figure 0.3 1,3 dibutylurea calibration curve used in Chapter 6, obtained by GC-MS analysis of standard solution prepared from commercial DBU174

Figure 0.4 Butylamine calibration curve used in Chapter 6, obtained by GC-MS analysis of standard solution prepared from commercial butylamine.....175

Figure 0.5 Calibration curves obtained by AAS using standard solutions prepared by commercial copper (II) nitrate dissolved in nitric acid176

Figure 0.6 Calibration curves obtained by AAS using standard solutions prepared by commercial iron (III) nitrate dissolved in nitric acid 177

Figure 0.7 Calibration curves obtained by AAS using standard solutions prepared by commercial zinc (II) nitrate dissolved in nitric acid.....178

List of Tables

| | |
|--|----|
| Table 2.1 The amount of CO ₂ used for the production of chemicals | 11 |
| Table 2.2 Heterogeneous catalysts used for the cycloaddition of different epoxides | 14 |
| Table 2.3 Heterogeneous catalysts employed for the two-step or direct synthesis of DMC | 18 |
| Table 2.4 Heterogeneous catalysts employed for the hydrogenation of carbon dioxide for methanol formation | 22 |
| Table 2.5 Heterogeneous catalysts used for methylamines synthesis from CO ₂ , H ₂ and NH ₃ at 570 K and 0.6 MPa | 27 |
| Table 2.6 Catalysts used for the synthesis of urea derivatives from different amines | 32 |
| Table 4.1 Carbon mass balance over amine amounts | 61 |
| Table 4.2 Catalytic conversion of butylamine with CO ₂ into DBU using different metal oxide catalysts | 66 |
| Table 4.3 The effect of reaction time on the synthesis of N,N-dibutylurea at optimised reaction conditions | 69 |
| Table 4.4 The synthesis of 1,3-disubstituted urea from different amines and CO ₂ over Fe ₂ O ₃ at optimised conditions | 71 |
| Table 4.5 Iron concentration over different amines | 74 |
| Table 4.6 Leached iron concentrations for different iron-based catalysts | 75 |
| Table 5.1 Surfactant effect on catalyst stability and reactivity towards DBU synthesis | 83 |
| Table 5.2 Solvent influence on catalyst stability against CuO leaching and reactivity for DBU synthesis | 88 |

| | |
|---|-----|
| Table 5.3 The influence of ethyl acetate amount on catalyst reactivity and stability | 90 |
| Table 5.4 Effect of ethanolamine amount on silica preparation for stability and reactivity | 93 |
| Table 5.5 The influence of synthesis temperature on catalyst stability and reactivity | 95 |
| Table 5.6 Effect of drying temperature on catalyst leaching and DBU yield | 95 |
| Table 5.7 Catalyst stability and activity over different calcination ramp rates | 97 |
| Table 5.8 Copper (II) oxide loading of catalysts over various TEOS amount and their catalytic performances..... | 103 |
| Table 6.1 Carbon mass balance changes over CO ₂ pressure..... | 121 |
| Table 6.2 Changes in butylamine conversion and DBU selectivity under the influence of different gases..... | 122 |
| Table 6.3 Catalytic conversion of butylamine with CO ₂ into DBU using different solvents | 129 |
| Table 6.4 Catalytic conversion of butylamine with CO ₂ into DBU using different metal oxide catalysts..... | 132 |
| Table 6.5 Catalyst leaching for metal oxides catalysts at optimised reaction conditions | 134 |
| Table 6.6 The synthesis of 1,3-disubstituted urea from different amines and CO ₂ over CuO at optimised conditions | 135 |
| Table 6.7 Copper oxide catalyst leaching in different amines | 137 |
| Table 6.8 Catalyst screening for the prepared core-shell catalysts for the synthesis of N,N-dibutylurea at optimised reaction conditions | 140 |

List of Equations

| | |
|--|-----|
| Equation 2.1 The cycloaddition of carbon dioxide with epoxides to the corresponding cyclic carbonates | 12 |
| Equation 2.2 The direct catalytic synthesis of DMC from methanol and CO ₂ | 16 |
| Equation 2.3 The two-step dimethyl carbonate synthesis from epoxide, methanol and CO ₂ | 20 |
| Equation 2.4 Reactions occur in the hydrogenation of CO ₂ and reactions produce methanol | 24 |
| Equation 2.5 Proposed reaction pathways for methylamine synthesis | 26 |
| Equation 2.6 Urea synthesis from CO ₂ and NH ₃ via Bosch-Meiser urea process ... | 28 |
| Equation 2.7 Urea derivatives synthesis from the reaction of amines with CO ₂ | 30 |
| Equation 4.1 The proposed reaction mechanism for the urea derivatives synthesis from CO ₂ and amines | 51 |
| Equation 4.2 The reaction occurs between DMF and butylamine | 56 |
| Equation 4.3 The side reaction occurs by the use of acetonitrile as a solvent | 56 |
| Equation 4.4 A side reaction pathway occurs in the presence of methanol..... | 57 |
| Equation 6.1 The side reaction occurs between DMF and butylamine | 117 |

Chapter 1: Introduction

Global warming and climate change refer to an enhancement of global temperatures due to increased concentration of anthropogenically generated greenhouse gases (GHGs) such as methane, ozone and CO₂ (Rinkesh, 2015). Hence, the global temperature has risen 1 °C since the pre-industrial period, and it is projected to exceed 4 °C by 2100 (IPCC, 2022). There are several measures available to limit this upsurge in greenhouse gases, especially the biggest contributor to global warming which is CO₂, such as lower energy consumption, increasing the efficiency of power generation, renewable energy, CO₂ capture and storage (CCS) and CO₂ utilisation (Kenarsari et al., 2013).

CCS is the process by which carbon dioxide is captured from major emission points like power stations and cement & steel industries for storing within enduring geological sites (Department of Energy & Climate Change, 2012). It is calculated that CCS has the potential to cut CO₂ emissions by 85-90% from the large volume of emitters. Three carbon dioxide capture technologies have already been proved for CCS: post-combustion, pre-combustion and oxyfuel combustion (Leung et al., 2014). The former the only commercially available can be the most prominent candidate for a short-term solution as no significant upgrade is required to be fitted to existing power plants (D’Alessandro et al., 2010).

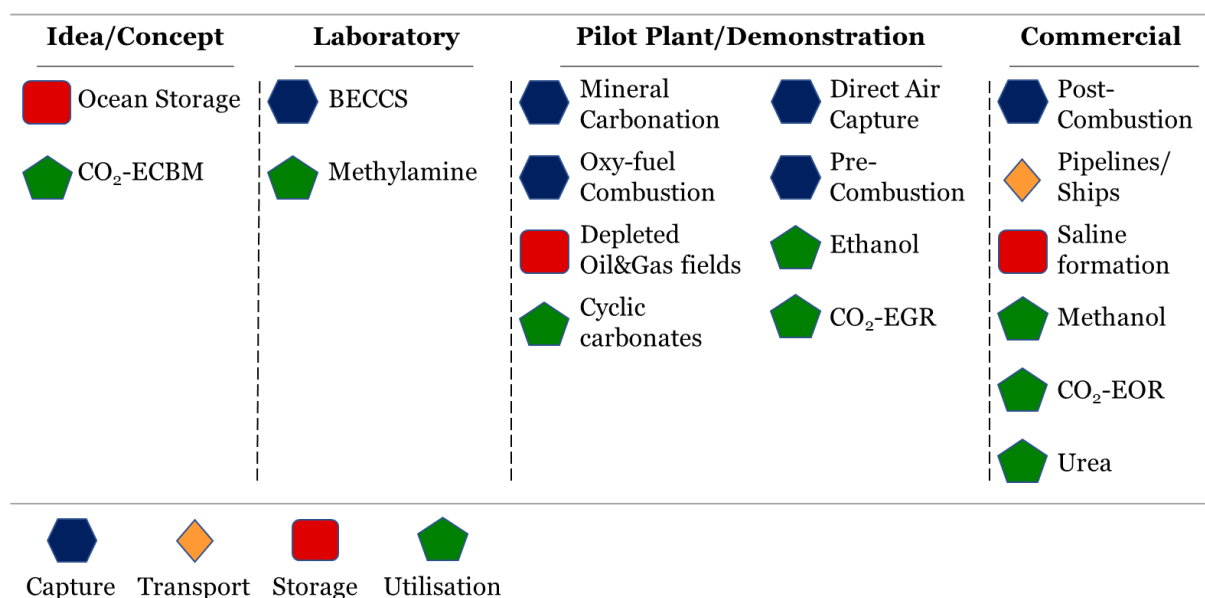


Figure 1.1 Innovative phases of technologies for CCS and CCU (Dziejarski et al., 2023)

Technical developments in the storage technologies of captured carbon dioxide showed similar trends with capture techniques, generating greater outcomes for CCS resulting in over 100 facilities in operation or under development worldwide (Global CCS Institute, 2021). Storing captured CO₂ in depleted oil and gas fields and saline formations are the most advanced options of which the latter has already been in use for over a decade (Chadwick et al., 2008). In this method, CO₂ is stored into a major saline aquifer placed several km below the surface, which is believed that it has the biggest potential volume for CCS (NETL, 2015). However, a recent report revealed that the annual capacity of all CCS facilities is around 45 million tonnes and it is estimated that over 5600 Mtpa is required by 2050 to limit the increase in global temperature by 2 °C (Global CCS Institute, 2021; IEA, 2022a). Therefore all accessible tools need to be employed to meet our goal for net-zero, among which the utilisation of CO₂ can be a promising approach as marketable products can be produced from captured CO₂. (Cuéllar-Franca & Azapagic, 2015). Additionally, CO₂ utilisation can be implemented with CCS cooperatively as a combination for broader applications (DECC & BIS, 2014). The primary assessment of the fixation of CO₂ is that the process should manufacture energy and chemicals with high efficiency and release less CO₂ into the atmosphere (Angunn et al., 2014).

CO₂ already has a wide range of applications, from the food and drink industry to Enhanced Oil Recovery (EOR), at which it can be used without requiring any further process. It can also be used as a reactant to produce chemicals and fuels. CO₂ has been utilised directly by the food and drink industry as a carbonating agent, preservative, packaging gas and inert gas to provide a controlled atmosphere to expand the shelf life of fruit and vegetables. However, food and drink industry applications require high purity of CO₂ (Cuéllar-Franca & Azapagic, 2015; Leitner et al., 2015).

Carbon dioxide has also been used to improve the yield of petroleum and natural gas extraction since the 1980s. By injecting high-pressure CO₂ into an oil field, 15% more petroleum can be obtained (Leitner et al., 2015). Furthermore, oil's viscosity can be reduced, and a greater yield can be obtained using supercritical CO₂. Although it has a potential to remain underground after the injection as per geological storage, the process has some uncertainty in terms of leakage because the equipment used on these sites to monitor CO₂ is mainly designed to boost productivity (Bui et al., 2018).

The utilisation of CO₂ also has a wide range of applications, from dry cleaning to foaming agents or solvents to fire extinguishers where CO₂ acts as an inert gas (Arakawa et al., 2001; Leitner et al., 2015). The physical or direct utilisation of CO₂ is least attractive due to its rapid release into the atmosphere. Producing value-added products from CCU makes this approach a better alternative for direct utilisation (Leitner et al., 2015). Several existing industrial applications use CO₂ to synthesise chemicals such as carbonates, urea, and salicylic acid, whilst it has more potential to be converted into synthetic fuels like hydrogen, methanol, dimethyl ether and alkane fuel (Laosiripojana & Faungnawakij, 2014; Omae, 2012). Among all these marketable compounds that could potentially be produced from CO₂, urea industries were the biggest consumer in 2019 with 130 Mt out of 230 Mt of carbon dioxide according to the report published by IEA, 2022. Additionally, more recent medical studies highlighted the importance of substituted ureas which can be used for many different treatments from HIV to various cancer diseases (Ghosh & Brindisi, 2020; Özgeriş et al., 2022).

Urea derivatives are organic compounds formed by the substitution of hydrogen atoms on urea with alkyl or aryl groups that has a variety of use in several industries including pharmaceuticals and agrochemicals (Lv et al., 2022). However, their traditional synthesis still relies on the reaction between amines and toxic and hazardous phosgene, isocyanates or carbon monoxide (Bigi et al., 2000). As an alternative to all of these harmful chemicals, carbon dioxide as a carbonyl source was proposed, since not only the elimination of toxic compounds would be achieved but also an alternative method would be created for the utilisation of captured CO₂ (Yang et al., 2011). This method also enables to produce various urea derivatives including both symmetrical and asymmetrical. A market research reported in 2018 revealed that one of the substituted urea, ethylene urea, has a quite large market in the global urea industry with a production of 12,000 t annually, considering that only one of them has such a high market size, all compounds would create a considerable potential for CO₂ utilisation (Koizumi et al., 2021).

Despite the fact that urea derivatives can be produced from amines and CO₂ for preventing any harmful chemicals, the process still requires the use of a catalyst. A catalyst is a substance that accelerates chemical reaction rates by reducing the activation energy for the reaction without being consumed. The use of catalysts provides a more favourable reaction route, thereby allowing desired products to be synthesised at reduced temperatures and pressures. Catalysts are mainly categorised into three different forms: biocatalysts also known as an enzyme that catalyse biological reactions; homogeneous catalysts are substrates in the same phase as reactants; heterogeneous catalysts that can catalyse reactions by being in a different phase compared to the reaction media (Chorkendorff & Niemantsverdriet, 2007). Although the use of homogeneous and heterogeneous catalysts in industrial catalysis has characteristic advantages, heterogeneous catalysts are more advantageous thanks to the ease of separation and reuse for sustainability (Thomas & Thomas, 2015). Hence, employing these catalysts in CCU could provide a sustainable economic profit from captured while avoiding the use of harmful substances for urea derivatives synthesis.

1.1. Project aim and objectives

The main aim of the project is to develop an alternative method to produce symmetrical urea derivatives from CO₂ and various amines with different attached groups by avoiding the use of fossil fuels or toxic chemicals such as carbon monoxide and phosgene. Global warming and climate change due to the increase of CO₂ levels in the atmosphere are the main motivations of the project. The project is divided into three main objectives to achieve this goal:

- Optimisation of urea derivatives synthesis from amines and CO₂ using different metal oxide heterogeneous catalysts
- Developing novel, highly reactive mesoporous silica-coated copper-based catalysts for the conversion of CO₂ with high selectivity and stability
- Employing prepared core-shell catalysts at optimised reaction conditions method to produce urea derivatives with a greater atom-efficiency.

A detailed literature review is presented which covers the conversion of CO₂ into different value-added products over several heterogeneous catalysts in Chapter 2. The experimental procedures and analytical methods used are described in Chapter 3 with the principles analyses. Chapter 4 outlines the results obtained from urea derivatives synthesis over various heterogeneous catalysts after an exhaustive process optimisation. After that, conditions for the preparation of copper-based core-shell catalysts are found in Chapter 5, along with the assessment of these prepared catalysts in terms of stability and reactivity for urea derivatives synthesis. The results of experimental work for employing prepared core-shell catalysts for urea derivatives synthesis at optimised reaction conditions are presented in Chapter 6. The final conclusion of the study, along with recommendations for future work, are listed in Chapter 7.

Chapter 2: Literature Review

Despite the development of clean energy systems, eighty per cent of the global energy demand was still fulfilled by fossil fuels in 2021, and energy-related emissions together with industrial processes were responsible for 36.3 Gt of CO₂ annual emissions out of about 40 Gt/y global CO₂ emission (Friedlingstein et al., 2022; IEA, 2023). As a result of this massive consumption of fossil fuels, the concentration of CO₂ has consequently risen from 280 ppm to just above 420 ppm since the industrial revolution, and it is estimated that it could reach 570 ppm by the end of this century (ESRL, 2023; W. Wang et al., 2011). In order to limit this elevation and keep the global average temperature within the Paris agreement target of 2 °C, CO₂ emission needs to be halved by 2050 (Arakawa et al., 2001; UNFCCC, 2015). It was calculated that the utilisation of CO₂ has the potential to cut one-tenth of carbon emissions every year, which is about 3 gigatonnes of carbon dioxide (Dibenedetto et al., 2014).

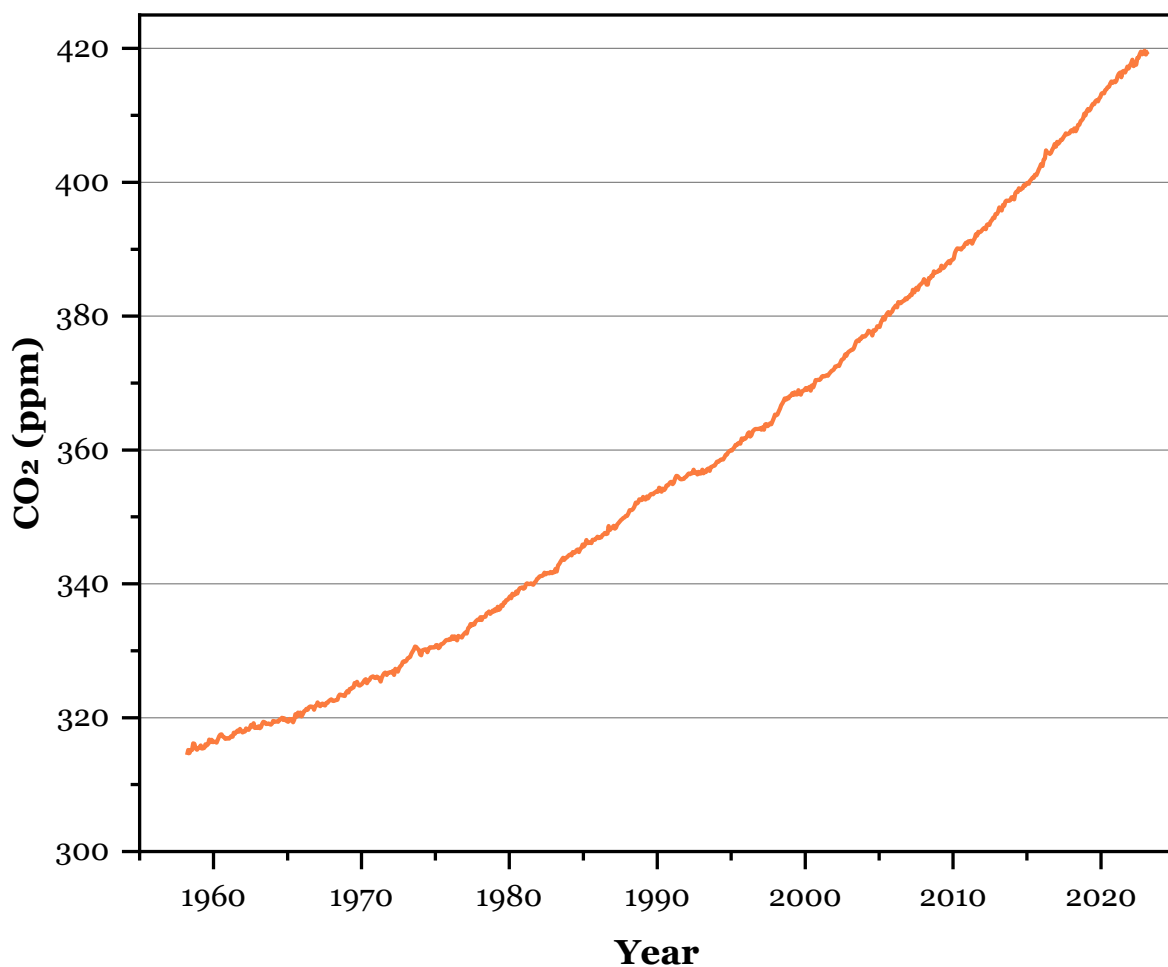


Figure 2.1 The changes in CO₂ level since 1958, adapted from Earth Science Communications Team (NASA) (2019)

CO₂ is an abundant, non-toxic, non-flammable, easily available and renewable carbon source emitted mostly from anthropogenic emission sources such as fossil fuels burning and deforestation (Laosiripojana & Faungnawakij, 2014; He, Sun, & Han, 2013; He & Sci, 2012). Although it is usually considered a useless compound or harmful waste that has a colossal impact on current global warming, it is now seen as a business opportunity for different industries to synthesise compounds formed by C-C, C-N, C-O and C-H bonds. Still, CO₂ conversion is a highly energy-intensive process because of its stability, but industrial drawbacks like chemical supply shortages or increases in fossil fuel prices could assist it being an industrial process, though (Cuéllar-Franca & Azapagic, 2015). Even though its use in the chemical industry has stayed under its potential due to this stability, it is known that CO₂ shows a powerful affinity toward nucleophiles to give a reaction at moderate conditions (Sakakura et al., 2007). Significant energy input is nonetheless required, or else highly reactive catalysts need to be employed for any feasible CO₂ utilisation routes under reduced reaction conditions (Road, 2010).

2.1. Activation of CO₂

Gibbs free energy differences between the reactants and products are the main driving factor for any chemical reactions. Both ΔH° and $T\Delta S^\circ$ terms of the Gibbs free energy do not favour CO₂ conversion into other chemicals, so substantial energy input is required to break C-O solid bonds (Road, 2010). There are two main categories of reaction in which CO₂ is involved: the first one is low energy process that C-atom maintains its +4 oxidation state like carbamates, ureas, carbonates and polymeric materials such as polycarbonates, polyurethanes and so on; the other one is high energy process that carbon atom goes down to oxidation states +2 or lower like formic acid, methanol, alkane and hydrocarbons etc. (Aresta et al., 2014). Although the market size of the chemicals produced from the latter is significantly greater than the first one owing to the use of these substrates as fuels or fuel additives, the requirement of higher energy-input and energy-intensive reactants like hydrogen for their production makes this pathway less viable in terms of CO₂ emission mitigation (Zheng et al., 2017). In this perspective, the synthesis of urea and its derivatives from CO₂ could be more a feasible option by employing catalysts to lower the activation energy for a faster reaction.

2.2. Value-added product synthesis by CO₂ utilisation

CO₂ is defined as a non-reactive compound, yet thanks to catalysis, it can be utilised to produce numerous chemicals from urea to carbonates and from methanol to syngas as fuel or fuel additives, as seen in Figure 2.2 (Aresta, 1993). The total amount of utilized CO₂ was just above 200 Mt/y in 2016, and it is estimated that it could reach up to 332 Mt/y in 2030 (Aresta et al., 2017).

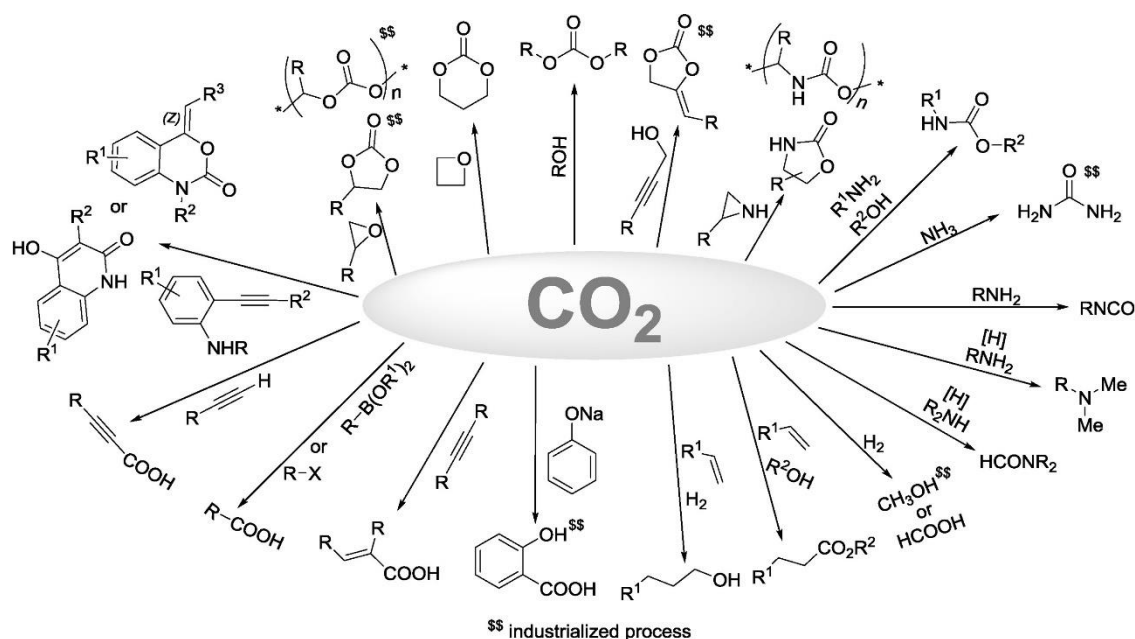


Figure 2.2 Possible routes of CO₂ utilisation in chemical production, adapted from Yu et al. (2018)

A review paper analysed several commercial CCU routes reveals that urea was the biggest application of CO₂ utilisation, with the usage of 132 Mt out of 180 Mt annual production in 2016 (Table 2.1). Following that, methanol synthesis was reported as the second biggest route where 60 Mt were produced from 10 Mt CO₂. It was projected that the market size of urea and methanol will be 210 and 80 Mt in 2030, respectively. Moreover, carbonates synthesis is one of the new approaches for CCU and it is estimated that the amount of several carbonates produced from CO₂ could potentially increase from 7 to 10 Mt between 2016 and 2030 by the use of 9 Mt of CO₂ (Aresta et al., 2017). Overall, the amount of CO₂ used in either chemical synthesis or EOR was over 230 Mt in 2022 and the roadmap on CO₂ utilisation stated that it has a potential to reach 7 Gt in 2030 (Global CO₂ Initiative, 2016; IEA, 2022a).

Table 2.1 The amount of CO₂ used for the production of chemicals, adapted from Aresta et al. (2017)

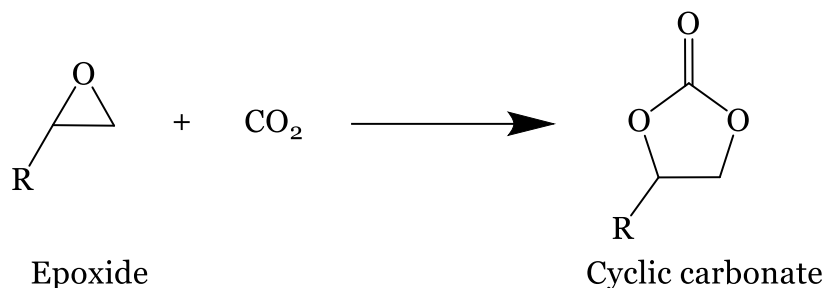
| Product | Market in 2016 (Mt/y) | CO₂ use in 2016 (Mt/y) | Market in 2030 (Mt/y) | CO₂ use in 2030 (Mt/y) |
|--------------------|------------------------------|--|------------------------------|--|
| Urea | 180 | 132 | 210 | 154 |
| Methanol | 60 | 10 | 80 | 28 |
| Carbonates | 7 | 1.5 | 10 | 8 |
| Acrylates | 5 | 1.5 | 8 | 5 |
| Formic acid | 1 | 1 | 10 | 9 |

In order to meet its potential, new more feasible routes are required to be introduced for CCU, which highly relies on novel effective catalyst designs. An effective heterogeneous catalyst is defined by Thomas & Thomas (2015) that it needs to be reactive and stable as well as selective for desired products. Although active sites and mechanisms of homogeneous catalysis are generally well-defined, compared to heterogeneous catalysis even though the heterogeneous ones have wide applications in the industry (Pelletier & Basset, 2016). Therefore, several heterogeneous catalysts employed for the synthesis of different chemicals from CO₂ have been examined in this chapter to identify catalysts that can be effective for CO₂ conversion and selective for urea derivatives.

2.2.1. Cyclic carbonates synthesis

Cyclic carbonates are significant types of commercial chemicals that can find a use themselves in batteries and chemical industries; as well as in degreasing, paints and cleaning as polar aprotic solvents, thanks to their outstanding characteristics like the ease of biodegradation, having high boiling and flash points (Cokoja et al., 2015; Tamura et al., 2014; Yoshida & Ihara, 2004). Their traditional synthesis is mainly based on a reaction between phosgene/carbon monoxide and reactants such as diols, olefins, cyclic ketals, propargyl alcohols, oxetanes and epoxides (McGuire et al., 2018).

This toxic phosgene can be eliminated by the use of CO₂ as a carbonyl source as can be seen in Equation 2.1; however, employing CO₂ in this non-spontaneous reaction relies on effective catalysts although the reaction is exothermic (Alves et al., 2017).



Equation 2.1 The cycloaddition of carbon dioxide with epoxides to the corresponding cyclic carbonates

In this perspective, the conversion of carbon dioxide with heterocyclic compounds can be a greener pathway by eliminating toxic chemicals where epoxides are used for corresponding five-membered cyclic carbonates synthesis, and oxetanes are utilized for corresponding six-membered cyclic carbonates synthesis. Today, cyclic carbonates are obtained using these heterocycles over suitable catalysts under challenging reaction conditions. This main drawback of the process needs to be resolved to make the process more atom economical. Therefore, new, viable and relatively cheap catalysts and procedures are required in order to produce cyclic carbonates at lower temperatures and pressures for sustainable industrial production (Cokoja et al., 2015; North et al., 2010; Tamura et al., 2014).

In this regard, the cyclic carbonate synthesis in the literature using epoxides and CO₂ over several heterogeneous catalysts has been reviewed in Table 2.2. Yano et al. (1997) tested MgO as a catalyst for the reaction and proposed a mechanism for the reaction. It was reported that the catalyst adsorbs reactants CO₂ and epoxide to synthesise an intermediate complex; then, oxyanion is formed by the attack of carboxylate anion to β -carbon of epoxide; thus, cyclic carbonate is produced by the reaction between the oxyanion and carbonyl group. Although MgO has strong adsorption sites, its catalytic activity was relatively lower than the homogeneous counterparts owing to the lower total uptake of CO₂. Nb₂O₅ was then employed to enhance the reactivity of the reaction by Aresta et al. (2003) and it was stated that the carboxylation of epoxide was successfully accomplished with greater a conversion rate compared to the other

heterogeneous catalysts. In these catalytic routes, it was deduced that a ring-opening of epoxides by O-atom or pre-forming carbonate group was encouraged by Nb-O bonds.

Moreover, the investigation using magnesium and aluminium-based mixed oxide catalyst with different ratios for the reaction revealed that the acid-base sites of the catalyst formed by the Mg-O-Al structure were highly influential for the activation of reactants. Results showed that the Mg/Al ratio could affect dramatically the acid-basic sites on catalysts and this ratio needs to be optimised for greater reactivity (Yamaguchi et al., 1999). Similarly, Tu & Davis (2001) highlighted the significance of the base site number and strength for CO₂ activation.

Different from the others, the cycloaddition of CO₂ with several epoxides was succeeded with a moderate yield by the absence of any solvents over Cs/Al₂O₃; nevertheless, the promotion effect of water as a solvent was noted for a greater yield. Later, Yasuda et al. (2002) investigated any potential route for a solvent-free process over Lanthanum-based heterogeneous catalysts and managed to generate considerable yield. It was reported that this elimination of solvent from the process was achieved by acid-base sites provided from the catalyst. The mechanism of the reaction proposed was the activation of CO₂ by the Lewis base O²⁻ site adjacent to Ln³⁺ and the activation of epoxides the by Lewis acid Ln³⁺ site adjacent to Cl⁻. Also, a novel-designed catalyst, Ti-SBA-15, was tested and the same mechanism was reported with the absence of any solvents. An experiment was conducted with and without the presence of titanium and a significant amount of decrease in the yield was observed for the catalyst without titanium. This approach proved the effect of Lewis acid sites (Ti⁴⁺ in this case) on the activation of epoxides by adsorbing the reactants and retaining the intermediates (Srivastava et al., 2005).

Table 2.2 Heterogeneous catalysts used for the cycloaddition of different epoxides

| Catalyst | Reactant | Solvent | Product | Reference |
|---------------------------------------|-----------------|---------|---------------------|---------------------------|
| Cs/Al₂O₃ | Ethylene oxide | - | Ethylene carbonate | (Tu & Davis, 2001) |
| MgO | Ethylene oxide | DMF | Ethylene carbonate | (Yano et al., 1997) |
| LnOCl | Propylene oxide | - | Propylene carbonate | (Yasuda et al., 2002) |
| MS-MCN | Propylene oxide | DMF | Propylene carbonate | (Ansari et al., 2011) |
| Ti-SBA-15 | Propylene oxide | - | Propylene carbonate | (Srivastava et al., 2005) |
| TS-1 | Propylene oxide | DMAP | Propylene carbonate | (Srivastava et al., 2003) |
| Mg-Al | Octene oxide | DMF | Octene carbonate | (Yamaguchi et al., 1999) |
| Nb₂O₅ | Octene oxide | DMF | Octene carbonate | (Aresta et al., 2003) |
| ZnHAP | Styrene oxide | TEA | Styrene carbonate | (Mori et al., 2005) |
| CuO@SiO₂ | Styrene oxide | - | Styrene carbonate | (Rajabzadeh et al., 2020) |
| Cu-Al₂O₃ | Styrene oxide | - | Styrene carbonate | (Khalifeh et al., 2020) |

* TS-1¹: Titanosilicate; DMAP: N, N- dimethylaminopyridine; HAP: Hydroxyapatite; TEA: Triethylamine; MS-MCN: Mesoporous silica-mesoporous carbon nitrides

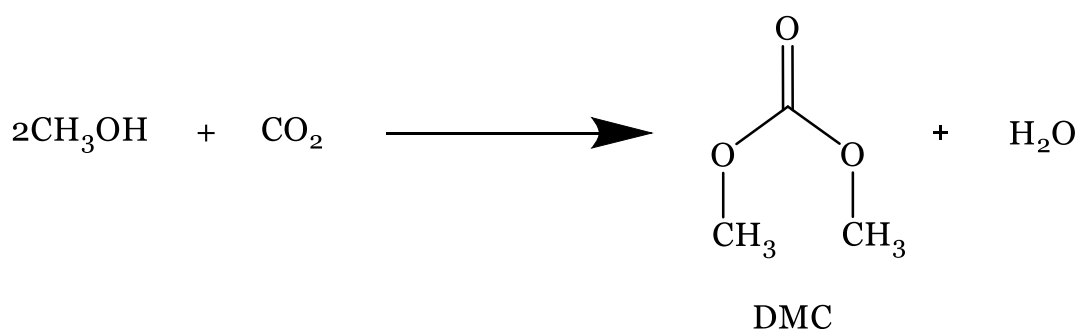
Nonetheless, all of these solvent-free pathways rely on the use of rare-earth elements, and recent developments in catalyst design enable to provide alternative options for this drawback. Copper-based core-shell catalysts were proposed to eliminate these expensive catalysts in solvent-free cycloaddition of CO₂ with various epoxides. These core-shell catalysts with multiple shell layers approved their reactivity and stability for the reaction but, similar yields compared to rare metal-based catalysts were accomplished by only using organic bases such as TBAB and TBAI as cocatalysts. Although Lewis acid Cu²⁺ sites were reported highly effective for the epoxy ring opening step, it was reported that organic bases were necessary to activate C atom on epoxide through nucleophilic attack of Br⁻ or I⁻ anions (Khalifeh et al., 2020; Rajabzadeh et al., 2020).

2.2.2. Dimethyl carbonate synthesis

Dimethyl carbonate is the simplest organic carbonate that smells like methanol with less toxicity in terms of being easy to handle without any precaution and non-hazardous when inhaled. Being biodegradable and environmentally friendly provides the compound wide range of applications as a fuel additive, solvent for lithium-ion batteries and reactant to produce polycarbonate, polyurethane and other chemicals. All these features facilitate being a promising alternative for toxic chemicals like ketones, acetate esters, phosgene and dimethyl sulphate (Razali et al., 2012; Tamboli et al., 2017). Processes including the reaction of phosgene with methanol; transesterification of cyclic carbonates by methanol; the reaction between CO and methyl nitrate; and oxidative carbonylation of methanol have been studied for the production of DMC over the years. However, these approaches suffer from the use of toxic chemicals. CO₂ utilization is able to address the problems in DMC production through different reaction routes: one-pot production of DMC using CO₂, methanol and epoxides; the carbonylation of acetals or ortho-esters; and direct synthesis of DMC from CO₂ and methanol. The latter can minimise feedstock's cost by increasing the efficiency if active catalysts can be developed (Abdalla & Liu, 2018; Dai et al., 2009).

The proposed mechanism for the one-pot DMC synthesis from methanol and CO₂ is a three-step reaction: the attraction of base sites of the catalyst to the hydroxyl groups on methanol, where methoxy groups are formed by converting t-OH and b-OH groups; the reaction between the t-methoxy group and CO₂ to produce methyl carbonate on the base site; the activation of methanol by Brønsted acid sites to obtain methyl cation that reacts with methyl carbonate to form DMC. Catalyst selectivity for DMC relies on converting t-OCH₃ to methyl carbonate in the overall reaction (Jiang et al., 2003). Since $\Delta_r G^\ominus_{298\text{ K}} = 26.21\text{ kJ/mol} > 0$ for the overall reaction of DMC, it does not occur spontaneously at room temperature, and substantial energy needs to be given to the system to run the reaction (Cai et al., 2009). Although higher temperature increases the activation of methanol and CO₂, DMC yield tends to reduce at temperatures above 150 °C due to the decrease in CO₂ adsorption of the catalyst and the decomposition of DMC (Bian, Xiao, Wang, Wang, et al., 2009; X. L. Wu et al., 2006). Because of the thermodynamic limitations, the stability of CO₂ and the lack of reactive catalysts, the direct synthesis of DMC has not been widely used industrially (Cai et al., 2009).

Therefore, several heterogeneous catalysts, namely organometallic compounds, metal tetra-alkoxides, potassium carbonate, zirconia and supported copper-nickel bimetallic catalysts, were employed in order to find an effective catalyst for the direct synthesis of DMC as seen in Eq 2.2. Experiments conducted for DMC synthesis over ZrO₂ stated that the efficiency of the process highly depends on the presence of acid-base sites similar to cyclic carbonates synthesis discussed above. The basic sites of the catalyst were related to activating methanol and carbon dioxide to produce methoxy carbonate intermediate; a methyl group that reacts with the intermediate compound was formed by acidic sites of the catalyst from methanol (Tomishige et al., 2000).



Equation 2.2 The direct catalytic synthesis of DMC from methanol and CO₂

Furthermore, Jiang et al. (2003) highlighted the methyl formation on acidic sites of the catalyst as a rate-determining step, and thereby 12-tungstophosphoric acid was incorporated on the surface of the zirconium oxide to provide more acidity for the process. It was reported that $\text{H}_3\text{PW}_{12}\text{O}_{40}/\text{ZrO}_2$ showed better reactivity under milder conditions over ZrO_2 catalyst and about 2% yield was achieved by both catalysts. Later, Chiang et al. (2018) employed $\text{H}_3\text{PW}_{12}\text{O}_{40}/\text{ZrO}_2$ for the reaction and doubled the yield at elevated temperatures. Various other Zr-based heterogeneous catalysts for the direct synthesis of DMC from methanol and CO_2 were also studied, and the influence of both acid-base sites on the catalyst surface was highlighted. Using weak acidity is significant in the selectivity of DMC due to DMF (by-product) formation caused by strong acid sites (Jung & Bell, 2001; Tomishige et al., 2001).

An evaluation to compare ZrO_2 and CeO_2 for direct synthesis of DMC revealed that not only the reaction rate is affected, but also the reaction mechanism can change with the catalyst. The proposed mechanism over CeO_2 differs in intermediates formed during the reaction where carbomethoxide is formed on the surface of ceria by the reaction between methanol and adsorbed CO_2 rather than methyl carbonate formed by ZrO_2 (Chen et al., 2014). The reactivity of CeO_2 was assessed by Honda et al. (2013) but the DMC was lower than ZrO_2 . Although experiments using different Ce-based catalysts were performed to enhance the catalyst reactivity, the increase in the yield was limited and yet no more than 1% yield was achieved, this led to the conclusion that the route proposed for CeO_2 is less favourable than ZrO_2 (Kumar et al., 2021; N. Liu et al., 2023; S. Wang et al., 2013; J. Zhang, Huang, et al., 2021; J. Zhang, Zhao, et al., 2021).

Table 2.3 Heterogeneous catalysts employed for the two-step or direct synthesis of DMC

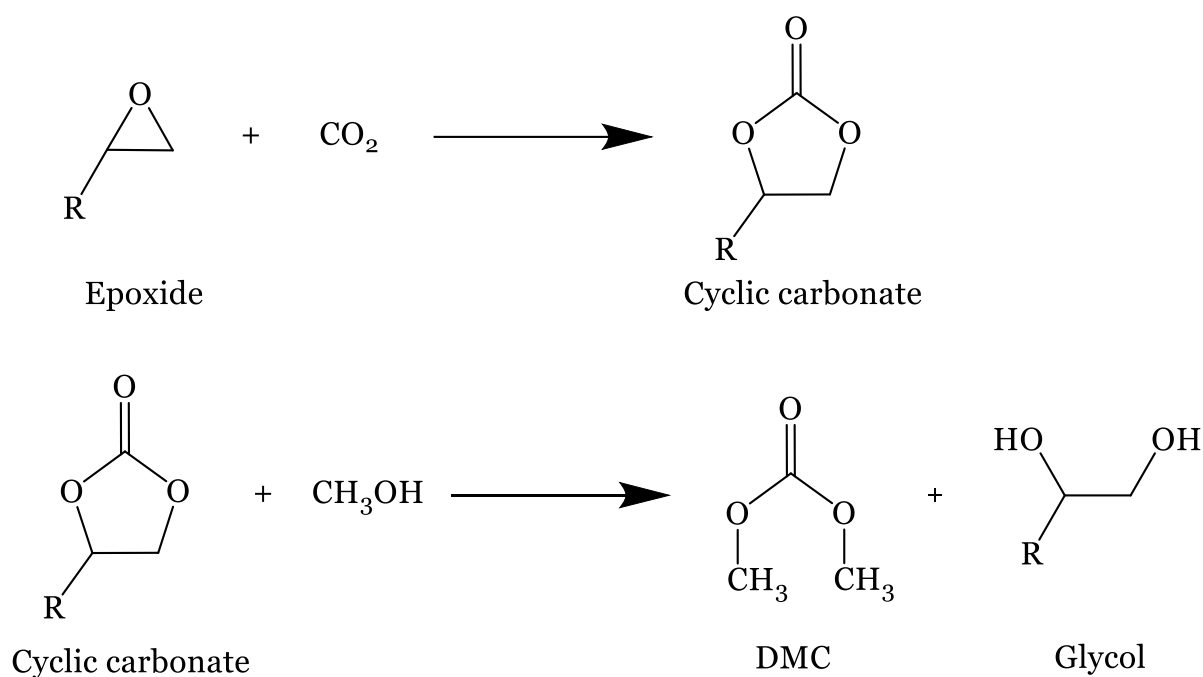
| Catalyst | Reactant | Yield (%) | Reference |
|---|------------------|------------------|--|
| Cu-Ni/AC | Methanol | 7 | (Bian, Xiao, Wang, Lu, et al., 2009a) |
| Cu-Ni/Graphite | Methanol | 9 | (Bian, Xiao, Wang, Wang, et al., 2009) |
| Cu-Ni/MWCNT | Methanol | 4 | (Bian, Xiao, Wang, Lu, et al., 2009b) |
| H₃PO₄/V₂O₅ | Methanol | 2 | (X. L. Wu et al., 2005) |
| H₃PW₁₂O₄₀/ZrO₂ | Methanol | 4 | (Chiang et al., 2018) |
| H₃PW₁₂O₄₀/ZrO₂ | Methanol | 2 | (Jiang et al., 2003) |
| ZrO₂ | Methanol | 2 | (Tomishige et al., 2000) |
| MnO₂/CeO₂ | Methanol | <1 | (Kumar et al., 2021) |
| CeO₂ | Methanol | <1 | (Honda et al., 2013) |
| MgO | Epoxide/methanol | 60 | (Bhanage et al., 2001) |
| Na₂WO₄·2H₂O | Epoxide/methanol | 80 | (Sankar et al., 2006) |
| CaO/C | EC/ methanol | 81 | (Wei et al., 2021) |
| Ca-Al LDHs | PC/ methanol | 60 | (Liao et al., 2018) |
| Co-CaO | PC/ methanol | 73 | (Huo et al., 2021) |

*MWCNT: Multi-walled carbon nanotubes; AC: Activated carbon; EC: Ethylene carbonate; PC: Propylene carbonate; LDHs: Layered double hydroxides

Furthermore, vanadium-based catalysts were tested for the reaction and a similar yield was obtained for $\text{H}_3\text{PO}_4/\text{V}_2\text{O}_5$ compared with CeO_2 . It was reported that weak Brønsted acid sites of the catalyst formed by the interaction between V and P are more influential than Lewis acid sites of V_2O_5 for the activation of methanol (X. L. Wu et al., 2005). Another vanadium-based supported bimetallic Cu-Ni catalyst was examined and a modest increase in the yield was received thanks to the synergetic effect of metallic copper and nickel along with the Cu-Ni alloy (X. L. Wu et al., 2006). This bimetallic Cu-Ni catalysts were then studied with different carbon-based support materials and a dramatic change in the yield was detected. The aforementioned synergetic effect was also observed for carbon-based supported Cu-Ni catalysts, which boosted DMC yield owing to enhanced MeOH and CO_2 activation. Lastly, the importance of active sites dispersion was evaluated by comparing these support materials and it was deduced that Cu-Ni/graphite had greater catalyst reactivity provided by the well-dispersion of metallic active species (Bian, Xiao, Wang, Lu, et al., 2009a, 2009b; Bian, Xiao, Wang, Wang, et al., 2009). However, recent developments in heterogeneous catalysis were unable to exceed 10% DMC yield from the direct synthesis using methanol and CO_2 due to the water produced from the reaction, requiring dehydrating agents to achieve a higher yield by eliminating water (Kohli et al., 2022).

Two-step DMC synthesis can be an alternative approach for avoiding these dehydration agents using epoxide, methanol and CO_2 Eq 2.3, but excess methanol is essential for moderate yield because of the unfavourable reaction occurring between methanol and alkylene carbonates (Chaemchuen et al., 2019; Tomishige et al., 2020). The first reaction in the process is broadly discussed in the previous section. The proposed mechanism for the second reaction occurs after activating methanol by basic sites of the catalysts to form CH_3O^- and H^+ . Afterwards, CH_3O^- attacks the carbonyl C atom of cyclic carbonates to form an intermediate which reacts with H^+ to produce a second intermediate. In the last step, the reaction between another CH_3O^- and the second intermediate happen to form DMC and the third intermediate of which produces glycol by the reaction H^+ (Liao et al., 2018). The mechanism explains the significance of basic sites on the catalyst, this was also confirmed by Huo et al. (2021) who investigated the effects of basic sites catalyst on DMC yield over Co-doped CaO. It was found that the more strong basic sites, the greater DMC yield was achieved owing

to better methanol activation. Hence, the DMC yield drastically changed and boosted from 10% to a minimum of 60% with this reaction pathway (Table 2.3).



Equation 2.3 The two-step dimethyl carbonate synthesis from epoxide, methanol and CO₂

Similarly, another Ca-based catalyst CaO on carbon support employed for the reaction and great reactivity was obtained thanks to basic site amounts and homogeneously dispersed active species on support material (Wei et al., 2021). Bhanage et al. (2001) investigated the reactivity of several metal oxide catalysts for the transesterification of cyclic carbonates to DMC by methanol and it was revealed that MgO achieved the highest methanol conversion thus the highest DMC yield. It was also reported that the yield was decreased from ethylene carbonate to propylene carbonate because of steric hindrance. Since MgO was found effective for the cyclic carbonate synthesis from epoxides and CO₂, it was then employed for two reactions in one-pot synthesis of DMC directly from epoxides, methanol and CO₂. Although the overall yield declined dramatically compared to the two-pot process, it was still significantly higher than one-pot synthesis from methanol and CO₂. Likewise, an assessment for the reactivity of tungsten-based heterogeneous catalysts was performed on both two-step and one-step DMC synthesis and great catalytic performance was detected for both routes (Sankar et al., 2006).

2.2.3. Methanol synthesis

Methanol is one of the commodity liquid petrochemicals, which is a primary raw material for several industries such as plastic, paints and antifreeze. It has also been widely used as an intermediate for the synthesis of various chemicals such as formaldehyde, acetic acid, methyl methacrylate, dimethyl terephthalate, methylamines and chloromethanes; and has directly been used in fuel cells and fuel additives (Álvarez et al., 2017; Jadhav et al., 2014). There are a number of methods and sources to produce methanol: coal, oil shale, agricultural products, wood and biomass. Today, it is mainly produced from a catalytical conversion of CO and H₂ along with a small amount of CO₂; however, the main drawback of the process is using highly toxic carbon monoxide. Although CO₂ has an excellent effect on increasing the efficiency of this traditional method, it can be used alone as a carbonyl source to produce methanol without using CO. Because CO is a toxic reactant, a new way for synthetic methanol production is a highly demanding challenge, so a search for reactive catalysts with high stability and low water inhibition is still an on-going task (Centi et al., 2013; Z. Jiang et al., 2010; Olah et al., 2009).

Many different reaction mechanisms have been proposed over the years and the most accepted one is the formate intermediated route (Zhong et al., 2020). In this pathway, activated CO₂ by Lewis acid sites of the catalyst reacts with adsorbed H⁺ to form formate (HCOO) which is then converted to methanol. The rate-determining step of this route was reported to be the activation of CO₂ and therefore, various heterogeneous catalysts were tested to find a reactive one for this step of the reaction (Ye et al., 2019). Copper-based catalysts were reported to be highly effective for the reaction as can be seen in Table 2.4. This was investigated by the use of Cu/Al₂O₃ and a relatively low methanol yield was obtained. Although the catalysts was doped with vanadium in order to enhance its performance, the effect of this functional group stayed limited (Y. Zhang et al., 2007). The reason for this relatively low yield could be explained by the formation of water as a by-product. Because the support material used in these catalysts was hydrophobic Al₂O₃, the presence of water negatively affected the catalyst performance. This shows that support material choice has a significant influence as much as active species for catalyst development.

Table 2.4 Heterogeneous catalysts employed for the hydrogenation of carbon dioxide for methanol formation

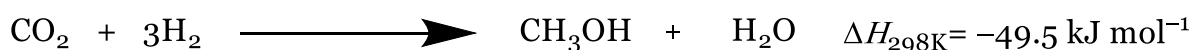
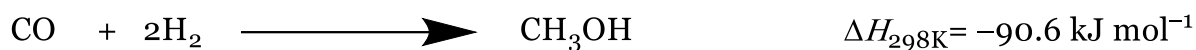
| Catalyst | T (K) | P (MPa) | Yield (%) | Reference |
|--|------------------|--------------------|----------------------|-----------------------------|
| CuO-ZnO/ZrO₂ | 473 | 2 | 8.7 | (Gallucci et al., 2004) |
| CuO-ZnO/ZrO₂ | 513 | 2 | 6.3 | (Hong et al., 2002) |
| CuO-ZnO/ZrO₂ | 513 | 3 | 9.6 | (Guo et al., 2009) |
| CuO-ZnO/ZrO₂ | 493 | 3 | 8.5 | (Guo et al., 2010) |
| Cu/Al₂O₃ | 513 | 3 | 3.0 | (Y. Zhang et al., 2007) |
| Cu/Zn/ZrO₂ | 513 | 4 | 12.5 | (X. An et al., 2007) |
| Cu/ZnO/ZrO₂ | 523 | 5 | 22.0 | (Saito & Murata, 2004) |
| Cu/SiO₂+ZnO/SiO₂ | 700 | 5 | 2.0 | (Y. Choi et al., 2001) |
| Cu/ZnO | 523 | 5 | 7.5 | (Fujitani & Nakamura, 2000) |
| Cu/ZnO/ZrO₂ | | | 14.0 | |
| Ag/ZnO/ZrO₂ | 493 | 8 | 1.9 | (Słoczyński et al., 2004) |
| Au/ZnO/ZrO₂ | | | 1.5 | |
| In₂O₃ | 603 | 4 | 2.8 | (K. Sun et al., 2015) |
| Pd-In₂O₃ | 573 | 5 | 14.0 | (Rui et al., 2017) |
| Ag/In₂O₃ | 573 | 5 | 8.0 | (K. Sun et al., 2022) |
| In₂O₃/ZrO₂ | 573 | 5 | 5.2 | (Martin et al., 2016) |

Alternatively, ZnO was used as a support material to prevent this negative impact of alumina and a considerable amount of improvement was detected in the yield (Fujitani & Nakamura, 2000). However, it is believed that this increase in the methanol yield occurred due to a different reaction pathway via syngas that was generated by the redox mechanism over metallic copper which was oxidised during the reaction by CO₂ to Cu⁺ to produce CO and then reduced back to Cu⁰ by H₂ (Roy et al., 2018). Similarly, Słoczyński et al. (2004) employed a number of different metals namely Cu, Ag and Au doped with ZnO on ZrO₂ that the catalyst with copper showed greater reactivity over others and Cu/ZnO by the addition of ZrO₂. This represents the impact of zirconium oxide support that exhibits Lewis acid Zr⁴⁺ sites and Lewis basic O²⁻ sites to activate CO₂ (Marcos et al., 2022). It was also reported that the reactivity of ZrO₂ highly depends on the crystal phases and it can be improved with the monoclinic phase as it provides stronger acid-basic sites compared to tetragonal and cubic phases (Marcos et al., 2019). Besides, the comparison work between metals assessed by Słoczyński et al. (2004) to evaluate the influence of active species on selectivity towards methanol revealed that the selectivity of copper over methanol was slightly lower than other metals even though the overall methanol yield was almost doubled for the presence of copper. This again confirms the parallel reaction pathway stated for Cu/ZnO catalyst.

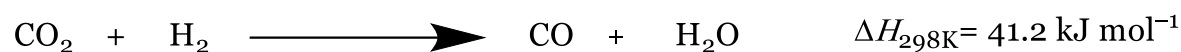
There are two reactions that occur in the CO₂ hydrogenation process, which are a synthesis of methanol and the reverse water-gas shift (RWGS) that produce methanol through syngas formed from CO₂ (Joo et al., 1999). Methanol synthesis from CO is more favourable than CO₂ as seen in Eq 2.4, thus metallic copper-based catalysts that promote syngas production from CO₂ had better yields at higher temperatures (Zhong et al., 2020). Also, higher temperatures promote endothermic RWGS reactions for the hydrogenation of CO₂ and hence the selectivity for methanol declined at elevated temperatures, especially for metallic copper catalysts discussed (X. Jiang et al., 2020). Similarly, iron-based catalysts known to be active for the RWGS route had limited use for methanol synthesis from CO₂ owing to the very low selectivity (Garba et al., 2021). It was reported that Fe₂O₃ also follows the same route as Cu and activates CO₂ by a redox reaction mechanism that oxidise to Fe₃O₄ at higher temperatures (Galvita et al., 2013) Although some metal oxide additives were monitored to improve its stability as

well as reactivity, the selectivity of Fe₂O₃ for methanol remained inadequate (Hakeem et al., 2015; Keturakis et al., 2016).

Methanol synthesis



Reverse water-gas-shift reaction (RWGS)



Equation 2.4 Reactions occurs in the hydrogenation of CO₂ and reactions produce methanol

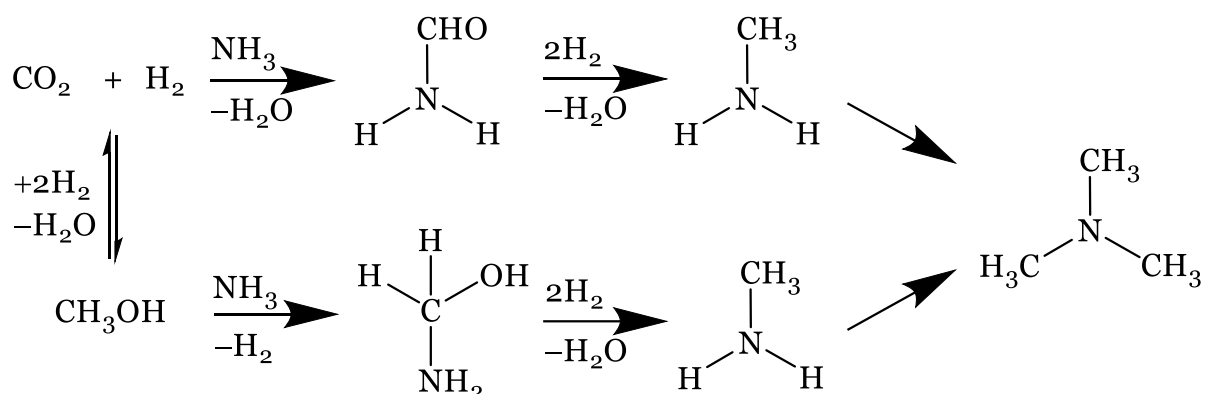
Numerous studies have been conducted using CuO as active species to prevent oxidation of metallic copper during the reaction, thereby avoiding syngas synthesis from the hydrogenation of CO₂. In that direction, CuO-ZnO/ZrO₂ was employed for formate intermediated methanol synthesis and a significant increase in the selectivity for methanol was observed thanks to the influence of finely dispersed CuO species (Guo et al., 2010). A modest growth in the yield was obtained with increasing reaction temperature as a consequence of better CO₂ activation whereas a restricted decline was monitored on methanol selectivity as higher temperatures favour RWGS reaction (Guo et al., 2009).

Indium-based catalysts that also follow the formate pathway for methanol synthesis drew attention in late research as they showed substantially effective performance for the reaction (Ye et al., 2019). They showed not only greater reactivity for the hydrogenation of CO₂ but also better stabilisation for intermediates like H₂COO and H₂CO that copper-based catalysts were unable to do so, which allowed the opportunity to trace more favourable reaction routes (Dang et al., 2019). This highlights another important factor that needs to be considered for catalyst design to achieve superior selectivity. Results gained from the experiments using In-based catalysts have shown that the yield remained relatively low for bulk In₂O₃ whilst it can be improved rapidly

with the synergistic effect provided by functional additions (K. Sun et al., 2015). A dramatic increase in the yield was gained over Ag-doped catalysts whilst it was boosted to a yield as much as RWGS by the presence of Pd (Rui et al., 2017; K. Sun et al., 2022). In addition, the use of In-based catalysts eliminated the promotion of RWGS at higher temperatures reported for copper-based catalysts and thus almost 100% methanol selectivity was achieved even above 573 K (Martin et al., 2016).

2.2.4. Methylamines synthesis

Methylamines are valuable compounds with an annual production of over 800,000 tonnes to be used in pesticides, solvents and water treatment. Monomethylamine (MMA), dimethylamines (DMA), and trimethylamines (TMA) are the most common types of methylamines that have applications as intermediates to synthesise several chemicals such as N-methyl pyrrolidone, alkylalkanolamines, dimethylformamide and dimethylacetamide. In industry, they are mainly produced from the exothermic reaction of methanol and ammonia using solid acid catalysts at 390-430°C and 20 atm (Corbin et al., 1997; S. V. Gredig et al., 1997). Since MMA and DMA are more desired products of methylamines on the market and TMA is more favoured due to the thermodynamic equilibrium, research on developing more selective catalysts over MMA and DMA has been focused on. Although several efficient methods for methylamines synthesis from CO and H₂ through the formation of methanol as an intermediate have been developed, using toxic carbon monoxide is limited their use in commercial production. Consequently, the synthesis of methylamines from CO₂ and NH₃ by adding H₂ has the potential to address problems faced in the conventional approach. Thus, new efforts are needed to develop non-expensive, highly selective, demanding products and stable catalysts to create environmentally friendly and sustainable processes (S. V Gredig et al., 1995; S. V Gredig, Maurer, et al., 1997).



Equation 2.5 Proposed reaction pathways for methylamine synthesis adapted from S. Liu et al. (2022)

The synthesis of methylamines such as monomethylamine (MMA), dimethylamine (DMA) and trimethylamine (TMA) prepared by the reaction of ammonia, hydrogen and CO₂ through the catalytic route has been studied as a carbon utilization method (Corbin et al., 1997). Several supported metal catalysts have been examined for methylamine synthesis, and copper, nickel, cobalt and palladium have been found to be reactive metals given in Table 2.5 (S. V. Gredig et al., 1997). Copper-based catalysts can assist the catalytic activity of methylamine synthesis thanks to the acidity and basicity of the catalyst surface (S. V Gredig, Maurer, et al., 1997). On the other hand, S. V. Gredig, Koepfel, & Baiker (1997) concluded that ammonia and methylamines are effectively adsorbed on the catalysts thanks to their Brønsted and Lewis acid sites. Although MMA and DMA are commercially in-demand products, the highlighted process favours TMA synthesis from NH₃, H₂ and CO₂. Thus, catalysts chosen for the synthesis of methylamines should be selected for either MMA or DMA. The group also examined copper-based alumina supported as a heterogeneous catalyst for MMA synthesis, which was achieved from CO₂, H₂ and NH₃ using the copper-based catalyst with high selectivity. Although a combination of this route on existing ammonia plants could provide new opportunities, the synthesis of methylamines through this pathway appears to be impracticable because of the very low yield (Artz et al., 2018).

Table 2.5 Heterogeneous catalysts used for methylamines synthesis from CO₂, H₂ and NH₃ at 570 K and 0.6 MPa

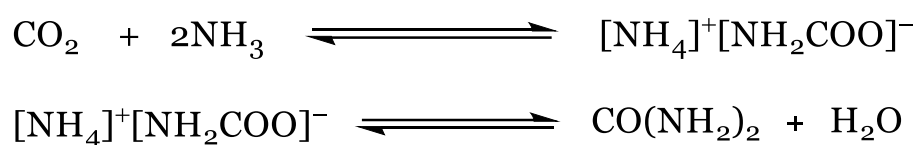
| Catalyst | MMA yield (mol%) | DMA yield (mol%) | TMA yield (mol%) | Reference |
|---------------------------------------|---------------------------------|---------------------------------|---------------------------------|--------------------------------------|
| Cu/Al₂O₃ | 0.9 | 0.2 | 0.1 | (S. V Gredig et al., 1995) |
| Cu/Cr₂O₃ | 0.7 | 0.1 | 0.05 | (S. V Gredig, Maurer, et al., 1997) |
| Cu/ZrO₂ | 0.55 | 0.06 | 0.03 | |
| Cu-Mg-Al/LDH | 0.8 | 0.1 | 0.05 | (Auer et al., 1999) |
| Fe/Al₂O₃ | 0.07 | 0.02 | 0.01 | (S. V Gredig, Koepfel, et al., 1997) |
| HMOR20 | ~20 | ~20 | ~50 | (Gründling et al., 1996) |
| HMOR20-M | ~30 | ~50 | ~4 | |

*LDH: Layered double hydroxides; HMOR20: (Mordenite) Zeolite-based catalysts

On the other hand, a different reaction route to produce methylamines from methanol and NH₃ was proposed, which has been seen as a promising option in terms of the green chemistry aspect as it can be synthesized with greater yields (Artz et al., 2018). Also, the aforementioned developments on catalysis for the hydrogenation of CO₂ into methanol indicate that this route could be an alternative for CCU. In this matter, mordenites were employed for the reaction and a dramatic increase was observed for all types of methylamines compared to the other reaction routes thanks to high adsorption capacities provided by Brønsted acid sites. In addition, it was reported that the selectivity of desired methylamines can be controlled by the modifications that can be made on these mordenites. It was stated that catalysts with narrow pores promote low-substituted methylamines like MMA and DMA (Gründling et al., 1996). However, studies on this route remained limited and more catalytic developments are required for commercial applications.

2.2.5. Urea and its derivatives synthesis

Urea, a di-amine of carbonic acid, is a significant type of bioactive organic compound that is widely used in several industries such as plastic, pesticides, pharmaceuticals and fertilisers thanks to being relatively cheap, colourless and odourless. The process known as Bosch-Meiser, which was developed in 1922 to synthesise urea, is still being used to produce it today. The annual production is about 180 Mt and could reach 200 Mt by 2030 (Aresta et al., 2017; IEA, 2021). Urea is produced from synthetic ammonia and carbon dioxide without using any catalysts, and the process occurs through two equilibrium reactions: an exothermic reaction between CO₂ and ammonia at 150–250 °C and 5-25MPa to form ammonium carbamate; and then it is dehydrated to urea driven by the heat recovered from the first reaction, which is the rate-determining step (Eq 2.6). The overall reaction is exothermic, and the conversion of CO₂ to ammonium carbamate could yield up to 78%. Among chemicals produced by CO₂ utilization, urea has the most prominent conversion application with the use of 130 Mt/y CO₂ (Alper & Yuksel Orhan, 2017; Aresta et al., 2014).



Equation 2.6 Urea synthesis from CO₂ and NH₃ via Bosch-Meiser urea process

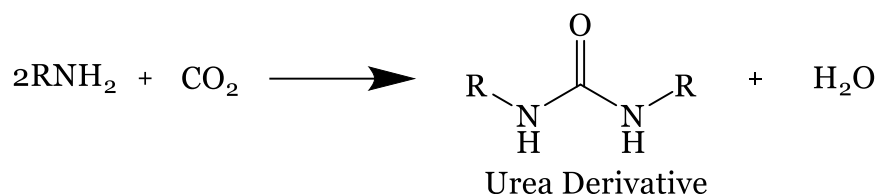
Having a carbonyl group in the structure of urea promotes research for the synthesis using different chemicals with carbonyl groups. Although countless R&D effort has been carried out to obtain it using phosgene, isocyanates, carbon monoxides or carbon dioxide since the middle of the 20th century, a new method is still necessary to make the process more sustainable and environment-friendly due to the toxicity of these chemicals under milder reaction conditions (H. Wang et al., 2018). Not only has there been an increase in demand for urea to be used as a fertilizer, but also the development of new applications in polymer synthesis as intermediates or monomers raises the price of urea. Moreover, the market price of urea is primarily reliant on natural gas prices in order that ammonia, based on the Haber process, is produced by the reaction of nitrogen and hydrogen over iron-based catalysts at 400-500 °C and 150-300 atm with a conversion rate as low as 10-15%. Therefore, alternatives for ammonia and new

catalytic approaches for CO₂ utilization are required to produce urea at lower temperatures and pressures (Srinivas et al., 2012).

A number of papers had been reviewed by Ragaini & Cenini (1996) for catalytically producing urea using different reactants, and it was found that palladium-based catalysts had relatively greater reactivity over others even though the catalyst had some drawbacks in terms of stability and the high prices of the metal. The catalyst, which has Pd as an active metal either with or without co-metal species, was partially leached in the reaction system. The homogeneous species formed due to the leaching of catalysts lower the conversion rate and make product separation more difficult. It was also noted that Pd catalysts doped with active metals such as Cu, Zn, Ni, Ru, Fe and V are highly corrosive against steels, which caused the deposition of Pd on the wall of autoclaves. Furthermore, Barzagli, Mani, & Peruzzin (2011) examined several catalysts that have different active metals such as Cu, Zn, Ni, Ru, Mn and Fe and their oxides and salts for the synthesis of urea from the solid mixture obtained by CO₂ capture with ammonia as a promising solution for the energy penalties faced in the regeneration step of carbon capture facilities. It has been reported that copper-based catalysts had a higher conversion rate even under milder reaction conditions than the conventional urea synthesis, as well as other catalytic conversions. However, the stability of catalysts was shallow owing to the formation of metal-ammonia complexes, making product separation and catalyst recycling more difficult.

The synthesis of urea derivatives from amines has also been of interest in terms of utilizing CO₂ after the first synthesis of urea from ammonia and CO₂ by Bazarov in 1870 (H. Wang et al., 2018). Since urea derivatives have several usages in pesticides, polymer, chemistry and pharmaceuticals manufacturing, much effort has been placed into producing them using carbon monoxide, urea, phosgene, carbonates or carbamates, as well as direct carbonylation reaction between amines and CO₂ (Eq 2.7) (H. Wang et al., 2017). Recently, a considerable amount of concentration has been given to the development of new methods with non-toxicity, efficiency and environment-friendly for the synthesis of urea derivatives owing to the increase in the significance of these chemicals thanks to the discovery of the use of these substituted ureas for cancer and HIV treatments (Ghosh & Brindisi, 2020). Nevertheless, there is no well-established commercial process for urea derivatives; the lack of reactive, stable

and inexpensive catalysts was proposed as the main reason for that. Thus, research on developing new cost-effective catalytic routes is still an ongoing process (H. Wang et al., 2017).



Equation 2.7 Urea derivatives synthesis from the reaction of amines with CO₂

Urea derivatives are produced from CO₂ and amines via SN₂ nucleophilic substitution reactions. There are two common mechanisms for aliphatic nucleophilic substitution reactions: SN₂ (substitution nucleophilic bimolecular) and SN₁ (substitution nucleophilic unimolecular). SN₂ mechanisms occur in one step where the nucleophile approaches the substrate to form a transition state and then the bond between the leaving group and carbon is broken while the bond between nucleophile and carbon is formed, simultaneously. On the other hand, the SN₁ mechanism is stepwise: the first (slow) reaction involves the ionisation of the substrate to form carbocation; the second (fast) reaction between the carbocation and the nucleophile to form the product. The mechanism of reactions can be controlled by the polarity of the solvent used in the reaction. Polar protic solvents like water and alcohols promote the SN₁ mechanism whereas SN₂ mechanism is promoted by the presence of polar aprotic solvents such as acetone, DMSO and DMF (Hart et al., 2007; Smith & March, 2006).

Alkali metals, their carbonates and salts were first used as catalysts (Table 2.6) for the synthesis of 1,3-disubstituted urea (DSU) from 2-heptylamine/n-butylamine and CO₂, and the highest yield was obtained by using Cs-based catalysts (Ion et al., 2007). Similarly, C. Wu et al. (2010) employed Cs-based catalysts for DSU synthesis using butylamine and CO₂ but lesser yield was obtained because base compounds were used as a co-catalyst by Ion et al. (2007). More recent studies conducted using Cs-based catalysts showed that salts of this active metal have better reactivity (Truong et al., 2017, 2020) Alternatively, the synthesis of DSU was driven by polymer-immobilised nanogold catalysts with great reactivity thanks to the acid-base sites of the catalyst. The study pointed out that basic sites are more influential than acidic active sites and it was

also reported that the size of the nanogold particles had more influence on catalyst performance than the loading of active species (Shi et al., 2005). The carboxylation of amines by CO₂ in the presence of K₃PO₄ was also conducted to form corresponding 1,3-dialkylureas in the presence of NMP and the rise in the yield was attributed to the basicity of the catalyst (Y.-S. Choi et al., 2014). In addition, Zhang et al. (2013) prepared Mg-Al-based bimetallic layered double hydroxide catalysts that provide weak and moderate basic sites to promote the reaction. The effect of the support material was also highlighted and LDH with a high CO₂ adsorption capacity also played a key role in the reactivity of the catalyst.

Late studies have shown that metal oxides are highly effective catalysts for the conversion of CO₂ into various chemicals, thereby their reactivity in urea derivatives synthesis was assessed broadly. D.-L. Sun et al. (2016) conducted experiments over Y₂O₃ and a moderate yield was obtained in a relatively long reaction time. The catalyst was then modified with oxalate to increase its reactivity, which enabled to elevate the yield but was not as successful as the efficiency in shortening the reaction time. Following, the same group employed Y₂O₃-ZrO₂ mixed oxide catalyst for the process and revealed the synergetic effect of the catalyst which generated more yield than each metal oxides individually. It is believed that this was achieved by the dispersion of Y₂O₃ in ZrO₂ framework, resulting in an improvement of CO₂ adsorption and activation by active oxygen sites. However, the yield obtained from the reaction was lesser than yttrium oxalate complexes even though a dehydrating agent was used to remove the water from the system in order to shift the direction of the reaction into the product's side (D. Sun et al., 2018).

Table 2.6 Catalysts used for the synthesis of urea derivatives from different amines

| Catalyst | Reactant | Urea Derivative | Yield (%) | Reference |
|---|-----------------|------------------------|------------------|--------------------------|
| CuCl₂ | Propylamine | 1,3-dipropylurea | 60 | (Casiello et al., 2015) |
| CeO₂ | Butylamine | 1,3-dibutylurea | 72 | (Tamura et al., 2016) |
| ZnO | | | 41 | |
| Y₂O₃ | Butylamine | 1,3-dibutylurea | 43 | (D.-L. Sun et al., 2016) |
| Y₂O₃-ZrO₂ | Butylamine | 1,3-dibutylurea | 58 | (D. Sun et al., 2018) |
| MnO₂ | Butylamine | 1,3-dibutylurea | 43 | (D. Sun et al., 2021) |
| ZnO/KF/Al₂O₃ | Butylamine | 1,3-dibutylurea | 65 | (Kulal et al., 2020) |
| Sn-Ni-O | Butylamine | 1,3-dibutylurea | 76 | (Kulal et al., 2021) |
| Cs₂CO₃ | Butylamine | 1,3-dibutylurea | 55 | (C. Wu et al., 2010) |
| CuCl₂.2H₂O | Butylamine | 1,3-dibutylurea | 39 | (Barzagli et al., 2016) |
| K₂PdI₄ | Butylamine | 1,3-dibutylurea | 97 | (Ca' et al., 2011) |

| | | | | |
|--|-----------------|----------------------|----|---------------------------|
| K₃PO₄ | Butylamine | 1,3-dibutylurea | 62 | (Y.-S. Choi et al., 2014) |
| KHCO₃/ KH₂PO₄ | | | 65 | |
| Mg-Al/LDH | Butylamine | 1,3-dibutylurea | 66 | (R. Zhang et al., 2013) |
| PdI₂ | Butylamine | 1,3-dibutylurea | 46 | (Gabriele et al., 2004) |
| Ph₃SbO/P₄S₁₀ | Butylamine | 1,3-dibutylurea | 88 | (Nomura et al., 1992) |
| InI₃ | Cyclohexylamine | 1,3-dicyclohexylurea | 39 | (Son et al., 2018) |
| RuCl₃·3H₂O/ n-Bu₂P | Cyclohexylamine | 1,3-dicyclohexylurea | 61 | (Fournier et al., 1991) |
| Cu-Fe-ZrO₂ | Aniline | 1,3-diphenylurea | 3 | (H. An et al., 2014) |
| CeO₂ | Ethylenediamine | Ethylene urea | 96 | (Tamura et al., 2013) |
| CeO₂-np | Ethylenediamine | Ethylene urea | 37 | (Primo et al., 2013) |
| KOH/PEG1000 | Ethylenediamine | Ethylene urea | 82 | (Tamura et al., 2014) |

*LDH: Layered double hydroxides, np: nanoparticles, PEG: polyethylene glycol

Moreover, Mn-based catalysts were broadly assessed as a catalyst for the reaction and showed greater reactivity over yttrium-based catalysts in the absence of any dehydrating agents owing to the basicity of O^{2-} on the surface of the catalyst. It was also reported that the crystal structure of the catalyst can affect the basicity drastically (D. Sun et al., 2021). The basicity of the catalyst can also be improved by the modification with alkali metals and hence the reactivity can be boosted by the presence of richer acid-base sites (D. Sun et al., 2022). Later, the effect of oxidation states for the metal was examined by D. Sun et al. (2023) over different metal oxides of manganese and MnO_2 and Mn_3O_4 showed greater activity among others, this signifies the impact of oxidation states on active acid-base sites and the reactivity of catalysts. As an alternative, the carbonylation of several alkylamines by CO_2 was examined to their corresponding urea derivatives using various catalysts. Ce-based catalysts, other than catalysts tested in the study like ZnO , ZrO_2 , MgO and TiO_2 , had superior reactivity for the synthesis of 1,3-dibutylurea (DBU) from n-butylamine and CO_2 using NMP as a solvent. It was also reported that the combination of CeO_2 and NMP had a synergetic effect and exhibited a dramatic increase in reactivity compared to individual use of them (Tamura et al., 2016).

After seeing the synergetic effect of mixed oxides catalysts on Y_2O_3 - ZrO_2 , different metal oxides were used together as a catalyst for the reaction. $ZnO/KF/Al_2O_3$ was employed by Kulal et al. (2020) and a yield similar to Mn-based catalysts was obtained in shorter reaction times. Additionally, it was concluded that acid-base sites play a key role in reactivity and they can be controlled by the concentration of ZnO and KF on the support material. The study also showed the effect of calcination temperature on the number of active sites. The reactivity of another mixed oxide catalyst, Sn-Ni-On, was investigated and the enhanced yield was attributed to the better distribution of active species on NiO. TPD analysis conducted on the prepared catalyst provided evidence that weak and moderate acid-base sites had more influence than stronger sites (Kulal et al., 2021).

Different types of urea derivatives like cyclic ureas, other than disubstituted alkylureas, can also be produced using the same approach where the reaction between diamines and CO_2 was catalysed by Ph_3SbO . Although the catalyst was moderately active for the carbonylation reaction, it was reported that the modified catalyst Ph_3SbO/P_4S_{10} had a

better catalytic performance at 80-150 °C. The group also synthesised alkyl ureas using the modified catalyst: trisubstituted from the co-carbonylation of butylamine and diethylamine at 80 °C; 1,3-dibutylurea at 120 °C. It was concluded that reaction temperature has a serious impact on the selectivity of the process where lower temperatures favour the trisubstituted urea whilst higher ones assist the formation of disubstituted urea (Nomura et al., 1992). Furthermore, the synthesis of 1,3-diphenylurea (DPU) from aniline and CO₂ was studied over mixed oxide catalysts using acetonitrile as a solvent. Among the number of different support materials such as SiO₂, MgO and Al₂O₃ tested in the study, the catalyst with ZrO₂ had greater reactivity due to the acid-base sites. Lewis acid Zrⁿ⁺ and Lewis base Zr-O⁻ sites were the active sites for the activation of CO₂ and aniline, respectively. However, no reactivity was detected with the lack of copper in any prepared catalyst. Metallic copper and CuO were the main active species on the catalyst while metallic iron and Fe₂O₃ acted as promoters for the catalyst (H. An et al., 2014).

A new method was highlighted for synthesising DSU from the decomposition of solid amine carbamates produced by the capture of CO₂ in non-aqueous amine solutions without using any catalysts. Because the reaction time was comparatively long, copper-based catalysts were employed in the thermal conversion of amine carbamates in order to decrease the heating time. It was discovered that the catalyst lowered the reaction time to one-third as well as increased the yield. Difficulties arose, on the other hand, including the leaching problem, as stated in their previous studies as still being one major drawback of the use of copper-based catalysts (Barzagli et al., 2016). All the studies reviewed so far, however, suffer from a number of limitations in terms of either using a rare and expensive catalyst with low stability or cost-intensive and inefficient processes in order for the use of co-catalyst or dehydrating agents under challenging reaction conditions. Thus, further developments for reactive heterogeneous catalysts without requiring to these additional agents would enable to provide promising approaches for urea derivatives synthesis from CO₂ under milder conditions (H. Wang et al., 2017).

2.3. Core-shell catalysts

One of the main challenges in catalysis, maintaining the active phase stability of catalysts, can be addressed by lately developed production methods. In this perspective, the preparation of catalysts in the form of a core-shell structure that the active phase encapsulated with a porous and more stable material can be a groundbreaking approach for catalyst stability. Additionally, a distinguished improvement in reactivity is also observed as a consequence of the interaction resulting from the presence of multiple species (Q. Zhang et al., 2013). These noticeable properties in stability, reactivity, adsorption capacity as well as the possibility of adaptation to biomaterials enable such nanomaterials to be used in broad areas such as energy storage, bio-medical engineering and mostly catalysis. There are endless possibilities for the catalysts produced in this structure that are mainly manufactured using several components: organic materials like polymer, carbon nanotubes and graphene; inorganic materials like metal and metal oxides; and their combinations (Das et al., 2020; Knežević et al., 2013).

Core-shell catalysts employed in a number of different processes provide numerous advantages in terms of activity and stability. R. Shi et al. (2018) used carbon-encapsulated copper nanoparticles for oxidative carboxylation of methanol to DMC and achieved greater yield over commercial CuCl catalysts. It was also reported that carbon shell used over Cu particles considerably prevented the aggregation and leaching of copper nanoparticles. Similarly, the performance of functionalised core-shell Fe₂O₃ nanospheres as shell components for active Pd(o) species were assessed in Sonogashira and Heck coupling reactions and superior reactivity was observed thanks to the synergetic effect of different species in the catalyst. The core-shell structure also enabled the catalyst to be used several times with a slight loss of activity and negligible Pd leaching (Sadjadi et al., 2018). It was also stated that the encapsulation of active species with an effective shell material could bring new benefits to the catalyst of which cerium oxide encapsulated Ni-SiO₂ showed improved activity owing to high redox potential and oxygen capacity provided by CeO₂ shell. The stability of the catalyst was also dramatically enhanced against the coke formation under harsh conditions of syngas dry reforming, which makes it possible to be used for 72 hours compared to 22 hours of use of the catalyst without coatings (Das et al., 2018).

Although different materials are used, silica has attracted more attention as a shell due to the ease of production, cost-effectiveness, high thermal stability and being highly resistance against agglomeration (Das et al., 2020). The investigation on the catalytic activity of mesoporous silica encapsulated Pt for ethylene hydrogenation and CO oxidation confirmed that similar reactivity can be obtained as metal platinum with limited deactivation and aggregation. It was also deduced from the study that Pt@m-SiO₂ showed superior thermal stability up to 750 °C where Pt would struggle to handle without any coating (S. H. Joo et al., 2009). In addition, bimetallic Fe-Cu alloy highly active catalyst for the ozonation of salicylic acid was coated with silica shell and a considerable amount of increase in the catalyst reactivity with negligible metal leaching was observed thanks to the synergetic effect of alloy core and silica shell (W. Chen et al., 2019). Likewise, the stability of cobalt and gold-based catalysts was improved against thermal sintering by the presence of silica shell in different processes. Co@SiO₂ escalated the selectivity for methanol from the hydrogenation of CO/CO₂ compared with bulk cobalt (Ilsemann et al., 2019). The reactivity of gold-based catalysts was raised with high surface area and porosity of silica for CO oxidation (Sekhar et al., 2013). Differently, a polymeric ionic liquid was surrounded by stable silica shell formations and this provided an opportunity to recycle the ionic liquid without complicated separation processes. This structure, besides from advancements in metal and metal oxide-based catalysts, has created a novel path for the development of heterogeneous ionic liquids (S. Liu, Su, et al., 2022).

In addition to its outstanding performance in different applications, silica-coated core-shell catalysts were also employed in the conversion of CO₂. Firstly, methanol synthesis from the hydrogenation of CO₂ was examined over core-shell catalysts and enhanced reactivity was reported for both Cu/ZnO@m-SiO₂ and Cu-Zn@m-SiO₂, more importantly, excellent resistance to sintering problem (Kosari et al., 2021; H. Yang et al., 2016). Furthermore, the structure was used for CO₂ methanation over NiO-MgO@SiO₂ core-shell catalyst and great reactivity and selectivity were obtained. This catalytic activity was attributed to the high dispersion of Ni nanoparticles and avoiding NiO and MgO reduction provided by the silica shell. It was also revealed that the core-shell catalyst used for the reaction showed stable performance for 100 hours at low temperatures around 300 °C (Li et al., 2014). Additionally, core-shell catalysts were tested for cyclic carbonates synthesis from CO₂ by Cu(III) salen functionalised

$\text{Fe}_3\text{O}_4@\text{SiO}_2$ catalyst which showed superior catalytic activity and selectivity over cyclic carbonates with ease of separation and reusability over 5 times without any reactivity loss (Min et al., 2021).

Silica that showed outstanding performance as a shell species in core-shell catalysts in terms of catalytic activity and stability for CO_2 conversion reactions and others, is generally produced using the Stöber method (Stöber et al., 1968). In this method, silica nanospheres were manufactured by the hydrolysis of silica precursor TEOS over ammonium hydroxide catalyst. In order to encapsulate active core species, a surfactant-templating sol-gel method is widely used for the preparation of silica-covered core-shell catalysts (Du et al., 2017; C. Sun et al., 2018). However, it was reported that it is relatively hard to adjust the pore size and shell thickness with these routes. Identically, El-Nahhal et al. (2016) used CTAB surfactant as a template and prepared core-shell catalysts with around 15 nm silica shell formations using NH_3 assisted sol-gel method whilst X. Wang et al. (2017) prepared silica nanosheets with the assistance of ethyl acetate. It is known that shell thickness is vital to prepare reactive catalysts with high stability (Tian et al., 2022). Thus, a surfactant-templating & ethyl acetate-assisted sol-gel method which is the combination of these two routes by El-Nahhal et al. (2016) and X. Wang et al. (2017), was proposed herein as a solution for the preparation of silica encapsulated core-shell catalysts that highly reactive and stable enough to prevent leaching of active core species into reaction media.

2.4. Summary of literature review

Recent advances in catalysis reveal that CO_2 that is known to be a highly stable compound can be used as a reactant for the synthesis of marketable compounds, enabling CO_2 utilisation to control CO_2 emissions when it is employed together with carbon capture and storage technologies. For CO_2 conversion reactions, heterogeneous catalysts draw great attention owing to the ease of separation and reusability, and they showed comparable reactivities as to their homogeneous counterparts thanks to the developments of novel catalyst designs discussed in this chapter. Concerning, it has been seen that urea derivatives synthesis as an alternative pathway for CO_2 utilisation is now possible over heterogeneous catalysts by the carboxylation of amines to eliminate the use of toxic phosgene or carbon monoxide for the process. This route;

however, highly relies on expensive and rare-earth elements as a catalyst such as cerium, yttrium and ruthenium. Unlike these rare metal-based catalysts, more abundant catalysts like alkali metals or alumina and magnesium-based catalysts are still required the use of base co-catalysts or dehydrating agents to enhance the disubstituted urea yield. Although copper and zinc-based catalysts were reported to be highly reactive for the reaction, their use remained limited due to the leaching of catalysts into the reaction media. Therefore, it is essential to find cost-effective, reactive and especially stable catalysts that do not need any promoters like co-catalyst or dehydrating agents for urea derivatives synthesis from CO₂ and amines (H. Wang et al., 2017).

In this perspective, iron-based catalysts proven their stability and reactivity in the Fischer-Tropsch process, may be a promising candidate as a catalyst for urea derivatives synthesis. (H. An et al., 2014) investigated the effect of iron-modified heterogeneous catalysts and reported that both Fe and Fe₂O₃ had a critical promoting influence on the catalysts. Nonetheless, the reactivity of iron-based catalysts has not been yet assessed broadly for the process. Thus their catalytic performances need to be investigated without the use of any co-catalyst or dehydrating agents. Likewise, copper-based catalysts that are widely used in methanol synthesis from the dehydrogenation of CO₂, have not been employed for urea derivatives synthesis because of the leaching detected. A novel catalyst design, core-shell structure, revealed that the stability of active species can be protected by inert shell formation. Silica-encapsulated core-shell catalysts in particular showed superior performance in preventing leaching and sintering as well as reactivity improvements by having high surface area. Thus, the implementation of this design could address the leaching problem that has been reported for copper-based catalysts and provide a promising and cost-effective catalyst with good stability and reactivity for urea derivatives synthesis.

Chapter 3: Materials and Methodology

3.1. Materials

Copper (II) oxide, copper, copper (I) oxide copper (II) sulphate anhydrous, methanol, DMF, nitric acid, pyridine, urea, silica and zinc nitrate hexahydrate, ethanol, hexanol, 2-propanol, DMSO, aniline, THF, pyridine, ethyl acetate, Pluronic P123, CTAB, TEOS, ethanolamine were purchased from Sigma-Aldrich (UK); CO₂, helium, argon and acetylene were supplied from BOC (UK) with a GC grade; ammonia solution, iron oxides and zinc oxide were purchased from Fisher Scientific (UK), and copper (II) nitrate trihydrate, NMP, methylamine, ethylamine, butylamine, cyclohexylamine, dimethylamine, diethylamine, N,N-dimethylurea, N,N-diethylurea, N,N-dibutylurea, N,N-dicyclohexylurea, N,N-diphenylurea, tetramethylurea and tetraethylurea were supplied from Acros-Organics (UK). All the chemicals were used as they were received.

3.2. Experimental method

3.2.1 Set-up

A stainless-steel high-pressure reactor with a volume of 45 ml was employed for the catalytic synthesis of urea derivatives from the reaction of CO₂ with different amines in organic solvents over various metal oxide catalysts (Figure 3.1). The reactor manufactured by Parr Instruments (Model 4714) comprises a pressure relief system to protect it from overpressure to be operated up to 100 bar. Despite the high equipment limit, the reactor loaded with a maximum of 50 bar CO₂ and a maximum 80 bar was observed during the reaction. The reaction is stirred by a magnetic stirrer and heated using a stainless-steel jacket placed on a heating plate with adjustable temperature and stirring speed. CO₂ was loaded from a gas cylinder at the inlet valve of the reactor and the connection line was checked to avoid any gas leakage. All the reactions were performed in a fume cupboard because of the safety considerations.

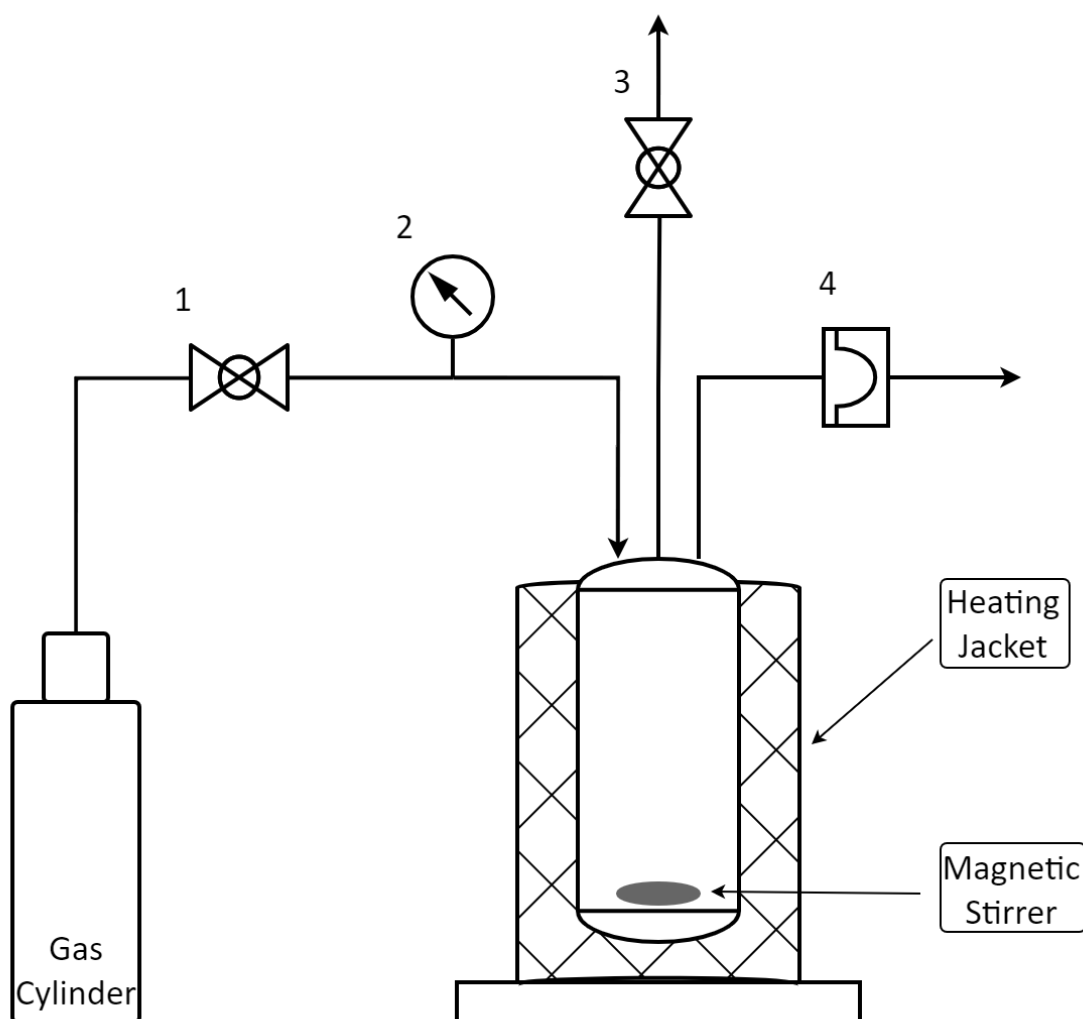


Figure 3.1 The diagram of setup used for the synthesis of urea derivatives from CO₂ and amines (1: Inlet valve; 2: Pressure gauge; 3: Outlet valve; 4: Pressure relief valve)

The procedure of the CO₂ conversion into urea derivatives was performed using the reactor loaded with 10-80 mmol of various amines as a liquid, 1-4 mmol of catalysts and 1-8 ml of several organic solvents. The reactor was then purged twice with CO₂ by loading the reactor with 10 bar of CO₂ and depressurised to eliminate the air trapped in the reactor. After that, the reactor was pressurised with the desired amount of CO₂ which is 5-50 bar. Later, the reactor was placed on the heater set to the desired temperature, and it was stirred when the temperature was reached. It was then left to run for the preferred time, the system was stopped, placed in an ice bath to cool down and depressurised slowly in the fume cupboard. The pressure changes before and after the cooling step were recorded. Catalysts used in the reaction were separated by grade

1 filter paper placed in a Buchner funnel situated on the Buchner flask to collect liquid samples. The collected catalyst was then washed with 50 ml of water four times and once methanol to eliminate any remaining reactant or product, and dried overnight in an oven at 80 °C to be reused. The liquid sample collected from the filtration step was stored in a container for further analysis.

3.2.1. Core-shell catalysts preparation

Mesoporous silica-coated core-shell catalysts were prepared using a novel method by combining two ways reported by El-Nahhal et al. (2016) and Wang et al. (2017). In a typical preparation method, 0.5 g of active metal oxide particles were placed in a round bottom flask with 2 g of surfactant (CTAB or Pluronic P 123), 15 ml of deionised water and 7.5 ml of ethyl acetate. The flask was then placed in a sonic bath for ultrasonication to increase the dispersion of metal oxide particles in the solvent. After 30 minutes of treatment, the flask was moved to a heating jacket sitting on a hot plate equipped with a thermocouple. The mixture was further stirred using a magnetic stirrer for 15 min after adding 1.2 ml of ethanolamine. After that time, silica precursor, TEOS, was added to the mixture dropwise by dropping funnel, and the reaction was run for 4 hours under reflux at 80 °C using the setup shown in Figure 3.2. After the completion of silica precipitation, samples were collected from the flask and filtered. The filtered particles were then washed with 4x50 ml of deionised water to remove any excess surfactant and washed samples were placed in an oven at 80 °C for drying overnight. It was then calcined at 550 °C with a temperature ramp rate of 1 °C/min, and the temperature was held for one hour when it reached the set temperature. Samples prepared using CTAB are directly used after the calcination, whereas catalysts prepared with Pluronic P123 and no surfactant are ground before use.

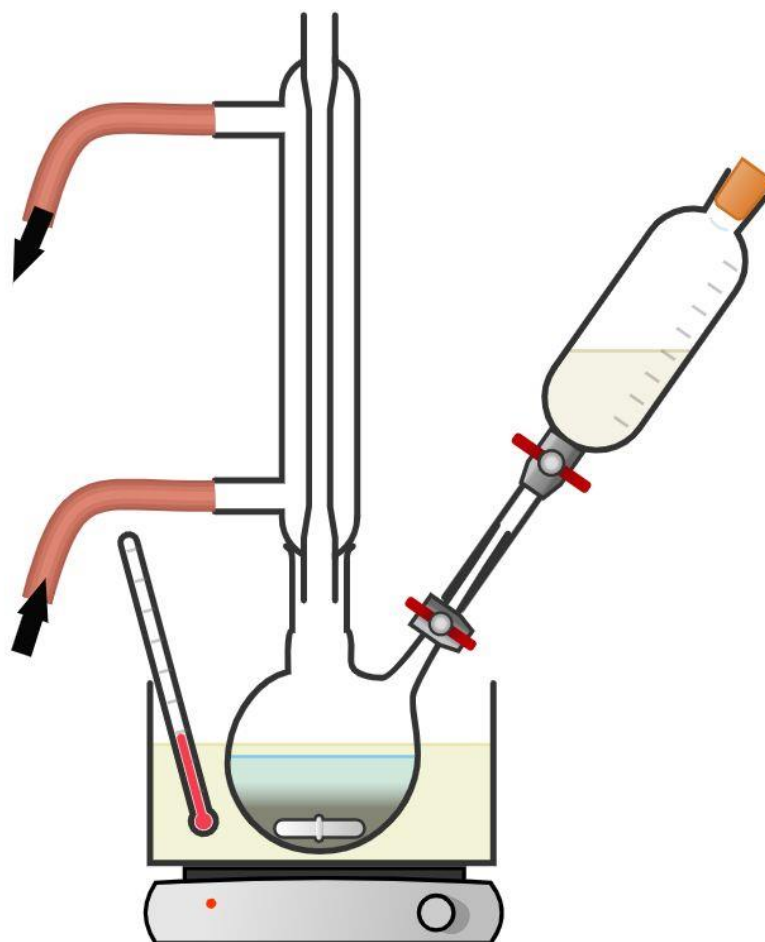


Figure 3.2 The schematic diagram of reflux setup used for the preparation of core-shell catalysts

3.3. Analytical methods

3.3.1. Analysis of urea derivatives by GC-MS

Gas chromatography (GC) is an analytical method that separates components in a sample according to their affinities in a GC column. This separation is carried out with two phases: a mobile phase which is an inert carrier gas like helium or nitrogen; a stationary phase that is generally a material with high molecular weight (Annino & Villalobos, 1992). A typical gas chromatography mainly consists of an injection port, column, oven and detector. In the first step of the analysis, the sample is introduced to the injection port that is set to a temperature high enough to volatilise all the components (Sparkman et al., 2011). The injected sample is then carried with the mobile phase through the fractional column where the separation occurs. The principle

of separation for compounds into the column relies on the affinity of chemicals against the stationary phase on the column—the stronger affinity to the phase, the longer retention times. The retention time is used to describe the total time spent by each component passing through the column (Annino & Villalobos, 1992). Components separated by GC then reach a detector where signals are generated. Mass spectrometry (MS) is one of the main detector types that are equipped with GC in order to produce electronic signals from the separated analytes (Sparkman et al., 2011). MS consists of three major parts: the ion source where the introduced analytes are converted into their ionised forms; mass analyser that accelerates and then separates the ions according to their mass to charge ratio (m/z); ion detector of which electrical signals are generated from the separated ions by a detector. These generated signals are then used to plot a chromatogram in the data system (Downard, 2004).

The qualitative and quantitative analysis of the derivatized product was done by Gas chromatography equipped with mass spectrometry (Shimadzu, GCMS QP2012SE) using a non-polar Agilent DB-5 column (30m x 0.25 mm x 0.25 μ m). The method used for the analysis of urea derivatives was adopted from Zhao et al. (2012) with small modifications. Helium was used as a carrier gas, and the column was washed with methanol before and after the running analysis. The injection amount of the analysis was set to 50 μ l on the programme of the GC-MS and this pre-diluted analyte was loaded to the carrier gas stream using the splitless method at the injection temperature of 250 °C, where the sample was volatilised to be able to flow along the column. The temperature of the column was programmed by setting the initial temperature of 100 °C (held for 5 min), then it was increased to 250 °C (hold for 5 min.) at a rate of 10 °C/min. The chromatogram generated by the signal from MS was analysed by a computer program in terms of peak height and area. Amines conversion, urea derivatives selectivity and product yields were calculated by calibration curves generated with external standard solutions. The plots and equations used in the calculations are shown in Appendices A.

3.3.2. Scanning electron microscopy

Scanning electron Microscopy (SEM) is an instrument to analyse the particle size and its morphology with high resolution using the emission of electron beams reflected from the sample (Dann et al., 2000). These electron beams generated by an electron gun are accelerated by a high voltage system and focused on the sample via objective lens for scanning. This scanning occurs continuously on the sample surface and SEM images are formed by a detector using electrons reflected from the sample. From the interaction between the sample and electron beams, various emissions are produced such as low-energy, secondary electrons, elastically scattered back-scattered electrons, Auger electrons and characteristic X-rays (Reimer, 1998). Secondary electrons are generally used to produce images of the sample whereas X-rays are employed for qualitative and quantitative analysis of the specimen as these emissions are distinctive for elements (Leng, 2013). Therefore, this technique known as energy dispersive X-ray spectrometry (EDS) is performed together with SEM for elemental analysis of the sample (Schatten, 2012).

The size and morphology of catalysts were analysed using Jeol JSM-6010 LA Scanning Electron Microscopy (SEM). Non-conductive catalysts were placed on an adhesive carbon tape, pre-coated with gold using Agar Sputter Coater for 8 seconds under argon to provide conductivity. For the coating process, 40 mA of current and 0.04 mbar of argon pressure were used. The measurement took place using accelerating voltage from 10 to 20 kV and the working distance of 11 mm from the sample. Images magnified from 100 to 1000 times are used to measure the particle size and in order to analyse the surface morphology of the particles.

3.3.3. X-ray diffraction

X-ray diffraction (XRD) is an analytical technique in order to analyse the crystalline phase and structure of materials by diffracted X-ray beams from the sample (Leng, 2013). A typical XRD consists of three main components which are an X-ray source, a sample holder and a detector (Suryanarayana & Norton, 1998). X-rays emitted from the X-ray source are reflected in different directions after hitting the sample due to the crystal phase of the materials. A diffraction pattern is then produced by the angle and

intensity of these diffracted X-rays measured by a detector. Because this generated diffraction pattern is unique for each materials and their crystal phases, diffraction patterns can be used to analyse the composition of the sample (Dann et al., 2000). In this analysis, the crystallite size of the components can be calculated using the Scherrer equation:

$$\tau = \frac{K\lambda}{\beta \cos(\theta)}$$

where τ is the crystallite size, λ is the X-ray wavelength of X-ray source, β is the peak broadening, and θ is the angle of the incident. K value which is the dimensionless shape factor of the crystal shape is typically around 0.9 for spherical particles (Leng, 2013).

The structure of the catalyst is analysed using a Bruker D2 Phaser XRD as the diffraction pattern can be described as a fingerprint for each crystal that has unique diffraction. The instrument is operated in transmission mode at 20 kV voltage and 5 mA current. The pattern measured at room temperature with Cu-K α radiation ($\lambda = 1.5406 \text{ \AA}$ and 2θ from 10° to 60°) is used to identify the characterisation of the catalysts by comparing XRD patterns in the database Powder Diffraction Files (PDF) (Dutrow & Clark, 2017).

3.3.4. Atomic absorption spectroscopy

The examination of metal leaching in the filtrate collected from the filtration step was performed by Atomic Absorption Spectrometer (AAAnalyst 400) by preparing standard solutions and samples diluted using 1% nitric acid blank solution. Since each element has unique absorption radiation at a specific radiation, it is possible to perform qualitative and quantitative analysis by this method (Ivanova, 2005). The programme called Winlab32 was used to operate the instrument and the appropriate lamp was selected for each metal examined. The calibration curve given in Appendices B was plotted by preparing standard solutions for each metal with 1.25, 2.5, 5 and 10 ppm to determine sample concentrations. Each sample was diluted 200 times before the analysis to work within the calibrated analysis range of the instrument, and the results are given as it is read from the analysis. The reading was performed three times for each sample and the mean value is taken into account.

3.3.5. Fourier transform infrared spectroscopy

The functional group of a compound absorb IR radiation at specific frequencies and Fourier transform infrared (FTIR) spectroscopy analysis relies on this absorption to identify the intramolecular bonds for the compositional analysis of a sample (Stuart, 2004). The difference in the dipole moment of molecular bonds due to the absorption of IR radiation is linked to the atoms in the bond and the type of vibrations such as bending and stretching. FTIR spectrum is then plotted by either absorbance or transmission against the wavenumber (Driggers et al., 2012).

The chemical properties of prepared core-shell catalysts were analysed using Shimadzu IRAffinity-1S and Specac Quest ATR FTIR spectroscopy. The analysis herein is performed using FTIR with ATR configuration in transmission mode on the diamond crystal, and the instrument is controlled by LabSolutions IR software. The experimental configuration was controlled by the software, and the measurement was performed for the wavenumber range of 380-4000 cm^{-1} with a scan resolution of 0.5 cm^{-1} . FTIR spectrum generated from the analysis was then used to identify any left organic species after the core-shell catalyst preparation by comparing results with fresh metal oxide samples.

3.3.6. Transmission electron microscopy

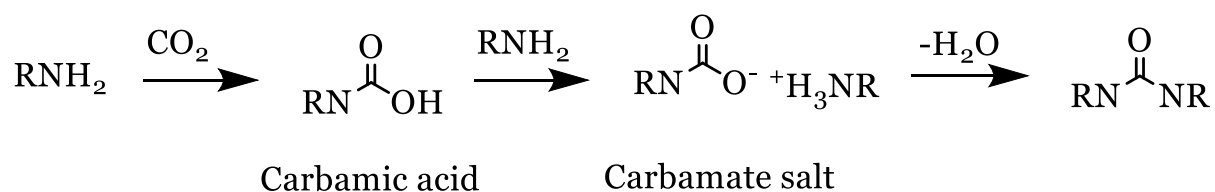
Transmission electron microscopy (TEM) is a technique that is being used to analyse the morphology of nanoparticles by transmitted electron beams through very fine samples (Nasrollahzadeh et al., 2019). An electron gun generates electron beams that are accelerated and focused by an electromagnetic field and then travel through the sample (Dorfs et al., 2011). The interaction between the sample and electrons produces images due to the changes in material composition or the thickness of its components. Since it has a capacity for accelerating voltages ranging from 100 to 1000 kV and electron wavelength ranging between 0.004 and 0.001 nm, it has a potential to image the material in nanometre dimensions (Pennycook, 2005). It is also possible to run a compositional analysis of the specimen by using secondary signals diffracted from the sample (Dorfs et al., 2011). Unlike SEM, it is relatively hard to investigate the surface morphology of the material; however, this technique enables to conduct internal

structure imaging for solid materials and interfaces between different components of the specimen (Stachowiak et al., 2004).

The morphology of prepared core-shell catalysts was examined by an FEI Tecnai T20 TEM instrument equipped with a CCD camera using a high tilt to obtain the images of analytes in both bright and dark fields. For TEM analysis, a small amount of samples were dispersed in ethanol and then placed on holey carbon films for the analysis. All analyses were conducted by Dr Colm O'Regan from the materials science and engineering department at the University of Sheffield. Images gained from the TEM images were then used to compare results from SEM analysis and to calculate the particle size, shell thickness and interface between core and shell materials of core-shell catalysts.

Chapter 4: Conversion of CO₂ Into Urea Derivatives Over Heterogeneous Metal Oxide Catalysts

Urea derivatives synthesis can be an alternative approach for the conversion of captured CO₂. A weak acid CO₂ can give a reaction with amines to carbamate acid or carbamate anions even under room temperature and low pressures (Eq 4.1). However, dehydrating these intermediates into urea derivatives requires dehydrating agents or harsh reaction conditions (H. Wang et al., 2017). On the other hand, reaction conditions can be manipulated by employing catalysts to enhance the overall yields at moderate conditions without any additional promoters (Ion et al., 2007). As discussed in Section 2.3.5, the synthesis of urea derivatives is highly dependent on catalysts that can subsequently increase the selectivity towards corresponding ureas. It was also highlighted that iron oxides are highly effective, abundant and inexpensive catalysts that have the great basicity desired for urea derivatives synthesis (Hakim et al., 2016). Additionally, Gomez (2017) showed that iron oxides were highly reactive for CO₂ conversion with excellent stability, and also (H. An et al., 2014) confirmed that they had a great impact on urea derivatives synthesis. Since Tamura et al. (2016) reported that the interaction between catalyst and solvent is highly distinctive for the production, it is essential to evaluate this relationship using different metal oxide catalysts with several solvents. Therefore, iron-based catalysts with various oxidation states were employed herein to understand this interaction better and assess their reactivity for the production of urea derivatives using a number of different amines over the conversion of CO₂.



Equation 4.1 The proposed reaction mechanism for the urea derivatives synthesis from CO₂ and amines

4.1. Results and discussion

4.1.1. Optimisation of the reaction conditions for DBU production

Prior to any experiments, the chemical kinetics of the reaction needs to be evaluated. Reaction law or reaction rate expresses the mathematical equation of a chemical reaction and shows the relationship between the rate of the reaction and the concentration or pressure of the reactants. A complicated rate equation can be simplified by the isolation method in which the dependence of the reaction rate for the concentration of a reactant is isolated by having excess amounts for other reactants. The assumption is made that the concentration of other reactants remains stable during the reaction, thereby the reaction rate depends only on the chosen reactant's concentration. Using this method, the reaction is identified as a pseudo-first-order reaction (Atkins, 1998).

With reference to this, Tamura et al. (2016) applied this method by having one reactant in large excess and running a series of experiments with changing concentrations. Then, the reaction's initial rates were determined using the method of initial rates at varied concentrations. Therefore, the reaction rate below

$$V = k[A]^a[B]^b$$

can be simplified and can be written as a pseudo-ordered reaction rate as follows

$$V = k[A]^a.$$

This equation can be rearranged by taking the natural logarithm of each side of the equation and can be represented as follows

$$\ln V = \ln k + a \ln[A]$$

By the use of this equation, a plot of $\ln V$ against $\ln [A]$ will give the reaction order with the slope of the plot (Atkins, 1998).

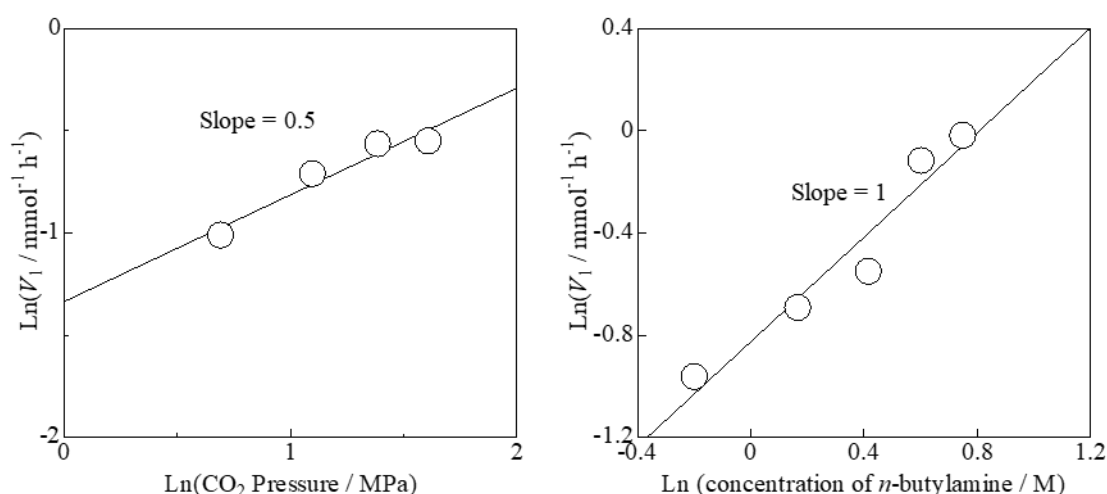


Figure 4.1 Dependence of CO₂ pressure and butylamine concentration on the reaction rate using solvent only experiments, adapted from Tamura et al. (2016)

Figure 4.1 shows the slopes obtained by Tamura et al. (2016) using this approach with experimental data found with the presence of NMP only as a solvent. It can be seen from the figure that the slopes are 0.5 and 1 for CO₂ and butylamine, respectively. Thus, the reaction rate can be written as follows

$$V = k[\text{CO}_2]^{0.5}[\text{C}_4\text{H}_{11}\text{N}]^1$$

This equation states that the reaction rate depends on the concentration of both CO₂ and butylamine.

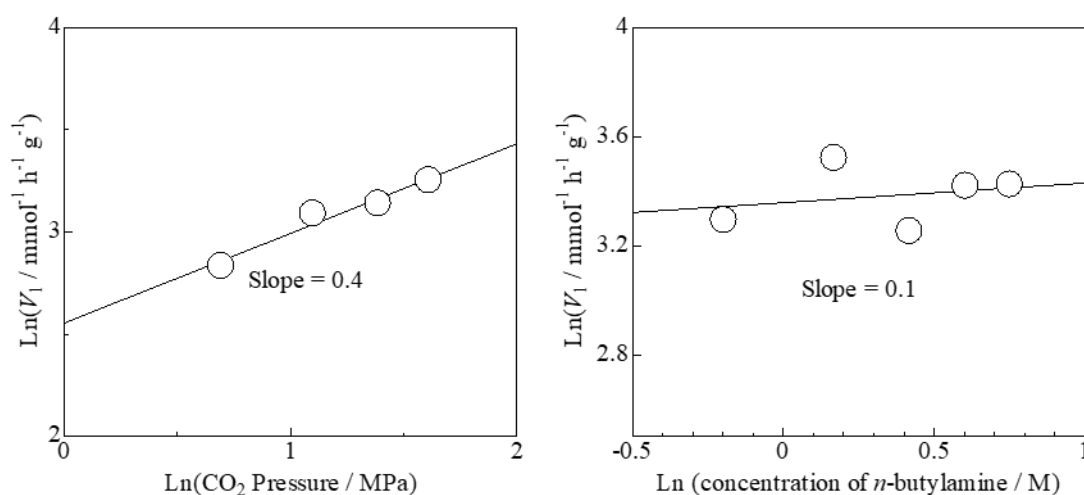


Figure 4.2 Dependence of CO₂ pressure and butylamine concentration on the reaction rate using CeO₂ in THF, adapted from Tamura et al. (2016)

After that, the plot of $\ln V$ versus $\ln [A]$ was drawn with the experimental data obtained using solvent and CeO_2 as a catalyst. The slopes gained from Figure 4.2 give the reaction orders which are 0.4 and 0.1 for CO_2 and butylamine, respectively. Using these reaction orders, the reaction rate of the catalytic route can be written as

$$V = k[\text{CO}_2]^{0.4}[\text{C}_4\text{H}_{11}\text{N}]^{0.1}$$

This again shows the dependence of the reaction rate on reactants' concentrations for the catalytic route. It can also be said that the reaction follows a different path by the presence of the catalyst as the reaction orders and reaction rates are different for two routes. Therefore, it can be said that it is essential to optimise the reaction conditions as the rate law depends on the concentration of reactants for both routes.

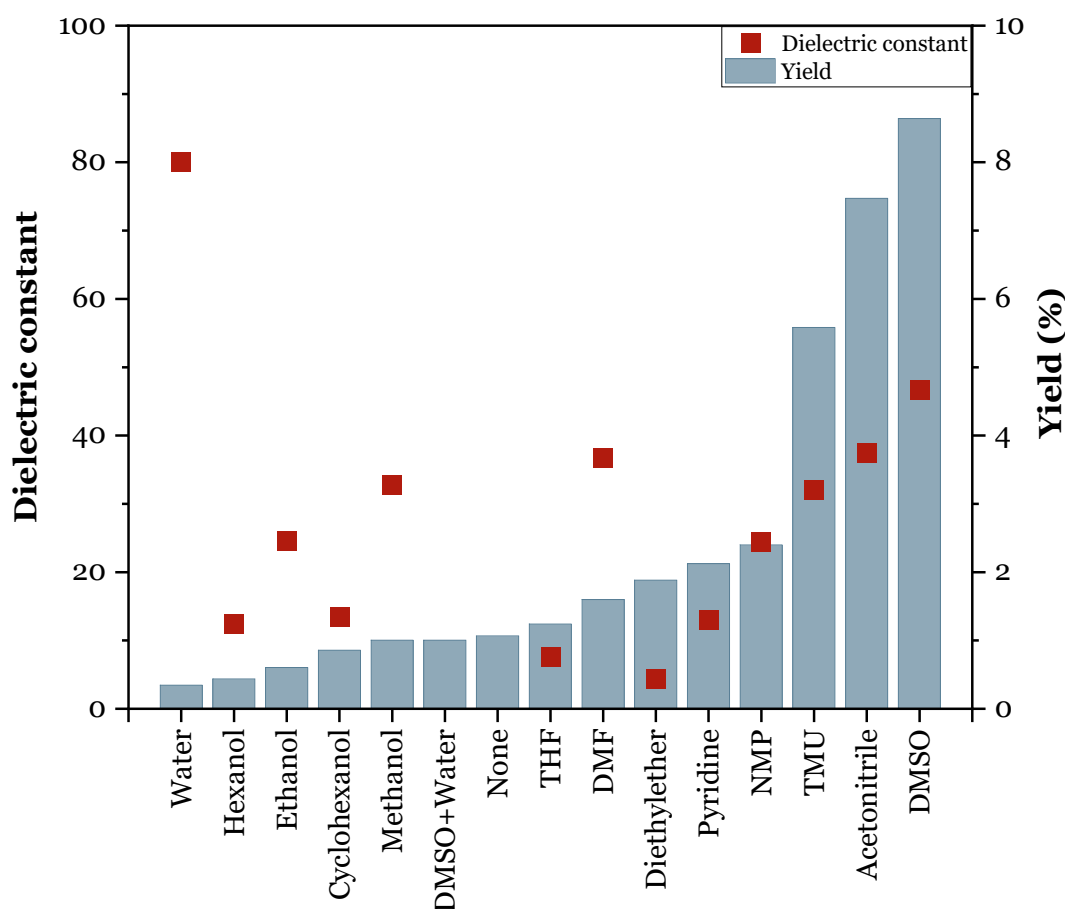
In order to evaluate the catalytic performance of iron-based catalysts, the variables such as temperature, time, reactant and solvent amounts will be first studied to identify the optimum conditions. The results found for these experiments are reported below.

4.1.1.a. The influence of solvent

Solvents greatly influence nucleophilic substitution reactions; polar protic solvents promote $\text{S}_{\text{N}}1$ reactions, whereas aprotic solvents facilitate $\text{S}_{\text{N}}2$. Experiments were first carried out to evaluate the effect of solvent on the procedure by employing several organic solvents as the nucleophilicity of amines very much depends on the solvent polarity (Kanzian et al., 2009). A set of experiments were then followed that to find an optimum amount of solvent for greater yield.

The experiments herein were conducted using 20 mmol butylamine, 4 ml solvent, 2 mmol Fe_2O_3 and 3 MPa of CO_2 at 423 K for 2 hours and the results are given in Figure 4.3 with yields and dielectric constant of solvents together (Cerón-Carrasco et al., 2014; Reichardt, 2002). Firstly, a test was undertaken without any solvent to see the procedure's feasibility, which only gave 1% yield for N,N-dibutylurea at the chosen reaction condition. As the process is an $\text{S}_{\text{N}}2$ nucleophilic substitution reaction, studies with polar aprotic solvents namely THF, DMSO, acetonitrile and NMP, were performed as they favour the $\text{S}_{\text{N}}2$ reaction (Hart et al., 2007). Polar aprotic solvents are able to dissolve the nucleophiles without making any hydrogen bonding as they do

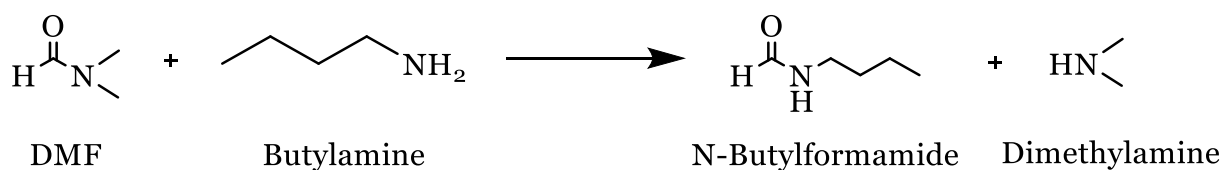
not have any O-H or N-H bonds. This allows nucleophiles to freely move around in the solvent and improve their reactivity in the reaction (Lowry & Richardson, 1987).



(Polar protic solvents: Water, hexanol, ethanol, cyclohexanol, methanol;
Polar aprotic solvents: THF, DMF, pyridine, NMP, Acetonitrile, DMSO; Non-polar: Diethyl ether)

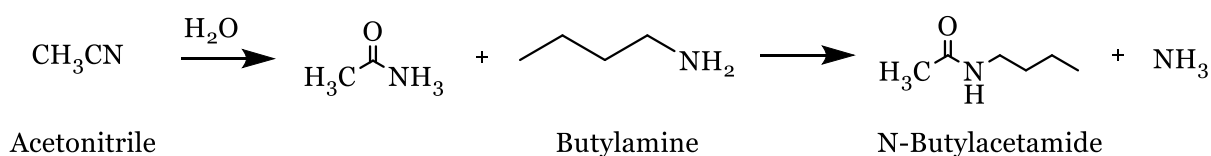
Figure 4.3 Influence of solvent on DBU synthesis and the correlation between DBU yield and dielectric constants of solvents (Reaction conditions: 20 mmol butylamine, 2 mmol Fe₂O₃, 3 MPa CO₂, 4 ml solvent at 423 K for 2 hours)

In the light of that, THF with the lowest dielectric constant of 7.5 had the minimum yield at 1.2% and then the yield of DBU was increased to 2.4% and 7.5% for NMP and acetonitrile, respectively. It reached its highest point of 8.6% using DMSO, with the highest dielectric constant at 47. This peak was achieved by 47% butylamine conversion and 21% DBU selectivity. Likewise, the graph indicates that the effectiveness of polar aprotic solvents was enhanced when the dielectric constant increased. This demonstrated a similar trend with the literature: the higher the dielectric constant, the more yield was achieved (Tamura et al., 2016).



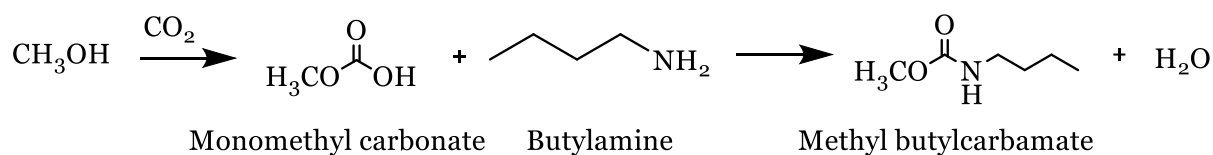
Equation 4.2 The reaction occurs between DMF and butylamine

The only inconsistency for the statement above was detected using DMF, where the yield was found just above 1% even though it has the second-highest dielectric constant among others. The main product detected on the GC-MS chromatogram was N-Butylformamide due to the reaction between DMF and butylamine, as reported by Tamura et al. (2016) (Eq 4.2). The yield, therefore, dramatically dropped to 1.2% for DBU synthesis from 8.6% with DMSO; however, it was still slightly higher than THF and the solvent-free experiment. Another side reaction occurring in the presence of acetonitrile as seen in Eq 4.3 was also reported where N-butylacetamide is formed due to the reaction between acetonitrile and water produced from the dehydration of carbamate salt to produce disubstituted urea. However, the yield was still higher than other solvents and it is believed that the removal of water from the system by the reaction with acetonitrile was the main reason for this increase, which shifted the main reaction to the product's side.



Equation 4.3 The side reaction occurs by the use of acetonitrile as a solvent

Polar protic solvents like water and several alcohols were also examined for the production of DBU from butylamine; no more than 1% yield was observed. That demonstrated identical results with the literature as polar protic solvents reduce the yield by stabilising carbocation that occurs in the first step of SN₁ reactions (Choi et al., 2014; Hart et al., 2007). This promotes an SN₁ reaction rather than SN₂; therefore, fewer yields were obtained compared to the experiment without any solvent and polar aprotic solvents. This decline can be seen in Figure 4.3 where the water dropped the DBU yield under 1% even though the butylamine conversion was the maximum at 93%. Experiments with a number of different alcohols also showed similar results in which DBU selectivity was smaller than 4% owing to the reaction seen in Eq 4.4, even though the conversion rate was 60% for ethanol and about 20% for others.



Equation 4.4 A side reaction pathway occurs in the presence of methanol

The effect of the presence of water on the procedure was discussed by Wu et al. (2010), and it was reported that the small amount of water would promote the reaction, whereas the yield dropped with excess water as it would shift towards the reactant side. In the light of that, an experiment with a solvent mixture of water and DMSO (1:1) was conducted, and the result was compared with water-only and DMSO-only experiments. Although the addition of DMSO tripled the yield from 0.3% to 1%, it drastically dropped from 8.6% to 1% with the presence of water. The amount of water used in the experiment was 2 ml, which was relatively high compared to the literature. That might be the reason for this dramatic drop, but this also indicated the importance of using non-aqueous chemicals in order to achieve greater selectivity.

Finally, diethyl ether was employed to study the influence of nonpolar solvents as they facilitate an elimination reaction, instead of nucleophilic substitution reactions (Hart et al., 2007). The overall result was just under 2%, with 17.6% conversion and 10.7% selectivity. Although diethyl ether favours the elimination reaction, relatively higher selectivity and consequently a better yield was achieved compared to polar protic solvents and the experiment without any solvent. Nonetheless, it was still significantly lower than polar aprotic solvents; thus, DMSO was used for subsequent experiments.

The influence of solvent amount was also assessed at different amounts of DMSO. Reactions run at 423 K using 3 MPa CO₂, 20 mmol butylamine and 2 mmol Fe₂O₃; the results are shown in Figure 4.4. As the experiment without any solvent in the previous section had an extremely low yield, it is important to assess the effect of the solvent amount. Only 1% yield was achieved for the experiment with no solvent and it rose to 2% with the addition of 2 ml DMSO. It was then boosted to its peak at 8.6% with 4 ml solvent, and remained almost flat with increased amount. The slight decrease for 8 ml of solvent is clearly in the range of error so the yield was accepted as alike for these experiments. This constant yield between 4 and 8 ml of solvent can be explained with the solubility of CO₂ (Tamura et al., 2016). Since no significant change was observed after 4 ml DMSO, it was selected as an optimum amount for the following experiments.

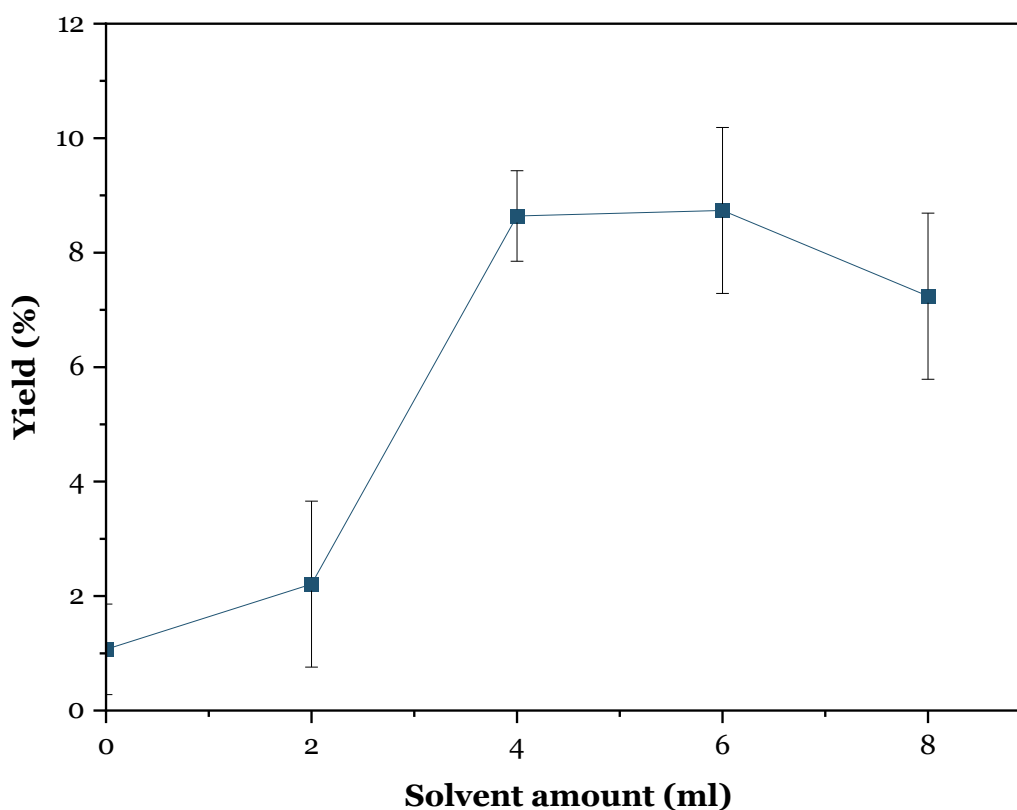


Figure 4.4 The effect of solvent amount on DBU synthesis from butylamine and CO₂ using DMSO (Reaction conditions: 20 mmol butylamine, 2 mmol Fe₂O₃, 3 MPa CO₂, 0-8 ml DMSO at 423 K for 2 hours)

4.1.1.b. The effect of reactant amounts

The evaluation of the substance amounts is essential to understand the kinetics of the reaction better and have optimum reaction conditions for an enhanced product yield. For that reason, experiments were next conducted to find an optimum amount of reactants by varying butylamine and CO₂ amounts to maximise the catalyst reactivity for the production of DBU.

It was reported that pressure substantially influences the DBU synthesis where the yield drops for exceeding CO₂ pressures (Zhang et al., 2013). Therefore experiments were performed to see the effect of CO₂ pressure on the reaction yield and the changes in DBU yield over pressure are presented in Figure 4.5.

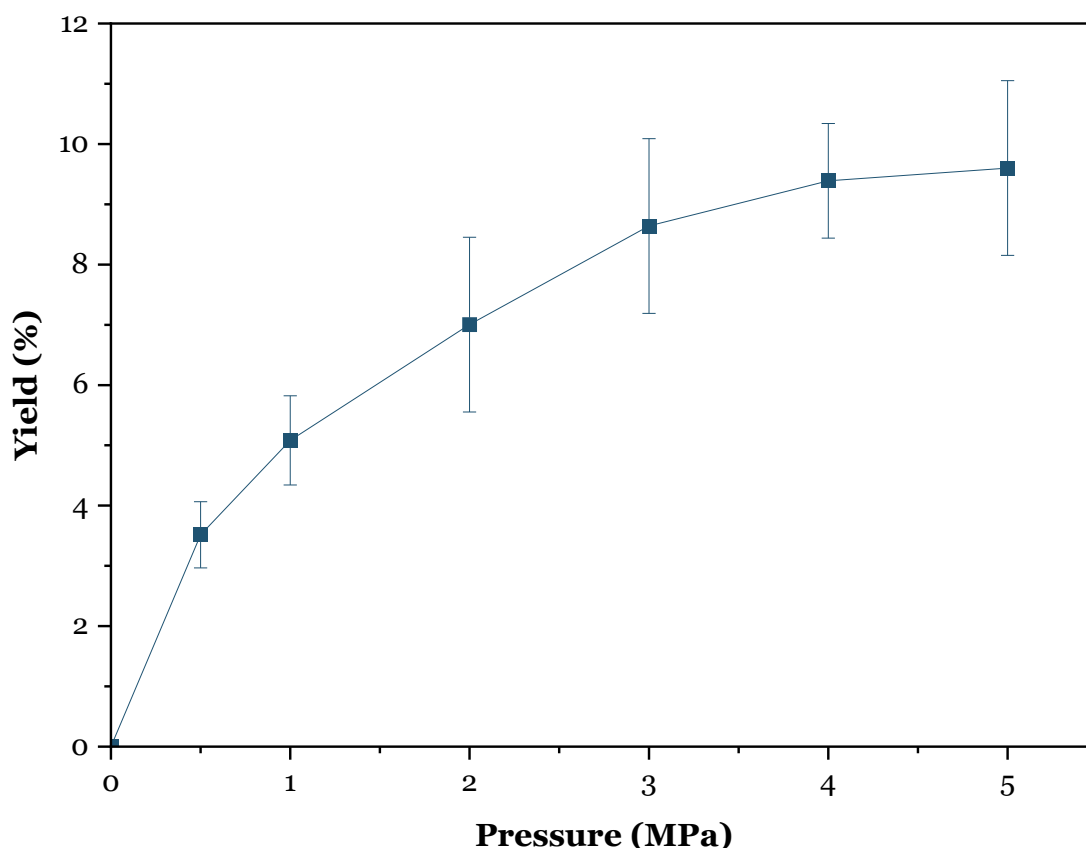


Figure 4.5 Changes in DBU yield over increased CO₂ pressure (Reaction conditions: 20 mmol butylamine, 2 mmol Fe₂O₃, 0-5 MPa CO₂, 4 ml DMSO at 423 K for 2 hours)

It is clear that no DBU was produced in the absence of CO₂, which confirms that the reaction only happens between CO₂ and butylamine. Only 3.5% DBU yield was obtained at 0.5 MPa and it was boosted to 9.6% when the pressure reached 5 MPa. There was a rapid increase from 0.5 MPa to 3 MPa in the yield, and then it was slowed down between 4 and 5 MPa. This can be explained again with CO₂ solubility in the solvent. The amount of CO₂ dissolved in the solvent was relatively high for the first three pressures, and then it reached the saturation around 4 MPa. This also showed a similar trend as reported by Zhang et al. (2013), where the yield declined after 3 MPa with the use of 2 ml NMP. It was also reported that the dilution effect occurred at higher pressures dropped the yield dramatically owing to more CO₂ being adsorbed around catalysts, making it harder for butylamine to reach catalysts' surface compared to lower pressures. Hence, 4 MPa was selected as an optimum pressure as there was only a slight difference in the DBU yield between 4 and 5 MPa.

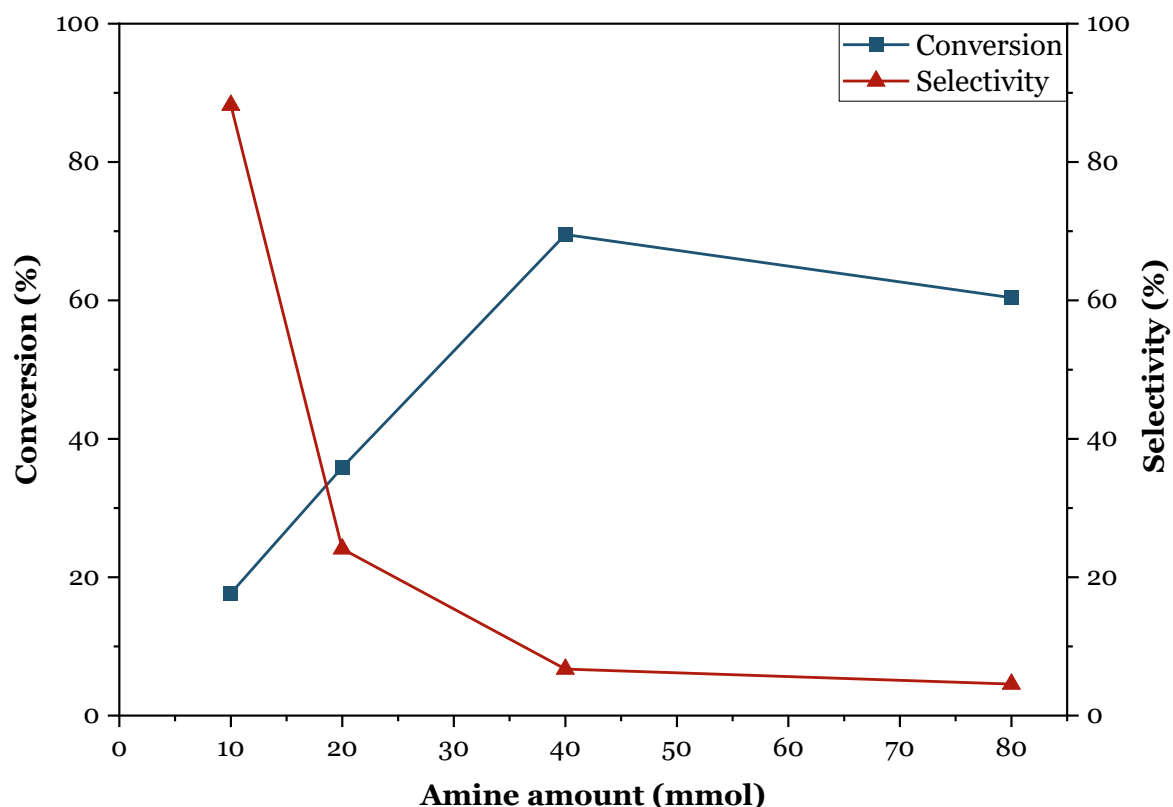


Figure 4.6 Butylamine conversion at different concentrations and the effect of amine amount on DBU selectivity (Reaction conditions: 10-80 mmol butylamine, 2 mmol Fe₂O₃, 3 MPa CO₂, 4 ml DMSO at 423 K for 2 hours)

To broaden the scope, tests with butylamine amounts between 10-80 mmol were performed, and results for butylamine conversion and DBU selectivity are given in Figure 4.6. Almost 90% selectivity was obtained with 18% butylamine conversion, which yielded 15% DBU in overall, for the first run. After that, the conversion had a gradual increase by amine amount whilst the selectivity significantly dropped. The production yield was just about 8.5% due to the decrease in selectivity from 90% to 24%, even though the conversion was doubled to 36%. The rise in butylamine conversion continued and reached its highest rate of 70% at 40 mmol butylamine and remained above 60% after that point. However, only 4.5% DBU was synthesised owing to the dramatic decline in selectivity to 5% for higher butylamine amounts. This indicates similar trends with pressure experiments (Figure 4.5), as using more amine may limit the access of CO₂ to catalysts because of the excess amount of butylamine adsorbed around active sites. Although the experiment with 10 mmol butylamine had the highest selectivity for DBU, the optimum amount for butylamine was selected as 20 mmol, where the conversion and selectivity lines were encountered.

Table 4.1 Carbon mass balance over amine amounts

| Amine amount (mmol) | Used butylamine (mmol) | Used C (mmol) | Formed DBU (mmol) | Formed DBU C (mmol) | DBU Selectivity (%) |
|----------------------------|-------------------------------|----------------------|--------------------------|----------------------------|----------------------------|
| 10 | 1.78 | 8.01 | 0.79 | 7.09 | 88.5% |
| 20 | 7.25 | 32.61 | 0.87 | 7.86 | 24.1% |
| 40 | 28.09 | 126.4 | 0.94 | 8.49 | 6.72% |
| 80 | 48.79 | 219.6 | 1.11 | 10 | 4.55% |

Further investigation on carbon mass balance was conducted to obtain the effect of reactant concentrations on DBU selectivity and its yield. Table 4.1 indicates the mass balance of carbon atoms in the reaction, confirming the dependence of the reaction rate on reactant concentration discussed above.

4.1.1.c. The influence of temperature and time

The effect of temperature and time were also investigated for the last step of the optimisation procedures. It has been reported that the reaction is highly dependent on the temperature as much as the reaction times, which both dramatically change the DBU yield (Tamura et al., 2016). Hence, finding the optimum reaction temperature and time for better DBU production is essential. Since the reaction needs a moderately high temperature for the activation energy of CO₂, no reactivity was detected below 413 K. Experiments were mainly focused on temperatures above 413 K and temperatures lower than 413 K were excluded. For a clear assessment, DMSO with a high boiling point which is around 462 K was selected after evaluating many different solvents in Section 4.2.1.a, and changes in the conversion of butylamine and the selectivity for DBU over temperatures between 413 and 473 K are given in Figure 4.7. Although no reactivity was reported for lower temperatures, experiments from 373 to 413 K were conducted and it is confirmed that a maximum 1% yield was achieved at that temperatures.

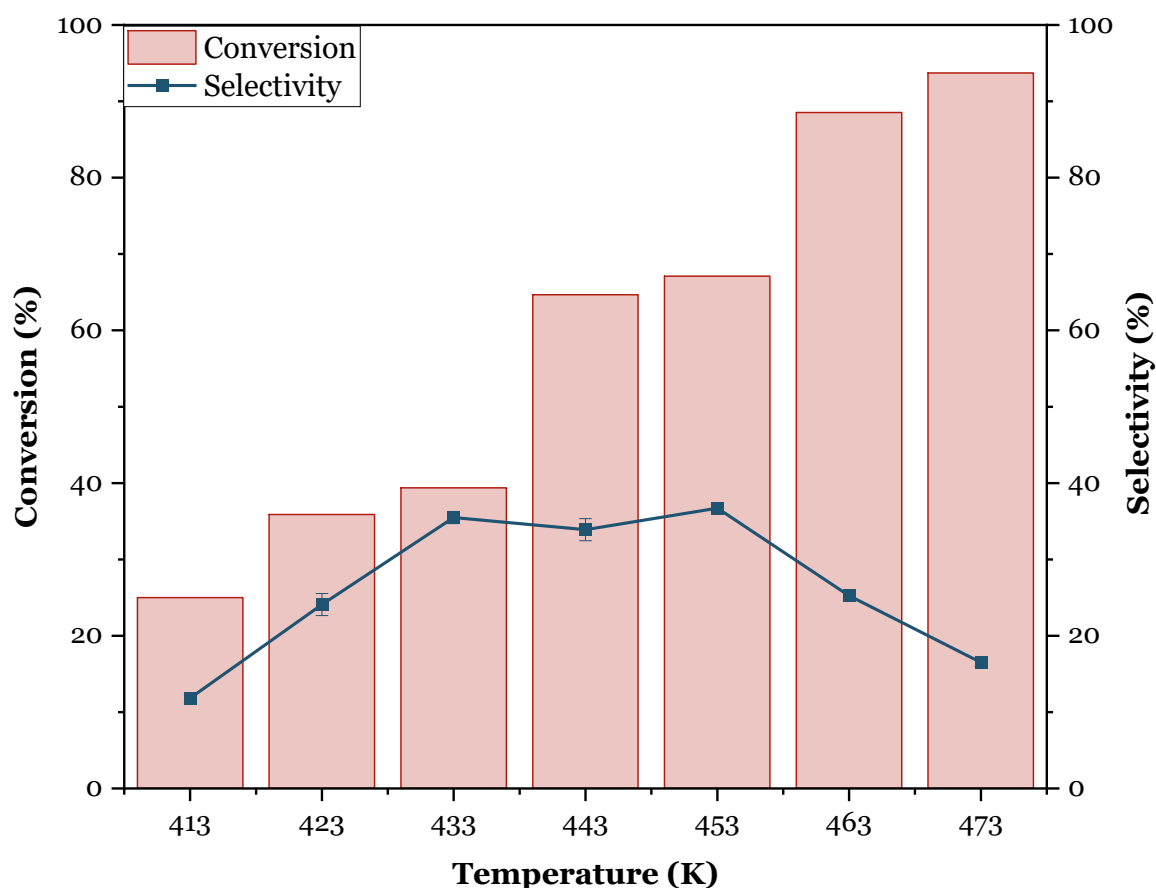


Figure 4.7 The influence of temperature on butylamine conversion and DBU selectivity (Reaction conditions: 20 mmol butylamine, 2 mmol Fe₂O₃, 3 MPa CO₂, 4 ml DMSO for 2 hours at different reaction temperatures)

The yield for DBU was initially just under 3% at 413 K with 12% selectivity and 25% butylamine conversion. Then it gradually increased to its peak of 24.6% at 453 K by 37% selectivity and 67% conversion. The butylamine conversion had a continuous increase by elevated temperatures until it reached 93% at 473 K. However, the DBU selectivity did not exhibit a similar trend and fluctuated over temperature. It was initially raised till 433 K, and then it remained steady at around 35% between 433 and 453 K. After that point, the selectivity started to drop when it was only about 16.5% at 473 K. This decline in the selectivity can be explained with the decomposition of DMSO. Although DMSO has a relatively higher boiling point, it was discovered that it starts to decompose around its boiling point at 463 K, which can be the main reason for this downward trend in selectivity (Deguchi et al., 2020). The timing for experiments was started when it reached the desired temperature, so if the solvent decomposed at the very beginning, it would not be able to promote the reaction as

intended. Thus, the yield was reduced from 25% to 22% for 463 K because of this decomposition noted. Furthermore, the drop continued with the increase in temperature, and only a 15% DBU yield was obtained at 473 K owing to the further decomposition of the solvent at higher temperatures.

In addition to the dramatic fall in selectivity, a change in the physical properties of the product was also noticed after the reaction at and above 473 K. The colour of the filtered product was yellow at lower temperatures, but it was turned to red after reactions on or after 473 K. There was also a fall in the amount of catalysts recovered after the reaction so it is presumed that the catalyst leaching was the primary reason for this colour change and the difficulty for catalyst recovery. As the decomposition of DMSO is a highly exothermic reaction, this decomposition has the potential to produce several chemicals including some acids like formic acid, acetic acid and sulfuric acid, which could be the major cause of this catalyst leaching (Deguchi et al., 2020; Yang et al., 2020).

A set of experiments at different reaction times was performed at the final part of the optimisation reactions. The experiments were run from 2 to 24 hours using 20 mmol butylamine, 2 mmol Fe₂O₃ and 3 MPa CO₂ at 423 K and the results are shared in Figure 4.8. It is easy to read from the graph that there is a parallel increasing trend in both DBU selectivity and butylamine conversion until 24 h. The conversion achieved was 36% in 2 hours and then, it gradually increased until 12 h and peaked at 80%. The selectivity rate also had a similar curve; it was raised from 22% to 38% for the experiments at 2 and 4 hours, respectively. Later, the increase continued steadily and reached the highest point of DBU selectivity at 43% in 24 hours. Overall, only an 8.6% yield was obtained in two hours, and it was boosted to 33% in 12 hours, then slowly enhanced to 34% until 24 hours.

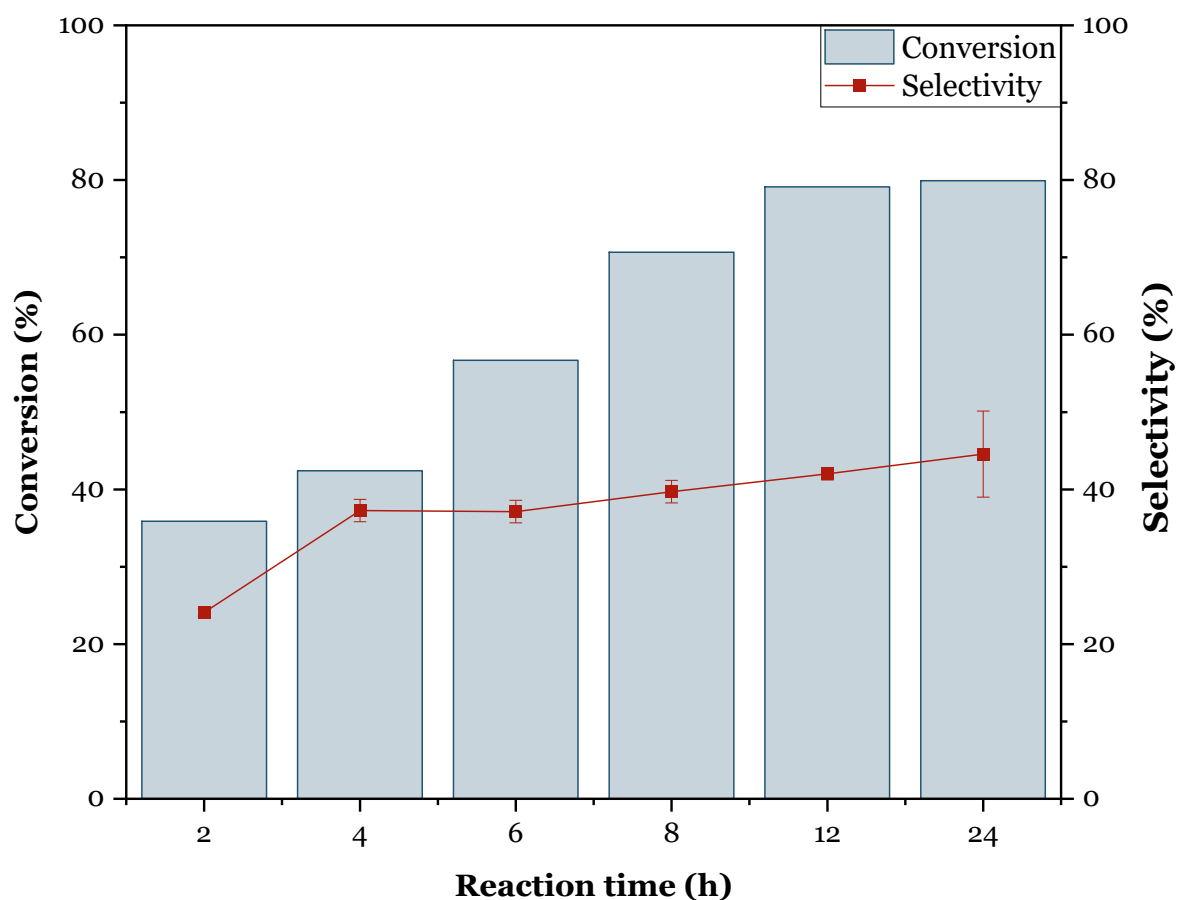


Figure 4.8 Changes in butylamine conversion and DBU selectivity over reaction times (Reaction conditions: 20 mmol butylamine, 2 mmol Fe₂O₃, 3 MPa CO₂, 4 ml DMSO at 423 K)

The reaction was run further for 72 hours to evaluate the effect of longer reaction times on the DBU production, as it was continuously enhanced; however, the yield dipped to 9% in 72 h. Moreover, it was observed that the product mixture collected from the reactor also had a change after 24 h. The colour of the collected liquid sample turned to dark deep red, and the amount of catalyst filtered from the reaction severely dropped after the reaction in the same way as reported at higher temperatures. Head & McCart (1973) stated that DMSO could completely decompose after 68 hours under moderate conditions, so both dramatic cut in yield and catalyst recovery at 72 hours can be attributed to the solvent decomposition happened for longer reaction times. Consequently, the temperature selected for the optimisation of the procedure was 453 K in this study, as the greatest yield was achieved without any catalyst leaching observed. Also, reactions were run for 2, 12 and 24 hours for subsequent experiments to evaluate the DMSO decomposition at the optimised condition over times.

4.1.2. Catalytic performance on urea derivatives synthesis

The reactivity of different metal oxide catalysts on urea derivatives synthesis was investigated as their influence was discussed in the literature. After optimisation reactions, several heterogeneous metal oxide catalysts were employed at the chosen reaction conditions. Additionally, amines with different attached groups were tested for the production of their corresponding ureas to investigate the effect of nucleophilicity on the reaction.

4.1.2.a. The effect of metal oxide catalysts

Catalyst reactivity was investigated at the chosen reaction condition after the optimisation, which was 20 mmol butylamine, 4 ml DMSO, 2 mmol catalysts and 4 MPa of CO₂ at 453 K for 2 hours and the results are given in Table 4.2. The catalyst amount used for supported catalysts was calculated for active species, and provided under the table with their loading value.

The first thing noticed in the table is that the lowest yield was obtained with CuO, even though it was concluded above that copper-based catalysts are highly reactive for this procedure. The result obtained was just above the half of the next one on the table, and this significant difference in the yield could be explained with the state of the product after the reaction. In the previous experiments with Fe₂O₃, the product mixture was yellow liquid with dispersed catalysts, and a simple filtration separated catalysts easily. Nevertheless, no catalyst was recovered after the reaction employing CuO and blue-yellow solid material with very little liquid was separated afterwards.

To evaluate the reason for this formation, copper (II) oxide was studied in different polar aprotic solvents like DMF and NMP. No solid material was observed after the filtration, including the catalyst itself. The filtrate was dark blue, which demonstrates that the catalyst used in the reaction was completely dissolved into these solvents. An experiment without any CO₂ using DMSO was also conducted to assess the reported reaction between CO₂ and CuO (Tanvir et al., 2016). No changes were detected, and the product recovered after the reaction was still limited other than that blue solid material mentioned above. In consequence, it indicates that CO₂ did not have any influence on this formation, and DMSO was the main reason as it was only observed

with the presence of DMSO. Because of the lack of promotion effect from either solvent or catalyst due to the reaction that occurred between DMSO and copper (II) oxide, the lowest yield at 18% was gained for the experiment with CuO even though the conversion was 87.5%.

Table 4.2 Catalytic conversion of butylamine with CO₂ into DBU using different metal oxide catalysts (Reaction conditions: 20 mmol butylamine, 2 mmol catalyst, 4 MPa CO₂, 4 ml DMSO at 453 K for 2 hours)

| Entry | Catalyst | Surface Area (m ² /g) ^a | Conversion (%) | Selectivity (%) | Yield (%) |
|-------|---------------------------------------|--|-------------------|--------------------|--------------|
| 1 | CuO | 29 | 87.5 | 20.9 | 18.3 |
| 2 | CuO/Al ₂ O ₃ * | | 74.2 | 43.9 | 32.5 |
| 3 | Pt/Al ₂ O ₃ ** | | 73.0 | 45.9 | 33.5 |
| 4 | None | | 80.8 | 42.5 | 34.3 |
| 5 | Al ₂ O ₃ | 181 | 78.0 | 45.2 | 35.3 |
| 6 | Pd/Al ₂ O ₃ *** | | 80.0 | 45.9 | 36.8 |
| 7 | Cu | | 76.8 | 48.9 | 37.5 |
| 8 | Cu ₂ O | | 90.3 | 42.1 | 38.0 |
| 9 | FeO | | 66.9 | 58.0 | 38.8 |
| 10 | ZrO ₂ | 59 | 83.2 | 48.6 | 40.4 |
| 11 | Fe ₃ O ₄ | 7 | 74.7 | 56.8 | 42.4 |
| 12 | Fe | | 67.2 | 61.1 | 42.4 |
| 13 | MnO ₂ | 10 | 77.7 | 58.2 | 45.2 |
| 14 | La ₂ O ₃ | 14 | 87.2 | 52.9 | 46.2 |
| 15 | SiO ₂ | 535 | 94.5 | 49.2 | 46.4 |
| 16 | Fe ₂ O ₃ | 11 | 76.1 | 62.4 | 47.5 |
| 17 | CeO ₂ | 88 | 86.9 | 61.9 | 53.8 |

*0.16 g of 13 mol% CuO/Al₂O₃ **0.39 of 0.5 mol% Pt/Al₂O₃ ***0.21 g of 5 mol% Pd/Al₂O₃

a: surface area of the catalysts was adopted from Quintana Gomez (2017); N. Razali (2017)

An experiment with supported CuO on alumina was also conducted to observe the impact of the support material on catalyst stability. The same solid material was observed after the reaction, similar to the one with CuO. Still, the amount of this solid material was reduced as the lower amount of CuO loaded. Used catalyst particles were also examined, and it was noted that particles had dramatic changes in their

appearance. Fresh CuO/Al₂O₃ has black CuO placed on white alumina particles, whereas used particles were completely white after the filtration. This implies that CuO on alumina was displaced from the support material and reacted with the solvent again. Although the yield for the experiment was higher than CuO, the DBU yield was only 32.5%, with 74% conversion and 44% DBU selectivity, making it the second-lowest yield among the catalysts tested.

Moreover, Pt/Al₂O₃, Pd/Al₂O₃ and bulk alumina were also tested for the reaction, and it can be undoubtedly concluded that alumina was not as effective as other metal oxides. Employing these catalysts only slightly increased DBU selectivity; the highest product yield at 37% was achieved with the presence of Pd for alumina-based catalysts. The yield obtained for these experiments was around the experiments with no catalyst.

The table also exhibits that copper-based catalysts at different oxidation states were effective as low as the alumina counterparts. Even though one of the highest butylamine conversions was achieved by Cu₂O, the yield was 38%, just over alumina. Again, some solid material was observed after the reaction, although this species dramatically declined for this experiment compared to CuO. SiO₂ with the highest surface area, converted the maximum amount of butylamine with 94.5%, whilst only 46.5% yield was achieved owing to the relatively low DBU selectivity. Similarly, ZrO₂ showed a moderate selectivity with comparatively higher butylamine conversion but only showed a 40% production rate, similar to iron-based catalysts such as Fe, FeO and Fe₃O₄. Although they had the same reactivity, DBU selectivity was better for these iron-based catalysts than ZrO₂. Another iron-based catalyst, Fe₂O₃, showed excellent reactivity for the reaction after CeO₂, which was defined as a highly reactive catalyst for the procedure. CeO₂ is an expensive, rare-earth element whilst Fe₂O₃ is a non-expensive metal oxide catalyst with a large abundance (Quintana Gomez, 2017; Tamura et al., 2016). Consequently, Fe₂O₃ was selected for the following experiments as DBU selectivity was the greatest for Fe₂O₃, and the difference in the yield between CeO₂ and Fe₂O₃ was relatively modest.

After a detailed consideration of catalysts, a set of experiments was also performed to assess the impact of catalyst amount in DBU synthesis. Experiments were conducted under the same conditions using a range of Fe₂O₃ amounts and the results are presented in Figure 4.9. There was a clear trend in both conversion and selectivity

where butylamine conversion gradually declined whilst DBU selectivity was enhanced with an increase of catalyst amount from 0 to 4 mmol. The yield for the experiment without any catalyst was 34.3%, then it was slightly raised to 36.6% for 1 mmol Fe₂O₃ with 78.7% butylamine conversion and 46.5% DBU selectivity. Furthermore, there was a considerable increase in selectivity to 62% at 2 mmol, then it reduced marginally to 54% at 4 mmol. It was noticed that some Fe₂O₃ particles were stuck to the bottom of the reactor afterwards. It is assumed that this was the main reason for this decline in the selectivity at 4 mmol, as the solvent was not enough to disperse 0.66 g of Fe₂O₃.

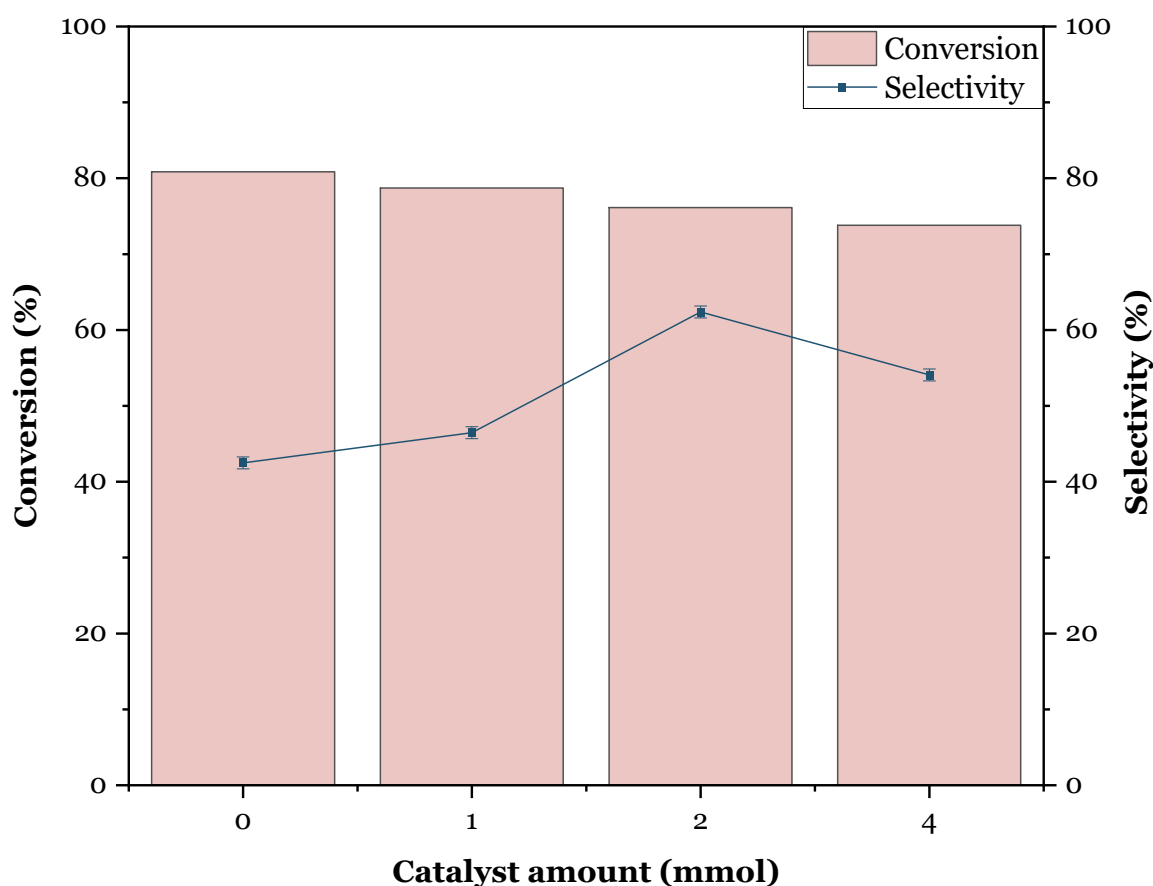


Figure 4.9 Changes in butylamine conversion and DBU selectivity over Fe₂O₃ amounts (Reaction conditions: 20 mmol butylamine, 0-4 mmol catalyst, 4 MPa CO₂, 4 ml DMSO at 453 K for 2 hours)

Finally, a set of experiments was conducted to evaluate how reaction times affect the production of DBU under the optimised conditions (Table 4.3). The yield increased from 2 to 12 hours and stayed stable up to 24 hours at 423 K and 3 MPa. However, results from experiments at 453 K and 4 MPa showed an opposite trend where the yield dropped from 47.5% to 8.7% by the rise of reaction time from 2 to 24 hours. Optimised

conditions boosted the yield from 8.6% to 47.5% in 2 hours (Entry 1 & 2, Table 4.3) whereas it dipped from 35.6% to 8.7% in 24 hours (Entry 5 & 8, Table 4.). Moreover, a similar decline was also detected for the experiments at 12 hours, of which the yield was slightly reduced to 24% from 33% at the elevated temperature and pressure. Products obtained after reactions were examined to identify the reason for the decline in yield at 12 and 24-hour experiments under optimised conditions. As reported previously, similar changes were observed at higher temperatures and longer reaction times. Additionally, the catalyst amount recovered from the reactor dramatically declined for these experiments, and the liquid sample collected from the reaction turned to dark red compared to one at 2 hours. It was estimated that the catalyst leaching was again the main reason for the colour changes and the reduction of DBU yield for longer reaction times under the chosen conditions. Hence, experiments using different amines were planned for 2 hours under optimised conditions.

Table 4.3 The effect of reaction time on the synthesis of N,N-dibutylurea at optimised reaction conditions

| Entry | Time (h) | Pressure (MPa) | Temperature (K) | Yield (%) |
|--------------|-----------------|-----------------------|------------------------|------------------|
| 1 | 2 | 3 | 423 | 8.6 |
| 2 | | 5 | 453 | 47.5 |
| 3 | 12 | 3 | 423 | 33.2 |
| 4 | | 5 | 453 | 24.3 |
| 5 | 24 | 3 | 423 | 35.6 |
| 6 | | 5 | 453 | 8.7 |

4.1.2.b. Conversion of different amines into urea derivatives


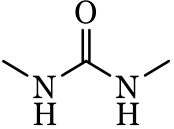
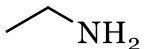
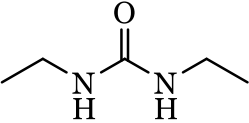
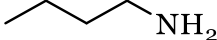
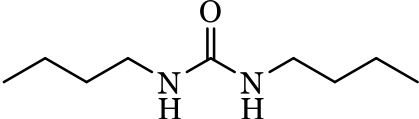
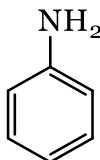
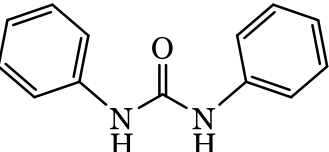
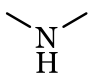
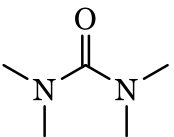
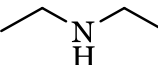
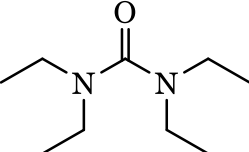
As the procedure herein involves nucleophilic substitution reactions, it is essential to consider the influence of the nucleophilicity of various amines on urea derivatives yield. It is known that amines' nucleophilicity changes with the alkyl/aryl group attached to the nitrogen atom on amines, and also steric hindrance affects the reactivity of amines during the procedure. Therefore, several different amines were used to test these effects and their reactivity for CO₂ utilisation at optimised reaction conditions.

The selection of amines was made to be applicable to the synthesis of a wide variety of urea derivatives since various symmetrical urea derivatives with different attached groups are being used in the industry (Koizumi et al., 2021).

Reaction conditions for the catalytic conversion of different amines were 20 mmol amines, 4 ml DMSO, 2 mmol Fe₂O₃ and 4 MPa CO₂ at 453 K for 2 hours. The results of these experiments are presented in Table 4.4 with a list of amines and their corresponding ureas. First, primary amines with different alkyl groups were tested, where the highest yield of 47.5% was achieved with butylamine. Then it was decreased by shorter alkyl substituents by more than half to 22.9 and 19.7% for N,N-Diethylurea and N,N-Dimethylurea synthesis, respectively. Because these amines were aqueous solutions, another reason for this decline could be the presence of water in those amines, which could severely decrease the yield, as mentioned in Section 4.2.1.a.

Bulky amines, namely aniline and cyclohexylamine, were also examined for CO₂ conversion. Although dry aniline was used herein, it showed almost no reactivity because of the conjugation that reduces the amine's nucleophilicity. This would make aniline more stable than other primary amines; however, this is not enough to explain the really low reactivity observed for aniline, as a steric hindrance was also in effect for this specific example. Another experiment using cyclohexylamine was also conducted to examine the impact of conjugation by comparing results with aniline. As cyclohexylamine does not have any unpaired electrons on its substituents, running the experiment with cyclohexylamine would show the effect of steric hindrance more precisely because they both have similar bulky substituents. Nonetheless, the product obtained from the cyclohexylamine conversion could not be analysed on GC-MS because of the low solubility of N,N-dicyclohexylurea. A number of different solvents alcohols, acetone, and hexane were tested, but no attempt was successful to dissolve for analysis. Thus, cyclohexylamine was excluded from the table. Still, it was expected to have a higher yield than aniline and comparatively lower than other primary amines owing to the steric hindrance reported (Brotzel, 2008).

Table 4.4 The synthesis of 1,3-disubstituted urea from different amines and CO₂ over Fe₂O₃ at optimised conditions (Reaction conditions: 20 mmol amine, 2 mmol Fe₂O₃, 4 MPa CO₂, 4 ml DMSO at 453 K for 2 hours)

| Amine | Urea | Yield (%) |
|--|--|-----------|
| Methylamine  | N,N'-Dimethylurea  | 19.7 |
| Ethylamine  | N,N'-Diethylurea  | 22.9 |
| Butylamine  | N,N'-Dibutylurea  | 47.5 |
| Aniline  | N,N'-Diphenylurea  | <1 |
| Dimethylamine  | Tetramethylurea  | <1 |
| Diethylamine  | Tetraethylurea  | 3.3 |

Finally, reactions with dimethylamine and diethylamine were employed under the same conditions, and it can be seen that the reactivity for secondary amines was also limited. Only a 3% yield was achieved for ethylamine, and less than 1% yield was obtained for methylamine conversion. Although they have stronger nucleophilicity than primary amines, the result for these amines dipped because steric hindrance has more influence on SN₂ reactions than nucleophilicity. Additionally, the difference between the yield at these secondary amines can be explained by the nucleophilicity, as the longer the alkyl group on amines, the greater nucleophilicity (Hart et al., 2007).

4.1.3. Catalyst leaching

Catalyst stability and reusability are vital elements of heterogeneous catalysts as much as their reactivity, as discussed in the literature review. For this aspect, the stability of Fe₂O₃ was monitored along with its reactivity during the experiments. Fe₂O₃ showed great stability against most of the experimental conditions; however, some catalyst leaching was detected, especially at elevated temperatures and longer reaction times. In order to confirm this leaching and assess the effect of these parameters on catalyst stability, AAS analysis was performed using by analysing the iron concentration in the product mixture collected after reactions. Results showed that no iron concentration was detected for a series of experiments by varying time, catalyst, solvent and solvent amount. Changes in the concentration were reported below specifically for temperature, amines, catalysts, and amine amount.

The first examination on catalyst leaching was conducted for the experiments over temperatures as colour changes were detected at higher temperatures (Section 4.2.1.c). The iron concentrations detected from the analysis are given in Figure 4.10. To clarify these changes, products were characterised using AAS to see whether iron was the leading cause of these changes. It can be seen that there were no significant changes in iron concentration at lower temperatures; it was about 1 ppm up to 433 K, and after that, it slightly increased to 2 ppm until 453 K. However, a sharp increase to 17.8 ppm was gained when the temperature was raised to 463 K. This dramatic increase could identify the reason for the colour change reported at elevated temperatures and the decrease in DBU selectivity.

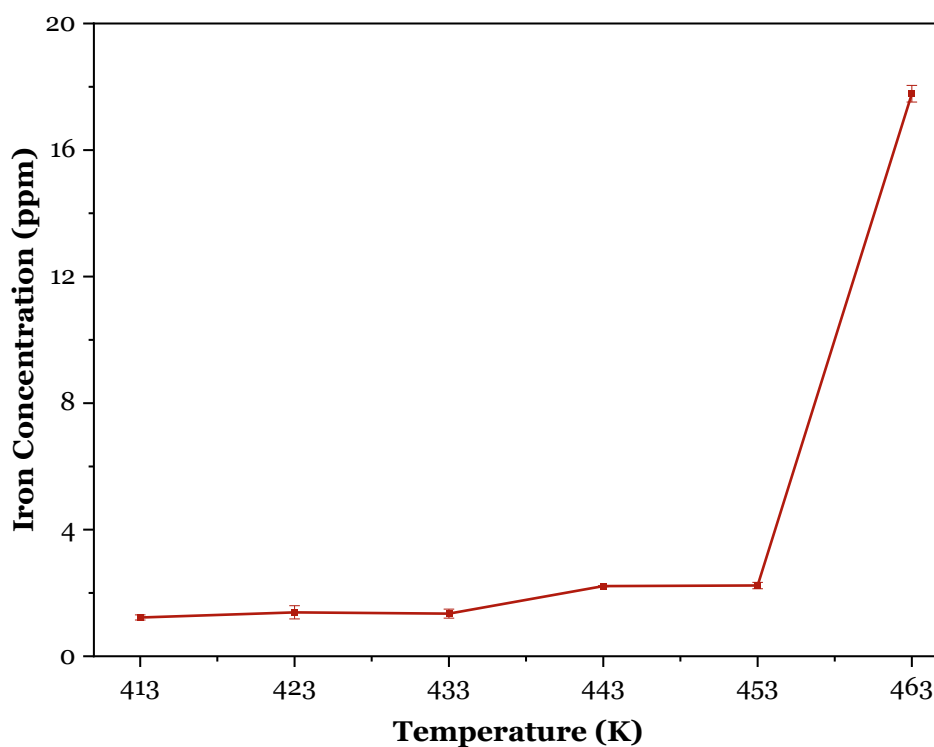


Figure 4.10 The impact of temperature on the iron concentration detected after the reaction (Reaction conditions: 20 mmol butylamine, 2 mmol Fe₂O₃, 3 MPa CO₂, 4 ml DMSO for 2 hours at different reaction temperatures)

The changes in iron concentration over amine amount were also analysed, and the results are given in Figure 4.11, which clearly indicates that amine amount has a significant influence on catalyst leaching. There was trace to no iron concentration detected at 10 mmol butylamine; however, it was slightly increased to about 1 ppm for the experiment with 20 mmol butylamine. Next, the concentration was lifted to 4.7 ppm when the amount doubled from 20 mmol to 40 mmol and then slightly increased to its highest point around 5.6 ppm. This curve appears to be the butylamine conversion trend, as discussed in Section 4.2.1.b. More butylamine conversion might cause the higher iron leaching into the reaction; therefore, this could give an explanation for the dramatic decline in the DBU selectivity mentioned over the amine amount experiments. This clearly shows that butylamine has a substantial impact on catalyst leaching; the more butylamine amount used in the investigation, the more Fe₂O₃ catalyst leached into the reaction mixture.

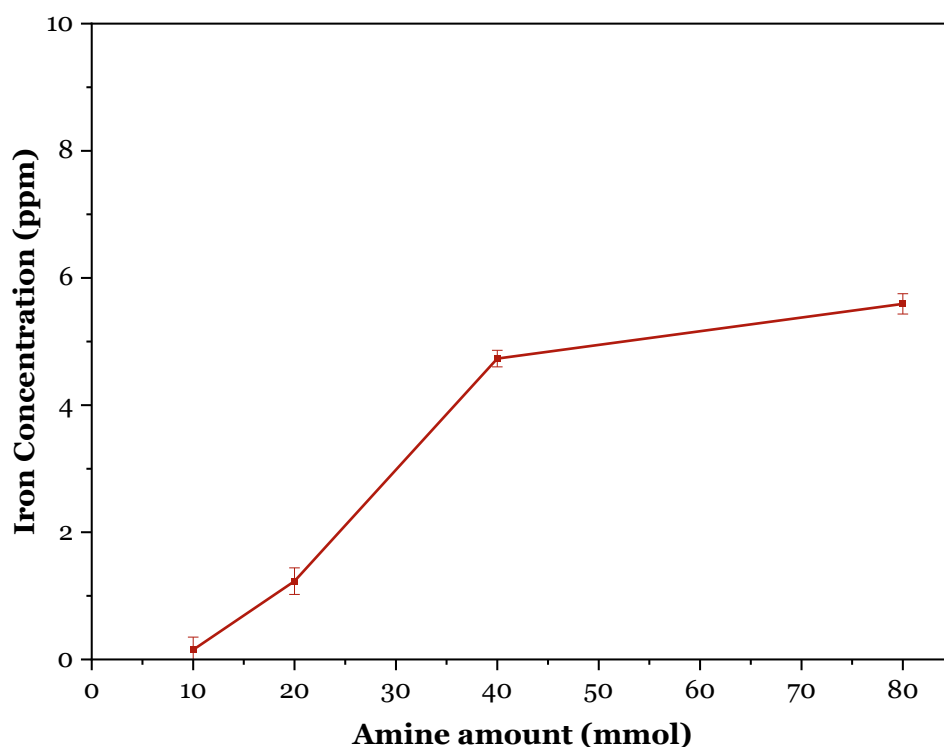


Figure 4.11 Effect of amine amount on iron concentration leached after the reaction (Reaction conditions: 10-80 mmol butylamine, 2 mmol Fe₂O₃, 3 MPa CO₂, 4 ml DMSO at 423 K for 2 hours)

Table 4.5 Iron concentration over different amines

| Entry | Amine | Iron Concentration (ppm) |
|-------|-----------------|--------------------------|
| 1 | Methylamine | 1.1 |
| 2 | Ethylamine | 2.8 |
| 3 | Butylamine | <1 |
| 4 | Cyclohexylamine | 1.7 |
| 5 | Aniline | 1.7 |
| 6 | Dimethylamine | 1.4 |
| 7 | Diethylamine | 4.4 |

After seeing the importance of amine on catalyst leaching, experiments with different amines were also tested in terms of iron concentration leached in the product mixture after reactions (Table 4.5). Butylamine caused less than 1 ppm iron concentration among those amines tested, whilst higher iron concentration was detected for others.

Methylamine and dimethylamine had relatively low catalyst leaching, which were 1.1 and 1.4 ppm, respectively. The iron concentration was then slightly increased to 1.7 ppm for both experiments using aniline and cyclohexylamine. The highest iron concentration detected for amines was 4.4 ppm for diethylamine, right after ethylamine with 2.8 ppm.

Table 4.6 Leached iron concentrations for different iron-based catalysts

| Catalyst | Crystal Structure^a | Basicity (mgCO₂/g_{cat})^b | Iron Conc. (ppm) | Conversion (%) | Selectivity (%) |
|--------------------------------|--------------------------------------|--|-------------------------|-----------------------|------------------------|
| Fe ₂ O ₃ | Rhombohedral | 3.01 | <1 | 76.1 | 62.4 |
| Fe | Cubic | | 2.6 | 67.2 | 61.1 |
| FeO | Cubic | 1.36 | <1 | 66.9 | 58 |
| Fe ₃ O ₄ | Cubic | 1.23 | <1 | 74.7 | 56.8 |

a: crystal structure of the catalysts was found using XRD analysis conducted by Gomez (2017)

b: basicity data was adapted from Hakim et al. (2016)

Finally, experiments with different iron catalysts were tested for catalyst leaching, and it can be said that iron oxides showed superior stability at the reaction conditions tested as almost none to trace iron concentration was detected in product mixtures (Table 4.6). The only noticeable iron concentration at 2.6 ppm was identified for metallic iron compared to other iron-based catalysts.

In addition, the effect of basic sites on catalysts was also monitored by comparing the reactivities of iron-based catalysts with different basicity determined by Hakim et al. (2016). Fe₂O₃ had greater basicity with 3.01 mgCO₂/g_{cat} compared to other iron oxides. Table 4.6 indicates that the higher the basicity, the greater the selectivity for DBU, which shows a similar trend reported by D. Sun et al. (2023). This again confirms the importance of catalyst basicity for urea derivatives synthesis from amines and CO₂.

4.2. Conclusion

In this chapter, urea derivatives were produced from butylamine and CO₂ using an effective and stable Fe₂O₃ catalyst with the promotion effect of DMSO under moderate conditions. In the first part of this chapter, the optimisation of the procedure was determined by varying solvents, solvent amount, temperature, reaction time and reactant amounts, considering the chemical kinetic analysis of the reaction indicated that the reaction rate is linked to reactant concentrations. It was first noticed that solvent greatly influences amine reactivity to maximise the yield as polar aprotic solvents favour the reaction. The peak at 8.6% was obtained for DMSO at that particular reaction conditions over Fe₂O₃. Furthermore, the solvent amount was evaluated where an optimum amount of 4 ml was found after running experiments in the range of 0-8 ml of DMSO. Reactant amount experiments followed this by adjusting CO₂ pressure and butylamine concentration, which indicated that the butylamine amount increased the conversion rate. In contrast, it dramatically dropped the selectivity for DBU at higher concentrations. CO₂ pressure also influenced heavily the yield for DBU where it was gradually increased from just above 3% to almost 10% by the pressure increase between 0.5 and 5 MPa. This confirms the chemical kinetics of the reaction where the concentration of reactants increases the reaction rate, so the optimum amount determined for a greater yield was 20 mmol of butylamine and 4 MPa of CO₂ pressure. In the final step of the optimisation of DBU synthesis, the effect of reaction temperature and time were assessed in the range of 413-473 K at 2-72 hours. It was observed that a rise in temperature was able to promote the reaction up to 47.5% at 453 K, and then the yield started to drop due to the decomposition of the solvent. Reaction time also had a substantial impact on the DBU production, where higher butylamine was converted for longer reaction times. The yield was increased over time up until 12 hours and reached 45%, at which it remained nearly constant for up to 24 hours.

As the importance of the catalyst was discussed several times in the literature review, several different metal oxide catalysts were employed for the catalytic conversion of CO₂ to urea derivatives using several amines at the conditions optimised in the first part. CuO was tested for the first of all metal oxides, and it was observed that it showed extremely low reactivity and stability because of the reaction between DMSO and CuO.

Numerous different supported catalysts on alumina were also used, and they did not show any reactivity towards the DBU as they gave similar results to the absence of the catalyst. Furthermore, it was detected that iron-based catalysts showed great activity for the reaction where Fe₂O₃ was superior by 47.5% yield amongst all the catalysts screened in terms of DBU selectivity. After that, the effect of the Fe₂O₃ amount was evaluated, and it was found that 10% of the butylamine amount was sufficient to maximise the yield. After deciding the catalyst and the right amount for it, the reaction was then run up to 24 at optimised conditions. The DBU yield was dropped by the reaction time compared to previous reactions done for the optimisation experiments, where the yield gradually increased over time. Finally, the reactivity of the catalyst was tested for the conversion of different amines with various substituent groups. It was found that primary amines were highly reactive; however, the bulky group drastically reduced the yield due to steric hindrance. Similarly, experiments performed with secondary amines showed nearly no reactivity even though they have strong nucleophilicity. This demonstrates that steric hindrance has more influence on amines reactivity than nucleophilicity of amines.

In the final part, the stability of Fe₂O₃ was assessed against catalyst leaching, and it showed exceptional stability as much as its reactivity under optimised conditions. The catalyst can be employed for the reaction at the optimised conditions with negligible catalyst leaching. The quantitative analysis of catalyst leaching was also performed using AAS as some loss was detected in the recovered catalyst amount after the reaction under certain conditions. The catalyst was highly stable for the experiments, but some limited leaching was detected due to the decomposition of the solvent at higher temperatures or longer reaction times. It was also reported that amine amount also affected catalyst recyclability where a trace to no iron was detected at the lower concentration of amines. However, iron was identified in the product mixture, particularly at higher amine concentrations. Experiments with iron-based catalysts with different oxidation states also showed that the basicity of the catalyst plays a key role in DBU selectivity. For this reason, it can be concluded that Fe₂O₃ is a great alternative catalyst with superior reactivity and stability for urea derivatives synthesis from amines and CO₂. This research also represents the impact of reaction parameters on catalyst leaching, and quantitative assessment of leached metal in the process.

In the next chapter, core-shell catalysts with different metal oxide core species and silica outer shell were prepared to reduce the catalyst leaching observed in this chapter. The findings gained herein were used as a foundation for Chapter 6 and the comparison of the results obtained from these two chapters will provide a better understanding on the influence of reaction variables.

Chapter 5: Preparation of Silica-Coated Metal Oxide Core-Shell Catalysts

In the previous section, numerous metal oxides were tested for urea derivatives synthesis and it was concluded from the experiments that some of them are highly effective catalysts for the reaction. Nevertheless, they had a major drawback in terms of stability, where the reusability of these heterogeneous catalysts, especially iron and copper-based metal oxides was restricted owing to the catalyst leaching. Therefore, mesoporous silica-coated core-shell catalysts arose considerable attention as an alternative solution for eliminating the disadvantages of these metal oxide catalysts.

Core-shell catalysts are a type of catalyst that has an egg-yolk formation that keeps metal oxide cores in an inert outer shell to enhance the catalyst stability while improving their reactivity by the interaction between core and shell materials. Silica, as an inert, chemically and thermally stable material, was selected for the shell formation of core-shell catalysts (Salgueiriño-Maceira & Correa-Duarte, 2006). In this chapter, a number of different silica-coated metal oxide catalysts were prepared, and their catalytic performances were investigated in the urea derivatives synthesis.

5.1. Experimental methods

The preparation method for core-shell catalysts was selected by combining two different procedures; the details of the procedures can be accessed in Section 2.3. A typical preparation of silica-encapsulated metal oxide core species was performed using 0.5 g CuO, 2 g CTAB, 15 ml water, 7.5 ethyl acetate and 4.2 ml of TEOS under reflux at 80 °C for 4 hours. The prepared particles were then dried at 80 °C (unless stated otherwise) and calcined at 550 C. Analytical methods used to examine prepared catalysts and their catalytical performances are also given in Section 3.3.

The reactivity of the catalysts prepared in this chapter was evaluated in urea derivatives synthesis from butylamine and CO₂ using 20 mmol butylamine, 0.16 g of prepared catalyst, 4 ml of NMP, and 3 MPa CO₂ at 423 K for 2 hours. The liquid product sample obtained after the reaction was analysed using GC-MS for DBU yield and AAS for copper amount leached into the reaction media during the reaction.

5.2. Results and discussion

5.2.1. Core-shell catalyst preparation

First attempts for core-shell catalyst synthesis were made via the sol-gel method reported by El-Nahhal et al. (2016) using a template; however, silica particles aggregated to each other, and no silica encapsulation was observed around the metal oxide cores. Therefore, a novel preparation method was proposed by combining two different approaches to address the problem. As reported, ethyl acetate was used to reduce the hydrolysis rate of TEOS to facilitate silica precipitation on the template placed around active core species (Wang et al., 2017). Since this is a new method, optimisation was required to find the right conditions for a uniform and complete shell preparation.

In the first stage of this chapter, copper (II) oxide particles were encapsulated at different reaction conditions with silica nanospheres to prepare a catalyst reactive for DBU synthesis and stable against active core leaching. Prepared catalysts were then employed in the reaction of urea derivatives from butylamine and CO₂ using NMP to assess their reactivity and stability for preventing CuO leaching. NMP was chosen as a solvent because no side reactions occurred between NMP and butylamine, as reported earlier for DMSO, DMF and acetonitrile. In the final part, the prepared core-shell catalysts prepared with uniform shell formation and high stability against leaching were analysed regarding their morphological and crystal structure as well as the elemental compositions of the catalysts.

5.2.1.a. The effect of surfactant on shell formation

The importance of surfactants in core-shell catalyst preparation has been broadly studied in the literature as discussed in the literature review. The surfactant takes a significant role between the solvent and the particles to prevent the aggregation of metal oxide species by providing better dispersion. In addition, it acts as a template that surrounds the metal oxide core species and allows the shell material to encapsulate the core. This provides a porous structure to the shell and boosts the accessibility of active core species (El-Nahhal et al., 2016).

In order to evaluate the effect of surfactant on silica formation for core-shell catalysts, silica-encapsulated particles were prepared using different surfactant amounts with 0.5 g CuO, 15 ml deionised water, 7.5 ethyl acetate, 1.2 ml ethanolamine and 4.2 ml TEOS under reflux at 80 °C for 4 hours. A set of experiments were also conducted using different surfactants, CTAB (cationic) and Pluronic P123 (non-ionic) in order to monitor their impact on the morphology of the particles by comparing with the catalyst prepared without any surfactant. The prepared catalysts were then employed in DBU synthesis from butylamine and CO₂ to examine their reactivity and stability for catalyst leaching in urea derivatives synthesis.

Results gained from the experiments are listed in Table 5.1 and it can be seen from the table that leached copper concentration in the reaction media after the reaction was minimum at 3 ppm by the catalyst without any surfactant and then gradually increased with the rise of CTAB amount. The copper concentration detected from the experiment conducted using the catalyst prepared with 0.0063 g of CTAB was 8 ppm and raised to 36 ppm for 2 g of CTAB, with a small increase in the DBU yield from 6.4 to 8%. This increase in catalyst leaching can be explained with the porosity effect of the surfactant, since more surfactant could facilitate more porous shell formations. Consequently, the porosity improvement on silica improved the accessibility to copper (II) oxide core species to catalyse the reaction. On the other hand, further addition of CTAB amount to 4 g declined the yield to 5% when the leached copper concentration reached its highest point at 48 ppm. In addition to cationic surfactant CTAB, a non-ionic surfactant Pluronic P123 was used to evaluate the effect of surfactant types on silica shell formation. By the use of Pluronic P123 the highest yield at 8.2% was achieved with relatively moderate catalyst leaching.

Table 5.1 Surfactant effect on catalyst stability and reactivity towards DBU synthesis (Reaction conditions: 20 mmol butylamine, 0.16 g catalyst, 3 MPa CO₂, 4 ml NMP at 423 K for 2 hours)

| Entry | Surfactant | Surfactant Amount (g) | Copper Conc. (ppm) | DBU Yield (%) |
|-------|---------------|--------------------------|-----------------------|------------------|
| 1 | None | - | 3 | 6.7 |
| 2 | CTAB | 0.0063 | 8 | 6.4 |
| 3 | CTAB | 0.125 | 11 | 7 |
| 6 | CTAB | 1 | 12 | 7 |
| 7 | CTAB | 2 | 36 | 8 |
| 8 | CTAB | 4 | 48 | 5 |
| 9 | Pluronic P123 | 2 | 22 | 8.2 |

The morphology of prepared catalysts was then investigated using SEM and TEM to assess the changes in the performance of catalysts. Figure 5.1 shows SEM images of the samples with various surfactants with different amounts. It can be seen from the figure that the catalyst prepared without any surfactant was relatively large, and no spherical species were detected (Figure 5.1-a). The appearance of the particles was also different from the ones prepared using CTAB and particles prepared with no surfactant had a rigid structure due to the lack of porosity. The particles with low surfactant amounts had a powder-like formation, whereas spherical species can only be seen after 0.25 g of CTAB. Although homogeneous silica spheres were obtained for 2 g CTAB, copper leaching was increased as aforementioned. This contrast can be explained with the SEM image of Figure 5.1-e; some silica spheres were broken, which lessened the stability and caused an increase in the leaching of copper (II) oxide into the reaction media.

The core-shell catalyst prepared by surfactant Pluronic P123 was also imaged and showed similar morphology to the one without any surfactant in terms of particle structure. They had very large rigid crystal-like formations and needed to be ground before using in the DBU synthesis. Although the catalyst prepared using this surfactant did not show any silica spheres on SEM images, they were analysed by TEM together with others to monitor the morphology of the particles in detail.

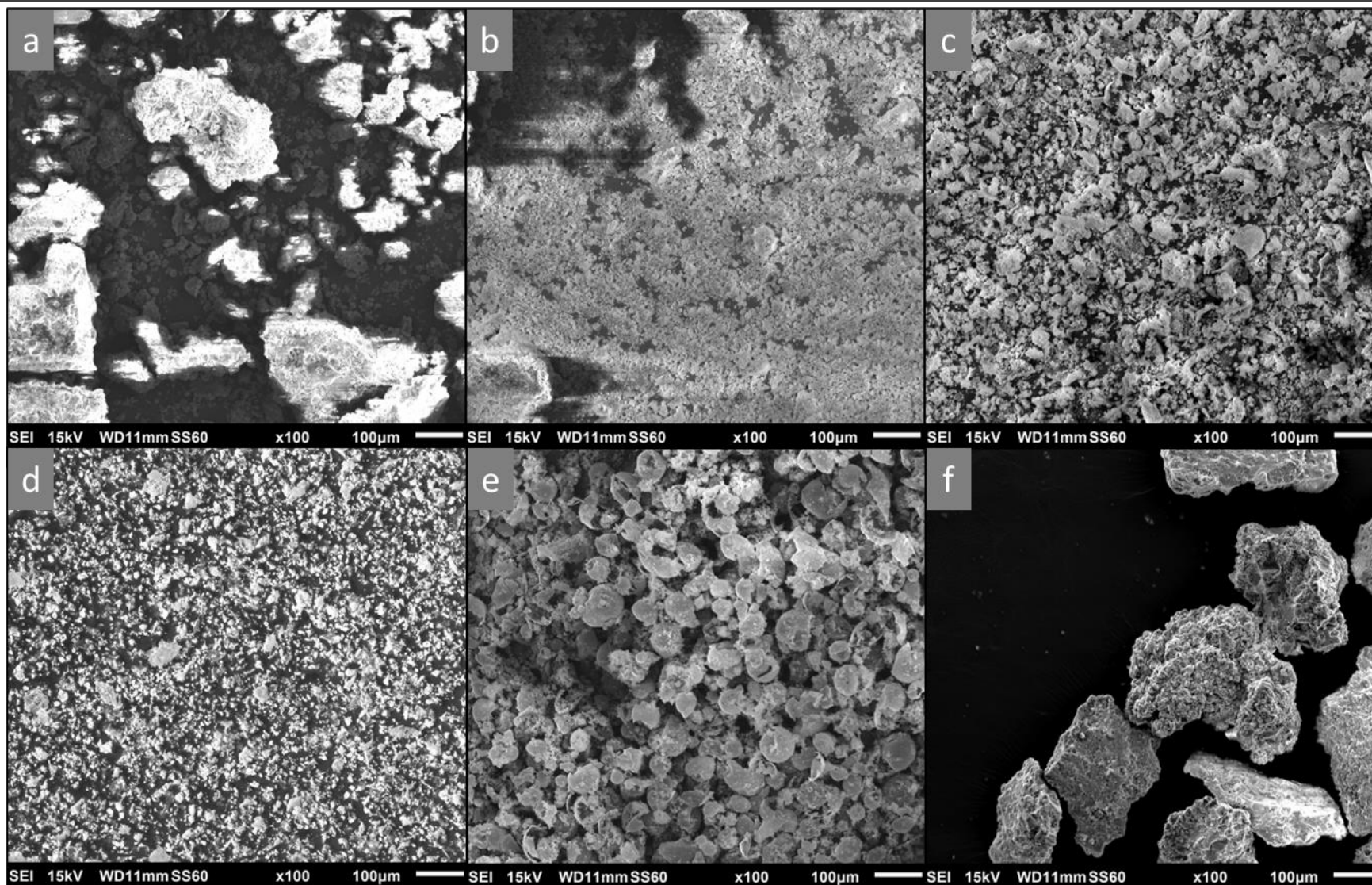


Figure 5.1 SEM images of prepared CuO@SiO₂ using different surfactants: a) No surfactant, b) 0.0063 g of CTAB, c) 0.25 g of CTAB, d) 1 g of CTAB, e) 2 g of CTAB, f) 2 g of Pluronic P123

TEM images given in Figure 5.2 showed that the use of surfactant successfully produced egg-yolk formation whilst the catalyst without any surfactant was relatively small where no shell formation was observed. Yet, CTAB facilitated apparent phase differences for core and shell, proving that the silica shell was accomplished (Figure 5.2-a&b). In contrast with SEM images, Pluronic P123 also gave core-shell structure; species were relatively small compared to those with CTAB, though. Particles prepared using Pluronic P123 and no surfactant had a rigid structure as mentioned above; TEM images confirm the difference in their morphology compared to CTAB ones as it enhanced the porosity.

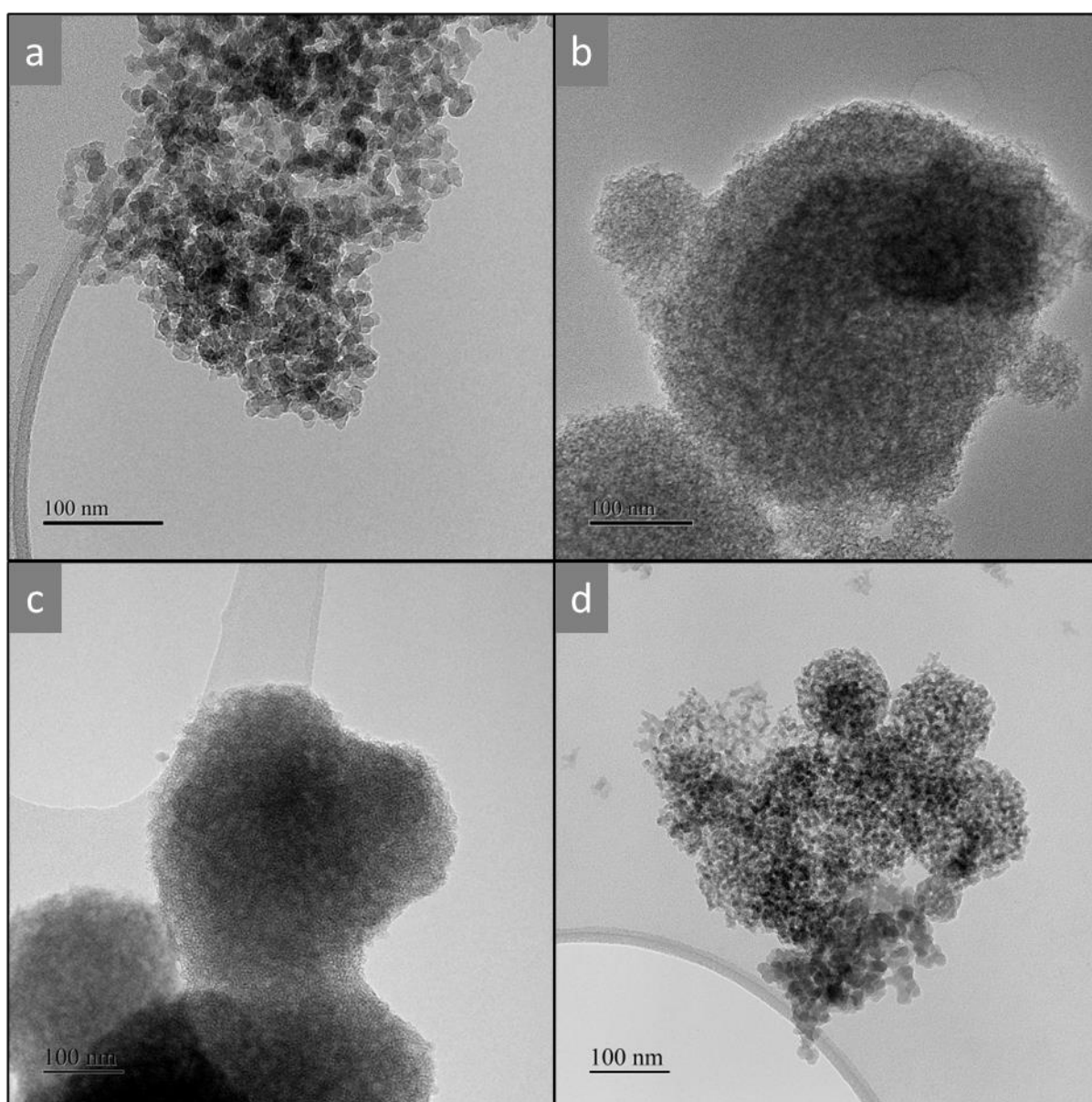


Figure 5.2 TEM images of prepared CuO@SiO₂ using different surfactants: a) No surfactant, b) 0.25 g of CTAB, c) 2 g of CTAB, d) 2 g of Pluronic P123

In conclusion, CuO@SiO₂ prepared without any surfactant showed the best performance on catalyst stability where the detected copper concentration was 3 ppm; however, the DBU yield noticeably dropped. Although Pluronic P123 had the highest yield, particles prepared using this surfactant was rigid and needed extra step before use. On the other hand, CTAB enabled to produce silica spheres after a certain amount even though some shell deformation was observed in the SEM images (Figure 5.1-e). It was proposed that this deformation can be avoided by the optimisation of the preparation conditions, and copper leaching could be restricted with a uniform and stable shell formation. Hence, CTAB was selected as a surfactant due to the less rigid particle formation in order to have better control over the porosity and thickness of the silica shell, thereby 2 g of CTAB was used for subsequent experiments.

5.2.1.b. Solvent influence on shell formation

The impact of solvents on the catalyst preparation was also investigated as they greatly influence the particle size and silica shell thickness (Joshi et al., 2017). Since 2 g of CTAB was selected for the surfactant amount, the conditions of the preparation method were varied in order to prevent the aforementioned shell deformation. Experiments with different water amounts were conducted using 0.5 g CuO, 2 g CTAB, 7.5 ml ethyl acetate, 1.2 ml ethanolamine and 4.2 ml TEOS under reflux at 80 °C for 4 hours, and prepared particles were then used for urea derivatives synthesis. Water with various amounts together with a water-ethanol mixture was tested to evaluate the effect of solvent, and the results are given in Table 5.2. It can be seen from the table that adding more water increased the catalyst leaching from 36 to 61 ppm, whereas DBU yield slightly dropped to 7.3% from 8%. The presence of ethanol in the preparation method also showed a similar copper concentration at 58 ppm when the yield remained almost stable. A couple more experiments were conducted using less than 15 ml of water, but the agitating was limited due to the lack of enough solvent in the system. It was also hard to recover samples after the reaction; therefore, they were excluded from the table.

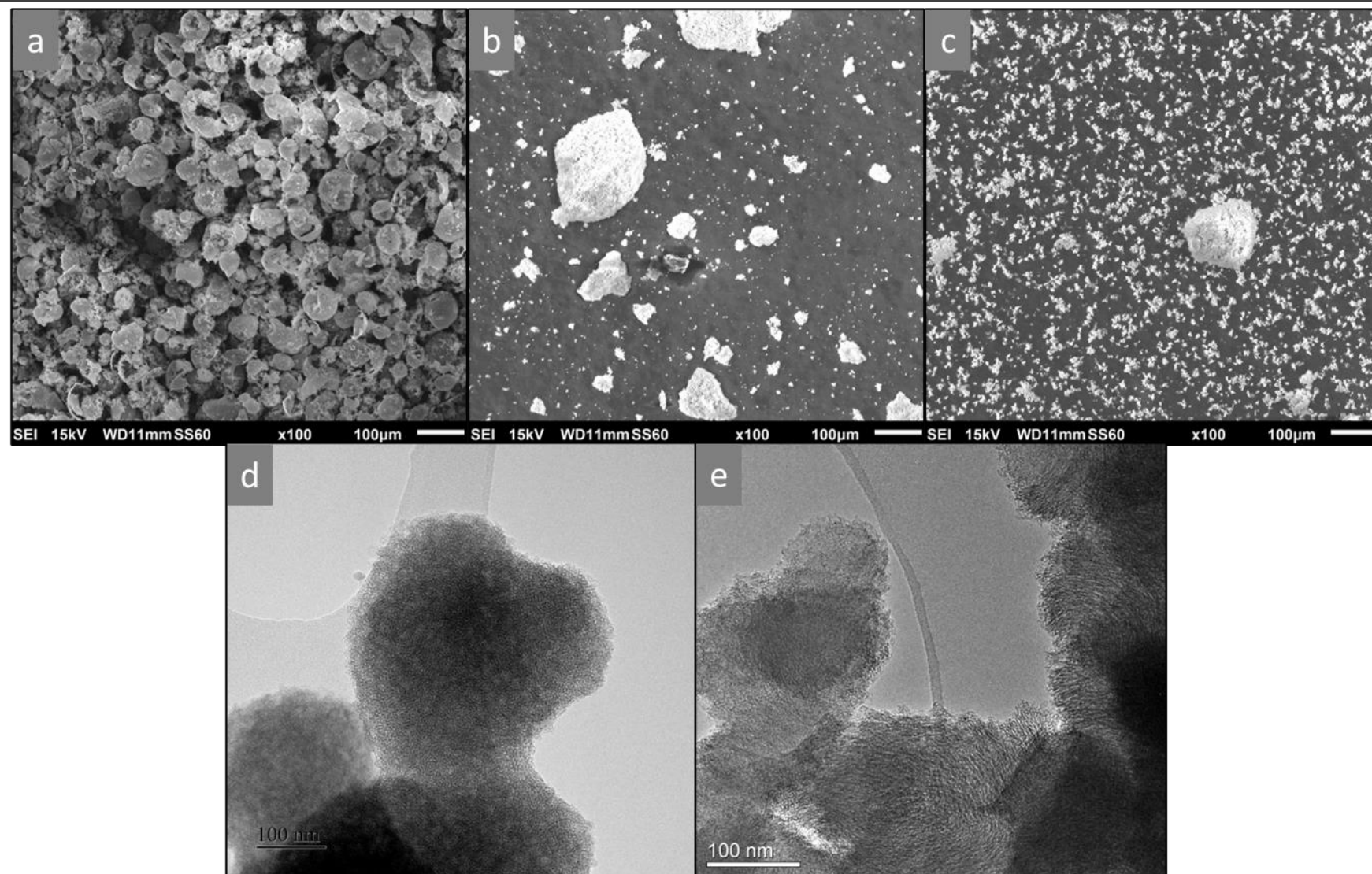


Figure 5.3 SEM images of core-shell catalysts prepared by different solvent amounts: a) 15 ml water, b) 60 ml water, c) 15 ml water : 15 ml ethanol; TEM images of CuO@SiO₂ prepared using 15 ml of water (d) and 60 ml of water (e)

Table 5.2 Solvent influence on catalyst stability against CuO leaching and reactivity for DBU synthesis (Reaction conditions: 20 mmol butylamine, 0.16 g catalyst, 3 MPa CO₂, 4 ml NMP at 423 K for 2 hours)

| Entry | Solvent | Solvent Amount (ml) | Copper Conc. (ppm) | DBU Yield (%) |
|-------|---------------|------------------------|-----------------------|------------------|
| 1 | Water | 15 | 36 | 8 |
| 2 | Water | 60 | 61 | 7.3 |
| 3 | Water&Ethanol | 15:15 | 58 | 7.9 |

The morphological analysis of the nanoparticles prepared using different solvents was conducted after drying and calcination steps via SEM, and the outcome of that analysis is given in Figure 5.3 (a-c) where SEM images demonstrate that increasing the amount of solvent in the system dramatically changes its appearance. A homogenous silica coating was achieved using 15 ml of water, whereas the excess amount drastically changed the particle size and morphology. It is believed that more solvent lowered the chance for the silica precursor to precipitate on copper oxide core species, so homogenous coating was not achieved. This would also explain the increase in copper concentration at higher solvent amounts. As better silica-coating was obtained at a lower water amount, less copper (II) oxide was leached into the reaction mixture. Since it was reported by Joshi et al. (2017) that ethanol significantly influenced the preparation of homogenous and well-structured silica, it was mixed with water at the same ratio, and relatively larger core-shell catalysts were produced together with fine silica nanoparticles. It is believed that the main reason for this difference is that Joshi et al. (2017) used only ethanol in their experiments.

Finally, the difference in the texture was analysed in detail using TEM, and Figure 5.3 (d&e) shows catalysts synthesised by two different water amounts. It can be deduced from the images that the solvent amount had an impact on particle morphology, especially the texture of the silica coating. This change can be seen on the edges of particles; the catalyst prepared using 15 ml of water had smooth circle edges, whilst 60 ml of water caused some deformation on the prepared silica shell. The differences spotted in SEM and TEM images can explain the dramatic increase in catalyst leaching from 36 to 61 ppm. Hence, 15 ml of water was selected as the optimum solvent for the preparation of CuO@SiO₂ nanoparticles.

5.2.1.c. Effect of acetate amount on shell formation

The acetate amount was also investigated as it was reported that using the right amount of ethyl acetate is important for producing uniform silica coating (Wang et al., 2017). Experiments with a range of ethyl acetate amounts from 0 to 15 ml were performed using 0.5 g CuO, 2 g CTAB, 15 ml water, 1.2 ml ethanolamine and 4.2 ml TEOS under reflux at 80 °C for 4 hours, and the outcomes in terms of DBU yield and leached copper concentration are given in Table 5.3.

The catalyst prepared without any ethyl acetate had the highest copper concentration after the reaction and showed the lowest reactivity with a 6.6% DBU yield. The detected copper concentration was then gradually reduced by the ethyl acetate amount. It was first dropped from 50 to 36 ppm with 7.5 ml acetate and then decreased further to 21 ppm at 15 ml. On the other hand, the DBU yield fluctuated with the increase in ethyl acetate amount, where it raised to 8% and then slightly dropped to 7.7% at the highest amount of ethyl acetate.

SEM analysis was then performed for morphological analysis to evaluate the reduction in the catalyst leaching (Figure 5.4). The presence of ethyl acetate made a noticeable difference for silica coating, where a better encapsulation was achieved compared to the catalysts prepared with no ethyl acetate experiments where mainly small silica particles and some large bulk species were detected. Liu et al. (2012) stated that the presence of ethyl acetate slows down the hydrolysis rate of TEOS, enabling silica to precipitate on copper (II) oxide core species. The addition of ethyl acetate facilitated a shell formation; hence, the spherical structure can be noticeably seen in SEM images (Wang et al., 2017). It was also noticed that the excess ethyl acetate caused an irregular aggregation of silica, as seen in Figure 5.4-c.

Table 5.3 The influence of ethyl acetate amount on catalyst reactivity and stability
(Reaction conditions: 20 mmol butylamine, 0.16 g catalyst, 3 MPa CO₂, 4 ml NMP at 423 K for 2 hours)

| Entry | Ethyl Acetate Amount (ml) | Copper Concentration (ppm) | DBU Yield (%) |
|-------|---------------------------|----------------------------|---------------|
| 1 | - | 50 | 6.6 |
| 2 | 7.5 | 36 | 8 |
| 3 | 15 | 21 | 7.7 |

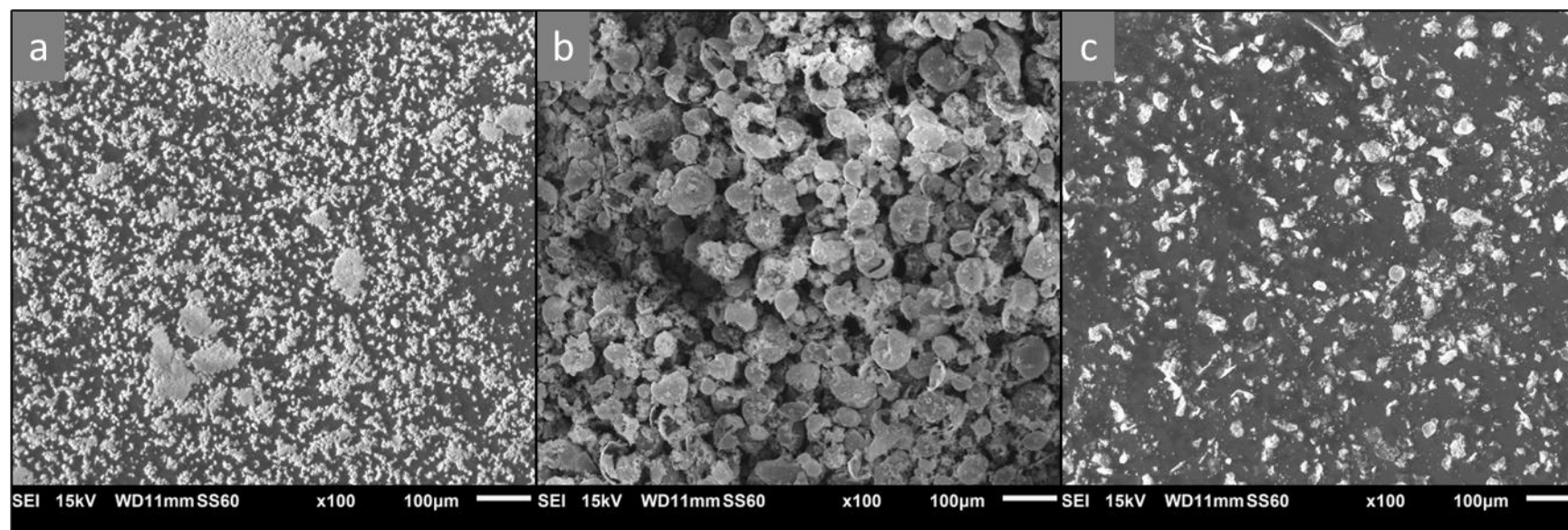


Figure 5.4 SEM images of silica-coated nanoparticles at various ethyl acetate amounts: a) None, b) 7.5 ml, c) 15 ml

To understand the DBU yield drop at a higher ethyl acetate amount, particles prepared with different amounts were examined using TEM (Figure 5.5). The increased ethyl acetate amount almost doubled the silica thickness from around 50 to 100 nm. As stated above, the higher the ethyl acetate amount, the slower the TEOS hydrolysis to allow growth on shell thickness. Having a thicker silica shell improved the stability by strengthening the core-shell interaction. In contrast, it reduced the reactivity due to the limited access to the active core species (Tian et al., 2022). That showed parallel results with the literature and highlighted the importance of control on shell thickness for core-shell catalysts.

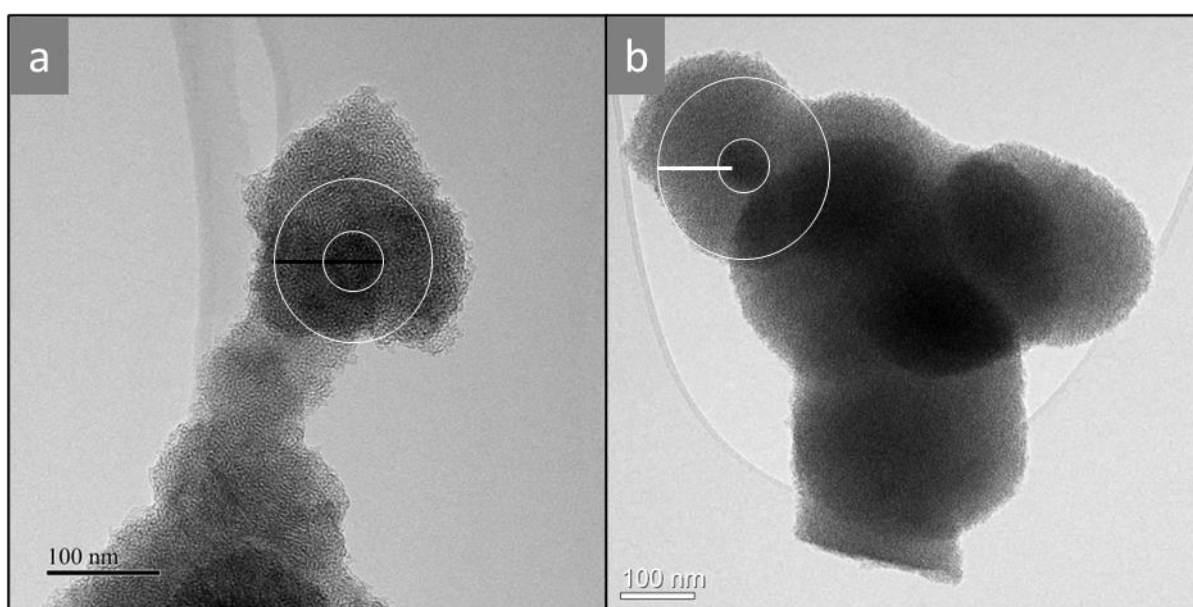


Figure 5.5 TEM images of prepared CuO@SiO₂ particles at several acetate amounts: a)7.5 ml, b)15 ml

In conclusion, experiments indicated the importance of ethyl acetate on silica precipitation rate and the significance of finding the optimum amount for preventing any aggregation of particles. Consequently, 7.5 ml of ethyl acetate was selected for the following experiments, as it demonstrated the highest reactivity with a uniform silica coating.

5.2.1.d. The influence of precipitation agent on mesoporous silica synthesis

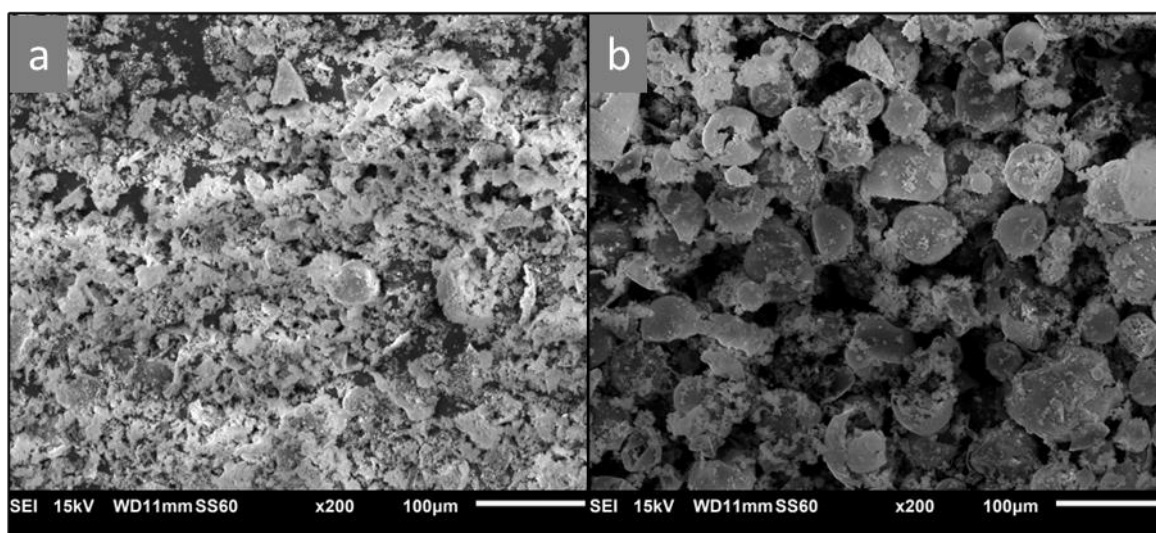
In the Stöber process, silica is mainly synthesised by the hydrolysis of TEOS using ammonium hydroxide as a catalyst (Stöber et al., 1968). It was also reported that pH considerably influences particle size, and the polycondensation reaction can be accelerated by higher pH (Greasley et al., 2016). In the preliminary experiments, ammonium hydroxide was used as a catalyst for silica synthesis. However, the copper oxide particles were dissolved by the presence of ammonium hydroxide as copper makes a complex with ammine ligands to form $[\text{Cu}(\text{NH}_3)_4]^{+2}$ (Lane & McDonald, 1946). Thus, ethanolamine was selected as a substitute for ammonium hydroxide as it proved the ability to catalyse the reaction (Meier et al., 2018).

A set of catalysts were prepared using different ethanolamine amounts to assess its effect as a precipitation agent on silica formations using 0.5 g CuO, 2 g CTAB, 15 ml water, 7.5 ml ethyl acetate and 4.2 ml TEOS under reflux at 80 °C for 4 hours. The first thing noticed during the synthesis was minimal silica precipitation from the lack of ethanolamine, which showed similar results to Stöber et al. (1968). The sample recovered after filtration were predominantly black, indicating that only copper oxide was filtered. That also explains the dramatic change in copper concentration in Table 5.4, as copper oxide cores with the absence of silica shell had the highest yield and catalyst leaching. The addition of ethanolamine dropped copper concentration noticeably from 56 to 36 ppm. The DBU yield was at the highest point of 9% for the catalyst without any ethanolamine because it was mainly copper (II) oxide due to the lack of silica precipitation. The yield on DBU synthesis was then dropped to 8% for 1.2 ml and even further to 6.2% with the addition of 0.6 ml ethanolamine while the catalyst leaching remained almost stable. In order to examine the decrease in the yield at lower ethanolamine concentrations, SEM analysis was performed to monitor the changes in the structure of the particles.

Table 5.4 Effect of ethanolamine amount on silica preparation for stability and reactivity (Reaction conditions: 20 mmol butylamine, 0.16 g catalyst, 3 MPa CO₂, 4 ml NMP at 423 K for 2 hours)

| Entry | Ethanolamine Amount (ml) | Copper Concentration (ppm) | DBU Yield (%) |
|-------|--------------------------|----------------------------|---------------|
| 1 | - | 54 | 9 |
| 2 | 0.6 | 38 | 6.2 |
| 3 | 1.2 | 36 | 8 |

Figure 5.6 shows that better encapsulation of copper oxide cores was achieved at higher ethanolamine amounts, although some spherical species were observed for lower amounts. A similar effect was also stated by Stöber et al. (1968) where the particle size of prepared silica was increased with ammonia concentrations. Since both catalysts demonstrated similar stability against leaching, it can be concluded that partial silica coating was achieved for both experiments. However, a higher ethanolamine concentration facilitated more homogeneous silica sphere formation with better TEOS hydrolysis as seen in the figure. Therefore, a greater reactivity was achieved for the particles prepared using 1.2 ml of ethanolamine due to the improved core-shell interactions discussed in the literature review, thus 1.2 ml of ethanolamine was selected as an optimum amount for the subsequent experiments.

**Figure 5.6** SEM images of prepared silica-coated copper (II) oxide nanoparticles using various ethanolamine amounts: a) 0.6 ml, b) 1.2 ml

5.2.1.e. Effect of synthesis and drying temperatures on silica shell formation

A series of experiments were performed to determine the impact of temperature changes at the synthesis and drying stages on silica encapsulation. As reported, the elevated synthesis temperature dropped the particle size; experiments were conducted at room temperature and 80 °C for the examination using 0.5 g CuO, 2 g CTAB, 15 ml of water, 1.2 ml ethanolamine and 4.2 ml of TEOS under reflux for 4 hours (Park et al., 2002). No substantial differences were detected in the structure of the particles synthesised at different temperatures. Nevertheless, some irregularities in terms of particle size were detected: particles synthesised at room temperature were irregular, whereas higher temperature produced rather homogenous species. Park et al. (2002) stated that particle size distribution became narrow by temperature as it raises the nucleation rate, which is considered the primary reason for well-formed silica coating.

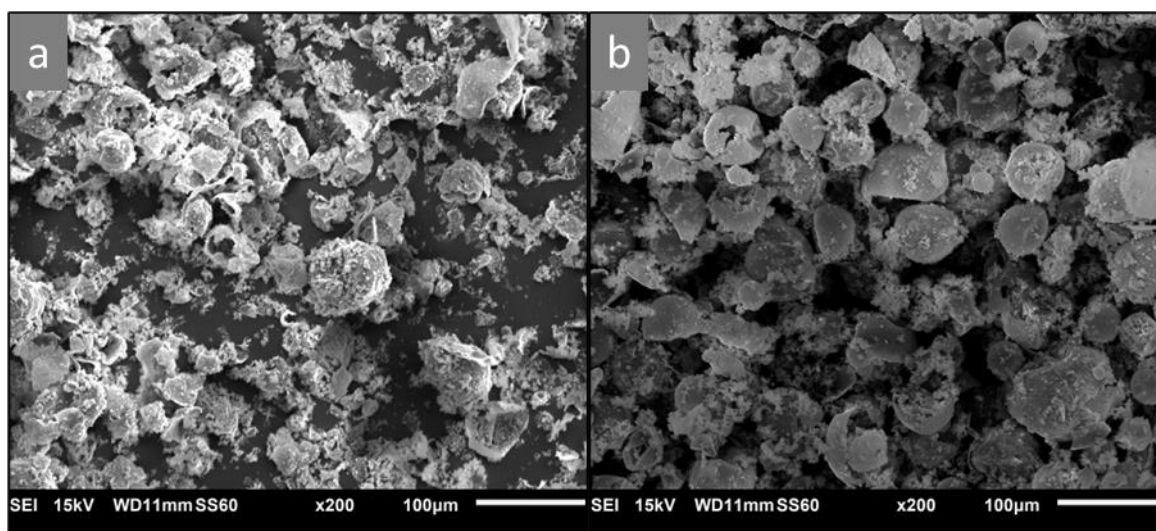


Figure 5.7 The synthesis of CuO@SiO₂ core-shell catalysts at room temperature (a) and 80 °C (b)

The performance of prepared catalysts was also evaluated for the DBU synthesis from butylamine and CO₂, and the outcome of the experiments can be seen in Table 5.5. Particles produced at a higher reaction temperature indicated superior catalyst stability and reactivity. Not only the yield for DBU was slightly enhanced from 7.1 to 8%, but also the copper oxide leaching was halved. This is attributed to a shell collapse detected in Figure 5.7, which reveals that more shell deformation happened at a lower temperature. Thus, catalyst stability was radically diminished, causing more copper oxide to leach.

Table 5.5 The influence of synthesis temperature on catalyst stability and reactivity (Reaction conditions: 20 mmol butylamine, 0.16 g catalyst, 3 MPa CO₂, 4 ml NMP at 423 K for 2 hours)

| Entry | Ageing Temperature (°C) | Copper Concentration (ppm) | DBU Yield (%) |
|-------|----------------------------|-------------------------------|------------------|
| 1 | 25 | 70 | 7.1 |
| 2 | 80 | 36 | 8 |

In addition to the synthesis temperature, the drying temperature of the procedure was also evaluated since Rahman et al. (2008) showed the drying effect on silica particles. Particles prepared using 0.5 g CuO, 2 g CTAB, 15 ml of water, 1.2 ml ethanolamine and 4.2 ml of TEOS under reflux at 80 °C for 4 hours, were collected after filtration and divided into two for drying at two different temperatures. Half of the sample was left at room temperature for drying overnight, and the rest was placed in the dryer oven at 80 °C overnight. Dried catalysts were employed for DBU synthesis after the calcination at the same condition. It is apparent from Table 5.6 that the stability was significantly improved where the concentration of copper was reduced from 46 to 28 ppm at elevated drying temperature when the reactivity nearly remained.

Table 5.6 Effect of drying temperature on catalyst leaching and DBU yield (Reaction conditions: 20 mmol butylamine, 0.16 g catalyst, 3 MPa CO₂, 4 ml NMP at 423 K for 2 hours)

| Entry | Drying Temperature (ml) | Copper Concentration (ppm) | DBU Yield (%) |
|-------|----------------------------|-------------------------------|------------------|
| 1 | 25 | 46 | 8.3 |
| 4 | 80 | 28 | 8.1 |

The morphology of the synthesised particles at two different drying temperatures was also examined by SEM. Figure 5.8 exhibits the images obtained from the analysis where the structure was slightly changed by the temperature. It is obvious that silica nanospheres were aggregated with fine bulk silica particles at a lower temperature. The elevated temperature enhanced the stability even though both species have broken silica coating. It is believed that drying samples at room temperature was unable to

remove all the water inside, so it created more cracks on the shell at the calcination step discussed in detail below. Subsequently, prepared particles were dried at 80 °C for the following experiments because more copper oxide leaching was detected for the samples dried at room temperature.

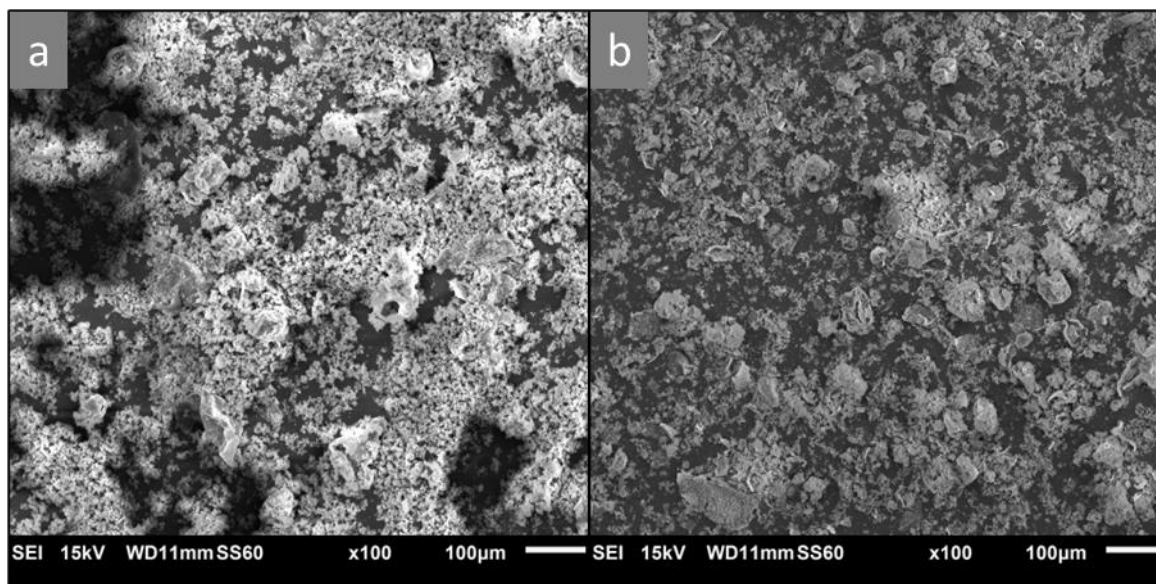


Figure 5.8 Samples morphology dried at room temperature (a) and 80 °C (b)

5.2.1.f. The effect of calcination temperature increase rate on shell formation

In the last part of the optimisation process for the synthesis of silica-coated copper oxide core-shell catalysts, the influence of calcination temperature ramp rate was controlled on the shell pattern. Since a higher copper concentration was detected above for the samples dried at room temperature, the calcination rate influence on the shell formation needed to be studied as well. Additionally, a study on the calcination effect for silica particles was held excessively before. It was stated that the control of calcination temperature broadly influences shell formation (Finsel et al., 2019). Since the template sits between the core and shell species, they need to pass through the shell at their removal stage. It is expected that template removal at higher ramp rate damage the silica shell structure, so it is essential to have control on the calcination ramp rate.

Nanospheres were prepared at the optimised reaction conditions where 0.5 g CuO, 2 g CTAB, 15 ml of water, 1.2 ml ethanolamine and 4.2 ml of TEOS were stirred under reflux at 80 °C for 4 hours and the samples divided into five after the drying at 80 °C overnight. All samples collected after the drying step were placed in a calcination oven set to 550 °C with various temperature increase rates: 0.5, 1, 2, 4 and 8 °C/m. After reaching the set temperature, samples were held for an hour. Later, samples were used for the DBU synthesis, and the changes in copper concentration and DBU yield over ramp rate are shown in Table 5.7.

Table 5.7 Catalyst stability and activity over different calcination ramp rates (Reaction conditions: 20 mmol butylamine, 0.16 g catalyst, 3 MPa CO₂, 4 ml NMP at 423 K for 2 hours)

| Entry | Calcination Rate (°C/m) | Copper Conc. (ppm) | DBU Yield (%) |
|--------------|------------------------------------|-------------------------------|--------------------------|
| 1 | 0.5 | 22 | 8.4 |
| 2 | 1 | 36 | 8 |
| 3 | 2 | 66 | 8.3 |
| 4 | 8 | 71 | 8.2 |

The first thing noticed from the table is that a similar DBU yield between 8.2 to 8.4% was achieved for all reactions. The minimum catalyst leaching was achieved for 0.5 °C/m, and it was increased with the calcination ramp rate to its peak of 71 ppm for 8 °C/m. SEM images show no considerable differences in the samples' morphology after the calcination, except for the species around the nanospheres before and after the calcination (Figure 5.9). This material is attributed to the surfactant used, as it disappeared after the calcination and only left formed CuO@SiO₂ particles. Another minor change spotted on the images was some deformation of the samples for 0.5 °C/m, which was attributed to heat exposure for a long time at their calcination step which was around 18 hours.

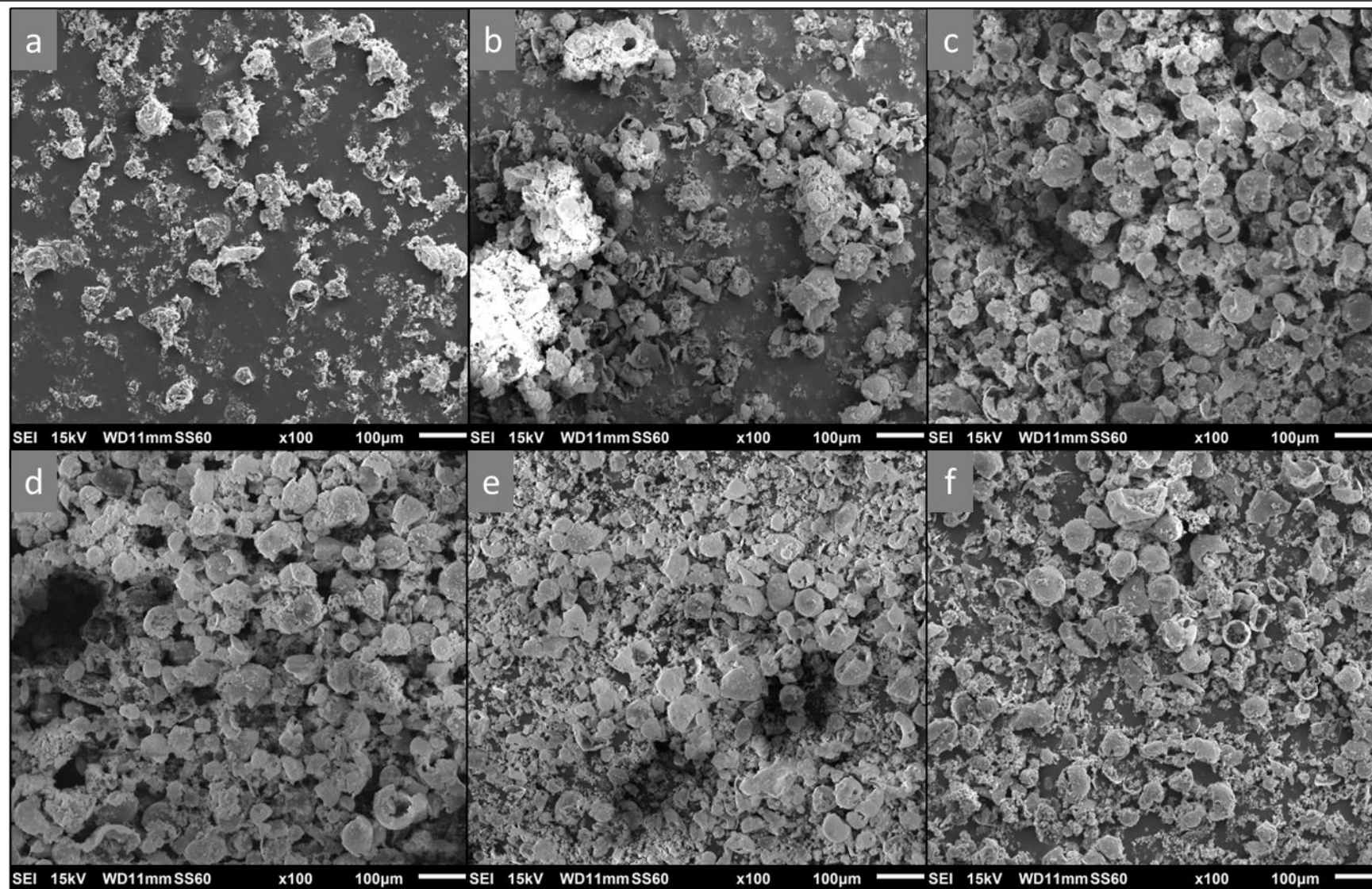


Figure 5.9 SEM images of catalysts before (a) and after the calcination with a ramp rate of 0.5 (b), 1 (c), 2 (d), 4 (e) and 8 °C/m (f)

For a details analysis on the morphology of the particles, TEM analysis was performed on the prepared samples calcined with the ramp rates of 1 and 4 °C/m (Figure 5.10). The analysis was mainly focused on the edge of the particles as no apparent changes were observed on SEM analysis. Samples calcined with the ramp rate of 1 °C/m had clearer and more smooth spherical edges, whereas some disorder was observed for the samples at a faster ramp rate. That kind of deformation on the shell structure could dramatically demolish the catalyst stability and cause more leaching for copper oxide species, as seen in Table 5.7 where the detected copper concentration was gradually increased with the calcination ramp rate. Similarly, this could explain the reason for having higher copper concentration from the catalysts dried at room temperature where the silica shell of the particles prepared without going through a correct drying step, might be deformed in the calcination phase, owing to the removal of any left water inside the samples.

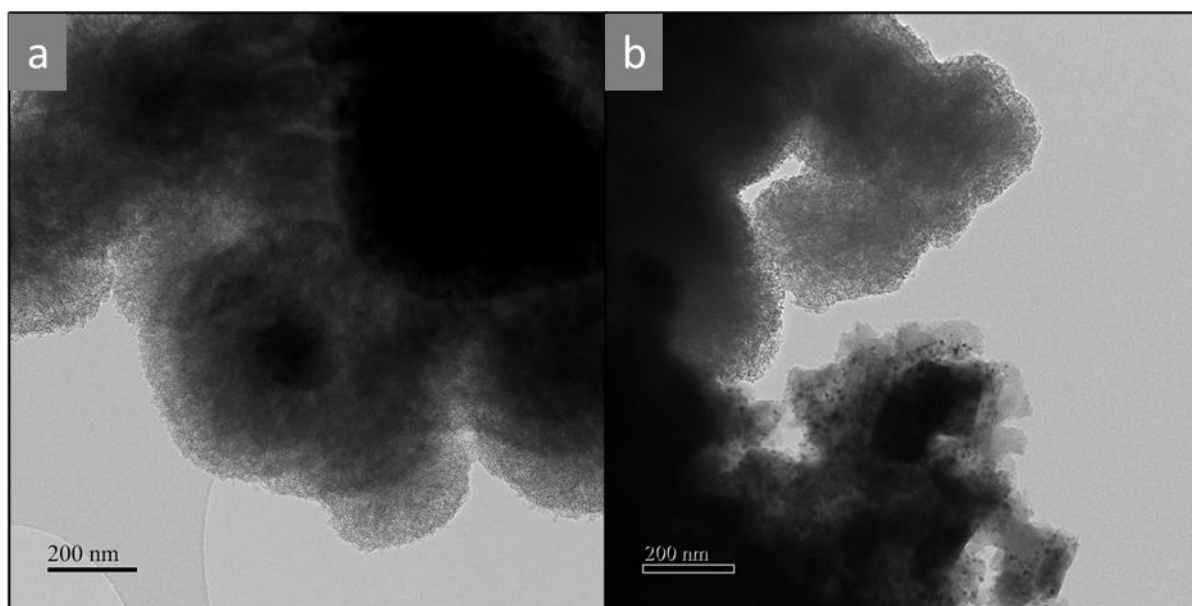


Figure 5.10 TEM images of samples with a calcination temperature ramp rate of 1 °C/m (a) and 4 °C/m (b)

Experiments showed the importance of thermal conditions on silica synthesis along with the other parameters of the reaction conditions. Consequently, findings from the optimisation experiments were then utilised to produce silica-coated metal oxide core-shell catalysts that to be employed in CO₂ conversion into DBU from butylamine.

5.2.2. Analysis of core-shell nanoparticles

Catalysts synthesised at the optimised reaction conditions were finally analysed by FT-IR, XRD, SEM and TEM and their catalytic performances were evaluated below.

5.2.2.a. Template removal assessment

For the preparation of CuO@SiO₂ particles, a sol-gel method was used with a template to enable silica coating to cover the active core copper oxide species. After assessing a couple of different templates with various amounts in the optimisation reactions, CTAB was employed to produce mesoporous silica-coated particles. It was implied that the calcination of samples removed the templates in Section 5.2.1.f, and an FT-IR analysis was conducted to confirm their removal (Figure 5.12).

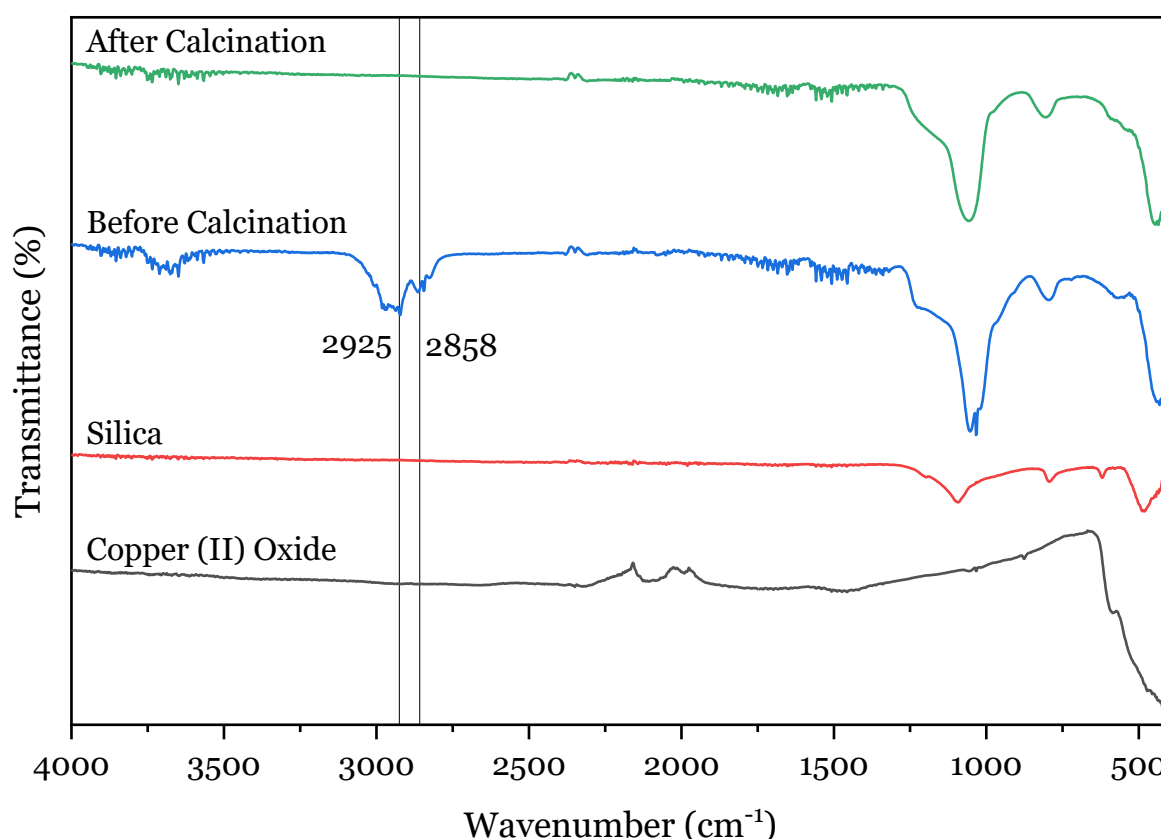


Figure 5.11 FT-IR spectrums of prepared core-shell catalysts before and after the calcination

Figure 5.11 demonstrates the FT-IR spectrum of synthesised CuO@SiO₂ nanoparticles before and after the calcination, along with fresh copper oxide and silica. No significant changes were observed for both samples below 1500 cm⁻¹. The vibration peak at 1060

cm^{-1} seen in both spectrums can be attributed to Si-O-Si stretching vibration bonds of silica, proving the successful production of silica for the particles. Cu-O bonds typically give peaks at 480 and 530 cm^{-1} ; however, it is hard to differentiate the peaks before 500 cm^{-1} as both silica and copper oxide have peaks at that area (El-Nahhal et al., 2016). Nevertheless, the vibration peak at 530 cm^{-1} can be seen in both particle spectra, confirming that CuO was maintained after the synthesis. The only difference reflected from the spectrums was peaks at 3100-2750 cm^{-1} , which were wiped out after the calcination. Peaks at 2858 and 2925 belonging to C-H bonds were observed only for the sample before the calcination, whereas it can be noticed that they disappeared after the calcination of core-shell catalysts (Keshavarz et al., 2020). This proves the complete elimination of the template from the samples by the calcination and supports the findings from the calcination experiments.

5.2.2.b. Compositional analysis of prepared core-shell catalysts

The elemental composition of the synthesised nanoparticles at optimised reaction conditions was analysed by SEM-EDS. Figure 5.12 shows the elemental composition of the CuO@SiO₂ particles synthesised using 0.5 g CuO, 15 ml water, 2 g CTAB, 7.5 ml ethyl acetate and 4.2 ml TEOS at 80 °C for 4 hours under reflux. The SEM-EDS analysis proves the successful precipitation of silica, as silicon and copper elements were detected at the examination.

Catalyst loading was also measured using SEM-EDS at several TEOS amounts. The amounts of TEOS were calculated to produce theoretical copper oxide loadings of 12.5, 25, 50, and 75 mol%, and the final loadings are shared in Table 5.8. It is revealed from the table that one-fifth of the copper oxide particles were lost during the synthesis process. This reduction can be attributed to drawbacks observed in the production where some particles stuck to the flask wall and could not be collected. Also, some of the CuO was dissolved during the agitating and caused a colour change in the filtrate, which was minimal compared to the ones obtained by the use of ammonium hydroxide.

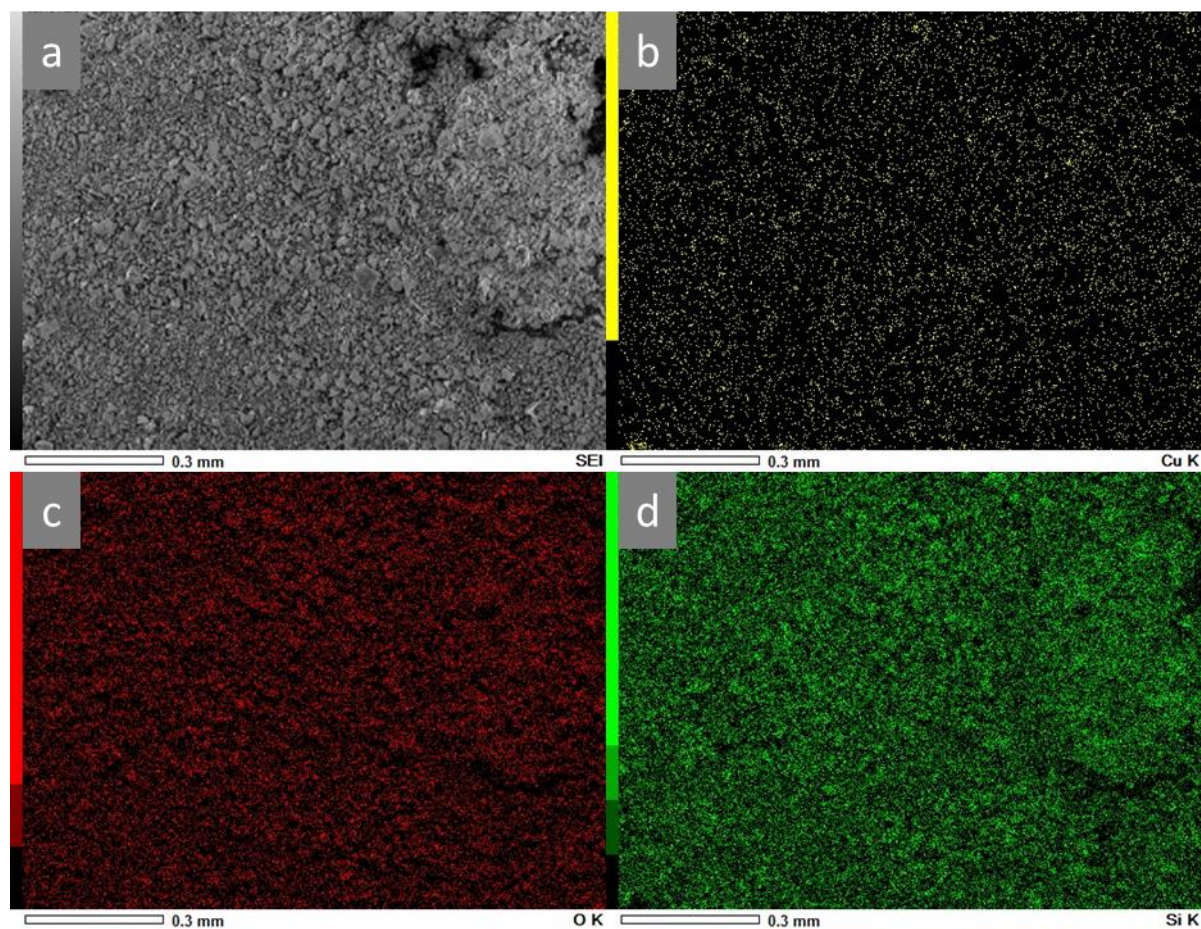


Figure 5.12 SEM-EDS analysis of silica-coated copper (II) oxide catalysts: a) SEM image of particles, b-d) images for EDS mappings of particles

Particles synthesised with different TEOS amounts were then used in DBU synthesis from butylamine and CO_2 in order to assess the influence of copper oxide loading on catalyst stability and reactivity. There is a clear trend in Table 5.8 for catalyst leaching, copper concentration dropped from 75 to 5.5 ppm when the CuO loading decreased. 0.16 g of catalysts were used for all experiments, so it was expected to have a higher concentration at higher loading. Still, another experiment was performed to monitor the ability of the silica shell against catalyst leaching by the use of 0.032 g bulk copper (II) oxide, which is the calculated amount of CuO in the core-shell catalysts with 20 mol% loading. The copper concentration was 33 ppm with a 5.7% DBU yield, whereas 20 mol% catalysts yielded 7.9% DBU with a more than 40% decrease in catalyst leaching.

Table 5.8 Copper (II) oxide loading of catalysts over various TEOS amount and their catalytic performances (Reaction conditions: 20 mmol butylamine, 0.16 g catalyst, 3 MPa CO₂, 4 ml NMP at 423 K for 2 hours)

| Entry | TEOS Amount (ml) | CuO Loading (mol%) | Copper Conc. (ppm) | DBU Yield (%) |
|-------|------------------|--------------------|--------------------|---------------|
| 1 | 0.47 | 60 | 75 | 7.3 |
| 2 | 1.4 | 40 | 36 | 8 |
| 3 | 4.2 | 20 | 19 | 7.9 |
| 4 | 9.7 | 10 | 5.5 | 7.1 |

Catalytic activities were improved over increased loadings where the DBU yield was only 7.1% for the experiment with 10 mol% CuO@SiO₂ whilst it slightly raised to around 8% for both 20 and 40 mol% loaded catalysts. After that point, a small decrease was measured for 60 mol% nanoparticles of which yielded 7.3% DBU after the reaction, which was just above the reaction with 10mol% loaded catalyst. Thus, it can be easily said that silica coating of copper oxide particles not only improves their catalyst stability but also enhances reactivity.

5.2.2.c. Morphological analysis of core-shell catalysts

The morphology of the particles prepared at optimised conditions with different copper oxide loadings was also examined by SEM and TEM. Figure 5.13 displays the SEM images of nanospheres with 20 to 60 mol% copper oxide loading catalysts. It is noticed from the figure that the silica encapsulation was successfully achieved at higher TEOS amounts: 20 mol% CuO@SiO₂ showed superior silica shell formation, whereas almost all nanoparticles were broken for 60 mol% loadings. It is assumed that the amount of TEOS used to synthesise 60 mol% catalysts was insufficient to facilitate adequate silica to cover all the metal oxides. This silica shell deformation can also help to explain the summit point in copper concentration shown in Table 5.8, as the lack of complete silica coatings in 60 mol% particles diminished their stability. The mesoporous silica capsulation can also be deduced from the figure for 40 mol% samples; however, a number of nanospheres with deformed silica shells still can be seen. Even though 20 mol% CuO@SiO₂ showed greater encapsulation, the leaching was still observed because there were very few nanospheres with a broken silica shell.

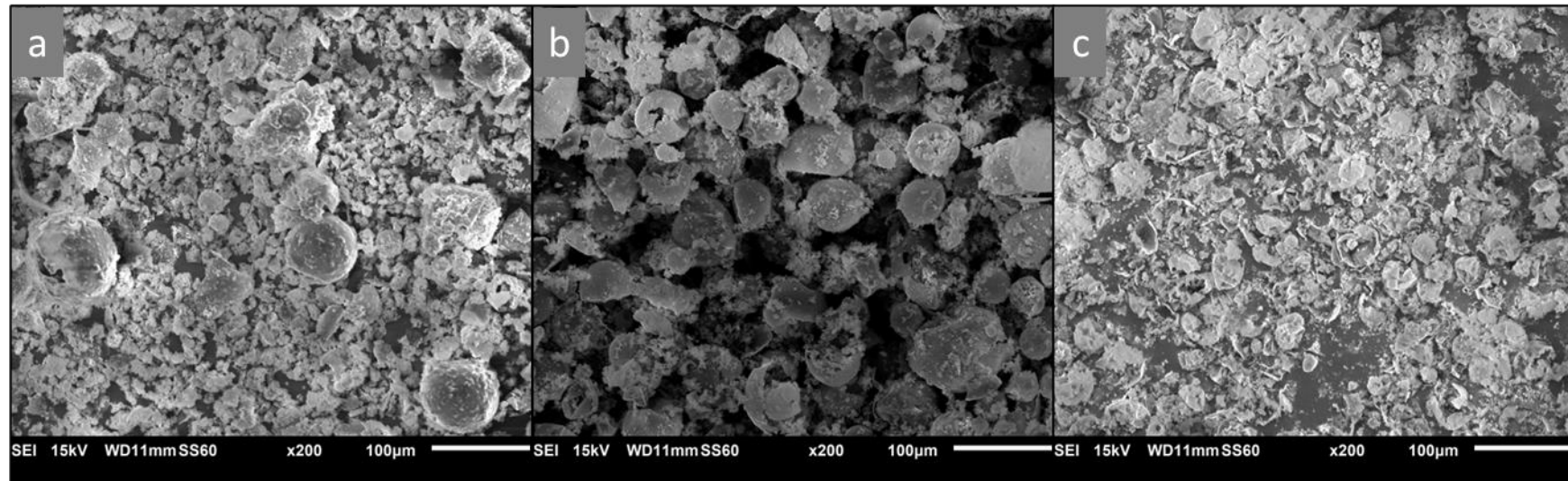


Figure 5.13 The morphological analysis of samples with several copper oxide loadings: a) 20 mol%, b) 40 mol%, c) 60 mol%

Since similar DBU yield was achieved for both 20 and 40 mol% catalysts, further investigation was made to address this superior activity accomplished by 20 mol%. Finsel et al. (2019) indicated that more TEOS amount facilitates a thicker silica shell, and this was confirmed with TEM analysis (Figure 5.14). Silica shell thickness was increased with the TEOS amount; 50, 100 and 200 nm thickness was measured for the catalysts loadings with 10, 20 and 40 mol%, respectively. The deformation of silica coating for 60 mol% nanospheres observed in SEM images was also detected by TEM analysis, where mesoporous silica structures had some irregularity compared to others. The particle size was also dramatically decreased and caused smaller particles than expected. Since the silica species collapsed with the lowest TEOS amount, it produced samples tinier than those with 20 mol% loadings.

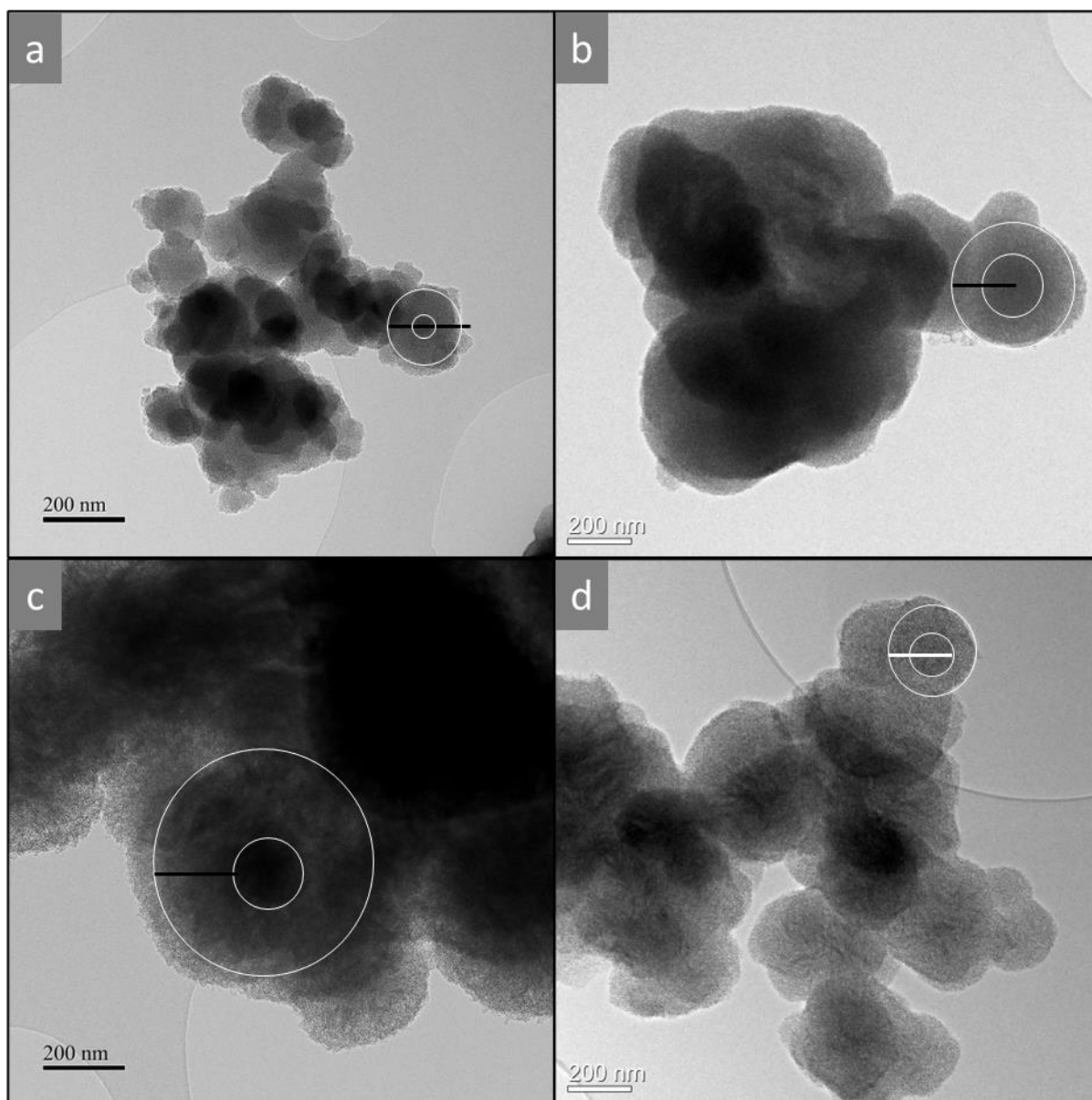


Figure 5.14 Particle size changes on mesoporous silica-coated copper oxide particles over TEOS amount: a) 9.7, b) 4.2, c) 1.4, and d) 0.47 ml

The reactivity of core-shell catalysts is heavily influenced by the thickness of the shell material, as discussed in 5.2.1.c. Having a thicker silica shell around the active core material declined their reactivity as a result of limited accessibility. Hence, 40 mol% catalysts with 200 nm shell thickness had similar DBU yield compared to 20 mol% nanospheres that have 100 nm. Therefore, an equivalent yield was achieved with a lower copper oxide loading.

5.2.2.d. The crystal composition of catalysts

The crystal structure of catalysts prepared via the sol-gel method was examined by XRD. For the synthesis, bulk copper (II) oxide was coated with silica particles, so no changes were expected in the particle structure. Diffraction peaks seen in Figure 5.15 at 35 and 39° approved the maintaining of the monoclinic phase for CuO, confirming that no changes were obtained after silica coating (El-Nahhal et al., 2016). There were also no shifts for diffraction peaks with different copper (II) oxide loading; however, changes in peak intensity were noticed, which could be associated with the particle size.

A broad peak between 15° to 25° belonging to amorphous silica can be seen for the catalysts with higher silica amounts. The peak was at its highest height for 10 mol% loadings and reduced by increased copper oxide loading as expected. Thus, this showed that silica coating was successfully achieved without having any changes in the crystal structure of core species.

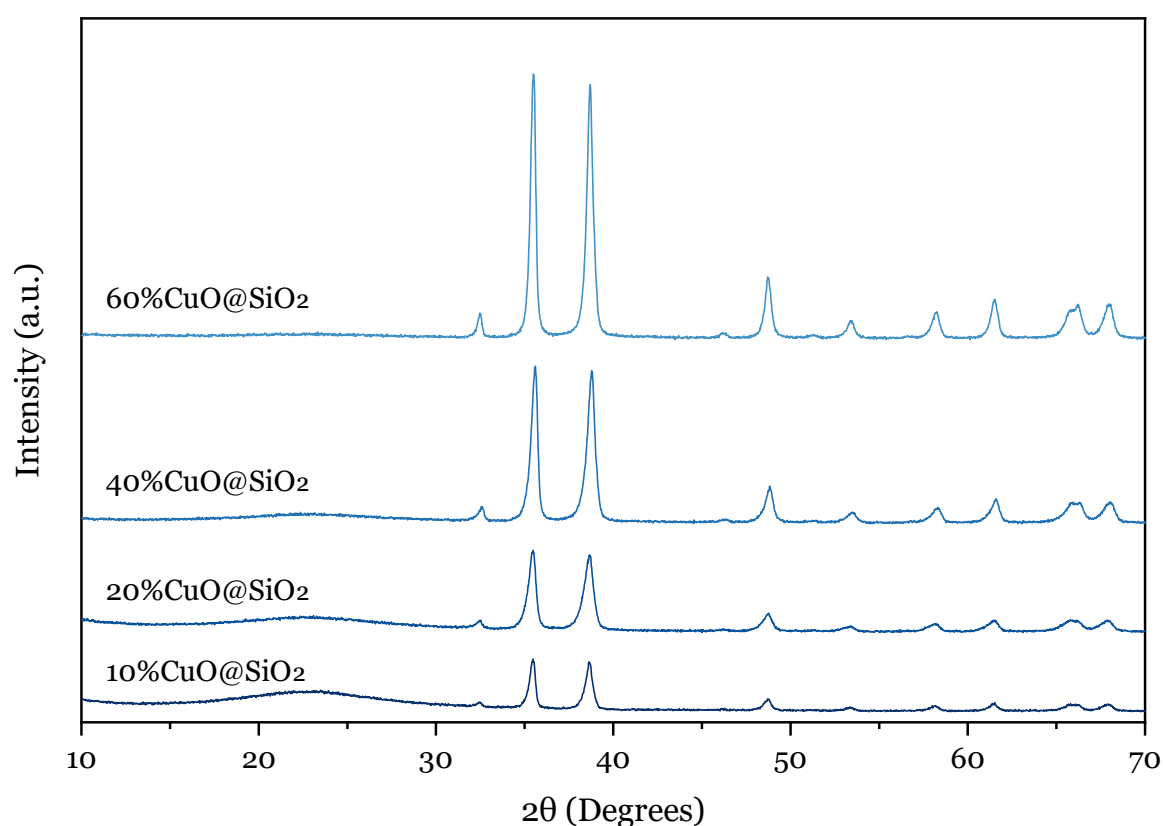


Figure 5.15 XRD patterns of core-shell nanoparticles with different loadings

5.2.2.e. Synthesis of different metal oxide core nanoparticles

After having well-capsulated nanospheres, a number of various metal oxides were then tested as a core species to prepare silica-coated core-shell catalysts. ZnO-based core-shell catalysts were prepared with 20 mol% whilst the ones with Fe₂O₃ and Fe₃O₄ were synthesised with 40 mol% loadings. Their morphological analysis was conducted using SEM to investigate the silica coating on different metal oxides. Figure 5.16 shows the silica-coated copper oxide and zinc oxide core-shell catalysts with the same active species. It can be seen from the figure that silica nanospheres were successfully produced for both experiments. However, particles prepared using zinc oxide exhibited more deformation on silica shells whilst this deformation stayed limited for copper oxide species.

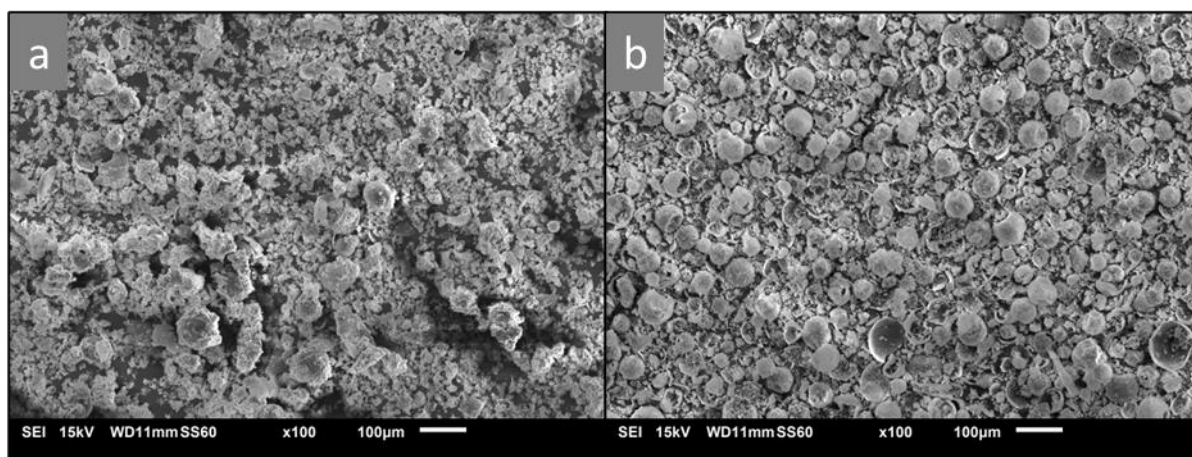


Figure 5.16 SEM images of core-shell catalysts with different metal oxides: a) CuO, b) ZnO

The encapsulation of copper oxide and zinc oxide cores was then analysed by TEM to see the phase difference between the active core and silica shell. Figure 5.17 shows the TEM images for both catalysts and it can be said that silica coating was achieved for both metal oxides. On the other hand, some empty silica species belonging to the broken silica nanospheres were also detected, as seen in the SEM image for zinc oxide. Additionally, a change in the silica shell thickness was also detected for the catalysts with different metal oxide core species. It was about 100 nm for particles with copper oxide, whereas it dropped to 50 nm for zinc oxide.

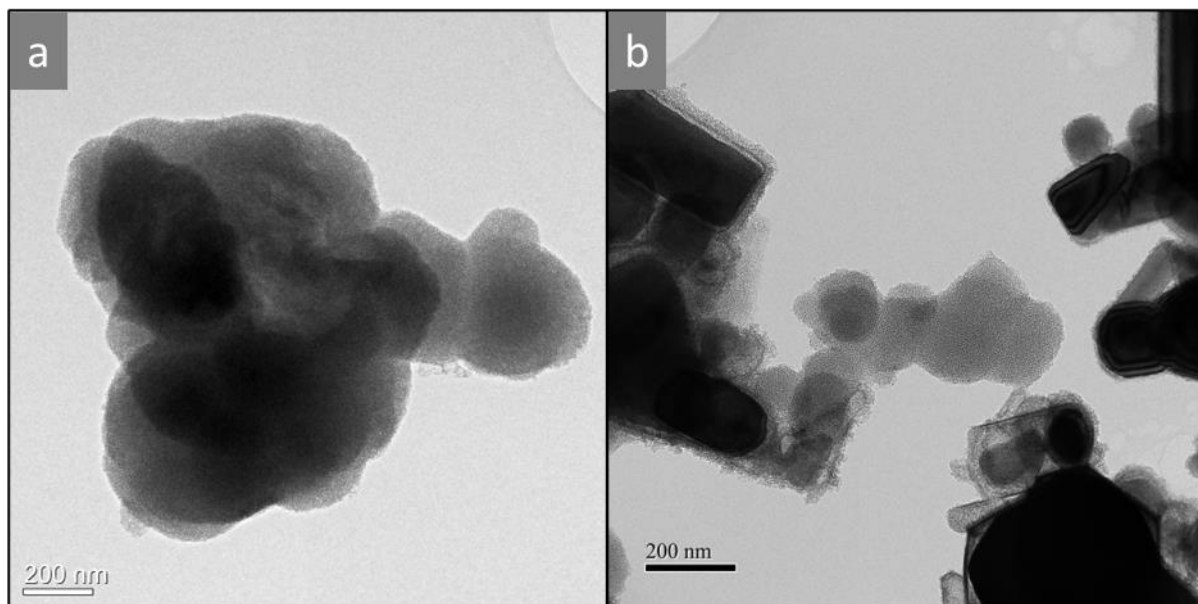


Figure 5.17 TEM images of different metal oxide cores coated with mesoporous silica: a) CuO, b) ZnO

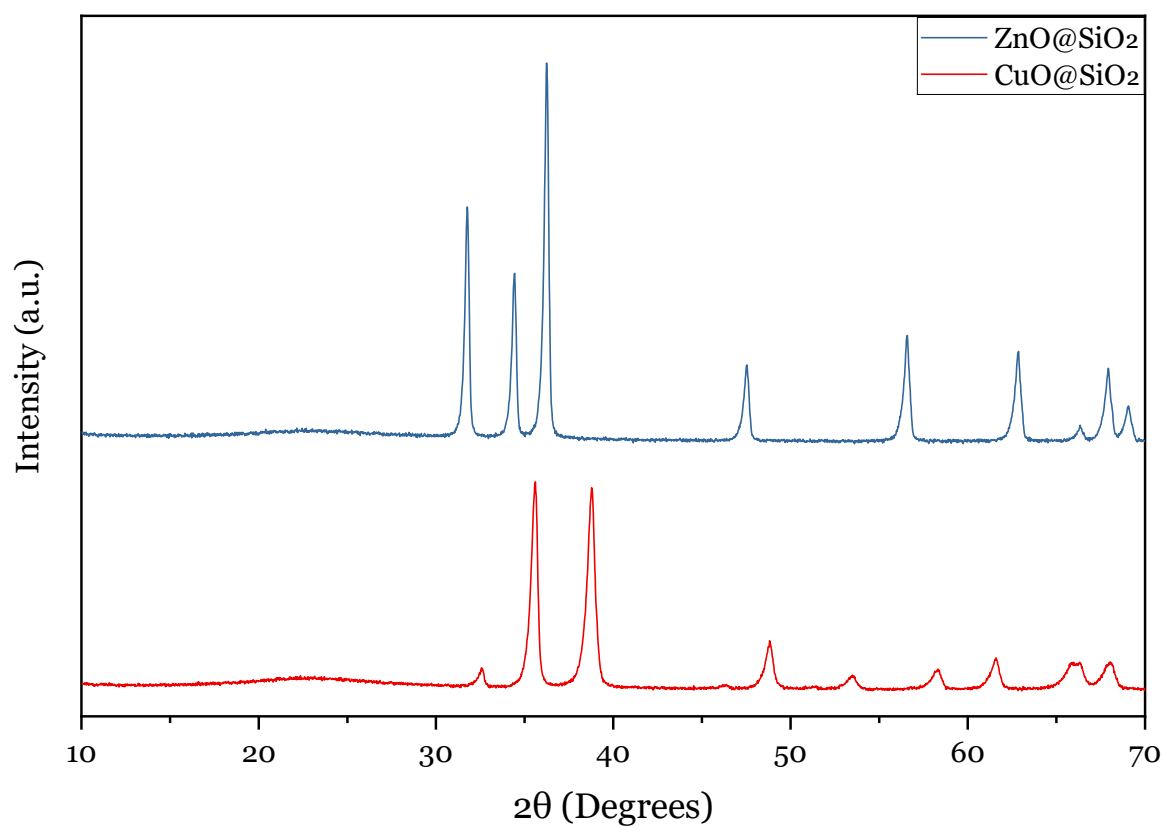


Figure 5.18 XRD pattern of CuO@SiO₂ and ZnO@SiO₂ core-shell catalysts

XRD analysis was then performed for both samples to evaluate the crystal structure of catalysts, and the results are given in Figure 5.18. A broad peak seen from 15° to 25° can be indexed to amorphous silica, confirming the successful silica precipitation for both particles. Copper oxide-silica nanoparticles showed diffraction peaks at 35° and 37° , which proves the presence of CuO. For the XRD pattern of the ZnO@SiO₂ catalyst, a range of diffraction peaks between 30° to 80° can be attributed to ZnO particles with hexagonal wurtzite structure (Galedari et al., 2017). This also explains the structure in the TEM image of ZnO@SiO₂ in Figure 5.17.

Additionally, an attempt to produce iron-based core-shell catalysts was made with 40 mol% loadings. The morphological analysis of synthesised samples given in Figure 5.19 shows that the catalyst structure was considerably changed with metal oxides used. TEM analysis indicates that the silica precipitation was achieved when Fe₂O₃ was used as core species; however, the encapsulation of these core materials remained inadequate since silica particles were attached to each other, rather than coating Fe₂O₃.

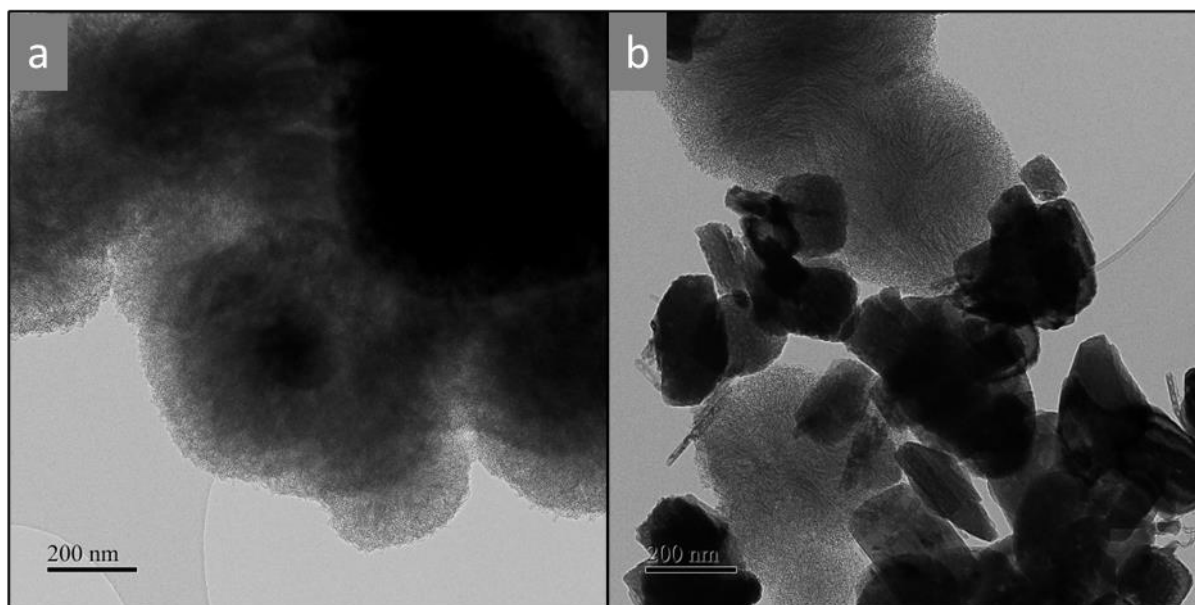


Figure 5.19 TEM images of silica-coated CuO (a) and Fe₂O₃ (b) with 40 mol% loadings

Due to the limitations of the instrument used for SEM-EDS analysis, the location of each element in core-shell catalysts could not be determined due to the formation of very small particles. For a better understanding, alumina-supported copper (II) oxide catalysts, CuO/Al₂O₃, were used for silica encapsulation and the prepared particles

were cut in half to monitor the phase differences better. Figure 2.20 shows the SEM image of the prepared $\text{CuO}/\text{Al}_2\text{O}_3@\text{SiO}_2$ along with the EDS mappings of the particle. For the preparation of this particle, alumina-supported copper (II) oxide was used and they were encapsulated with silica using the conditions chosen above. SEM-EDS analysis clearly shows the silica coating around the alumina support material and the presence of three different phases belonging to each element confirms the successful preparation of silica-encapsulated core-shell catalysts.

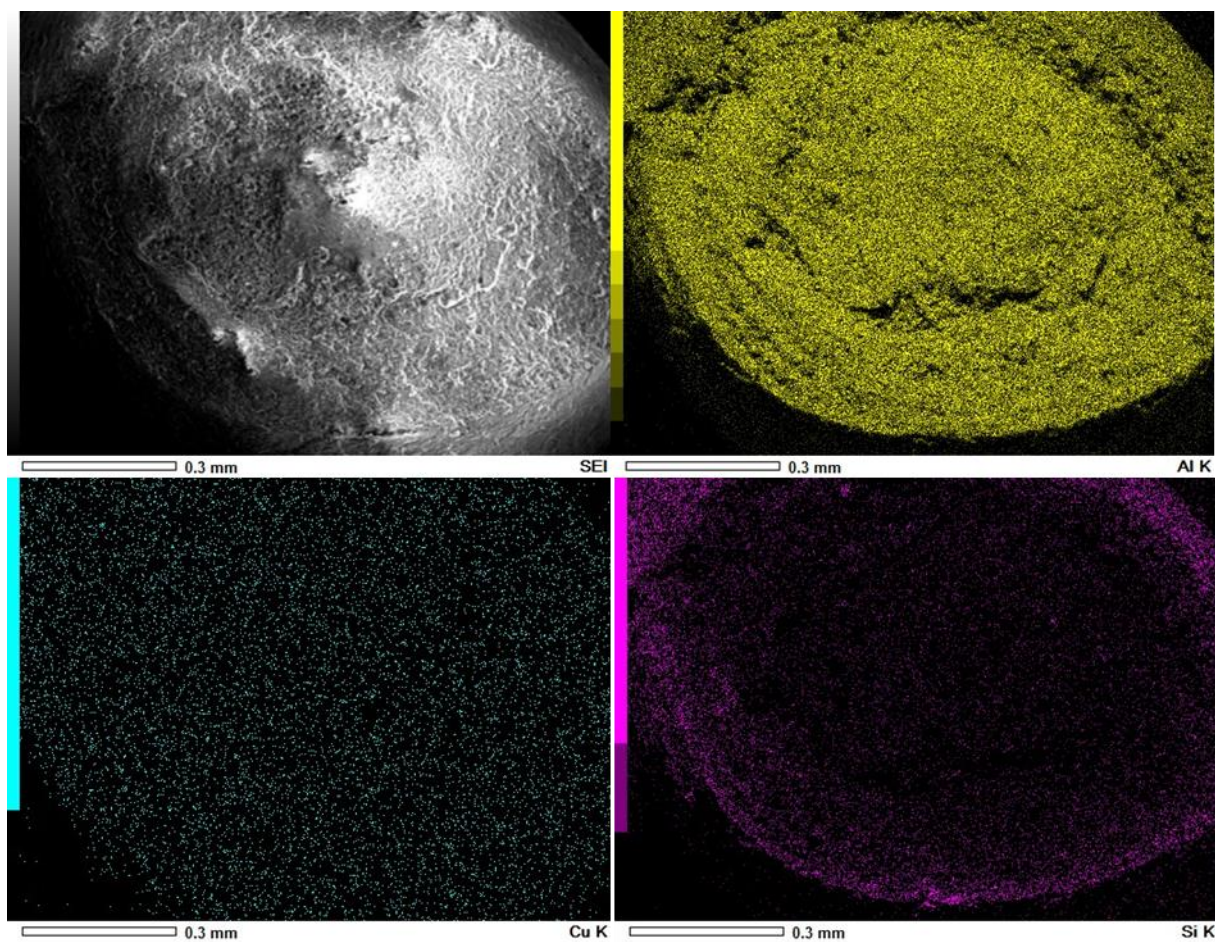


Figure 5.20 SEM-EDS analysis of the prepared $\text{CuO}/\text{Al}_2\text{O}_3@\text{SiO}_2$ catalyst

5.3. Conclusion

In this chapter, mesoporous silica-coated metal oxide-based core-shell catalysts were successfully synthesised with major stability and good reactivity. In the first stage of the chapter, the conditions of the preparation method for core-shell catalysts were optimised by varying surfactant, reactant amounts, solvent and temperature for drying and calcination. It was noticed from the analyses that the presence of a surfactant strongly influences silica encapsulation and also seen that surfactant types can radically change the silica shell structure. It was found that the use of CTAB as a surfactant achieved better silica encapsulation, since well-structured silica nanospheres were observed compared to the catalyst prepared without any surfactants. It was also deduced from the experiments that the shell porosity could be controlled by the amount of CTAB, as less rigid particles were produced compared to Pluronic P123 and no surfactant. Subsequently, the enhancement in the porosity of the particles improved their reactivity and a raise in the DBU yield was obtained from 6.4% to 8%, with a restricted change in the catalyst leaching.

A series of experiments were then conducted to find the optimum amount of solvent and ethyl acetate for a uniform silica encapsulation. It can be said that both of them have a substantial effect on silica precipitation: the presence of ethyl acetate enabled to produce uniform silica spheres by reducing TEOS hydrolysis whilst the addition of an excess amount of solvent can dramatically change the particle size and structure due to differences on the dispersion of active species. The outcome of the experiments highlighted the importance of using the optimum amount of water and ethyl acetate for homogeneous silica formation; therefore, it was found that 15 ml of water with 7.5 ml of ethyl acetate was the optimum amount for better silica coatings.

The influence of temperature was then assessed at the final stage of the optimisation reactions. It was found that synthesis temperature has a major impact on the production of homogeneous nanospheres; more homogeneous particles were produced at the elevated synthesis temperature owing to the increased nucleation rate for silica. SEM analysis was performed to investigate the effect of temperature changes on the particles, and images show that a better particle size distribution was achieved

at higher temperatures. The catalytic performances of the particles were also assessed and better reactivity was obtained for the particles synthesised at higher temperatures. In addition to synthesis temperature, the effect of the calcination temperature was evaluated using catalysts calcined with different temperature ramp rates after producing under the same reaction conditions. The outcomes from the experiments emphasised that the calcination ramp rate has a substantial influence on the catalyst stability. TEM images obtained from the particles showed that higher ramp rates at the calcination step could cause deformation on the silica shell, which then led to a dramatic increase in the concentration of leached active species from 22 to 71 ppm.

After an extensive assessment on the preparation conditions of core-shell catalysts, CuO@SiO₂ particles were prepared with a range of copper oxide loadings at carefully chosen conditions. The morphological analysis revealed that the amount of TEOS used for the preparation of catalysts can affect the silica formation radically. Higher TEOS amounts achieved more uniform silica coating whereas the silica spheres monitored for lower precursor amounts were mostly broken. The catalysts that have 20 mol% copper (II) oxide loading showed the greatest silica capsulation with around 100 nm shell thickness whereas particles coated with silica were mostly broken for higher CuO loadings. The reactivity of the prepared catalysts with different loading was also investigated for urea derivatives synthesis and experiments also showed that a similar DBU yield was achieved by both 20 and 40 mol% catalysts owing to the difference in their shell thickness, even though 20%mol CuO@SiO₂ had a lower amount of active species.

The analysis of the prepared particles was performed using several different methods: FT-IR analysis confirmed the complete removal of the template after the calcination; SEM-EDS and XRD were used to evaluate the elemental composition and crystal structure of particles, respectively. Analysis verified the presence of both silica and copper oxide species in the synthesised catalysts. Finally, several metal oxides were employed as a core species to produce core-shell catalysts; but the morphological analysis on these catalysts showed that silica-encapsulation was not successful for ZnO and Fe₂O₃. On the other hand, core-shell catalysts prepared using alumina-supported CuO particles showed a better and more uniform silica coating. SEM-EDS analysis

concluded that the formation of silica shell was well achieved around the active core species by the presence of different phases between silica and CuO/Al₂O₃ particles.

In the next chapter, silica-encapsulated copper-based catalysts prepared in this chapter were employed for the urea derivatives synthesis from CO₂ and amines. Following, their stability against leaching was assessed by the measurement of copper presence in the product mixture after the reaction.

Chapter 6: Urea Derivatives Synthesis Over Copper-Based Catalysts

Results gained from Chapter 4 showed that the interaction between a solvent and catalyst is highly distinctive, thereby it is fundamental to find the best solvent that can promote the catalyst reactivity and stability. As discussed in Section 2.3.5, copper-based catalysts are highly reactive for the synthesis of urea derivatives from carbon dioxide and amines. However, previous studies showed that besides their superior reactivity, they suffer from leaching into the reaction media during the experiments. This was also confirmed with the experiments conducted in Chapter 4 where DMSO reacted with CuO, which eliminated the promoting effect of both solvent and catalyst. A similar problem was also observed in Chapter 5 where bulk CuO was completely dissolved in the reaction media, and it was unable to recover the catalyst by filtration after the reaction.

To overcome this drawback, a core-shell catalyst was proposed as a solution for the catalyst leaching. Studies in Chapter 5 showed that mesoporous silica-coated copper (II) oxide catalysts could be successfully synthesised with different loadings. Having silica capsulation around copper oxide particles can dramatically improve their stability as well as their reactivity thanks to the interaction between shell and core species. Therefore, the catalytic performance of prepared silica-coated copper-based core-shell catalysts was assessed in this chapter for the production of urea derivatives from carbon dioxide and amines.

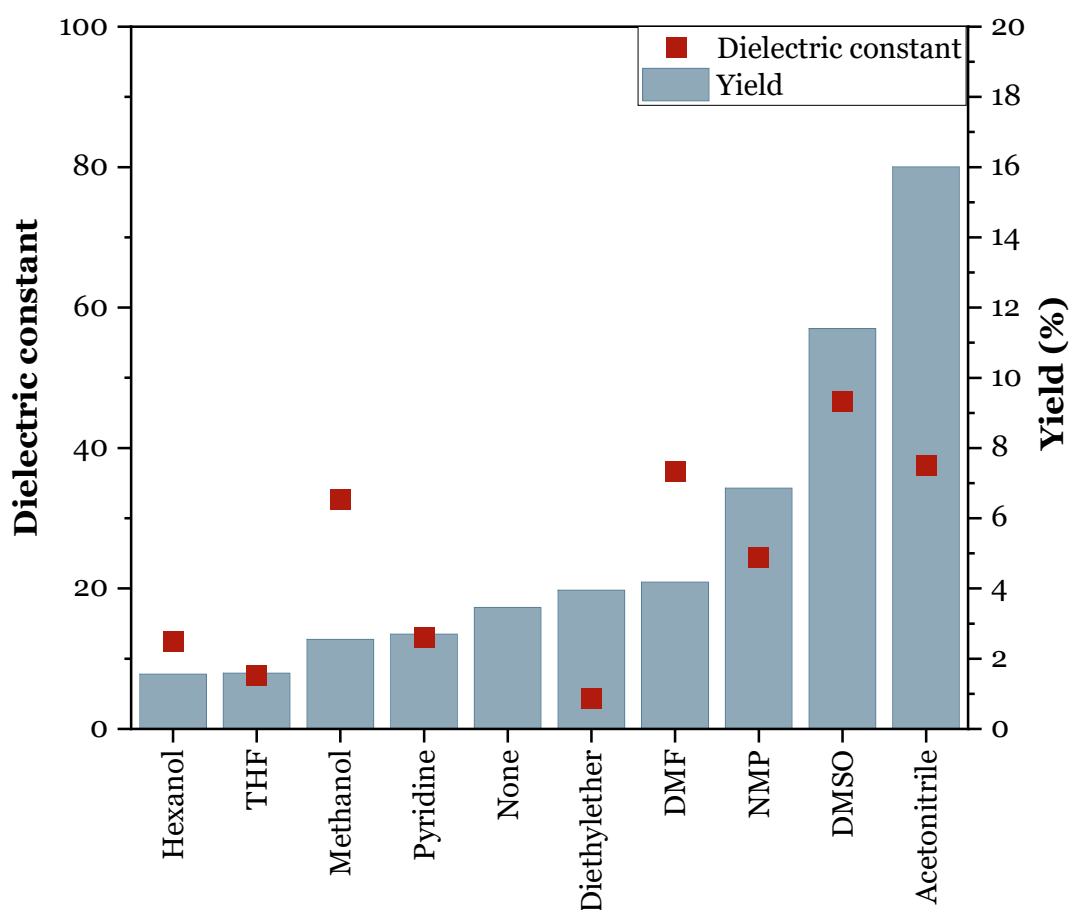
6.1. Results and discussion

6.1.1. Optimisation of the reaction conditions for urea derivatives synthesis

In order to produce urea derivatives from amines and carbon dioxide using silica-coated copper oxide catalysts, the optimisation of the reaction was undertaken using bulk copper (II) oxide catalysts. A series of experiments were performed to investigate the effect of reaction parameters on catalyst performance and stability against catalyst leaching.

6.1.1.a. The influence of solvent

The importance of using a suitable solvent for the reaction was highlighted by Kanzian et al. (2009) and also confirmed in Section 4.2.1.a where the solvent choice can drastically change the product yield for urea derivatives synthesis. It is known that polar aprotic solvents promote the SN₂ reaction by dissolving nucleophiles without making any hydrogen bonding, which allows them to move freely in the solvent (Hart et al., 2007). Therefore, a set of experiments with a number of different solvents were conducted to find the ideal solvent for CuO particles to promote its reactivity with a limited catalyst leaching.

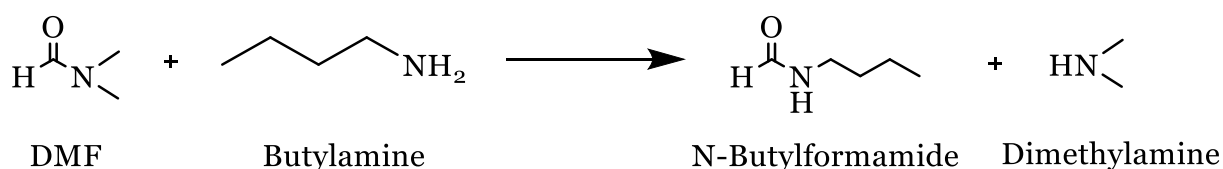


(Polar protic solvents: Hexanol, methanol; Non-polar solvent: Diethyl ether
Polar aprotic solvents: THF, pyridine, DMF, NMP, DMSO, Acetonitrile)

Figure 6.1 The influence of different solvents on DBU synthesis and the correlation between DBU yield and dielectric constants of solvents (Reaction conditions: 20 mmol butylamine, 2 mmol CuO, 3 MPa CO₂, 4 ml solvents at 423 K for 2 hours)

Experiments were performed using 20 mmol butylamine, 4 ml solvent, 2 mmol CuO and 3 MPa of CO₂ at 423 K for 2 hours in a stainless steel reactor with a volume of 45 ml. The DBU yield obtained from the experiments can be found in Figure 6.1, along with the dielectric constant of solvents (Cerón-Carrasco et al., 2014; Reichardt, 2002). Similar to the previous experiments in Chapter 4, higher yields were achieved with polar aprotic solvents: the DBU yield was only 3.5% for the experiment without any solvent whereas it was enhanced by the use of these solvents. Moreover, results showed the relationship between the yield and the dielectric constant of polar aprotic solvents; the overall yield was raised with dielectric constants among these solvents tested. The highest yield at 16% was obtained by the use of acetonitrile, even though DMSO has the highest dielectric constant. This could be explained by the aforementioned reaction between DMSO and copper oxide, which reduced the yield dramatically in Chapter 4 for CuO. However, about 11% yield was obtained herein owing to washing the reactor with methanol to dissolve all the products stuck on the wall of the reactor and inside the formed solid particles produced from the reaction between DMSO and CuO. Likewise, the experiment with NMP showed just above 2% DBU yield for the experiment with Fe₂O₃, whereas it was boosted to almost 7% this time in the presence of CuO as a catalyst. This increase can be attributed to the use of copper (II) oxide or washing the reactor with methanol, since DBU is not dissolved in NMP.

Finally, polar protic and non-polar solvents again demonstrated a minimal DBU yield because they favour different reaction routes. The yield obtained from the experiments with hexanol, THF, methanol and pyridine was lower than with no solvent, whilst it was nearly the same for diethyl ether. Another polar aprotic solvent, DMF with a relatively high dielectric constant, also showed poor performance for the reaction. The DBU yield was at the lowest point among all polar aprotic solvents at 4% because of the reaction between butylamine and DMF (Eq 6.1).



Equation 6.1 The side reaction occurs between DMF and butylamine

Although acetonitrile had the highest yield, NMP was selected for the subsequent experiments due to the reaction between acetonitrile and butylamine given in Eq 4.3. In addition to that, there was also an enormous difference in the leached copper concentrations after the reaction where 55 ppm of copper was measured for NMP whereas using acetonitrile drastically boosted it to about 240 ppm.

6.1.1.b. The effect of substance amounts

The chemical kinetic studies confirmed that reactant amounts greatly influence the reaction rate, so optimising the reaction conditions can aid to enhance the production yield. A series of experiments were performed to find the optimum amount of substances for greater yield by varying the amounts of solvent, butylamine, carbon dioxide and catalyst. Since the experiments with various solvents showed that NMP was a highly effective solvent for the reaction, a set of experiments was then performed to find the optimum amount.

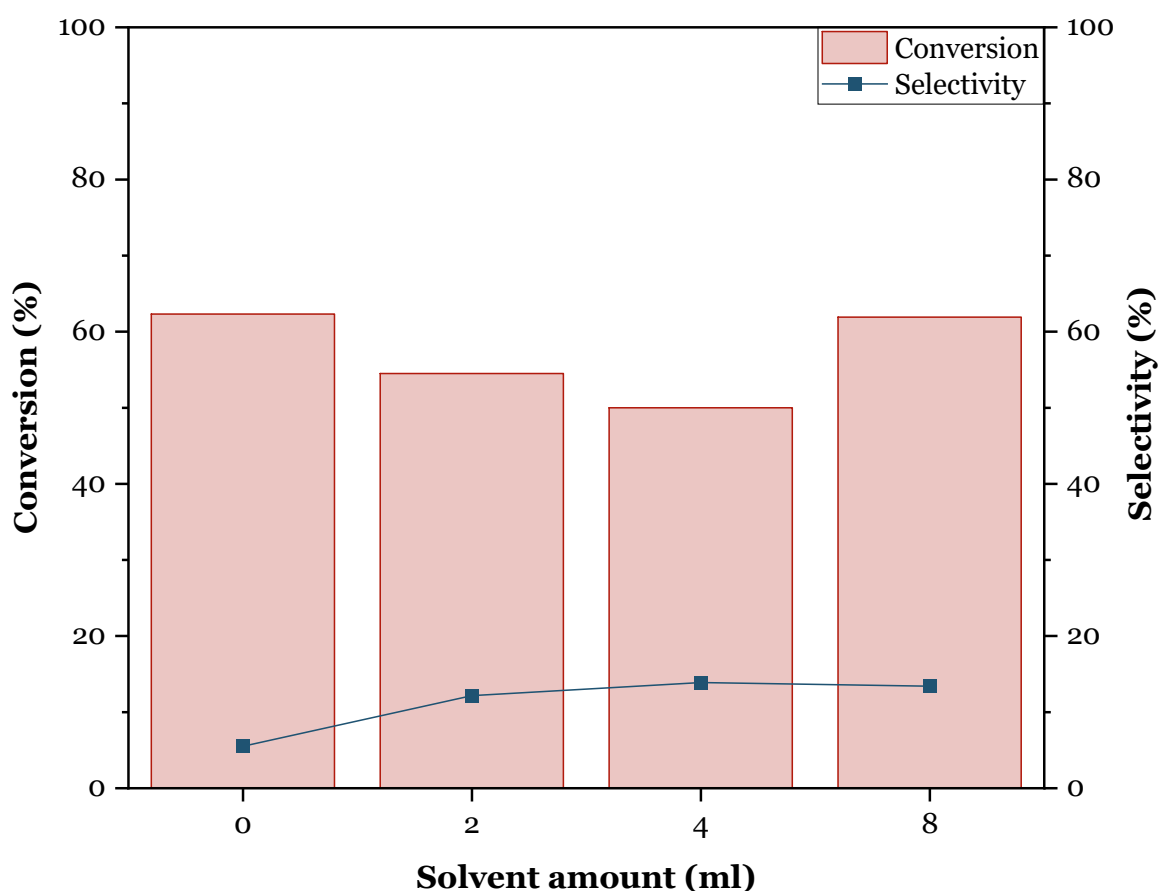


Figure 6.2 The effect of solvent amount on DBU synthesis from butylamine and CO₂ using DMSO over copper (II) oxide (Reaction conditions: 20 mmol butylamine, 2 mmol CuO, 3 MPa CO₂, 0-8 ml NMP at 423 K for 2 hours)

Figure 6.2 shows the changes in butylamine conversion and DBU selectivity by the solvent amount. It can be seen from the figure that the highest conversion rate was gained for the experiment with butylamine only; however, only a 3.4% yield was achieved due to the lowest DBU selectivity rate of 5%. The presence of the solvent drastically changed the selectivity, and the addition of 2 ml NMP almost doubled the yield to 6.6%, even though there was a slight reduction in the conversion from 62% to 55%. The decrease in butylamine conversion continued up to 4 ml of solvent, where the highest DBU selectivity was achieved by 13.9%. Then, there was a noticeable increase in the butylamine conversion with 8 ml solvent from 50 to 62%, improving the yield to 8.3%. However, the selectivity for the main product was slightly reduced by the increased amount of solvent. Therefore, 4 ml was selected as an optimum amount of NMP for the subsequent experiments, as it showed the highest selectivity for DBU.

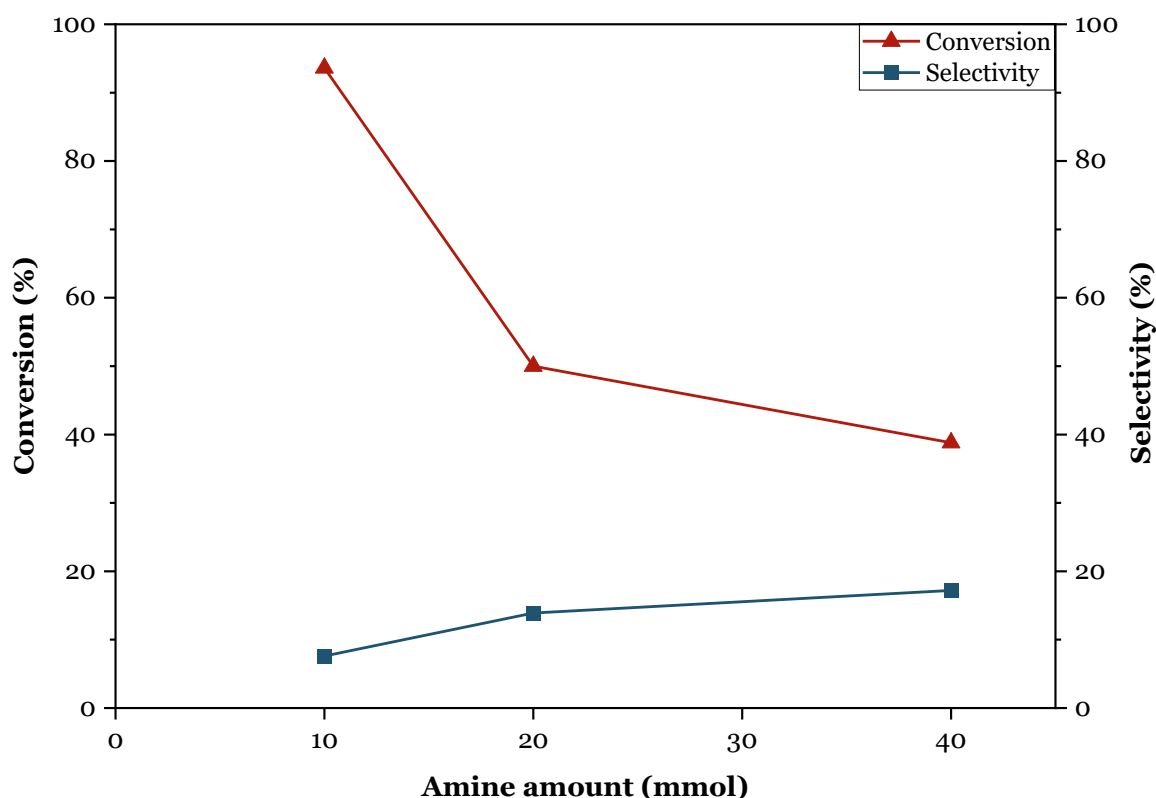


Figure 6.3 Butylamine conversion at different concentrations and the effect of amine amount on DBU selectivity (Reaction conditions: 10-40 mmol butylamine, 2 mmol CuO, 3 MPa CO₂, 4 ml NMP at 423 K for 2 hours)

A set of experiments with different butylamine amounts were then conducted to evaluate the effect of butylamine on its conversion and selectivity for DBU. A range of butylamine from 10 to 40 mmol was catalytically reacted with CO₂ using CuO and NMP at 423 K for 2 hours and the outcome of the experiments is presented in Figure 6.3. It is quickly noticed from the figure that more than 90% butylamine conversion was achieved in the first run; however, the DBU selectivity was only 7.5%. After that point, a clear trend for both the conversion and selectivity was spotted; the butylamine conversion was gradually decreased whereas the selectivity for DBU was increased progressively over amine amounts. The reduction in butylamine conversion was attributed to the capacity of the catalyst to activate butylamine, as the capacity at a time did not change when the amount of butylamine increased. Hence, the conversion was dropped to 39% but the selectivity for DBU increased more than twice and reached 17.2% at 40 mmol of butylamine. Nevertheless, 2 mmol was selected as it had a high selectivity with a good butylamine conversion.

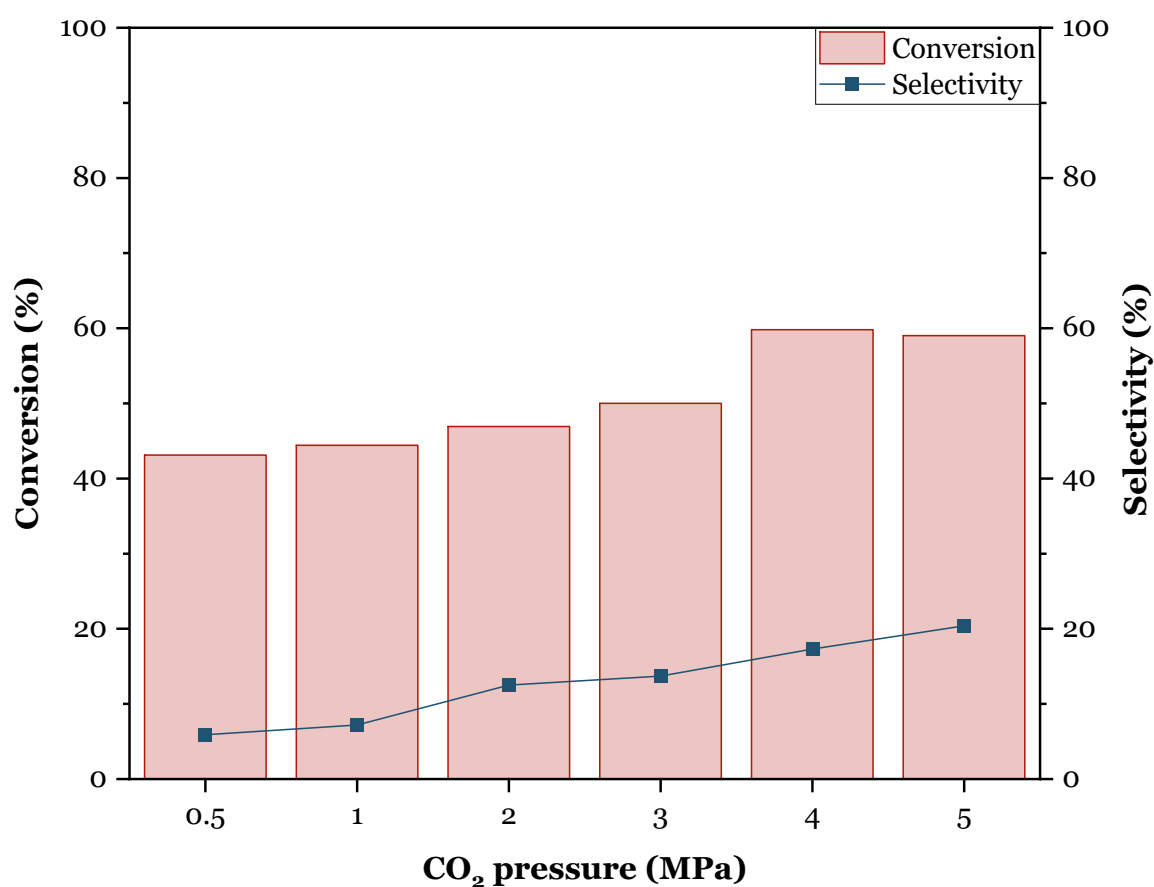


Figure 6.4 Changes in DBU yield over the increase of CO₂ pressure (Reaction conditions: 20 mmol butylamine, 2 mmol CuO, 0.5-5 MPa CO₂, 4 ml NMP at 423 K for 2 hours)

Since the influence of carbon dioxide pressure was observed in the previous experiments, the effect of pressure on the reaction with NMP and copper (II) oxide was also studied. Experiments with different CO₂ pressure were performed for the investigation, and the results can be seen in Figure 6.4. It was revealed from the results that DBU yield was continuously increased by CO₂ pressure from 2.6% to 12.1%, similar to previous experiments with Fe₂O₃. The figure demonstrates that both conversion and selectivity increased with the CO₂ pressure, where the initial conversion rate was 43% for 0.5 MPa and increased gradually to 60% at 5 MPa, whilst the selectivity boosted from 5.9% to 20.4%. In order to monitor the effect of pressure on the reaction in detail, changes in the carbon mass balance were evaluated with the increase of CO₂ pressure. Table 6.1 exhibits the carbon balance of the reaction before and after the reaction with different CO₂ pressures. The carbon balance for the reactions was calculated using the converted butylamine amount with taking into account the carbon provided from CO₂ and it can be said that the analysis shows a similar trend with Figure 6.4 where the selectivity of DBU was enhanced with the CO₂ amounts. This indicates that CO₂ is the limiting substrate of the reaction; hence, 5 MPa of CO₂ was used for urea derivatives synthesis at optimised conditions.

Table 6.1 Carbon mass balance changes over CO₂ pressure

| CO ₂ Pressure (MPa) | Used butylamine (mmol) | Used C (mmol) | Formed DBU (mmol) | Formed DBU C (mmol) | DBU Selectivity (%) |
|--------------------------------------|------------------------------|---------------------|-------------------------|---------------------------|---------------------------|
| 0.5 | 8.72 | 39.24 | 0.257 | 2.31 | 5.9% |
| 1 | 8.98 | 40.41 | 0.323 | 2.91 | 7.2% |
| 2 | 9.5 | 42.75 | 0.59 | 5.31 | 12.4% |
| 3 | 10.1 | 45.45 | 0.623 | 5.61 | 12.3% |
| 4 | 12.01 | 54.05 | 1.048 | 9.43 | 17.4% |
| 5 | 11.95 | 53.78 | 1.218 | 10.96 | 20.4% |

A set of experiments were also performed using CO₂ and argon with a pressure of 1 MPa to investigate the carbonyl source of the reaction. It was obtained from the reactions that 44.4% conversion was achieved by CO₂ with 7.2% selectivity, whilst the conversion jumped to 79.4% for the reaction with 1 MPa argon (Table 6.2). Nonetheless, no DBU was produced by the presence of argon, confirming that CO₂ is the only source of the carbonyl group for the urea derivative synthesis.

Table 6.2 Changes in butylamine conversion and DBU selectivity under the influence of different gases (Reaction conditions: 20 mmol butylamine, 2 mmol CuO, 1 MPa of gas, 4 ml NMP at 423 K for 2 hours)

| Entry | Gas | Conversion (%) | Selectivity (%) | Yield (%) |
|-------|----------------|----------------|-----------------|-----------|
| 1 | Carbon dioxide | 44.4 | 7.2 | 3.2 |
| 2 | Argon | 79.4 | 0 | 0 |

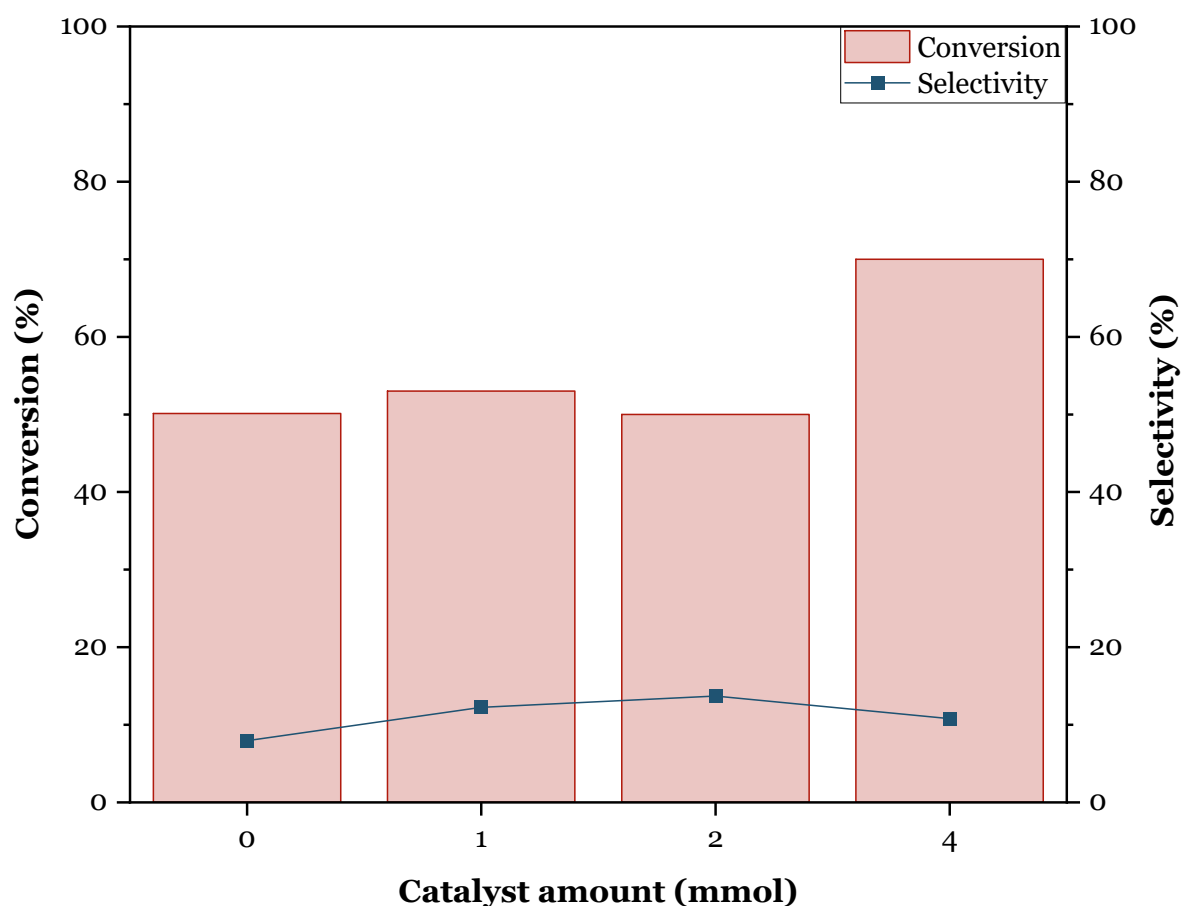


Figure 6.5 Changes in butylamine conversion and DBU selectivity over a range of CuO amounts (Reaction conditions: 20 mmol butylamine, 0-4 mmol CuO, 3 MPa CO₂, 4 ml NMP at 423 K for 2 hours)

In addition, the influence of catalyst amount on DBU synthesis was studied in the last part of the optimisation of substrates amounts. A range of copper oxide amounts from none to 4 mmol was tested for the reaction, and changes in butylamine conversion and DBU selectivity were recorded (Figure 6.5). A reaction without any catalysts yielded only 4% DBU with 50% butylamine conversion and just 8% selectivity. The conversion rate remained almost stable up to 2 mmol of copper oxide. In contrast, the DBU selectivity was steadily improved over catalysts amount and reached its maximum point of 13.7%, thereby a 6.9% DBU yield was achieved. The selectivity was then slightly dropped to 11% for 4 mmol of catalyst, even though it had the highest conversion rate of 70%.

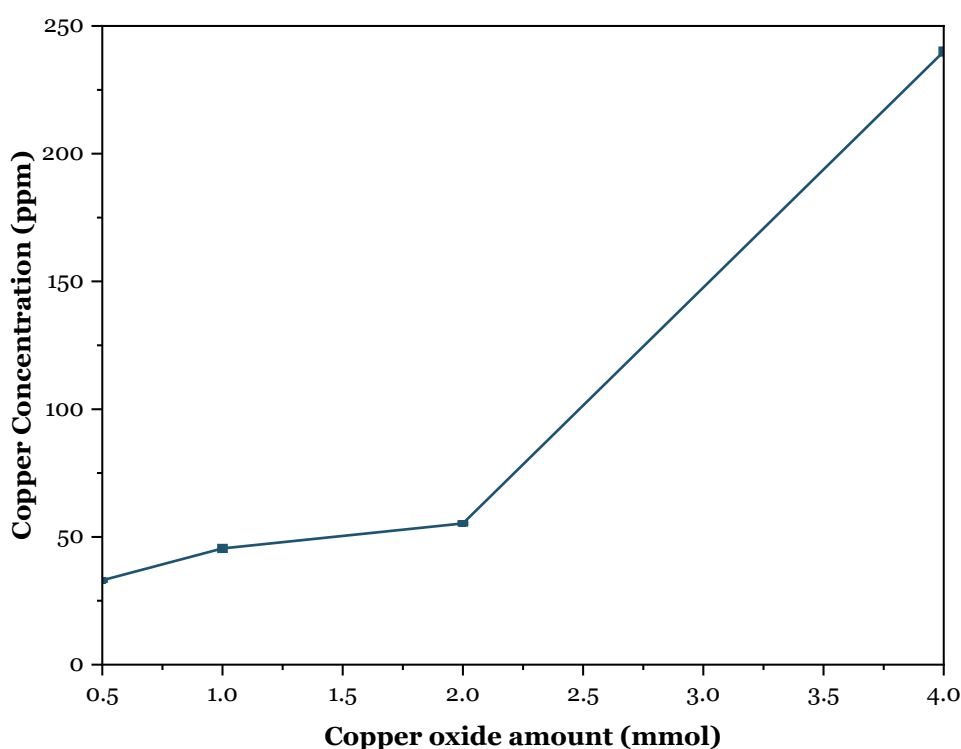


Figure 6.6 The catalyst leaching over copper (II) oxide amounts (Reaction conditions: 20 mmol butylamine, 0-4 mmol CuO, 3 MPa CO₂, 4 ml NMP at 423 K for 2 hours)

Catalyst leaching was investigated by AAS analysis using the samples obtained after reactions, and it was found that copper concentration was continually raised by catalyst amounts used in the reaction (Figure 6.6). The increase in the concentration was relatively slow at lower copper amounts, but it soared after 2 mmol. It was 33 ppm for the experiment with 0.5 mmol of catalyst and slightly increased to 55 ppm for 2 mmol.

However, a further increase in the catalyst amount caused a dramatic increase in the copper concentration from 55 to above 200 ppm. Although employing 4 mmol of copper oxide produced the highest DBU yield with a 7.8% yield, 2 mmol of catalysts was selected as an optimum amount of copper oxide because of the massive difference in catalyst leaching.

6.1.1.c. The influence of temperature and time

In the last part of the optimisation reactions, the effect of reaction time and temperature were examined as their substantial impact on the synthesis was observed in previous experiments with Fe_2O_3 in DMSO. Since CO_2 is a highly stable compound, adequate energy input is essential to overcome the activation energy (Road, 2010). Consequently, trace to zero DBU yield was observed for the experiments on and below 393 K, and only 2% yield was obtained up to 403 K. For that reason, results obtained from the experiments conducted lower than 413 K are excluded.

Previous experiments showed that the decomposition of the solvent is a determinative parameter for experiments at higher temperatures. NMP with a decomposition temperature of about 643 K enables to perform experiments at elevated temperatures (WHITE & SANKEY, 1979). Experiments using 20 mmol butylamine, 3 MPa CO_2 , 4 ml NMP and 2 mmol copper oxide were performed at temperatures between 413 and 493 K and the results for the butylamine conversion and DBU selectivity is given in Figure 6.7. Butylamine conversion was 43% at 413 K and remained nearly stable up to 473 K. In contrast to the conversion, DBU selectivity was also continuously raised by the temperature, where it was 6.8% at 413 K and reached its highest point of 76% at 463 K. After that point, it was slightly reduced and remained between 45 and 55% at higher temperatures. The comparison results with the previous experiments in DMSO showed that NMP remained stable and active at elevated temperatures. For the experiments in Chapter 4, the DBU selectivity was dipped to less than 20% due to the decomposition of DMSO at 473 K whereas DBU selectivity stayed above 50% with the use of NMP as a solvent.

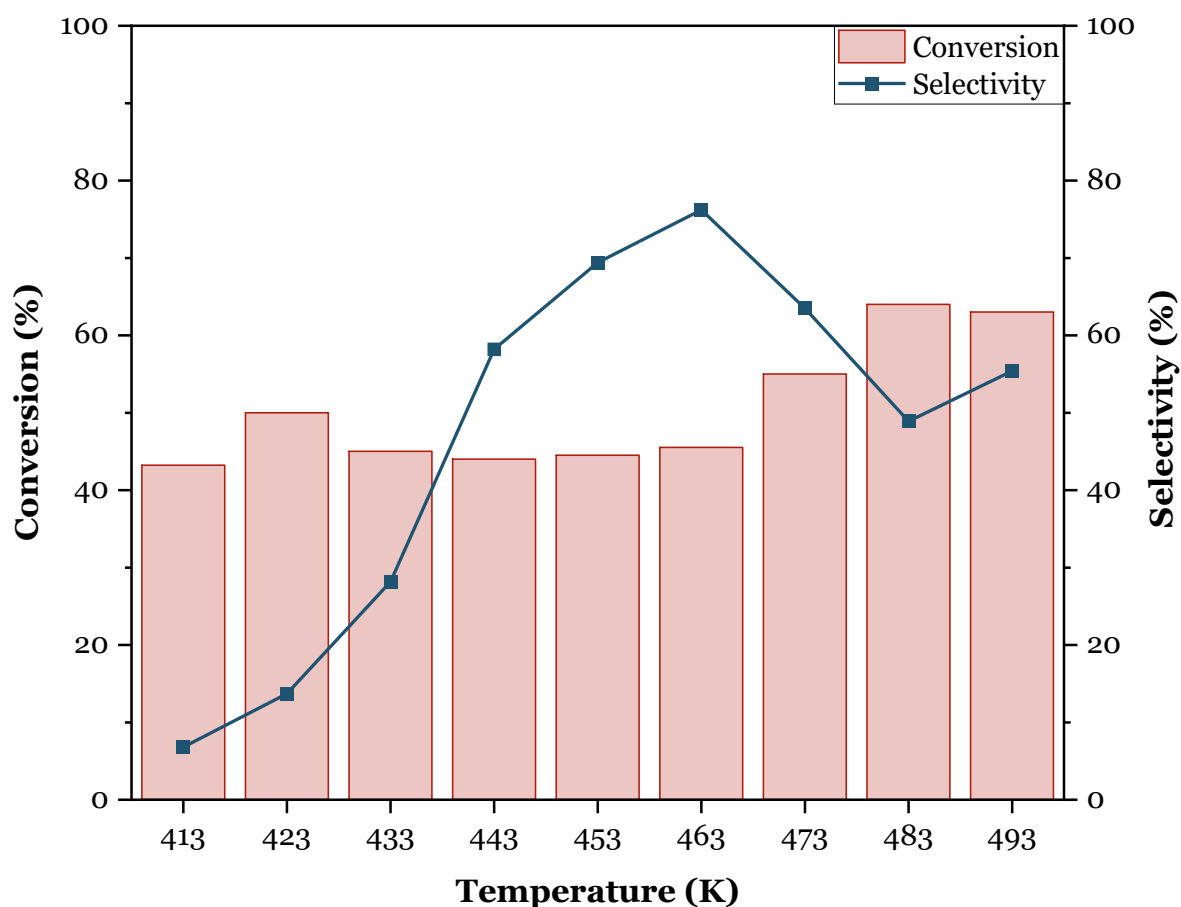


Figure 6.7 Changes in the conversion and selectivity over temperature (Reaction conditions: 20 mmol butylamine, 2 mmol CuO, 3 MPa CO₂, 4 ml NMP for 2 hours at different temperatures)

To investigate the selectivity decline after a certain point, catalyst leaching was analysed since a colour change was detected together with brown particles after the reaction for some experiments. Figure 6.8 shows the copper concentration over reaction temperature, and it is clear that the amount of copper oxide dissolved in the reaction media was increased until a cliff at 443 K. The concentration was dramatically decreased after that point where it is believed that leached copper oxide particles started to precipitate as metallic copper. The liquid recovered from the reaction was dark blue up to 463 K, which changed to brown because of the reduction of copper oxide after that temperature. Some metallic copper particles were also observed after the filtration, confirming the reduction of metal species to metallic copper.

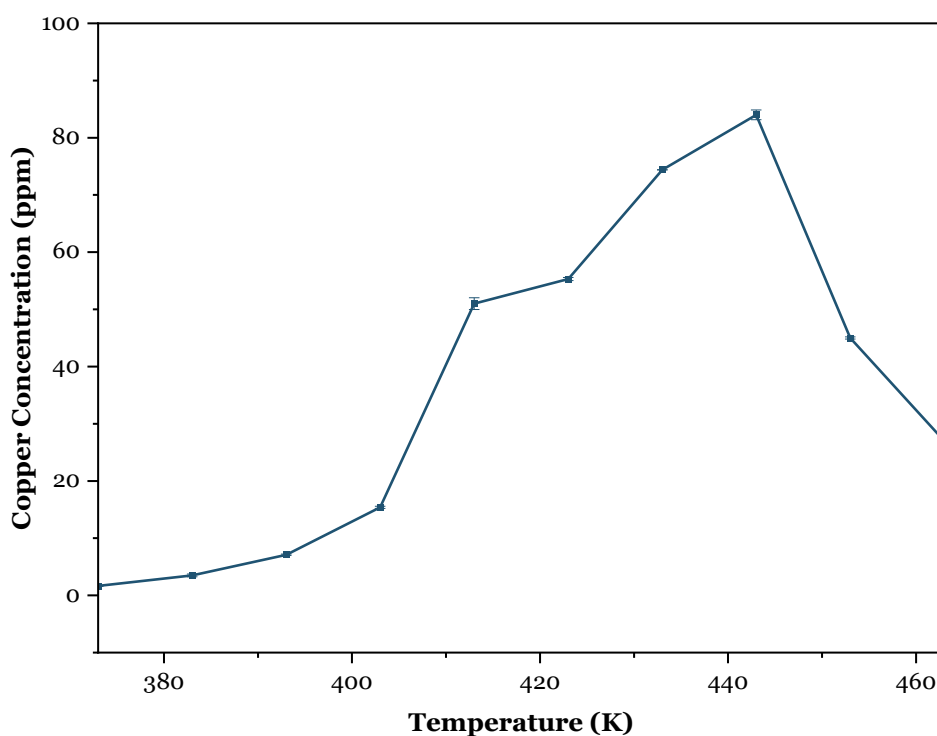


Figure 6.8 The impact of temperature on the leaching of copper (II) oxide (Reaction conditions: 20 mmol butylamine, 2 mmol CuO, 3 MPa CO₂, 4 ml NMP for 2 hours at different temperatures)

The influence of the oxidation states of catalysts was discussed in Section 4.2.2.a, where the DBU yield was declined when iron catalysts with different oxidation states used. Therefore, the reduction of copper (II) oxide to metallic copper could change its reactivity for the experiment and cause a decrease in DBU yield. It is believed that the reduction of copper (II) oxide to metallic copper changed the selectivity of the reaction and caused the decline observed in DBU selectivity after 463 K. For that reason, 463 K was selected as an optimum temperature since it had the highest selectivity with a limited reduction reaction happened.

Finally, reaction time was assessed from 1 to 72 hours under the same reaction conditions. It was found that only a 3.7% yield was achieved for the experiment run for one hour and then gradually increased over time. The butylamine conversion obtained for the experimentation in 2 hours was 50 %, which was enhanced to 60% in 24 hours (Figure 6.9). The selectivity also progressively improved over time and soared from 13.7% to 73.6% in the same time range. After that point, the conversion jumped to the peak at 75% for both 48 and 72 hours, whilst the selectivity was increased first to 79% and then dropped to 44.3% at 72 hours. This reduction can also be explained by catalyst

leaching, similar to the colour change detected at elevated temperatures. AAS analysis was conducted to investigate the copper oxide concentration over reaction time, and the outcome of the analysis is shown in Figure 6.10. The copper concentration was around 30 ppm at the beginning, and it was increased by reaction time to 8 hours, with the highest copper concentration of 90 ppm. It then started to fall and become steady at 24 hours, indicating that the copper reduction started around 12 hours. Although the copper concentration detected did not change after 24 hours, the selectivity only declined after 48 hours. It is believed that there were still enough copper oxides in the system to catalyse the reaction, and the amount of copper oxide reduced to metallic copper was increased over time and caused a decrease in selectivity for the experiment within 72 hours.

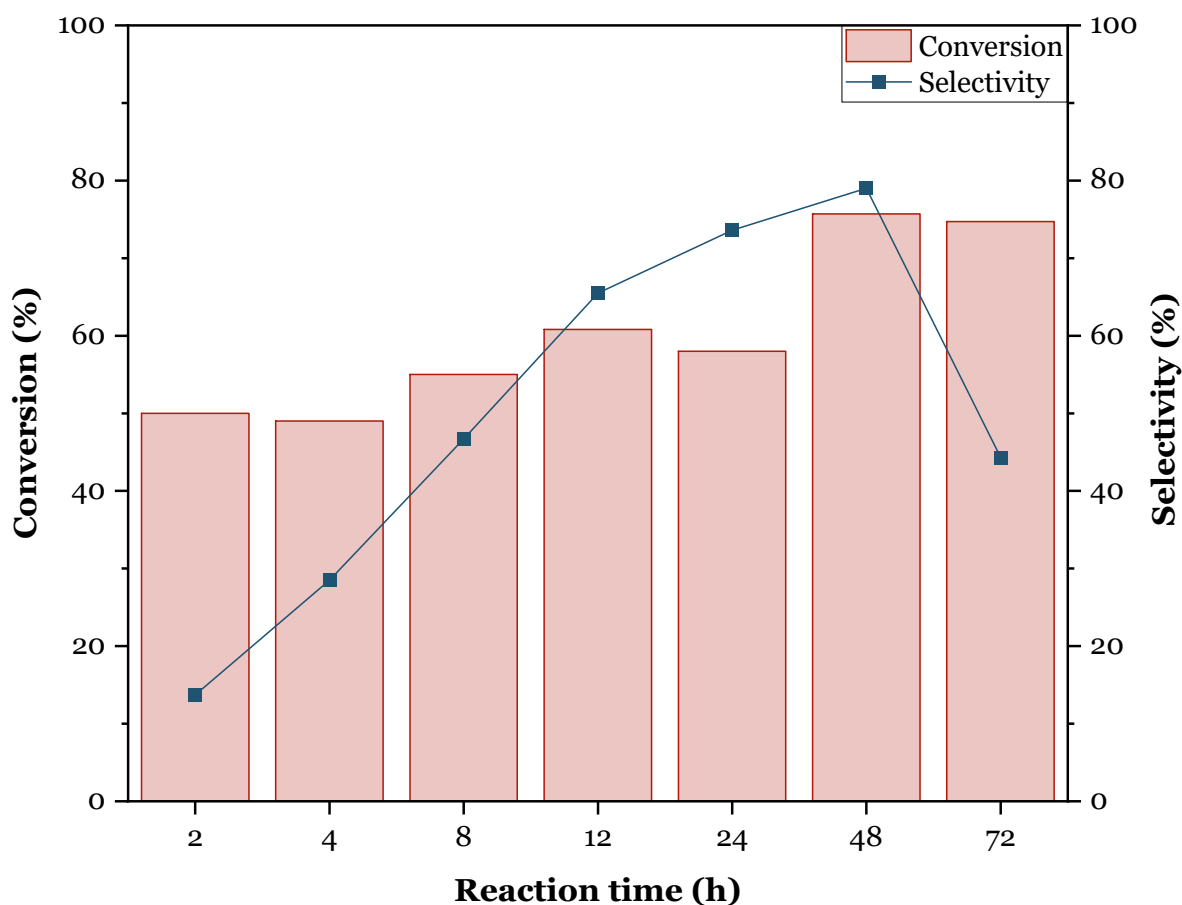


Figure 6.9 The synthesis of DBU from butylamine and CO₂ over copper oxide at different reaction times (Reaction conditions: 20 mmol butylamine, 2 mmol CuO, 3 MPa CO₂, 4 ml NMP at 423 K)

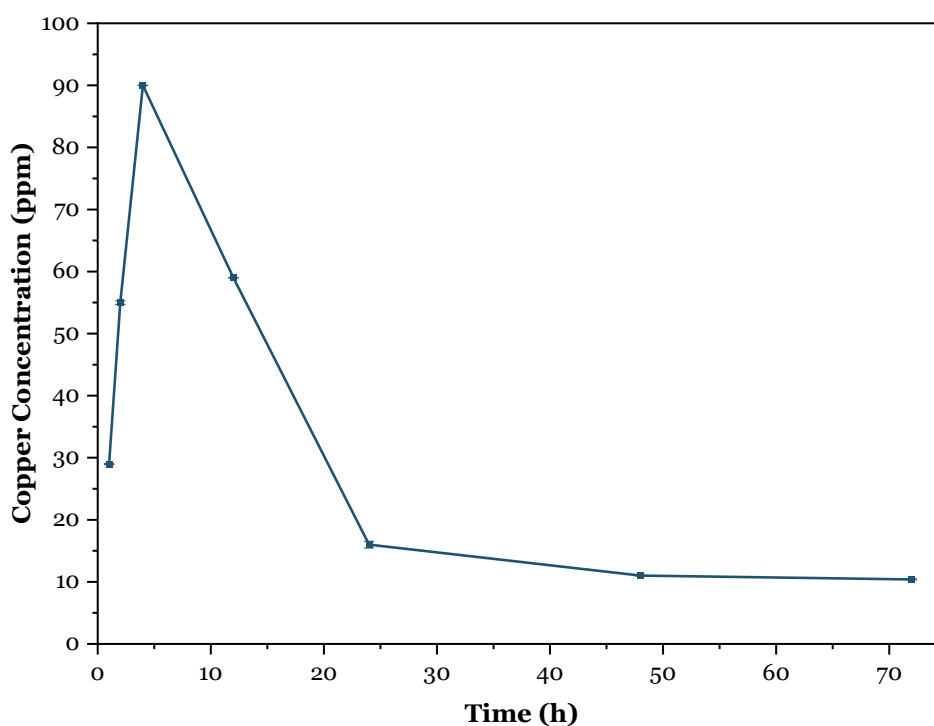


Figure 6.10 The effect of time on the leached copper concentration after the reaction (Reaction conditions: 20 mmol butylamine, 2 mmol CuO, 3 MPa CO₂, 4 ml NMP at 423 K)

Results from the experiments at various temperatures and times showed that NMP stayed stable at higher temperatures and longer reaction times; however, the reduction of copper oxide was restricted to run experiments at higher and longer experiments. Hence, a reaction of up to 4 hours was planned for the catalytic synthesis under optimised conditions for greater DBU selectivity.

6.1.2. Catalytic performance on urea derivatives synthesis

The optimisation reactions confirmed that a greater product yield could be achieved by adjusting reaction conditions. It was also noticed from comparing two sets of optimisation reactions that every solvent and catalyst employed for the reaction can dramatically change the direction of reactions. In this part of the chapter, the catalytic conversion of CO₂ from different amines to corresponding urea derivatives was studied under the conditions optimised above.

6.1.2.a. The effect of solvent at optimised conditions

The influence of solvent was studied broadly for both copper oxide and iron oxide previously at lower temperatures; however, experiments were not conducted to assess their effectiveness at higher temperatures. The reactions were run using 20 mmol butylamine, 2 mmol copper oxide, 5 MPa of CO₂, and 4 ml of solvent at 463 K for 2 hours. The table below shows the influence of solvents under optimised reaction conditions.

The first thing noticed from Table 6.3 was that the yield was increased for all solvents under optimised conditions. Moreover, polar protic solvents again showed the lowest reaction yields up to only 13%, still lower than the experiment without any solvents, similar to the experiments at lower temperatures. The DMF experiment had a slightly higher yield than the experiment with no solvent previously, but the yield dropped lower than that at optimised conditions. Although it had the second-highest conversion rate, DBU selectivity was the weakest due to the reaction with butylamine. Furthermore, the decrease in the selectivity indicated that the reaction between DMF and butylamine was increased by the temperature and dropped the overall yield for DBU, compared to others.

Table 6.3 Catalytic conversion of butylamine with CO₂ into DBU using different solvents (Reaction conditions: 20 mmol butylamine, 2 mmol CuO, 5 MPa CO₂, 4 ml solvent at 463 K for 2 hrs)

| Entry | Solvent | Dielectric Constant | Conversion (%) | Selectivity (%) | Yield (%) |
|-------|--------------|---------------------|----------------|-----------------|-----------|
| 1 | Cyclohexanol | 13.4 | 51.8 | 16.4 | 8.5 |
| 2 | Methanol | 32.7 | 30.0 | 32.0 | 9.6 |
| 3 | Ethanol | 24.5 | 33.6 | 32.0 | 10.7 |
| 4 | 2-Propanol | 17.9 | 25.5 | 45.9 | 11.7 |
| 5 | DMF | 36.7 | 94.7 | 12.9 | 12.3 |
| 6 | Hexanol | 12.5 | 51.1 | 25.8 | 13.2 |
| 7 | Pyridine | 13 | 63.9 | 32.2 | 20.6 |
| 8 | None | - | 55.7 | 37.2 | 20.7 |
| 9 | DMSO | 46.7 | 98.0 | 34.3 | 33.6 |
| 10 | NMP | 25.5 | 78.8 | 47.2 | 36.9 |
| 11 | Acetonitrile | 37.5 | 93.4 | 44.3 | 41.4 |

Moreover, only polar aprotic solvents such as DMSO, NMP and acetonitrile, had higher DBU yields than the experiment with no solvent. DMSO achieved a 33.6% yield with the highest butylamine conversion, but the selectivity was relatively low due to the decomposition stated before. Therefore, NMP showed better results than DMSO under optimised conditions with outstanding selectivity towards DBU with a moderate butylamine conversion. Lastly, acetonitrile showed again the highest yield of 41.4%, with 93.4% conversion and 44.3% selectivity. This increase for acetonitrile was attributed to the reaction seen in Eq 4.3 between acetonitrile and water, which is produced as a by-product of DBU and removing water from the system promotes the reaction to the product side.

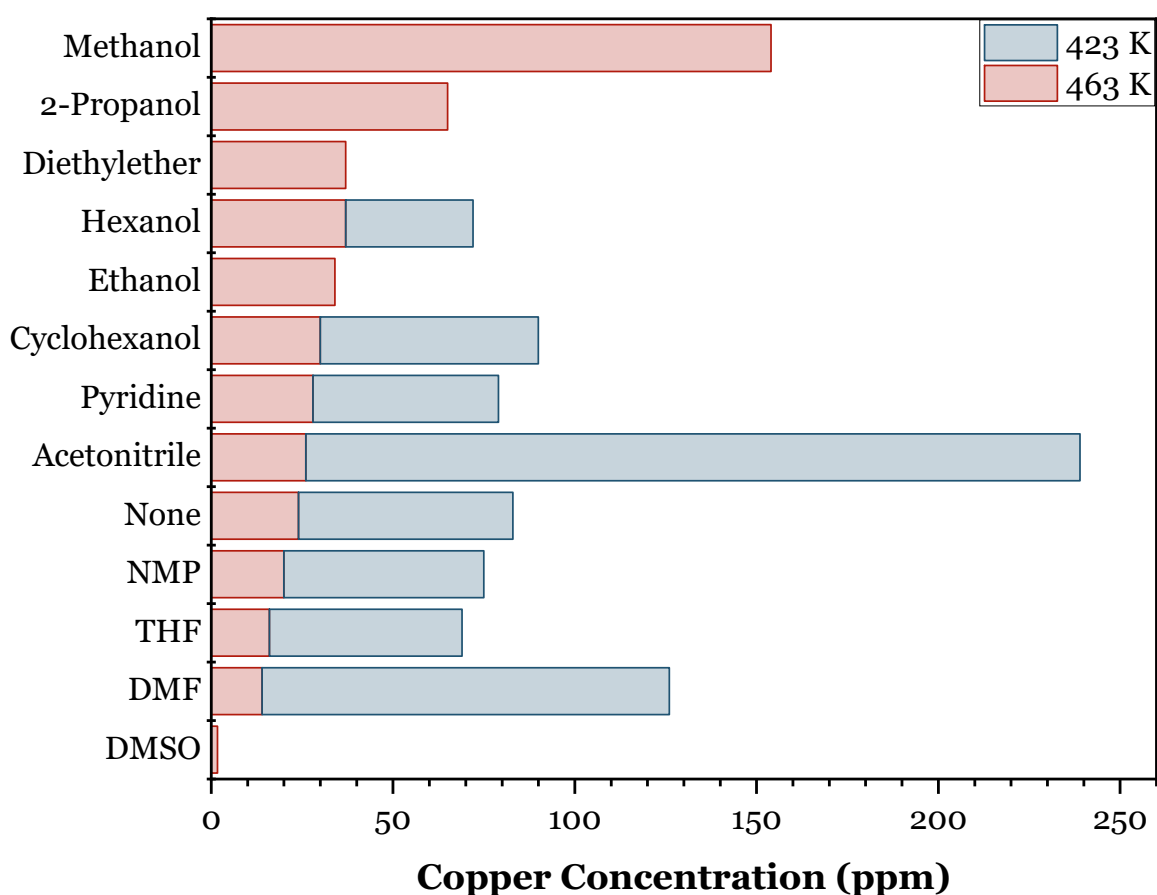


Figure 6.11 Catalyst leaching in various solvents at two different temperatures

Since catalyst leaching was detected for various experiments, AAS analysis was conducted to evaluate the changes in copper concentration by different solvents at two different reaction temperatures. Figure 6.11 indicates that the copper concentration declined for all samples obtained with polar aprotic solvents when the temperature increased from 423 K to 463 K. As acetonitrile had the highest copper concentration of 240 ppm at the lower temperature, NMP was selected as a solvent for the experiment from the optimisation reactions. The analysis for the experiment with DMSO showed trace to no copper oxide, which can be attributed to the particles that occurred due to the reaction between DMSO and CuO in this experiment. It is also clear that the copper concentration was relatively low for polar protic and non-polar solvents at lower temperatures than polar aprotic solvents, whereas it was increased by temperature in contrast to polar aprotic solvents. The highest concentration was detected for methanol at the elevated temperature, followed by other alcohols and diethyl ether. On the other hand, the leached copper concentration was dropped for polar aprotic solvents when the temperature increased.

6.1.2.b. The assessment on the reactivity of different metal oxide catalysts

Experiments showed that the catalyst reactivity heavily changed with the solvent used to produce urea derivatives from amines and carbon dioxide. An investigation was also performed for the catalytic conversion of CO₂ into DBU from butylamine using 2 mmol of several different metal oxides under optimised reaction conditions. The results are given in Table 6.4 with butylamine conversion, DBU selectivity and overall yield.

It was first deduced from the table that iron-based catalysts showed deficient activity for the reaction. They showed exceptionally high reactivity in the previous experiments run using DMSO in Chapter 4; however, the yield dropped to about 13% from 47.5% for Fe₂O₃. Other iron-based catalysts also showed similar trends and yielded lower than the experiments without any catalysts, highlighting the effect of the catalyst-solvent interaction for greater yield. Similarly, silica did not show any reactivity in the experiments, whilst it was one of the best catalysts in previous experiments with DMSO; the yield obtained with SiO₂ in DMSO was 46.4% but dipped to 12.7% when NMP was used as a solvent.

Table 6.4 Catalytic conversion of butylamine with CO₂ into DBU using different metal oxide catalysts (Reaction conditions: 20 mmol butylamine, 2 mmol catalyst, 5 MPa CO₂, 4 ml NMP at 463 K for 2 hrs)

| Entry | Catalyst | Surface Area (m ² /g) ^a | Conversion (%) | Selectivity (%) | Yield (%) |
|-------|--|--|-------------------|--------------------|--------------|
| 1 | FeO | | 67.4 | 9.7 | 6.5 |
| 2 | Fe | | 73.4 | 13.7 | 10.1 |
| 3 | Pd/Al ₂ O ₃ ^{***} | | 91.3 | 11.8 | 10.8 |
| 4 | SiO ₂ | 535 | 59.0 | 21.4 | 12.7 |
| 5 | Fe ₂ O ₃ | 11 | 47.0 | 27.9 | 13.1 |
| 6 | None | | 61.5 | 24.5 | 15.1 |
| 7 | MnO ₂ | 10 | 53.3 | 28.4 | 15.1 |
| 8 | Al ₂ O ₃ | 181 | 40.8 | 37.7 | 15.4 |
| 9 | ZrO ₂ | 59 | 52.3 | 29.6 | 15.5 |
| 10 | Pt/Al ₂ O ₃ ^{**} | | 69.2 | 22.8 | 15.8 |
| 11 | Cu | | 24.9 | 65.9 | 16.4 |
| 12 | CuO/Al ₂ O ₃ [*] | | 50.6 | 42.7 | 21.6 |
| 13 | La ₂ O ₃ | 14 | 91.3 | 30.5 | 27.8 |
| 14 | ZnO | | 86.7 | 40.2 | 34.8 |
| 15 | Cu ₂ O | | 45.9 | 82.6 | 37.9 |
| 16 | CuO | 29 | 78.8 | 56.9 | 44.8 |
| 17 | CeO ₂ | 88 | 98.4 | 85.7 | 84.3 |

*0.16 g of 13 mol% CuO/Al₂O₃; **0.39 g of 0.5 mol% Pt/Al₂O₃; ***0.21 g of 5 mol% Pd/Al₂O₃

a: surface area of the catalysts was adopted from Quintana Gomez (2017); N. Razali (2017)

Alumina showed similar reactivity for the experiment and gave only a 15.4% DBU yield, which was just above the reaction with no catalyst. However, adding active species on alumina drastically changed the catalyst reactivity, where butylamine conversion was increased for all alumina-supported catalysts. More than 90% butylamine conversion was achieved for Pd/Al₂O₃; however, the overall DBU yield was just about 10% due to low selectivity. Pt/Al₂O₃ also showed similar results: butylamine conversion was enhanced from 40% to almost 70%, while the selectivity was reduced to 22.8%. Nevertheless, only increase was observed in the addition of copper oxide for both conversion and selectivity, and a 21.6% yield was achieved by CuO/Al₂O₃.

Furthermore, the reactivity of copper-based catalysts was confirmed with these results as discussed in the literature; all copper catalysts showed higher activity than no catalyst experiment. Copper (II) oxide had the highest DBU yield among all the copper-based catalysts, with 79% butylamine conversion and 57% selectivity for DBU. Then, the DBU selectivity was improved by copper (I) oxide, whereas having lower butylamine conversion decreased the yield to 38% from almost 45%. The lowest reactivity observed for copper-based catalysts was for metallic copper particles, which had 16.4% DBU yield with 66% selectivity and 25% butylamine conversion. Since metallic copper has a higher density, particles stuck to the bottom of the reactor and the magnetic stirrer was unable to stir the particles properly. This could also be the cause of the decrease in butylamine conversion, as their contact was limited.

ZnO and La₂O₃ were also other reactive catalysts after copper-based particles; 34.8% and 27.8% DBU yield were achieved, respectively. La₂O₃ had one of the highest butylamine conversions with Pd/Al₂O₃, but both had low selectivity for DBU. Among all the catalysts tested, copper (II) oxide showed one of the best reactivity for the reaction after CeO₂, which 84% DBU yield in 2 h, similar to the literature reported (Tamura et al., 2016). The yield for CeO₂ was only 54% with DMSO and then boosted to 84% thanks to the unique interaction with NMP, as reported. Although it showed the highest yield for the experiment, Cu₂O had similar selectivity towards DBU. This shows the effectiveness of copper-based catalysts for the experiment, and it can be concluded that they can be an excellent alternative for this noble and expensive CeO₂ catalyst.

Catalyst leaching was also investigated for copper particles with different oxidation states and types of catalysts together with ZnO and Fe₂O₃. The results in Table 6.5 shows that Fe₂O₃ had low catalyst leaching at 463 K by the use of NMP, where it jumped from 2 ppm to 20 ppm by the increase in the reaction temperature from 453 K to 463 K in Chapter 4 in the presence of DMSO. It was stated that acid formed due to the decompositions of DMSO was the reason for this dramatic increase and this can be confirmed here, as it only had 1 ppm iron concentration at the same temperature.

Table 6.5 Catalyst leaching for metal oxides catalysts at optimised reaction conditions (Reaction conditions: 20 mmol butylamine, 2 mmol catalyst, 5 MPa CO₂, 4 ml NMP at 463 K for 2 hrs)


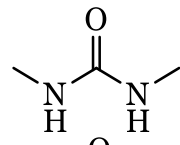

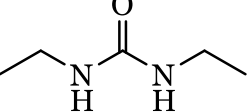
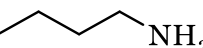
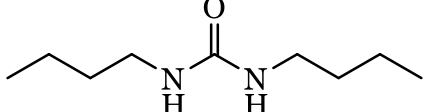
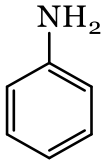
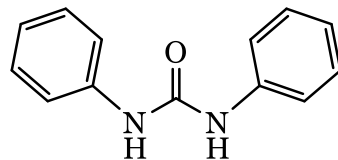
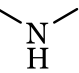
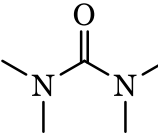
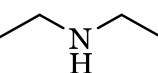
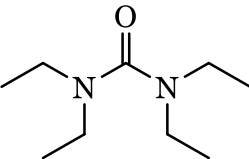
| Entry | Catalyst | Metal Concentration (ppm) |
|-------|------------------------------------|---------------------------|
| 1 | CuO | 20.1 ± 0.02 |
| 2 | Cu ₂ O | 11.1 ± 0.09 |
| 3 | Cu | 2.0 ± 0.7 |
| 4 | CuO/Al ₂ O ₃ | 4.8 ± 0.07 |
| 5 | ZnO | 35.7 ± 0.002 |
| 6 | Fe ₂ O ₃ | 1.1 ± 0.5 |

The observation after the experiment with ZnO showed that it was also dissolved in the reaction media as no particle was recovered after the reaction. AAS analysis confirms the catalyst leaching for ZnO, which had more than 35 ppm zinc concentration. A set of analyses for copper catalysts were also tested by AAS to investigate the effect of the oxidation state on leaching. It can be seen that mainly copper (II) oxides showed higher catalyst leaching whilst metallic copper only had 2 ppm copper concentration after the analysis. Copper (II) oxide had the highest concentration at 20 ppm, dropping it to 11 ppm for copper (I) oxide. Moreover, it was further decreased to 4.8 ppm by alumina-supported copper (II) catalysts, as expected. The loading for the catalyst was 13% on alumina particles, and the copper concentration detected can be attributed to the copper loading for this catalyst. That shows similar results with iron-based catalysts in Chapter 4, where iron concentration was changed with the oxidation states of iron, which shows the effect of the oxidation states in catalyst leaching.

6.1.2.c. Catalytic conversion of different amines into urea derivatives

After having a significant reactivity using butylamine over copper (II) oxide, the catalyst was then used for different amines with several attached groups like alkyl and aryl groups to produce their corresponding urea derivatives. It was discussed before that amine nucleophilicity highly depends on the attached group. Findings from the experiments with different amines are given in Table 6.6, with the structure of amines and their corresponding ureas.

Table 6.6 The synthesis of 1,3-disubstituted urea from different amines and CO₂ over CuO at optimised conditions (Reaction conditions: 20 mmol amine, 2 mmol CuO, 5 MPa CO₂, 4 ml NMP at 463 K for 2 hrs)

| | Amine | Urea | Yield (%) |
|---------------|---|--|-----------|
| Methylamine |  | N,N'-Dimethylurea  | 17.4 |
| Ethylamine |  | N,N'-Diethylurea  | 7.6 |
| Butylamine |  | N,N'-Dibutylurea  | 45 |
| Aniline |  | N,N'-Diphenylurea  | <1 |
| Dimethylamine |  | Tetramethylurea  | <1 |
| Diethylamine |  | Tetraethylurea  | 6.3 |

The highest yield was again achieved for DBU synthesis from butylamine with 44.8%, and the yield was dropped with a shorter alkyl group (Hart et al., 2007). The nucleophilicity of amines increases with the alkyl substituents, so a lower yield was obtained for the experiments with methylamine and ethylamine. It was also discussed in previous experiments that as methylamine and ethylamine used herein are aqueous solutions, lower yields were obtained for the experiments due to the presence of water.

An experiment with a bulky amine was also tested to investigate the effect of a steric hindrance on the reaction. The reaction was conducted using aniline with a phenyl group attached, and trace to no yield was achieved for the corresponding urea even though it has a larger substituent than other primary amines tested. This shows the influence of steric hindrance on the experiments, and it can be said that it is more influenced than the nucleophilicity of amines. Moreover, it was also reported that lower reactivity could be attributed to the conjugation of unpaired electrons, increasing the aniline's stability. For a better assessment, secondary amines were tested for the steric hindrance effect using aqueous solutions of dimethylamine and diethylamine. It can be seen that the yield was dropped for their corresponding ureas. Using aqueous solutions with different alkyl groups attached shows the effect of steric hindrance, where a 17.4% yield was achieved for methylamine. However, its secondary amines counterpart, dimethylamine, had no reactivity in the reaction. A similar reduction was also observed from ethylamine to diethylamine, from 7.6% to 6.3% yield. The slight difference between diethylamine and dimethylamine can be explained by the increased nucleophilicity of ethylamine thanks to longer alkyl substituents.

Catalyst leaching changes were also investigated in different amines for copper oxide, and results from the AAS analysis can be found in Table 6.7. The table indicated a similar pattern to the previous experiments, where the copper concentration was more than tripled from 17 to 60 ppm for methylamine and ethylamine, as reported for iron-based catalysts. Moreover, the copper concentration also had a similar increase to their secondary counterparts. However, secondary amines had lower copper concentrations in general, which were 6 and 20 ppm for dimethylamine and diethylamine, respectively.

Table 6.7 Copper oxide catalyst leaching in different amines

| Entry | Amine | Copper Concentration (ppm) |
|--------------|-----------------|---------------------------------------|
| 1 | Methylamine | 17.3 |
| 2 | Ethylamine | 59.5 |
| 3 | Butylamine | 20.1 |
| 4 | Cyclohexylamine | 31.6 |
| 5 | Aniline | 65 |
| 6 | Dimethylamine | 6.4 |
| 7 | Diethylamine | 19.6 |

The highest concentration was detected for aniline with a bulky attached group at 65 ppm. Another amine with a larger substituent, cyclohexylamine, showed a relatively higher concentration, but it was half the amount in aniline. That shows the effect of amine on copper oxide leaching, where it is clear that the structure of amines used for the experiment can dramatically change the catalyst leaching dissolved in the reaction mixture.

6.1.3. DBU synthesis over CuO@SiO₂ core-shell catalysts

Experiments in Chapter 5 showed that silica coating could dramatically enhance the catalyst reactivity and stability. The interaction between the silica shell and copper oxide core can improve the catalyst reactivity with a limited catalyst leaching detected. As up to 8% DBU yield was achieved with different copper oxide loading in 423 K, shown in Section 5.2.2.b, experiments in the optimisation reactions showed that bulk copper oxide had a lower yield at the same reaction condition, where the yield was 6.9% for the bulk copper (II) oxide. Results showed that all core-shell catalysts with different CuO loadings showed higher yields than bulk copper (II) oxide. As it shows this great reactivity, a set of experiments was then performed at optimised reaction conditions and the changes in butylamine conversion and DBU selectivity over copper oxide loading are given in Figure 6.12.

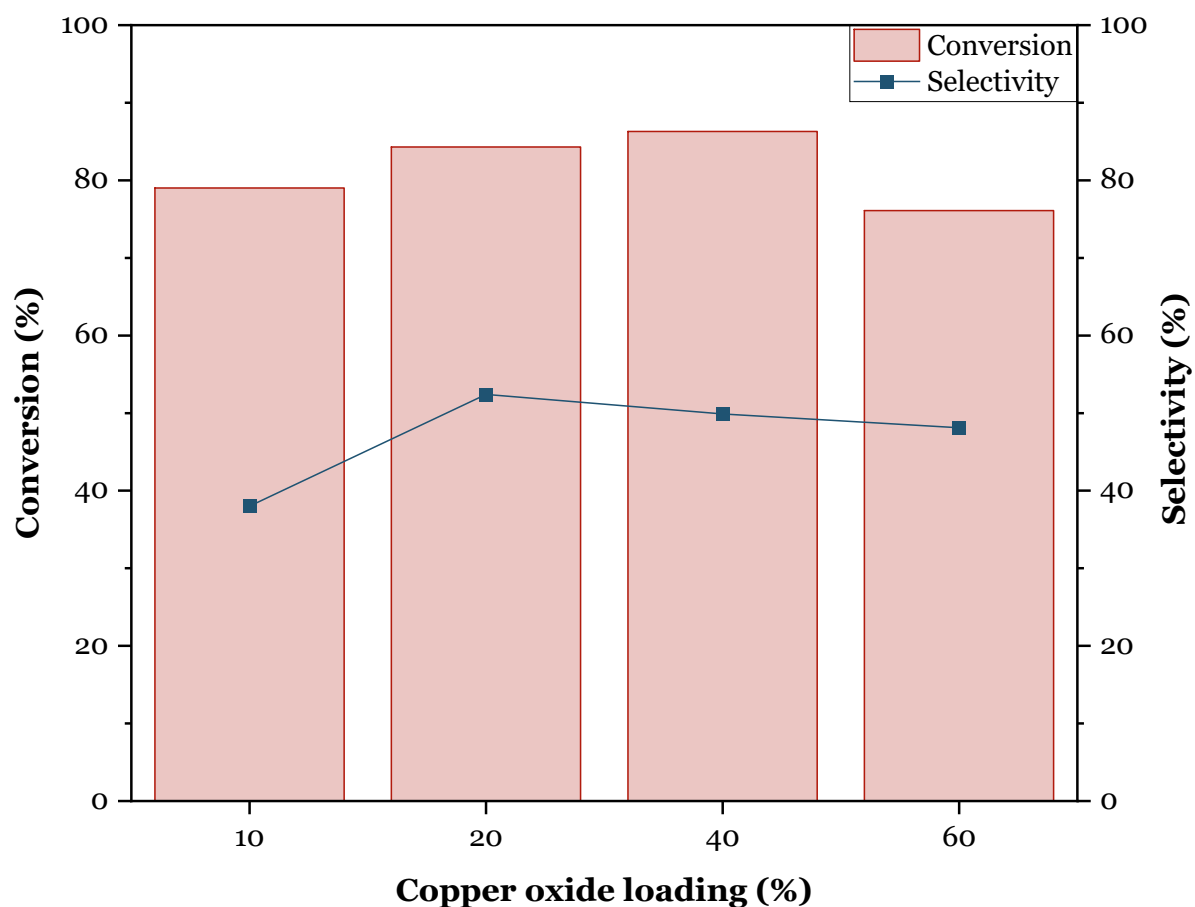


Figure 6.12 Changes in butylamine conversion and DBU selectivity over CuO@SiO_2 with various loadings (Reaction conditions: 20 mmol butylamine, 0.16 g catalyst, 5 MPa CO_2 , 4 ml NMP at 463 K for 2 hrs)

A yield between 7 and 8% yield was achieved in the previous chapter for the experiments with different copper oxide loadings. The optimisation reactions showed that bulk copper (II) oxide only showed 6.9% under the same reaction conditions, that proves the promotion effect of the core-shell catalyst in terms of reactivity. As core-shell catalysts showed their ability to produce more DBU with less catalyst leaching, their reactivity was then assessed under optimised reaction conditions. It can be seen from Figure 6.12 that butylamine conversion was slightly increased from just under 80% up to 86% for copper loading between 10 and 40%. It was then dropped to its lowest point at 76% for 60 mol% copper oxide loading, where the most deformation was observed for the silica shell. Core-shell catalyst with 20 mol% copper oxide loading with the best silica coating gave the highest selectivity of 44.2% for DBU among the others at optimised reaction conditions. It was 38% for 10 mol% CuO@SiO_2 and increased with the amount of copper oxide. However, catalysts with higher copper

oxide loading showed lower DBU selectivity than 20 mol% CuO@SiO₂. This was discussed before with the morphological analysis of the particles, where a better silica coating was observed for this copper oxide loading. Therefore a greater yield was achieved for the catalysts thanks to the interaction between the silica shell and copper oxide core. This increase in lower CuO loading can also be attributed to the complete silica shell formations; as limited broken silica spheres were detected for 20 mol% CuO@SiO₂ particles, it is believed that the yield obtained by this catalyst was higher because of the successful protection of active species against the leaching.

This interaction can be investigated with a comparison of the results with experiments in Section 4.2.2.b where only 12.7% yield was achieved by silica and 44.8% yield was obtained by bulk copper oxide particles with the butylamine conversion was under 80%, and the selectivity under 60%. It can be said that silica is not an effective catalyst for the reaction; however, the presence of mesoporous silica shell around copper oxide core particles increased the butylamine conversion from 80 to 85% with a lower copper oxide amount.

Since the highest yield was observed with a 20 mol% copper oxide loading with a well-formed silica coating, it was then used to run the experiment for different reaction times, and the results for both bulk CuO and mesoporous silica-coated copper oxide catalyst at different reaction times can be found in Table 6.8 along with other heterogeneous catalysts employed in the literature. The yields were almost the same in 2 hours, and then both increased with the reaction time, where CuO@SiO₂ showed 55.6% DBU yield, which is higher than bulk CuO particles. The comparison of the yield obtained with silica-coated copper-based catalysts showed that a similar yield to rare-earth element-based catalysts was achieved.

Experiments showed that a higher yield could be achieved with a lower amount of metal oxide loading, thanks to the great stability of core-shell catalysts against the catalyst leaching. The presence of silica coating around active species CuO reduced their leaching and thereby their reduction to metallic copper; thus the reactivity of the catalysts remained high and greater yield was achieved for longer reactions.

Table 6.8 Catalyst screening for the prepared core-shell catalysts for the synthesis of N,N-dibutylurea at optimised reaction conditions (Reaction conditions: 20 mmol butylamine, 0.16 g catalyst, 5 MPa CO₂, 4 ml NMP at 463 K)

| Catalyst | Solvent | Temp (K) | Pressure (MPa) | Time (h) | DBU Yield (%) | Ref |
|---|---------|----------|----------------|----------|---------------|-----------------------|
| CuO | NMP | 453 | 5 | 2 | 44.8 | - |
| CuO@SiO ₂ | NMP | 453 | 5 | 2 | 44.2 | - |
| CuO | NMP | 453 | 5 | 4 | 48.7 | - |
| CuO@SiO ₂ | NMP | 453 | 5 | 4 | 55.6 | - |
| Mn ₃ O ₄ | NMP | 433 | 5 | 4 | 40.8 | D. Sun et al. (2023) |
| Y ₂ O ₃ -ZrO ₂ | NMP | 433 | 2 | 24 | 58.0 | (D. Sun et al., 2018) |
| Sn-Ni-O | NMP | 433 | 4 | 4 | 57.8 | (Kulal et al., 2021) |
| MnO ₂ | NMP | 433 | 5 | 4 | 43.4 | (D. Sun et al., 2021) |
| ZnO/KF/ Al ₂ O ₃ | NMP | 453 | 1 | 4 | 64.8 | Kulal et al. (2020) |
| CeO ₂ | NMP | 433 | 5 | 4 | 72.3 | (Tamura et al., 2016) |

The improvement in catalyst stability by silica coating has already been discussed in Chapter 5, where the copper concentration was dropped by more than 40% by the presence of silica shell compared to bulk copper oxide. So, it can be said that higher catalytical activity can be achieved with limited leaching by the use of silica-coated copper-based core-shell catalysts.

6.2. Conclusion

Since the catalyst leaching was detected in Chapter 4 and reported in the literature, copper-based catalysts with inert outer silica shell were proposed as a solution for the problem. The synthesis of CuO@SiO₂ particles was discussed in Chapter 5 and it was observed that core-shell catalysts can limit the catalyst leaching considerably while they increase the reactivity of catalysts. To assess their reactivity at optimised reaction conditions for urea derivatives synthesis from CO₂ and amines, the reaction conditions need to be optimised since a different solvent and catalyst were employed in experiments. It was also stated in the literature that the interaction between a solvent and catalyst is unique, so an optimisation for the reaction conditions is required for each solvent and catalyst. Therefore, experiments in this chapter started with the optimisation reaction by varying solvent, reactant and solvent amounts and then followed by the reaction temperature and time. Experiments performed using different solvents confirmed again that polar aprotic solvents are highly effective owing to the lack of any hydrogen bonding, which allows nucleophiles to move freely in the reaction media. These findings showed similar results to Chapter 4 and the literature, and it was found that NMP is the most effective solvent that promotes the reaction without having any side effects. Although DMSO and acetonitrile had higher DBU yields than NMP, NMP was selected as a solvent for the experiments because of the side reactions occurring for these solvents. The leached copper concentration was also another parameter where acetonitrile caused the highest leaching for CuO whereas the concentration was limited for NMP.

After running experiments with different solvents, the impact of its amount was then evaluated using 0-8 ml of NMP. Results gained from the experiments revealed that 4 ml of NMP was the optimum amount to achieve greater yield for DBU. Later, the changes in the yield of DBU over varied butylamine amount was investigated using 10-40 mmol of butylamine. Results indicated that DBU selectivity was raised with butylamine amounts whereas its conversion was reduced. Thus, it was concluded that 20 mmol of butylamine was the optimum amount for the reaction with great DBU selectivity and a good butylamine conversion rate. After that, changes in butylamine conversion and DBU selectivity were determined over CO₂ pressure. Experiments with CO₂ pressures between 0.5 and 5 MPa were conducted, 5 MPa was selected as a CO₂

pressure for the optimised reaction conditions, since the selectivity for DBU was continuously raised over CO₂ amounts. In Chapter 4, an experiment without any CO₂ showed that CO₂ was the only source of the carbonyl group on DBU. Likewise, experiments with CO₂ and argon were performed to compare the results and it can be concluded that no DBU was produced with the presence of argon, confirming again that the carbonyl group on DBU comes from CO₂. In the last step of the optimisation of substance amounts, a set of experiments were performed with different CuO amounts. The experiment conducted without any catalyst had only a 4% DBU yield whilst it was boosted to 7% in the presence of 2 mmol CuO thanks to its superior selectivity towards DBU.

Experiments run at different reaction temperatures exhibited a dramatic effect on DBU synthesis in Chapter 4, but the decomposition of DMSO at higher temperatures was the limiting parameter for the experiments. The use of NMP that is a highly stable solvent against high temperatures, enabled to perform experiments at higher temperatures to evaluate the effect of temperature extensively. Similar to the experiments with DMSO, almost no reactivity was observed under 413 K, confirming the activation energy required for the reaction. Although butylamine conversion stayed flat between 413 and 463 K, the selectivity for DBU drastically changed over temperatures. The selectivity was under 10% at 413 K and increased to its peak point of 80% at 463 K. It then started to drop with the further increase in the temperature. AAS analysis conducted to investigate this decline revealed that the leached copper concentration was increased up to 463 K and then severely dropped after that temperature. It was concluded that the reduction of CuO was the main reason of this decrease; hence, 463 K was selected as an optimum reaction temperature. In the final stage of the optimisation process, the influence of reaction time was investigated up to 72 hours. The selectivity of DBU was just over 10% at 2 hours and reached over 80% with a gradual increase over time whilst the butylamine conversion was increased slowly from 50% to around 75% over time. In contrast to the gradual increase in the butylamine conversion, the selectivity of DBU dropped at 72 hours from 80 to 45%. Changes in the leached copper concentration determined by AAS explained that the main reason for this decline was the reduction of CuO into metallic copper, like reported for higher temperatures.

After an extensive study for the optimisation of reaction conditions, various catalysts were employed under the optimised conditions for the synthesis of urea derivatives from CO₂ and different amines. Experiments with different solvents at elevated temperatures displayed similar results and confirmed the effectiveness of NMP as a solvent for the reaction. The reactivity of different catalysts was then investigated under optimised conditions. The biggest difference detected between Chapter 4 and this chapter was the decline in the reactivity of iron-based catalysts. Fe₂O₃ was one of the best catalysts by the use of DMSO whereas it showed the lowest yields were obtained predominantly by iron-based catalysts, confirming again the unique interaction between a solvent and catalyst. On the other hand, copper-based catalysts showed superior catalytic performances together with CeO₂ by the use of NMP. Although CeO₂ showed the highest overall DBU yield, CuO was selected as a catalyst, since it is more abundant and cost-effective than CeO₂.

Catalyst leaching reported in the literature was also observed in the experiments, and it was concluded that the proposed core-shell copper-based catalyst is an excellent solution to the problem. Mesoporous silica-coated copper (II) oxide catalysts prepared in Chapter 5 showed similar reactivity with bulk copper (II) oxide catalysts with limited catalyst leaching. The presence of silica coating around active CuO particles reduced the leaching by 40%, compared to the same amount of bulk CuO employed. It was also found that 20 mol% CuO@SiO₂ had the greatest catalytic performance among the other core-shell catalysts with several CuO loadings and showed a similar DBU yield to bulk CuO with about 45%. The same DBU yield obtained with less amount of CuO was attributed to preventing the catalyst leaching by silica coating. Therefore, higher DBU yield was achieved by employing 20 mol% CuO@SiO₂ for longer reaction times: more than 55% DBU yield was obtained for the core-shell catalysts whereas it was only 49% for bulk CuO under optimised conditions for 4 hours.

In conclusion, experiments using copper (II) oxide catalysts showed that urea derivatives can be produced with excellent yields, similar to the literature. It was also concluded that the reported catalyst leaching can be avoided by the encapsulation of active species, CuO, with silica, consequently, the reactivity of the catalyst can be improved.

Chapter 7: Conclusions and Future Work

CO₂ is one of the main greenhouse gases that cause climate change, and there are a number of different measures that can be implemented to limit CO₂ emissions. Carbon capture and storage is one of the major approaches in these measures whilst the application of the utilisation of CO₂ instead of storing captured CO₂ can also enhance the global capacity of CO₂ removal from the atmosphere. Urea derivatives synthesis has gained considerable attention as an application of CO₂ utilisation, since recent studies showed that urea derivatives can be used as a drug for the treatment of HIV and different cancers. However, their traditional synthesis requires the use of toxic chemicals such as phosgene and carbon monoxide. Although studies showed that these chemicals can be produced from CO₂ and amines, the process highly depends on the use of rare-earth and expensive catalysts. In this aspect, a number of different chemicals that can be produced from CO₂ were assessed in order to evaluate the catalyst properties that are effective for the activation of stable CO₂.

In Chapter 2, an extensive literature review was conducted to highlight the active sites of several heterogeneous catalysts for CO₂ activation and the selectivity for the desired main product. The investigation on heterogeneous catalysts employed for the conversion of CO₂ into various chemicals such as cyclic carbonates, DMC, methanol and methylamines concluded that the acid sites of the catalysts play a key role in the activation of CO₂. It was also reported for different processes that the reactant used in the process can be activated by the basic sites of the catalysts. In the light of that, heterogeneous catalysts used for urea derivatives synthesis from CO₂ and different amines were analysed to find effective catalysts for the process. Studies showed that iron and copper-based catalysts with good basicity can be an alternative for the substitution of expensive metal oxide catalysts of cerium, yttrium and ruthenium. However, these catalysts have not been broadly studied for the reaction due to the catalyst leaching, especially for copper (II) oxide. To prevent this drawback, silica-encapsulated core-shell catalysts were proposed herein, as the stability of these catalysts against active core leaching was reported in the literature.

7.1. Conclusions

The main objective of the research was urea derivatives synthesis as an alternative approach for CO₂ utilisation using inexpensive and abundant heterogeneous catalysts. This was undertaken in three chapters: urea derivatives synthesis from CO₂ and amines over highly stable and reactive iron-based catalysts; developing silica-coated copper-based catalysts to increase the stability of copper-based catalysts against leaching; employing these prepared silica-encapsulated core-shell catalysts for the synthesis of urea derivatives from CO₂ and amines.

7.1.1. Conversion of CO₂ into urea derivatives over heterogeneous metal oxide catalysts

The lack of any catalytic conversion of CO₂ into urea derivatives using amines over cost-effective heterogeneous catalysts without requiring any additional co-catalyst or dehydration agents has prioritised the assessment of known to be stable and reactive iron-based catalysts. In this perspective, iron-based catalysts with different oxidation states were monitored for the process along with a number of different heterogeneous catalysts. Since the reaction rate equation revealed the dependence of reactant concentrations on the reaction, experiments were first conducted to optimise reaction conditions. It was seen that polar aprotic solvents had a good promoting effect for the reaction, and the overall yield for DBU can be enhanced by the use of 4 ml of DMSO. It was also concluded that the yield can be improved with the amount of reactants used in the reaction. The effect of reaction temperature and time was also assessed and it was found that the decomposition of DMSO was the limiting factor for the experiments.

Following the optimisation experiments, the catalytic conversion of CO₂ with various amines over several catalysts was conducted under the optimised reaction conditions. Iron-based catalysts showed great catalytic performance for the reaction of which Fe₂O₃ achieved the second highest yield for DBU with 47%, right after CeO₂. The comparison test using iron-based catalysts with different oxidation states uncovered the influence of catalyst basicity for the reaction. Thus, Fe₂O₃ with higher basicity compared to other iron-based catalysts tested showed greater selectivity for DBU. Experiments with different amines also showed that amine nucleophilicity heavily affects the yield as much as steric hindrance caused by the bulky attached groups.

AAS analysis was performed simultaneously for all experiments to determine the catalyst stability against leaching. The analyses obtained from the AAS revealed that Fe_2O_3 is highly stable for the reaction conditions tested, except for the leaching detected due to the decomposition of the solvent. Although there was a change in the leached iron concentration observed for different amines, it remained under 1 ppm for butylamine.

Overall, it can be said that Fe_2O_3 is a stable and reactive catalyst that can be an option to replace expensive and rare-earth-based catalysts for urea derivatives synthesis from CO_2 and amines.

7.1.2. Preparation of silica-coated metal oxide core-shell catalysts

Catalyst leaching that has been reported in the literature and seen in Chapter 4 for some catalysts, is one of the major problems for catalysis. A new catalyst design in a core-shell structure was proposed to address this problem. A number of different silica-coated core-shell catalysts with varied metal oxide cores were prepared in the second chapter of the thesis, and their stability and reactivity were assessed in the synthesis of urea derivatives from CO_2 and amines. Copper (II) oxide was first selected as a core material and the optimisation of the preparation method was undertaken before adapting the method for different core species. The experiments performed for the optimisation of catalyst preparation showed that the use of surfactant is essential for core-shell formation, together with ethyl acetate and ethanolamine as a catalyst for the precipitation of silica. Furthermore, the solvent used for the method and temperatures used at different stages of the method had a great influence on the formation of homogenous silica shells.

Core-shell catalysts with different CuO loadings were prepared using the preparation conditions that is carefully chosen after detailed analysis and performance tests at the optimisation steps for silica-encapsulated core-shell catalysts. Prepared core-shell catalysts were then analysed with several methods to evaluate their formations and structure. XRD analysis conducted on core-shell catalysts with different loading confirmed the maintenance of CuO crystal structure as well as silica formation. In addition, the removal of the surfactant after the calcination step was proved by FTIR analysis where the peak belonging to CTAB disappeared after the calcination of

particles. Also, the morphological analysis of the prepared core-shell particles was performed using SEM and TEM; the images gained from these analyses showed that core-shell particles with 20 mol% CuO loading have more uniform and complete silica formation around core species. In the light of the results obtained by the use of CuO, different metal oxides such as Fe₂O₃ and ZnO were used as core species; however, the analyses revealed that more optimisation steps were required to adapt conditions for different metal oxides. Finally, CuO/Al₂O₃ catalyst that has relatively large particles was coated with silica and SEM-EDS analysis performed on the prepared CuO/Al₂O₃@SiO₂ catalyst showed the successful deposition of silica shell around the particles.

Overall, the effectiveness of core-shell catalysts as a practical design to prevent catalyst leaching has been confirmed again by experiments conducted herein. It can also be said that the novel method developed in this study can be applied to different silica-coated core-shell catalysts and the catalyst leaching can be eliminated significantly using this model in different processes.

7.1.3. Urea derivatives synthesis over copper-based catalysts

The search for a reactive and cost-effective catalyst for the synthesis of urea derivatives synthesis from CO₂ and amines has put iron and copper-based catalysts at the forefront. The reactivity of iron-based catalysts was proved in Chapter 4, and the catalytic performances of copper-based catalysts were investigated in this chapter. However, the catalyst leaching observed especially for copper-based catalysts limited their use in this process. Core-shell catalysts have been proposed as a solution for preventing the catalyst leaching and the performances of prepared silica-coated core-shell catalysts were tested in this chapter along with the other copper-based catalysts. Since a different solvent and catalyst were employed compared to Chapter 4, optimisation reactions were performed before the assessment of the reactivity of catalysts.

Although similar results to Chapter 4 were obtained for most of the reaction parameters, a noticeable difference was detected for the experiments at different temperatures. By the use of NMP, the limiting factor detected due to the decomposition

of the solvent was eliminated thanks to the greater stability of NMP against higher temperatures. This provided an ability to perform experiments at elevated temperatures, but it was noticed from the experiments that the reactivity of CuO was reduced owing to the reduction into metallic copper at elevated temperatures. After the optimisation reactions, different catalysts were monitored for urea derivatives synthesis under the reaction conditions selected as a result of detailed assessments. As in Chapter 4, CeO₂ showed the greatest reactivity for the reaction, and it was followed by copper-based catalysts with 45% DBU yield. AAS analysis performed together with the reactivity tests indicated the effect of reaction conditions on the leached copper concentration.

In the final part of the study, the prepared core-shell catalysts in the previous chapter were employed for urea derivatives synthesis under the optimised reaction conditions. Results revealed that core-shell structures increased the active core reactivity as well as its stability. A similar yield to bulk CuO was achieved with the use of 20 mol% CuO@SiO₂ even though it has less amount of active species. This improved reactivity even overtook the bulk CuO catalysts with the increased reaction time; more than 55% DBU yield was obtained from the experiments run for 4 hours.

In overall, it can be easily said that copper-based catalysts are highly effective without requiring any additional promoters such as co-catalyst and dehydrating agents for urea derivatives synthesis from amines as an alternative approach for CO₂ utilisation. The main drawback of these reactive catalysts that is the catalyst leaching can be avoided by the preparation of silica-coated copper-based core-shell catalysts.

7.2. Recommendations for future work

Although it was presented that urea derivatives can be produced from CO₂ and amines over cost-effective heterogeneous catalysts without additional promoters, there are still many potential further research areas that need to be investigated to improve the potential of this process in order to be applied in CCU technologies.

Heterogeneous catalysis was adapted by a wide variety of industries; however, the working mechanism of the catalysts has been uncovered for most of the reactions. The evidence gained from the analytical methods used herein showed the reaction follows the proposed reaction pathway reported in the literature, further analysis can be performed to identify the intermediates of the reaction. C. Wu et al. (2010) performed the solid state ^{13}C NMR analysis for the identification of these compounds and it may also be used in the future to reveal the reaction routes for both iron and copper-based catalysts.

Moreover, the quantitative analysis was only performed for the main products obtained from the urea derivatives synthesis due to the limitations on time and financial resources. Further analysis is required for better carbon mass balance analysis and a better understanding of the reaction pathway. In addition, several different amines were used to form their corresponding ureas, but, the analysis of 1,3-dicyclohexylurea was not completed due to the low solubility of the compound. Although a number of different solvents were tested to dissolve it to analyse using GC-MS, all attempts were unsuccessful. A different solvent system or an alternative analytical method can be used to analyse these reactions in order to evaluate the conjugation effect on amine nucleophilicity reported for aniline. Also, products synthesised herein were symmetrical urea derivatives, experiments for the preparation of unsymmetrical urea derivatives using a mixture of two different amines could provide a different aspect for the area. Another further analysis required for the products obtained after the reaction is the identification of compounds formed because of the decomposition of DMSO. It was reported that the compound formed from this decomposition caused the catalyst leaching, thereby an analysis for these chemicals would be beneficial to prevent any catalyst leaching. Aside from that, a solid material produced from the reaction between DMSO and CuO needs to be analysed to understand the limitations of using these substances together.

It was broadly discussed in the literature review that the acid-base sites of the catalyst are responsible for the activation of both reactants. Some of the catalysts employed in this study were commercially available catalysts, therefore the characteristics of the catalysts were gained from data available in the literature. However, a characterisation of the catalysts used in the study is necessary to understand the properties effective for

the activation of both CO₂ and amines. Further catalyst characterisation can be performed using CO₂/NH₃-TPD analysis for the determination of acid-base sites of commercial and prepared catalysts. Moreover, it is known that the surface area of the catalyst is a key parameter for the accessibility of catalysts so, it is also important to perform BET analysis for all catalysts used in the study to evaluate the effect of surface area on catalyst reactivity.

The selection of catalysts used in the study was made with consideration of concerns such as the availability and cost-effectiveness of the catalysts. Iron and copper-based catalysts were selected as catalysts for urea derivatives synthesis, but CeO₂ showed greater reactivity in both chapters. Since core-shell catalysts showed that the reactivity of active species can be maintained with less amount of loadings, silica encapsulated cerium-based catalysts can be employed for the reaction for greater yield. Furthermore, several attempts made to prepare core-shell catalysts with different core materials failed to prepare a uniform coating of these cores with silica shell. Therefore, further optimisation is needed on the preparation conditions for these core-shell catalysts. In addition to the preparation method improvements, further analysis is also required using SEM-EDS for the mapping of prepared core-shell catalysts. Due to the limitations of the instrument used, an EDS analysis at higher magnification could not be performed. A different instrument for the analysis with SEM-EDS or advanced analytical techniques such as TEM-EDS can be conducted to monitor the silica coating around copper (II) oxide particles.

The prevention of catalyst leaching was one of the main focuses of the research and experiments were performed to minimize the leaching of catalysts tested. However, there was still some catalyst leaching observed for both iron-based and copper-based catalysts. The reactivity of these leached catalysts needs to be assessed for a better understanding of the heterogeneous nature of these catalysts. Sharma et al. (2014) used the hot filtration method to evaluate the effect of leached metal species on the reactivity of catalysts, which method can also be used to determine the effect of metal leaching on urea derivatives yields. Finally, iron-based catalysts showed great stability for the reaction conditions tested, even though there was some catalyst leaching detected due to the decomposition of the solvent. The reusability test of the catalysts, mainly iron-based catalysts should be monitored to show the advantages of catalysts.

References

- Abdalla, O. A. & Liu, D. (2018). Dimethyl Carbonate as a Promising Oxygenated Fuel for Combustion: A Review. *Energies*, 11(6).
- Alper, E. & Yuksel Orhan, O. (2017). CO₂ Utilization: Developments in Conversion Processes. *Petroleum*, 3(1), 109–126.
- Álvarez, A., Bansode, A., Urakawa, A., Bavykina, A. V, Wezendonk, T. A., Makkee, M., Gascon, J. & Kapteijn, F. (2017). Challenges in the Greener Production of Formates/Formic Acid, Methanol, and DME by Heterogeneously Catalyzed CO₂ Hydrogenation Processes. *Chemical reviews*, 117(14), 9804–9838.
- Alves, M., Grignard, B., Mereau, R., Jerome, C., Tassaing, T., & Detrembleur, C. (2017). Organocatalyzed coupling of carbon dioxide with epoxides for the synthesis of cyclic carbonates: catalyst design and mechanistic studies. *Catalysis Science & Technology*, 7(13), 2651–2684.
- An, H., Zhang, L., Zhao, X., & Wang, Y. (2014). Effect of preparation conditions on the catalytic performance of Cu–Fe/ZrO₂ for the synthesis of DPU from aniline and CO₂. *Chemical Engineering Journal*, 255, 266–273.
- An, X., Li, J., Zuo, Y., Zhang, Q., Wang, D. & Wang, J. (2007). A Cu/Zn/Al/Zr Fibrous Catalyst That Is an Improved CO₂ Hydrogenation to Methanol Catalyst. *Catalysis Letters*, 118(3), 264–269.
- Angunn, E., Nada, A. & Gaëlle, B.-C. (2014). Evaluation of Carbon Dioxide Utilisation Concepts: A Quick and Complete Methodology. *Energy Procedia*, 63, 8010–8016.

- Annino, R., & Villalobos, R. (1992). *Process Gas Chromatography: Fundamentals and Applications: On-line Analysis for Process Monitoring and Control*. Instrument Society of America.
- Ansari, M. B., Min, B.-H., Mo, Y.-H. & Park, S.-E. (2011). CO₂ Activation and Promotional Effect in the Oxidation of Cyclic Olefins over Mesoporous Carbon Nitrides. *Green Chemistry*, 13(6), 1416–1421.
- Appl, M. (2011). Ammonia, 2. Production Processes. *Ullmann's Encyclopedia of Industrial Chemistry*.
- A Arakawa, H., Aresta, M., Armor, J. N., Barteau, M. A., Beckman, E. J., Bell, A. T., Bercaw, J. E., Creutz, C., Dinjus, E., Dixon, D. A., Domen, K., DuBois, D. L., Eckert, J., Fujita, E., Gibson, D. H., Goddard, W. A., Goodman, D. W., Keller, J., Kubas, G. J., ... Tumas, W. (2001). Catalysis research of relevance to carbon management: Progress, challenges, and opportunities. In *Chemical Reviews* (Vol. 101, Issue 4, pp. 953–996).
- Aresta, M. (1993). The Fixation of Carbon Dioxide in Inorganic and Organic Chemicals. *Energy Conversion and Management*, 34(9), 745–752.
- Aresta, M., Dibenedetto, A. & Angelini, A. (2014). Catalysis for the Valorization of Exhaust Carbon : From CO₂ to Chemicals, Materials, and Fuels. Technological Use of CO₂.
- Aresta, M., Dibenedetto, A. & Dutta, A. (2017). Energy Issues in the Utilization of CO₂ in the Synthesis of Chemicals: The Case of the Direct Carboxylation of Alcohols to Dialkyl-Carbonates. *Catalysis Today*, 281, 345–351.
- Aresta, M., Dibenedetto, A., Gianfrate, L. & Pastore, C. (2003). Nb(V) Compounds as Epoxides Carboxylation Catalysts: The Role of the Solvent. *Journal of Molecular Catalysis A: Chemical*, 204–205, 245–252.
- Artz, J., Müller, T. E., Thenert, K., Kleinekorte, J., Meys, R., Sternberg, A., Bardow, A., & Leitner, W. (2018). Sustainable Conversion of Carbon Dioxide: An Integrated Review of Catalysis and Life Cycle Assessment. *Chemical Reviews*, 118(2), 434–504.
- Atkins, P. (1998). *Atkins' Physical Chemistry* (6th Ed). Oxford University Press.
- Auer, S. M., Gredig, S. V, Köppel, R. A. & Baiker, A. (1999). Synthesis of Methylamines from CO₂, H₂ and NH₃ over Cu–Mg–Al Mixed Oxides. *Journal of Molecular Catalysis A: Chemical*, 141(1), 193–203.
- Barzagli, F., Mani, F. & Peruzzini, M. (2011). From Greenhouse Gas to Feedstock: Formation of Ammonium Carbamate from CO₂ and NH₃ in Organic Solvents and Its Catalytic Conversion into Urea under Mild Conditions. *Green Chemistry*, 13(5), 1267–1274.
- Barzagli, F., Mani, F. & Peruzzini, M. (2016). Carbon Dioxide Uptake as Ammonia and Amine Carbamates and Their Efficient Conversion into Urea and 1,3-Disubstituted Ureas. *Journal of CO₂ Utilization*, 13, 81–89.
- Bhanage, B. M., Fujita, S., Ikushima, Y. & Arai, M. (2001). Synthesis of Dimethyl Carbonate and Glycols from Carbon Dioxide, Epoxides, and Methanol Using Heterogeneous Basic Metal Oxide Catalysts with High Activity and Selectivity. *Applied Catalysis A: General*, 219(1), 259–266.

- Bian, J., Xiao, M., Wang, S.-J., Lu, Y.-X. & Meng, Y.-Z. (2009). Carbon Nanotubes Supported Cu–Ni Bimetallic Catalysts and Their Properties for the Direct Synthesis of Dimethyl Carbonate from Methanol and Carbon Dioxide. *Applied Surface Science*, 255(16), 7188–7196.
- Bian, J., Xiao, M., Wang, S., Lu, Y. & Meng, Y. (2009). Direct Synthesis of DMC from CH₃OH and CO₂ over V-Doped Cu–Ni/AC Catalysts. *Catalysis Communications*, 10(8), 1142–1145.
- Bian, J., Xiao, M., Wang, S., Wang, X., Lu, Y. & Meng, Y. (2009). Highly Effective Synthesis of Dimethyl Carbonate from Methanol and Carbon Dioxide Using a Novel Copper–nickel/Graphite Bimetallic Nanocomposite Catalyst. *Chemical Engineering Journal*, 147(2), 287–296.
- Bigi, F., Maggi, R., & Sartori, G. (2000). Selected syntheses of ureas through phosgene substitutes. *Green Chemistry*, 2(4), 140–148.
- Bocuzzi, F., Coluccia, S., Martra, G. & Ravasio, N. (1999). Cu/SiO₂ and Cu/SiO₂–TiO₂ Catalysts: I. TEM, DR UV-Vis-NIR, and FTIR Characterisation. *Journal of Catalysis*, 184(2), 316–326.
- Brotzel, F. (2008). *Nucleophilicities of Amines, Amino Acids and Pyridines*
- Bui, M., Adjiman, C. S., Bardow, A., Anthony, E. J., Boston, A., Brown, S., Fennell, P. S., Fuss, S., Galindo, A., Hackett, L. A., Hallett, J. P., Herzog, H. J., Jackson, G., Kemper, J., Krevor, S., Maitland, G. C., Matuszewski, M., Metcalfe, I. S., Petit, C., ... Mac Dowell, N. (2018). Carbon capture and storage (CCS): the way forward. *Energy & Environmental Science*, 11(5), 1062–1176.
- Brunauer, S., Emmett, P. H. & Teller, E. (1938). Adsorption of Gases in Multimolecular Layers. *Journal of the American Chemical Society*, 60(2), 309–319.
- Ca', N. Della, Bottarelli, P., Dibenedetto, A., Aresta, M., Gabriele, B., Salerno, G. & Costa, M. (2011). Palladium-Catalyzed Synthesis of Symmetrical Urea Derivatives by Oxidative Carbonylation of Primary Amines in Carbon Dioxide Medium. *Journal of Catalysis*, 282(1), 120–127.
- Cai, Q., Lu, B., Guo, L. & Shan, Y. (2009). Studies on Synthesis of Dimethyl Carbonate from Methanol and Carbon Dioxide. *Catalysis Communications*, 10(5), 605–609.
- Cao, X., Sun, S. & Sun, R. (2017). Application of Biochar-Based Catalysts in Biomass Upgrading: A Review. *RSC Advances*, 7(77), 48793–48805.
- Casiello, M., Iannone, F., Cotugno, P., Monopoli, A., Cioffi, N., Ciminale, F., Trzeciak, A. M. & Nacci, A. (2015). Copper(II)-Catalysed Oxidative Carbonylation of Aminols and Amines in Water: A Direct Access to Oxazolidinones, Ureas and Carbamates. *Journal of Molecular Catalysis A: Chemical*, 407, 8–14.
- Centi, G., Quadrelli, E. A. & Perathoner, S. (2013). Catalysis for CO₂ Conversion: A Key Technology for Rapid Introduction of Renewable Energy in the Value Chain of Chemical Industries. *Energy & Environmental Science*, 6(6), 1711–1731.
- Cerón-Carrasco, J. P., Jacquemin, D., Laurence, C., Planchat, A., Reichardt, C., & Sraïdi, K. (2014). Solvent polarity scales: determination of new ET(30) values for 84 organic solvents. *Journal of Physical Organic Chemistry*, 27(6), 512–518.

- Chadwick, A., Arts, R., Bernstone, C., May, F., Thibeau, S., & Zweigel, P. (2008). *Best practice for the storage of CO₂ in saline aquifers : observations and guidelines from the SACS and CO₂STORE projects*. British Geological Survey.
- Chaemchuen, S., Semyonov, O. V, Dingemans, J., Xu, W., Zhuiykov, S., Khan, A., & Verpoort, F. (2019). Progress on Catalyst Development for Direct Synthesis of Dimethyl Carbonate from CO₂ and Methanol. *Chemistry Africa*, 2(4), 533–549.
- Chen, L., Wang, S., Zhou, J., Shen, Y., Zhao, Y., & Ma, X. (2014). Dimethyl carbonate synthesis from carbon dioxide and methanol over CeO₂ versus over ZrO₂: comparison of mechanisms. *RSC Advances*, 4(59), 30968–30975.
- Chen, W., Bao, Y., Li, X., Huang, J., Tang, Y., & Li, L. (2019). Mineralization of salicylic acid via catalytic ozonation with Fe-Cu@SiO₂ core-shell catalyst: A two-stage first order reaction. *Chemosphere*, 235, 470–480.
- Chiang, C. L., Lin, K. S., & Yu, S.-H. (2018). Preparation and characterization of H₃PW₁₂O₄₀/ZrO₂ catalyst for carbonation of methanol into dimethyl carbonate. *Research on Chemical Intermediates*, 44(6), 3797–3811.
- Choi, Y. S., Kim, H., Shin, S. H., Cheong, M., Kim, Y. J., Jang, H. G., Kim, H. S., & Lee, J. S. (2014). K₃PO₄-catalyzed carboxylation of amines to 1,3-disubstituted ureas: A mechanistic consideration. *Applied Catalysis B: Environmental*, 144, 317–324.
- Choi, Y., Futagami, K., Fujitani, T. & Nakamura, J. (2001). The Role of ZnO in Cu/ZnO Methanol Synthesis Catalysts – Morphology Effect or Active Site Model? *Applied Catalysis A: General*, 208(1), 163–167.
- Chorkendorff, I., & Niemantsverdriet, H. (2007). Introduction to Catalysis. In *Concepts of Modern Catalysis and Kinetics* (Second Edition).
- Cokoja, M., Wilhelm, M. E., Anthofer, M. H., Herrmann, W. A. & Kühn, F. E. (2015). Synthesis of Cyclic Carbonates from Epoxides and Carbon Dioxide by Using Organocatalysts. *ChemSusChem*, 8(15), 2436–2454.
- Copplestone, J. C., Kirk, C. M., Death, S. L., Betteridge, N. G., Fellows, S. M. & Wansbrough, H. Ammonia and Urea Production.
- Corbin, D. R., Schwarz, S. & Sonnichsen, G. C. (1997). Methylamines Synthesis: A Review. *Catalysis Today*, 37(2), 71–102.
- Cuéllar-Franca, R. M. & Azapagic, A. (2015). Carbon Capture, Storage and Utilisation Technologies: A Critical Analysis and Comparison of Their Life Cycle Environmental Impacts. *Journal of CO₂ Utilization*, 9, 82–102.
- D'Alessandro, D. M., Smit, B. & Long, J. R. (2010). Carbon Dioxide Capture: Prospects for New Materials. *Angewandte Chemie - International Edition*, 49(35), 6058–6082.
- Dai, W.-L., Luo, S.-L., Yin, S.-F. & Au, C.-T. (2009). The Direct Transformation of Carbon Dioxide to Organic Carbonates over Heterogeneous Catalysts. *Applied Catalysis A: General*, 366(1), 2–12.

- Dang, S., Yang, H., Gao, P., Wang, H., Li, X., Wei, W., & Sun, Y. (2019). A review of research progress on heterogeneous catalysts for methanol synthesis from carbon dioxide hydrogenation. *Catalysis Today*, 330, 61–75.
- Dann, S. E., Abel, E. W., Davies, A. G., Phillips, D. & Woollins, J. D. (2000). *Reactions and Characterization of Solids*. The Royal Society of Chemistry.
- Das, S., Ashok, J., Bian, Z., Dewangan, N., Wai, M. H., Du, Y., Borgna, A., Hidajat, K., & Kawi, S. (2018). Silica–Ceria sandwiched Ni core-shell catalyst for low temperature dry reforming of biogas: Coke resistance and mechanistic insights. *Applied Catalysis B: Environmental*, 230, 220–236.
- Das, S., Pérez-Ramírez, J., Gong, J., Dewangan, N., Hidajat, K., Gates, B. C., & Kawi, S. (2020). Core-shell structured catalysts for thermocatalytic, photocatalytic, and electrocatalytic conversion of CO₂. *Chemical Society Reviews*, 49(10), 2937–3004.
- DECC & BIS. (2014). *Demonstrating CO₂ Capture in the UK Cement, Chemicals, Iron and Steel and Oil Refining Sectors by 2025: A Techno-Economic Study Final Report for DECC and BIS About the Authors Element Energy University of Sheffield*.
- Deguchi, Y., Kono, M., Koizumi, Y., Izato, Y., & Miyake, A. (2020). Study on Autocatalytic Decomposition of Dimethyl Sulfoxide (DMSO). *Organic Process Research & Development*, 24(9), 1614–1620.
- Department of Energy & Climate Change. (2012). *CCS Roadmap: Supporting Deployment of Carbon Capture and Storage in the UK*. Retrieved from https://www.gov.uk/government/uploads/system/uploads/attachment_data/file/48317/4899-the-ccs-roadmap.pdf
- Dibenedetto, A., Angelini, A. & Stufano, P. (2014). Use of Carbon Dioxide as Feedstock for Chemicals and Fuels : Homogeneous and Heterogeneous Catalysis. , (October 2013), 334–353.
- Dorfs, D., Krahe, R., Falqui, A., Manna, L., Giannini, C., & Zanchet, D. (2011). 1.08 - Quantum Dots: Synthesis and Characterization. In D. L. Andrews, G. D. Scholes, & G. P. Wiederrecht (Eds.), *Comprehensive Nanoscience and Technology* (pp. 219–270). Academic Press.
- Downard, K. (2004). *Mass Spectrometry: A Foundation Course* (1st Edition). Royal Society of Chemistry.
- Driggers, R. G., Friedman, M. H., & Nichols, J. M. (2012). *Introduction to infrared and electro-optical systems* (2nd ed.). Artech House.
- Du, X., Zhao, C., Luan, Y., Zhang, C., Jaroniec, M., Huang, H., Zhang, X., & Qiao, S.-Z. (2017). Dendritic porous yolk@ordered mesoporous shell structured heterogeneous nanocatalysts with enhanced stability. *Journal of Materials Chemistry A*, 5(40), 21560–21569.
- Dutrow, B. L. & Clark, C. M. (2017). *Geochemical Instrumentation and Analysis, X-Ray Powder Diffraction (XRD)*.

- Dziejarski, B., Krzyżyńska, R., & Andersson, K. (2023). Current status of carbon capture, utilization, and storage technologies in the global economy: A survey of technical assessment. *Fuel*, 342, 127776.
- Earth Science Communications Team (NASA). (2019). *Carbon dioxide*. <https://climate.nasa.gov/vital-signs/carbon-dioxide/>
- El-Nahhal, I. M., Salem, J. K., Kuhn, S., Hammad, T., Hempelmann, R., & al Bhaisi, S. (2016). Synthesis and characterization of silica-, meso-silica- and their functionalized silica-coated copper oxide nanomaterials. *Journal of Sol-Gel Science and Technology*, 79(3), 573–583.
- ESRL. (2023). *Trends in Atmospheric Carbon Dioxide*. <https://gml.noaa.gov/ccgg/trends/global.html>
- Finsel, M., Hemme, M., Döring, S., Rüter, J. S. v, Dahl, G. T., Krekeler, T., Kornowski, A., Ritter, M., Weller, H., & Vossmeier, T. (2019). Synthesis and thermal stability of ZrO(2)@SiO(2) core-shell submicron particles. *RSC Advances*, 9(46), 26902–26914.
- Fournier, J., Bruneau, C., Dixneuf, P. H. & Lecolier, S. (1991). Ruthenium-Catalyzed Synthesis of Symmetrical N,N'-Dialkylureas Directly from Carbon Dioxide and Amines. *The Journal of Organic Chemistry*, 56(14), 4456–4458.
- Friedlingstein, P., O'sullivan, M., Jones, M. W., Andrew, R. M., Gregor, L., Hauck, J., Le Quéré, C., Luijkx, I. T., Olsen, A., Peters, G. P., Zeng, J., & Zheng, B. (2022). Global Carbon Budget 2022. *Earth System Science Data*, 14(11), 4811–4900.
- Froidevaux, V., Negrell, C., Caillol, S., Pascault, J.-P. & Boutevin, B. (2016). Biobased Amines: From Synthesis to Polymers; Present and Future. *Chemical Reviews*, 116(22), 14181–14224.
- Fujita, S.-I., Usui, M. & Takezawa, N. (1992). Mechanism of the Reverse Water Gas Shift Reaction over Cu/ZnO Catalyst. *Journal of Catalysis*, 134(1), 220–225.
- Fujitani, T. & Nakamura, J. (2000). The Chemical Modification Seen in the Cu/ZnO Methanol Synthesis Catalysts. *Applied Catalysis A: General*, 191(1), 111–129.
- Gabriele, B., Salerno, G., Mancuso, R. & Costa, M. (2004). Efficient Synthesis of Ureas by Direct Palladium-Catalyzed Oxidative Carbonylation of Amines. *The Journal of Organic Chemistry*, 69(14), 4741–4750.
- Galedari, N. A., Rahmani, M., & Tasbihi, M. (2017). Preparation, characterization, and application of ZnO@SiO₂ core-shell structured catalyst for photocatalytic degradation of phenol. *Environmental Science and Pollution Research*, 24(14), 12655–12663.
- Gallucci, F., Paturzo, L. & Basile, A. (2004). An Experimental Study of CO₂ Hydrogenation into Methanol Involving a Zeolite Membrane Reactor. *Chemical Engineering and Processing: Process Intensification*, 43(8), 1029–1036.
- Galvita, V. V., Poelman, H., Bliznuk, V., Detavernier, C., & Marin, G. B. (2013). CeO₂-Modified Fe₂O₃ for CO₂ Utilization via Chemical Looping. *Industrial & Engineering Chemistry Research*, 52(25), 8416–8426.

- Garba, M. D., Usman, M., Khan, S., Shehzad, F., Galadima, A., Ehsan, M. F., Ghanem, A. S., & Humayun, M. (2021). CO₂ towards fuels: A review of catalytic conversion of carbon dioxide to hydrocarbons. *Journal of Environmental Chemical Engineering*, 9(2), 104756.
- Ghosh, A. K., & Brindisi, M. (2020). Urea Derivatives in Modern Drug Discovery and Medicinal Chemistry. *Journal of Medicinal Chemistry*, 63(6), 2751–2788.
- Global CCS Institute. (2021). *The Global Status of CCS: 2021*.
- Global CO₂ Initiative. (2016). *Global Roadmap for Implementing CO₂ Utilization*.
- Greasley, S. L., Page, S. J., Sirovica, S., Chen, S., Martin, R. A., Riveiro, A., Hanna, J. v., Porter, A. E., & Jones, J. R. (2016). Controlling particle size in the Stöber process and incorporation of calcium. *Journal of Colloid and Interface Science*, 469, 213–223.
- Gredig, S. V., Koepfel, R. A. & Baiker, A. (1995). Synthesis of Methylamines from Carbon Dioxide and Ammonia. *Journal of the Chemical Society, Chemical Communications*, (1), 73–74.
- Gredig, S. V, Koepfel, R. & Baiker, A. (1997). Synthesis of Methylamines from CO₂, H₂ and NH₃. Catalytic Behaviour of Various Metal-Alumina Catalysts. *Applied Catalysis A: General*, 162(1), 249–260.
- Gredig, S. V, Maurer, R., Koepfel, R. & Baiker, A. (1997). Copper-Catalyzed Synthesis of Methylamines from CO₂, H₂ and NH₃. Influence of Support. *Journal of Molecular Catalysis A: Chemical*, 127(1), 133–142.
- Gründling, C., Eder-Mirrh, G., & Lercher, J. A. (1996). Selectivity Enhancement in Methylamine Synthesis via Postsynthesis Modification of Brønsted Acidic Mordenite: An Infrared Spectroscopic and Kinetic Study on the Reaction Mechanism. *Journal of Catalysis*, 160(2), 299–308.
- Guo, X., Mao, D., Lu, G., Wang, S. & Wu, G. (2010). Glycine–nitrate Combustion Synthesis of CuO–ZnO–ZrO₂ Catalysts for Methanol Synthesis from CO₂ Hydrogenation. *Journal of Catalysis*, 271(2), 178–185.
- Guo, X., Mao, D., Wang, S., Wu, G. & Lu, G. (2009). Combustion Synthesis of CuO–ZnO–ZrO₂ Catalysts for the Hydrogenation of Carbon Dioxide to Methanol. *Catalysis Communications*, 10(13), 1661–1664.
- Hakeem, A. A., Li, M., Berger, R. J., Kapteijn, F., & Makkee, M. (2015). Kinetics of the high temperature water–gas shift over Fe₂O₃/ZrO₂, Rh/ZrO₂ and Rh/Fe₂O₃/ZrO₂. *Chemical Engineering Journal*, 263, 427–434.
- Hakim, A., Marliza, T. S., Abu Tahari, N. M., Wan Isahak, R. W. N., Yusop, R. M., Mohamed Hisham, W. M., & Yarmo, A. M. (2016). Studies on CO₂ Adsorption and Desorption Properties from Various Types of Iron Oxides (FeO, Fe₂O₃, and Fe₃O₄). *Industrial & Engineering Chemistry Research*, 55(29), 7888–7897.
- Hart, H., Craine, L. E., Hart, D. J., & Hadad, C. M. (2007). *Organic Chemistry : A Short Course, 12th Edition*. Houghton Mifflin.
- Hashimoto, M., Eda, Y., Osanai, Y., Iwai, T. & Aoki, S. (1986). A Novel Decarboxylation of .ALPHA.-Amino Acids. A Facile Method of Decarboxylation by the Use of 2-Cyclohexen-1-One as a Catalyst.

- He, M., Sun, Y. & Han, B. (2013). Green Carbon Science: Scientific Basis for Integrating Carbon Resource Processing, Utilization, and Recycling. , 9620–9633.
- He, S. & Sci, E. E. (2012). Title : Carbon Dioxide Utilization with C – N Bond Formation : As Featured in : Energy & Carbon Dioxide Utilization with C – N Bond Formation : Carbon Dioxide Capture and Subsequent Conversion. , (207890).
- Head, D. L., & McCarty, C. G. (1973). The thermal decomposition of DMSO. *Tetrahedron Letters*, 14(16), 1405–1408.
- Honda, M., Tamura, M., Nakagawa, Y., Sonehara, S., Suzuki, K., Fujimoto, K., & Tomishige, K. (2013). Ceria-Catalyzed Conversion of Carbon Dioxide into Dimethyl Carbonate with 2-Cyanopyridine. *ChemSusChem*, 6(8), 1341–1344.
- Hong, Z., Cao, Y., Deng, J. & Fan, K. (2002). CO₂ Hydrogenation to Methanol Over Cu/ZnO/Al₂O₃ Catalysts Prepared by a Novel Gel-Network-Coprecipitation Method. *Catalysis Letters*, 82(1), 37–44.
- Huo, L., Wang, T., Pu, Y., Li, C., Li, L., Zhai, M., Qiao, C., & Bai, Y. (2021). Effect of Cobalt Doping on the Stability of CaO-Based Catalysts for Dimethyl Carbonate Synthesis via the Transesterification of Propylene Carbonate with Methanol. *ChemistrySelect*, 6(38), 10226–10237.
- IEA. (2021). *Ammonia Technology Roadmap*.
<https://www.iea.org/reports/ammonia-technology-roadmap>
- IEA. (2022a). *CO₂ Capture and Utilisation*. <https://www.iea.org/reports/co2-capture-and-utilisation>
- IEA. (2022b). *Carbon Capture, Utilisation and Storage*.
<https://www.iea.org/reports/carbon-capture-utilisation-and-storage-2>
- IEA. (2023). *CO₂ Emissions in 2022*. <https://www.iea.org/reports/co2-emissions-in-2022>
- Ilsemann, J., Straß-Eifert, A., Friedland, J., Kiewidt, L., Thöming, J., Bäumer, M., & Güttel, R. (2019). Cobalt@Silica Core-Shell Catalysts for Hydrogenation of CO/CO₂ Mixtures to Methane. *ChemCatChem*, 11(19), 4884–4893.
- Ion, A., Parvulescu, V., Jacobs, P. & Vos, D. De. (2007). Synthesis of Symmetrical or Asymmetrical Urea Compounds from CO₂ via Base Catalysis. *Green Chemistry*, 9(2), 158–161.
- IPCC. (2022). *Climate Change 2022: Mitigation of Climate Change. Contribution of Working Group III to the Sixth Assessment Report of the Intergovernmental Panel on Climate Change*.
- Ivanova, E. H. (2005). ATOMIC ABSORPTION SPECTROMETRY | Principles and Instrumentation. In P. Worsfold, A. Townshend, & C. Poole (Eds.), *Encyclopedia of Analytical Science (Second Edition)* (pp. 149–156).
- Jadhav, S. G., Vaidya, P. D., Bhanage, B. M. & Joshi, J. B. (2014). Catalytic Carbon Dioxide Hydrogenation to Methanol: A Review of Recent Studies. *Chemical Engineering Research and Design*, 92(11), 2557–2567.

- Jiang, C., Guo, Y., Wang, C., Hu, C., Wu, Y. & Wang, E. (2003). Synthesis of Dimethyl Carbonate from Methanol and Carbon Dioxide in the Presence of Polyoxometalates under Mild Conditions. *Applied Catalysis A: General*, 256(1), 203–212.
- Jiang, X., Nie, X., Guo, X., Song, C., & Chen, J. G. (2020). Recent Advances in Carbon Dioxide Hydrogenation to Methanol via Heterogeneous Catalysis. *Chemical Reviews*, 120(15), 7984–8034.
- Jiang, Z., Xiao, T., Kuznetsov, V. & Edwards, P. (2010). *Turning Carbon Dioxide into Fuel*.
- Joo, O.-S., Jung, K.-D., Moon, I., Rozovskii, A. Ya., Lin, G. I., Han, S.-H., & Uhm, S.-J. (1999). Carbon dioxide hydrogenation to form methanol via a reverse-water-gas-shift reaction (the CAMERE process). *Industrial and Engineering Chemistry Research*, 38(5), 1808–1812.
- Joo, S. H., Park, J. Y., Tsung, C.-K., Yamada, Y., Yang, P., & Somorjai, G. A. (2009). Thermally stable Pt/mesoporous silica core-shell nanocatalysts for high-temperature reactions. *Nature Materials*, 8(2), 126–131.
- Joshi, D. P., Pant, G., Arora, N., & Nainwal, S. (2017). Effect of solvents on morphology, magnetic and dielectric properties of (α -Fe(2)O(3)@SiO(2)) core-shell nanoparticles. *Heliyon*, 3(2), e00253–e00253.
- Jung, K. T. & Bell, A. T. (2001). An in Situ Infrared Study of Dimethyl Carbonate Synthesis from Carbon Dioxide and Methanol over Zirconia. *Journal of Catalysis*, 204(2), 339–347.
- Kanzian, T., Nigst, T. A., Maier, A., Pichl, S., & Mayr, H. (2009). Nucleophilic Reactivities of Primary and Secondary Amines in Acetonitrile. *European Journal of Organic Chemistry*, 2009(36), 6379–6385.
- Kenarsari, S. D., Yang, D., Jiang, G., Zhang, S., Wang, J., Russell, A. G., Wei, Q. & Fan, M. (2013). Review of Recent Advances in Carbon Dioxide Separation and Capture. *RSC Advances*, 3(45), 22739–22773.
- Keshavarz, H., Khavandi, A., Alamolhoda, S., & Naimi-Jamal, M. R. (2020). pH-Sensitive magnetite mesoporous silica nanocomposites for controlled drug delivery and hyperthermia. *RSC Advances*, 10(64), 39008–39016.
- Keturakis, C. J., Zhu, M., Gibson, E. K., Daturi, M., Tao, F., Frenkel, A. I., & Wachs, I. E. (2016). Dynamics of CrO₃–Fe₂O₃ Catalysts during the High-Temperature Water-Gas Shift Reaction: Molecular Structures and Reactivity. *ACS Catalysis*, 6(7), 4786–4798.
- Khalifeh, R., Karimi, M., Rajabzadeh, M., Hafizi, A., & Nogorani, F. S. (2020). Synthesis and morphology control of nano CuAl₂O₄ hollow spheres and their application as an efficient and sustainable catalyst for CO₂ fixation. *Journal of CO₂ Utilization*, 41, 101233.
- Kimura, M., Yamamoto, T. & Yamaguchi, S. (1999). Automated Metabolic Profiling and Interpretation of GC/MS Data for Organic Acidemia Screening: A Personal Computer-Based System. *The Tohoku Journal of Experimental Medicine*, 188(4), 317–334.

- Knežević, N. Ž., Ruiz-Hernández, E., Hennink, W. E., & Vallet-Regí, M. (2013). Magnetic mesoporous silica-based core/shell nanoparticles for biomedical applications. *RSC Advances*, 3(25), 9584–9593.
- Kohli, K., Sharma, B. K., & Panchal, C. B. (2022). Dimethyl Carbonate: Review of Synthesis Routes and Catalysts Used. *Energies*, 15(14).
- Koizumi, H., Takeuchi, K., Matsumoto, K., Fukaya, N., Sato, K., Uchida, M., Matsumoto, S., Hamura, S., & Choi, J.-C. (2021). One-pot catalytic synthesis of urea derivatives from alkyl ammonium carbamates using low concentrations of CO₂. *Communications Chemistry*, 4(1), 66.
- Kosari, M., Anjum, U., Xi, S., Lim, A. M. H., Seayad, A. M., Raj, E. A. J., Kozlov, S. M., Borgna, A., & Zeng, H. C. (2021). Revamping SiO₂ Spheres by Core-Shell Porosity Endowment to Construct a Mazelike Nanoreactor for Enhanced Catalysis in CO₂ Hydrogenation to Methanol. *Advanced Functional Materials*, 31(47), 2102896.
- Kulal, N., John, C., & Shanbhag, G. V. (2020). Rational design of bifunctional catalyst from KF and ZnO combination on alumina for cyclic urea synthesis from CO₂ and diamine. *Applied Catalysis A: General*, 598, 117550.
- Kulal, N., Vetrivel, R., Gopinath, C. S., Ravindran, R. K., Rao, V. N., Shetty, M., Shrikanth, R., Rangappa, D., & Shanbhag, G. V. (2021). Green route for carbonylation of amines by CO₂ using Sn-Ni-O bifunctional catalyst and theoretical study for finding best suited active sites. *Chemical Engineering Journal*, 419, 129439.
- Kumar, P., Matoh, L., Kaur, R., & Štangar, U. L. (2021). Synergic effect of manganese oxide on ceria based catalyst for direct conversion of CO₂ to green fuel additive: Catalyst activity and thermodynamics study. *Fuel*, 285, 119083.
- Lammens, T. M., Franssen, M. C. R., Scott, E. L. & Sanders, J. P. M. (2012). Availability of Protein-Derived Amino Acids as Feedstock for the Production of Bio-Based Chemicals. *Biomass and Bioenergy*, 44, 168–181.
- Lane, R. W., & McDonald, H. J. (1946). Kinetics of the Reaction between Copper and Aqueous Ammonia¹. *Journal of the American Chemical Society*, 68(9), 1699–1704.
- Laosiripojana, N. & Faungnawakij, K. (2014). Synthetic Fuel Production from the Catalytic Thermochemical Conversion. , 215–243.
- Leitner, W., Markewitz, P., Mu, T. E. & Kuckshinrichs, W. (2015). *Opportunities for Utilizing and Recycling CO₂*.
- Leng, Y. (2013). Materials Characterization: Introduction to Microscopic and Spectroscopic Methods. In *Materials Characterization*.
- Leung, D. Y. C., Caramanna, G. & Maroto-Valer, M. M. (2014). An Overview of Current Status of Carbon Dioxide Capture and Storage Technologies. *Renewable and Sustainable Energy Reviews*, 39, 426–443.
- Li, Y., Lu, G., & Ma, J. (2014). Highly active and stable nano NiO–MgO catalyst encapsulated by silica with a core–shell structure for CO₂ methanation. *RSC Advances*, 4(34), 17420–17428.

- Liao, Y., Li, F., Dai, X., Zhao, N., & Xiao, F. (2018). Dimethyl carbonate synthesis over solid base catalysts derived from Ca–Al layered double hydroxides. *Chemical Papers*, 72(8), 1963–1971.
- Liu, J., Bu, W., Zhang, S., Chen, F., Xing, H., Pan, L., Zhou, L., Peng, W., & Shi, J. (2012). Controlled Synthesis of Uniform and Monodisperse Upconversion Core/Mesoporous Silica Shell Nanocomposites for Bimodal Imaging. *Chemistry – A European Journal*, 18(8), 2335–2341.
- Liu, N., Xue, Y., Yu, Z., Li, Y., Xu, Y., Xu, J., Xue, B., Luo, J., & Wang, F. (2023). Zn-Doped CeO₂ Nanorods: a Highly Efficient Heterogeneous Catalyst for the Direct Synthesis of Dimethyl Carbonate from CO₂ and Methanol. *ChemistrySelect*, 8(3), e202203472.
- Liu, S., Su, Q., Fu, M., Deng, L., Wang, Y., Dong, L., Liu, Y., Ma, X., & Cheng, W. (2022). Core-Shell Dispersed Polymeric Ionic Liquids as Efficient Heterogeneous Catalyst for CO₂ Conversion into Cyclic Carbonates. *Catalysis Letters*.
- Liu, S., Wang, M., Cheng, Q., He, Y., Ni, J., Liu, J., Yan, C., & Qian, T. (2022). Turning Waste into Wealth: Sustainable Production of High-Value-Added Chemicals from Catalytic Coupling of Carbon Dioxide and Nitrogenous Small Molecules. *ACS Nano*, 16(11), 17911–17930.
- Look, G. van. (1988). *Silylating Agents: Derivatization Reagents, Protecting-Group Reagents, Organosilicon Compounds, Analytical Applications, Synthetic Applications*.
- Lv, C., Liu, D., Muschin, T., Bai, C., Bao, A., & Bao, Y.-S. (2022). From amides to urea derivatives or carbamates with chemospecific C–C bond cleavage at room temperature. *Organic Chemistry Frontiers*, 9(5), 1354–1363.
- Lowry, T. H., & Richardson, K. S. (1987). *Mechanism and Theory in Organic Chemistry, Third Edition* (Third Edition).
- Marcos, F. C. F., Assaf, J. M., Giudici, R., & Assaf, E. M. (2019). Surface interaction of CO₂/H₂ mixture on mesoporous ZrO₂: Effect of crystalline polymorph phases. *Applied Surface Science*, 496, 143671.
- Marcos, F. C. F., Cavalcanti, F. M., Petrolini, D. D., Lin, L., Betancourt, L. E., Senanayake, S. D., Rodriguez, J. A., Assaf, J. M., Giudici, R., & Assaf, E. M. (2022). Effect of operating parameters on H₂/CO₂ conversion to methanol over Cu-Zn oxide supported on ZrO₂ polymorph catalysts: Characterization and kinetics. *Chemical Engineering Journal*, 427, 130947.
- Markewitz, P., Kuckshinrichs, W., Leitner, W., Linszen, J., Zapp, P., Bongartz, R., Schreiber, A. & Müller, T. E. (2012). Worldwide Innovations in the Development of Carbon Capture Technologies and the Utilization of CO₂. *Energy & Environmental Science*, 5(6), 7281–7305.
- Martin, O., Martín, A. J., Mondelli, C., Mitchell, S., Segawa, T. F., Hauert, R., Drouilly, C., Curulla-Ferré, D., & Pérez-Ramírez, J. (2016). Indium Oxide as a Superior Catalyst for Methanol Synthesis by CO₂ Hydrogenation. *Angewandte Chemie International Edition*, 55(21), 6261–6265.

- McGuire, T. M., López-Vidal, E. M., Gregory, G. L., & Buchard, A. (2018). Synthesis of 5- to 8-membered cyclic carbonates from diols and CO₂: A one-step, atmospheric pressure and ambient temperature procedure. *Journal of CO₂ Utilization*, 27, 283–288.
- Meier, M., Ungerer, J., Klinge, M., & Nirschl, H. (2018). Formation of porous silica nanoparticles at higher reaction kinetics. *Powder Technology*, 339, 801–808.
- Min, J., Song, W., Hu, T., Zhi, Y., Xia, Z., Zhang, T., Shan, S., & Su, H. (2021). Fe₃O₄@SiO₂ nanoparticle-supported Co(III)-Salen composites as recyclable heterogeneous catalyst for the fixation of CO₂. *Ceramics International*, 47(24), 35320–35332.
- Mori, K., Mitani, Y., Hara, T., Mizugaki, T., Ebitani, K. & Kaneda, K. (2005). A Single-Site Hydroxyapatite-Bound Zinc Catalyst for Highly Efficient Chemical Fixation of Carbon Dioxide with Epoxides. *Chemical Communications*, (26), 3331–3333.
- Nasrollahzadeh, M., Atarod, M., Sajjadi, M., Sajadi, S. M., & Issaabadi, Z. (2019). Chapter 6 - Plant-Mediated Green Synthesis of Nanostructures: Mechanisms, Characterization, and Applications. In M. Nasrollahzadeh, S. M. Sajadi, M. Sajjadi, Z. Issaabadi, & M. Atarod (Eds.), *Interface Science and Technology* (Vol. 28, pp. 199–322). Elsevier.
- NETL. (2015). *Carbon Storage Atlas, Fifth Edition*. <https://doi.org/10.2172/1814017>
- Nishimura, S., Shishido, T., Ebitani, K., Teramura, K. & Tanaka, T. (2010). *Novel Catalytic Behavior of Cu/Al₂O₃ Catalyst against Daily Start-up and Shut-down (DSS)-like Operation in the Water Gas Shift Reaction*.
- Nomura, R., Hasegawa, Y., Ishimoto, M., Toyosaki, T. & Matsuda, H. (1992). Carbonylation of Amines by Carbon Dioxide in the Presence of an Organoantimony Catalyst. *The Journal of Organic Chemistry*, 57(26), 7339–7342.
- North, M., Pasquale, R. & Young, C. (2010). Synthesis of Cyclic Carbonates from Epoxides and CO₂. *Green Chemistry*, 12(9), 1514–1539.
- Olah, G. A., Goepfert, A. & Prakash, G. K. S. (2009). Chemical Recycling of Carbon Dioxide to Methanol and Dimethyl Ether: From Greenhouse Gas to Renewable, Environmentally Carbon Neutral Fuels and Synthetic Hydrocarbons. *The Journal of Organic Chemistry*, 74(2), 487–498.
- Omae, I. (2012). Recent Developments in Carbon Dioxide Utilization for the Production of Organic Chemicals. *Coordination Chemistry Reviews*, 256(13), 1384–1405.
- Quintana Gomez, L. (2017). *HYDROTHERMAL CONVERSION OF CO₂ INTO HIGHER HYDROCARBONS AND OXYGENATES* [PhD Thesis]. University of Sheffield.
- Özgeriş, F. B., Kaci, F. N., Özgeriş, B., & Görmez, A. (2022). The synthesis of unsymmetrical urea from substituted phenethylamine and the investigation of its antibacterial, anticancer, and antioxidant properties. *Biointerface Research in Applied Chemistry*, 12(5), 7052–7063.

- Park, S. K., Kim, K. do, & Kim, H. T. (2002). Preparation of silica nanoparticles: determination of the optimal synthesis conditions for small and uniform particles. *Colloids and Surfaces A: Physicochemical and Engineering Aspects*, 197(1–3), 7–17.
- Pelletier, J. D. A., & Basset, J.-M. (2016). Catalysis by Design: Well-Defined Single-Site Heterogeneous Catalysts. *Accounts of Chemical Research*, 49(4), 664–677.
- Pennycook, S. J. (2005). Transmission Electron Microscopy. In F. Bassani, G. L. Liedl, & P. Wyder (Eds.), *Encyclopedia of Condensed Matter Physics* (pp. 240–247). Elsevier.
- Pohanish, R. P. (2012). F, in: Pohanish, R. P. B. T.-S. H. of T. and H. C. and C. (Sixth E. (Ed.), *Sittig's Handbook of Toxic and Hazardous Chemicals and Carcinogens*, (pp. 1294–1373). Oxford: William Andrew Publishing.
- Primo, A., Aguado, E. & Garcia, H. (2013). CO₂-Fixation on Aliphatic α,ω -Diamines to Form Cyclic Ureas, Catalyzed by Ceria Nanoparticles That Were Obtained by Templating with Alginate. *ChemCatChem*, 5(4), 1020–1023.
- Ragaini, F. & Cenini, S. (1996). Mechanistic Studies of Palladium-Catalysed Carbonylation Reactions of Nitro Compounds to Isocyanates, Carbamates and Ureas. *Journal of Molecular Catalysis A: Chemical*, 109(1), 1–25.
- Rahman, I. A., Vejayakumaran, P., Sipaut, C. S., Ismail, J., & Chee, C. K. (2008). Effect of the drying techniques on the morphology of silica nanoparticles synthesized via sol–gel process. *Ceramics International*, 34(8), 2059–2066.
- Rajabzadeh, M., Khalifeh, R., Eshghi, H., & Hafizi, A. (2020). Design and synthesis of CuO@SiO₂ multi-yolk@shell and its application as a new catalyst for CO₂ fixation reaction under solventless condition. *Journal of Industrial and Engineering Chemistry*, 89, 458–469.
- Razali, N. (2017). *THE SYNTHESIS OF GLYCEROL CARBONATE FROM GLYCEROL AND CARBON DIOXIDE OVER HETEROGENEOUS CATALYSTS*. University of Sheffield.
- Razali, N. A. M., Lee, K. T., Bhatia, S. & Mohamed, A. R. (2012). Heterogeneous Catalysts for Production of Chemicals Using Carbon Dioxide as Raw Material: A Review. *Renewable and Sustainable Energy Reviews*, 16(7), 4951–4964.
- Reichardt, C. (2002). *Solvents and Solvent Effects in Organic Chemistry*. Wiley.
- Reimer, L. (1998). Scanning Electron Microscopy. In L. Reimer (Ed.), *Physics of Image Formation and Microanalysis*. Springer Berlin Heidelberg.
- Rinkesh, M. (2015). *What is Global Warming?* <http://www.conserve-energy-future.com/HowGlobalWarmingWorks.php>
- Road, S. P. (2010). Turning Carbon Dioxide into Fuel. , 3343–3364.
- Roy, S., Cherevotan, A., & Peter, S. C. (2018). Thermochemical CO₂ Hydrogenation to Single Carbon Products: Scientific and Technological Challenges. *ACS Energy Letters*, 3(8), 1938–1966.

- Rui, N., Wang, Z., Sun, K., Ye, J., Ge, Q., & Liu, C. (2017). CO₂ hydrogenation to methanol over Pd/In₂O₃: effects of Pd and oxygen vacancy. *Applied Catalysis B: Environmental*, 218, 488–497.
- Sadjadi, S., Heravi M., M., & Malmir, M. (2018). Pd(0) nanoparticle immobilized on cyclodextrin-nanosponge-decorated Fe₂O₃@SiO₂ core-shell hollow sphere: An efficient catalyst for CC coupling reactions. *Journal of the Taiwan Institute of Chemical Engineers*, 86, 240–251.
- Saito, M. & Murata, K. (2004). Development of High Performance Cu/ZnO-Based Catalysts for Methanol Synthesis and the Water-Gas Shift Reaction. *Catalysis Surveys from Asia*, 8(4), 285–294.
- Sakakura, T., Choi, J. & Yasuda, H. (2007). Transformation of Carbon Dioxide.
- Salgueiriño-Maceira, V., & Correa-Duarte, M. A. (2006). Cobalt and silica based core-shell structured nanospheres. *Journal of Materials Chemistry*, 16(36), 3593–3597.
- Sankar, M., Nair, C. M., Murty, K. V. G. K. & Manikandan, P. (2006). Transesterification of Cyclic Carbonates with Methanol at Ambient Conditions over Tungstate-Based Solid Catalysts. *Applied Catalysis A: General*, 312, 108–114.
- Schatten, H. (2012). Scanning Electron Microscopy for the Life Sciences. In *Advances in Microscopy and Microanalysis*. Cambridge University Press.
- Sekhar, A. C. S., Meera, C. J., Ziyad, K. V, Gopinath, Chinnakonda. S., & Vinod, C. P. (2013). Synthesis and catalytic activity of monodisperse gold–mesoporous silica core–shell nanocatalysts. *Catalysis Science & Technology*, 3(5), 1190–1193.
- Sharma, R. K., Monga, Y., & Puri, A. (2014). Magnetically separable silica@Fe₃O₄ core-shell supported nano-structured copper(II) composites as a versatile catalyst for the reduction of nitroarenes in aqueous medium at room temperature. *Journal of Molecular Catalysis A: Chemical*, 393, 84–95.
- Shi, F., Zhang, Q., Ma, Y., He, Y. & Deng, Y. (2005). From CO Oxidation to CO₂ Activation: An Unexpected Catalytic Activity of Polymer-Supported Nanogold. *Journal of the American Chemical Society*, 127(12), 4182–4183.
- Shi, R., Wang, J., Zhao, J., Liu, S., Hao, P., Li, Z., & Ren, J. (2018). Cu nanoparticles encapsulated with hollow carbon spheres for methanol oxidative carbonylation: Tuning of the catalytic properties by particle size control. *Applied Surface Science*, 459, 707–715.
- Sing, K. (2001). The Use of Nitrogen Adsorption for the Characterisation of Porous Materials. *Colloids and Surfaces A: Physicochemical and Engineering Aspects*, 187–188, 3–9.
- Śloczyński, J., Grabowski, R., Kozłowska, A., Olszewski, P., Stoch, J., Skrzypek, J. & Lachowska, M. (2004). Catalytic Activity of the M/(3ZnO·ZrO₂) System (M=Cu, Ag, Au) in the Hydrogenation of CO₂ to Methanol. *Applied Catalysis A: General*, 278(1), 11–23.
- Śloczyński, J., Grabowski, R., Olszewski, P., Kozłowska, A., Stoch, J., Lachowska, M. & Skrzypek, J. (2006). Effect of Metal Oxide Additives on the Activity and Stability of Cu/ZnO/ZrO₂ Catalysts in the Synthesis of Methanol from CO₂ and H₂. *Applied Catalysis A: General*, 310, 127–137.

- Son, G. M., Truong, C. C., Mishra, D. K., Mishra, V. & Kim, Y. J. (2018). One-Pot Synthesis of Disubstituted Urea from Carbon Dioxide, Propylene Oxide, and Amines Catalyzed by Imidazolium-Tetraiodoborate. *Bulletin of the Korean Chemical Society*, 39(2), 174–183.
- Smith, M. B., & March, J. (2006). Aliphatic Substitution: Nucleophilic and Organometallic. In *March's Advanced Organic Chemistry* (pp. 425–656).
- Sparkman, O. D., Penton, Z. E., & Kitson, F. G. (2011). Gas Chromatography and Mass Spectrometry: A Practical Guide. In O. D. Sparkman, Z. E. Penton, & F. G. Kitson (Eds.), *Gas Chromatography and Mass Spectrometry (Second Edition)*. Academic Press.
- Srinivas, B., Kumari, V. D., Sadanandam, G., Hymavathi, C., Subrahmanyam, M. & De, B. R. (2012). Photocatalytic Synthesis of Urea from in Situ Generated Ammonia and Carbon Dioxide. *Photochemistry and Photobiology*, 88(2), 233–241.
- Srivastava, R., Srinivas, D. & Ratnasamy, P. (2003). Synthesis of Polycarbonate Precursors over Titanosilicate Molecular Sieves. *Catalysis Letters*, 91(1), 133–139.
- Srivastava, R., Srinivas, D. & Ratnasamy, P. (2005). CO₂ Activation and Synthesis of Cyclic Carbonates and Alkyl/Aryl Carbamates over Adenine-Modified Ti-SBA-15 Solid Catalysts. *Journal of Catalysis*, 233(1), 1–15.
- Stachowiak, G. W., Batchelor, A. W., & Stachowiak, G. B. (2004). 8 - Surface Micrography and Analysis. In G. W. Stachowiak, A. W. Batchelor, & G. B. Stachowiak (Eds.), *Tribology Series* (Vol. 44, pp. 165–220). Elsevier.
- Stuart, B. H. (2004). *Infrared Spectroscopy: Fundamentals and Applications*.
- Stöber, W., Fink, A., & Bohn, E. (1968). Controlled growth of monodisperse silica spheres in the micron size range. *Journal of Colloid and Interface Science*, 26(1), 62–69.
- Sun, C., Zheng, Z., Wang, S., Li, X., Wu, X., An, X., & Xie, X. (2018). Yolk-shell structured Pt-CeO₂@Ni-SiO₂ as an efficient catalyst for enhanced hydrogen production from ethanol steam reforming. *Ceramics International*, 44(2), 1438–1442.
- Sun, D., Peng, L., Cheng, K., Zheng, Y., & Jiang, S. P. (2023). Comparative study of manganese oxides with different oxidation states for catalytic carbonylation of n-butylamine by CO₂. *Journal of CO₂ Utilization*, 68, 102382.
- Sun, D., Peng, L., Yang, Y., Fang, Y., Ping Jiang, S., & Shao, Z. (2022). Boosting catalytic activity of δ-MnO₂ through potassium incorporation for efficient carbonylation of amines by carbon dioxide. *Journal of Catalysis*, 409, 48–58.
- Sun, D., Xie, K., Fang, Y., & Yang, X. (2018). One-Pot Synthesis of N,N'-dialkylureas via Carbonylation of Amines with CO₂ Applying Y_{0.08}Zr_{0.92}O_{1.96} Mixed Oxide (YSZ-8) as a Heterogeneous Catalyst. *Catalysts*, 8(5).
- Sun, D.-L., Ye, J.-H., Fang, Y.-X., & Chao, Z.-S. (2016). Green Synthesis of N,N'-Dialkylureas from CO₂ and Amines Using Metal Salts of Oxalates as Catalysts. *Industrial & Engineering Chemistry Research*, 55(1), 64–70.

- Sun, K., Fan, Z., Ye, J., Yan, J., Ge, Q., Li, Y., He, W., Yang, W., & Liu, C. (2015). Hydrogenation of CO₂ to methanol over In₂O₃ catalyst. *Journal of CO₂ Utilization*, 12, 1–6.
- Sun, K., Zhang, Z., Shen, C., Rui, N., & Liu, C. (2022). The feasibility study of the indium oxide supported silver catalyst for selective hydrogenation of CO₂ to methanol. *Green Energy & Environment*, 7(4), 807–817.
- Suryanarayana, C., & Norton, M. G. (1998). Practical Aspects of X-Ray Diffraction. In C. Suryanarayana & M. G. Norton (Eds.), *X-Ray Diffraction: A Practical Approach* (pp. 63–94). Springer
- Tamboli, A. H., Chaugule, A. A. & Kim, H. (2017). Catalytic Developments in the Direct Dimethyl Carbonate Synthesis from Carbon Dioxide and Methanol. *Chemical Engineering Journal*, 323, 530–544.
- Tamura, M., Honda, M., Nakagawa, Y. & Tomishige, K. (2014). Direct Conversion of CO₂ with Diols, Aminoalcohols and Diamines to Cyclic Carbonates, Cyclic Carbamates and Cyclic Ureas Using Heterogeneous Catalysts. *Journal of Chemical Technology & Biotechnology*, 89(1), 19–33.
- Tamura, M., Ito, K., Nakagawa, Y. & Tomishige, K. (2016). CeO₂-Catalyzed Direct Synthesis of Dialkylureas from CO₂ and Amines. *Journal of Catalysis*, 343, 75–85.
- Tamura, M., Noro, K., Honda, M., Nakagawa, Y. & Tomishige, K. (2013). Highly Efficient Synthesis of Cyclic Ureas from CO₂ and Diamines by a Pure CeO₂ Catalyst Using a 2-Propanol Solvent. *Green Chemistry*, 15(6), 1567–1577.
- Tans, P. (NOAA/ESRL) & Keeling, R. (Scripps I. of O. (2022). Trends in Atmospheric Carbon Dioxide. Retrieved June 25, 2022, from <https://www.esrl.noaa.gov/gmd/ccgg/trends/>
- Tanvir, N. B., Yurchenko, O., Wilbertz, Ch., & Urban, G. (2016). Investigation of CO₂ reaction with copper oxide nanoparticles for room temperature gas sensing. *Journal of Materials Chemistry A*, 4(14), 5294–5302.
- Tavakoli Mohammadi, M. R. (2012). Ammonia Leaching in the Copper Industry: A Review
- Teng, Y., Scott, E. L., Witte-van Dijk, S. C. M. & Sanders, J. P. M. (2016). Simultaneous and Selective Decarboxylation of L-Serine and Deamination of l-Phenylalanine in an Amino Acid Mixture—a Means of Separating Amino Acids for Synthesizing Biobased Chemicals. *New Biotechnology*, 33(1), 171–178.
- Thomas, J. M., & Thomas, W. J. (2015). *Principles and Practice of Heterogeneous Catalysis*.
- Tian, Y., Ma, X., Chen, X., Chaoyue, Z., & Lu, X. (2022). The influence of shell thickness on coke resistance of core-shell catalyst in CO₂ catalytic reforming of biomass tar. *International Journal of Hydrogen Energy*, 47(29), 13838–13849.
- Tomishige, K., Furusawa, Y., Ikeda, Y., Asadullah, M. & Fujimoto, K. (2001). CeO₂-ZrO₂ Solid Solution Catalyst for Selective Synthesis of Dimethyl Carbonate from Methanol and Carbon Dioxide. *Catalysis Letters*, 76(1), 71–74.

- Tomishige, K., Gu, Y., Nakagawa, Y., & Tamura, M. (2020). Reaction of CO₂ With Alcohols to Linear-, Cyclic-, and Poly-Carbonates Using CeO₂-Based Catalysts. *Frontiers in Energy Research*, 8.
- Tomishige, K., Ikeda, Y., Sakaihorii, T. & Fujimoto, K. (2000). Catalytic Properties and Structure of Zirconia Catalysts for Direct Synthesis of Dimethyl Carbonate from Methanol and Carbon Dioxide. *Journal of Catalysis*, 192(2), 355–362.
- Toyir, J., Ramí rez de la Piscina, P., Fierro, J. L. G. & Homs, N. (2001). Catalytic Performance for CO₂ Conversion to Methanol of Gallium-Promoted Copper-Based Catalysts: Influence of Metallic Precursors. *Applied Catalysis B: Environmental*, 34(4), 255–266.
- Truong, C. C., Kim, J., Lee, Y., & Kim, Y. J. (2017). Well-Defined Cesium Benzotriazolide as an Active Catalyst for Generating Disubstituted Ureas from Carbon Dioxide and Amines. *ChemCatChem*, 9(2), 247–252.
- Tsai, M. Y., Oliphant, C. & Josephson, M. W. (1985). Identification of Metabolites Diagnostic for Organic Acidurias by Simultaneous Dual-Column Capillary Gas Chromatography. *Journal of Chromatography B: Biomedical Sciences and Applications*, 341, 1–10.
- Tu, M. & Davis, R. J. (2001). Cycloaddition of CO₂ to Epoxides over Solid Base Catalysts. *Journal of Catalysis*, 199(1), 85–91.
- UNFCCC. (2015). *Paris Agreement*. Retrieved from <https://unfccc.int/resource/docs/2015/cop21/eng/l09r01.pdf>
- United States Environmental Protection Agency. (2014). Climate Change Is Happening. Retrieved December 23, 2016, from <https://www.epa.gov/climatechange/climate-change-basic-information>
- Wang, H., Xin, Z., & Li, Y. (2017). Synthesis of Ureas from CO₂. *Topics in Current Chemistry*, 375(2), 49.
- Wang, H., Xin, Z. & Li, Y. (2018). Synthesis of Ureas from CO₂ BT - Chemical Transformations of Carbon Dioxide, in: Wu, X.-F. and Beller, M. (Eds.), (pp. 177–202). Cham: Springer International Publishing.
- Wang, S., Zhao, L., Wang, W., Zhao, Y., Zhang, G., Ma, X., & Gong, J. (2013). Morphology control of ceria nanocrystals for catalytic conversion of CO₂ with methanol. *Nanoscale*, 5(12), 5582–5588.
- Wang, W., Wang, S., Ma, X. & Gong, J. (2011). Recent Advances in Catalytic Hydrogenation of Carbon Dioxide. *Chemical Society Reviews*, 40(7), 3703–3727.
- Wang, X., Xu, J., Wang, Q., Xu, A., Zhai, Y., Luo, J., Jiang, Y., He, N., & Wang, Z. (2017). Wet Chemical Synthesis of Silica Nanosheets via Ethyl Acetate-Mediated Hydrolysis of Silica Precursors and Their Applications. *Small*, 13(13), 1603369.
- Wei, Q., Zhang, G., Yao, J., Chen, X., Wang, G., & Yang, X. (2021). One-step bulk fabrication of a CaO/carbon heterogeneous catalyst from calcium citrate for rapid synthesis of dimethyl carbonate (DMC) by transesterification of ethylene carbonate (EC). *New Journal of Chemistry*, 45(12), 5540–5550.

- Wu, C., Cheng, H., Liu, R., Wang, Q., Hao, Y., Yu, Y. & Zhao, F. (2010). Synthesis of Urea Derivatives from Amines and CO₂ in the Absence of Catalyst and Solvent. *Green Chemistry*, 12(10), 1811–1816.
- Wu, X. L., Meng, Y. Z., Xiao, M. & Lu, Y. X. (2006). Direct Synthesis of Dimethyl Carbonate (DMC) Using Cu-Ni/VSO as Catalyst. *Journal of Molecular Catalysis A: Chemical*, 249(1), 93–97.
- Wu, X. L., Xiao, M., Meng, Y. Z. & Lu, Y. X. (2005). Direct Synthesis of Dimethyl Carbonate on H₃PO₄ Modified V₂O₅. *Journal of Molecular Catalysis A: Chemical*, 238(1), 158–162.
- Yamaguchi, K., Ebitani, K., Yoshida, T., Yoshida, H. & Kaneda, K. (1999). Mg–Al Mixed Oxides as Highly Active Acid–Base Catalysts for Cycloaddition of Carbon Dioxide to Epoxides. *Journal of the American Chemical Society*, 121(18), 4526–4527.
- Yang, H., Gao, P., Zhang, C., Zhong, L., Li, X., Wang, S., Wang, H., Wei, W., & Sun, Y. (2016). Core-shell structured Cu@m-SiO₂ and Cu/ZnO@m-SiO₂ catalysts for methanol synthesis from CO₂ hydrogenation. *Catalysis Communications*, 84, 56–60.
- Yang, Z.-Z., Zhao, Y.-N., & He, L.-N. (2011). CO₂ chemistry: task-specific ionic liquids for CO₂ capture/activation and subsequent conversion. *RSC Advances*, 1(4), 545–567.
- Yang, Q., Sheng, M., Li, X., Tucker, C., Vásquez Céspedes, S., Webb, N. J., Whiteker, G. T., & Yu, J. (2020). Potential Explosion Hazards Associated with the Autocatalytic Thermal Decomposition of Dimethyl Sulfoxide and Its Mixtures. *Organic Process Research & Development*, 24(6), 916–939.
- Yano, T., Matsui, H., Koike, T., Ishiguro, H., Fujihara, H., Yoshihara, M. & Maeshima, T. (1997). Magnesium Oxide-Catalysed Reaction of Carbon Dioxide with an Epoxide with Retention of Stereochemistry. *Chemical Communications*, (12), 1129–1130.
- Yasuda, H., He, L.-N. & Sakakura, T. (2002). Cyclic Carbonate Synthesis from Supercritical Carbon Dioxide and Epoxide over Lanthanide Oxychloride. *Journal of Catalysis*, 209(2), 547–550.
- Ye, R.-P., Ding, J., Gong, W., Argyle, M. D., Zhong, Q., Wang, Y., Russell, C. K., Xu, Z., Russell, A. G., Li, Q., Fan, M., & Yao, Y.-G. (2019). CO₂ hydrogenation to high-value products via heterogeneous catalysis. *Nature Communications*, 10(1), 5698.
- Yoshida, M. & Ihara, M. (2004). Novel Methodologies for the Synthesis of Cyclic Carbonates. *Chemistry – A European Journal*, 10(12), 2886–2893.
- Yu, B., Zou, B. & Hu, C.-W. (2018). Recent Applications of Polyoxometalates in CO₂ Capture and Transformation. *Journal of CO₂ Utilization*, 26, 314–322.
- Zhang, J., Huang, S., Zhao, Y., Ma, X., & Wang, S. (2021). CeO₂ hollow nanosphere for catalytic synthesis of dimethyl carbonate from CO₂ and methanol: The effect of cavity effect on catalytic performance. *Asia-Pacific Journal of Chemical Engineering*, 16(1), e2554.
- Zhang, J., Zhao, S., Zhao, Y., Ma, X., & Wang, S. (2021). Influence of valence state of cerium ion on dimethyl carbonate synthesis from methanol and carbon dioxide over CeO₂. *Asia-Pacific Journal of Chemical Engineering*, 16(1), e2517.

- Zhang, Q., Lee, I., Joo, J. B., Zaera, F., & Yin, Y. (2013). Core-Shell Nanostructured Catalysts. *Accounts of Chemical Research*, 46(8), 1816–1824.
- Zhang, M., Zhu, G., Zhao, Y. & Feng, X. (2012). A Study of Recovery of Copper and Cobalt from Copper–cobalt Oxide Ores by Ammonium Salt Roasting. *Hydrometallurgy*, 129–130, 140–144.
- Zhang, R., Hua, L., Guo, L., Song, B., Chen, J. & Hou, Z. (2013). Calcined Mg-Al Layered Double Hydroxide as a Heterogeneous Catalyst for the Synthesis of Urea Derivatives from Amines and CO₂. *Chinese Journal of Chemistry*, 31(3), 381–387.
- Zhang, Y., Fei, J., Yu, Y. & Zheng, X. (2007). Study of CO₂ Hydrogenation to Methanol over Cu-V/ γ -Al₂O₃ Catalyst. *Journal of Natural Gas Chemistry*, 16(1), 12–15.
- Zhao, Y., Li, M., Fang, X., Li, X., Li, H. & Xu, B. (2012). Determination of Urea in Milk by Liquid Chromatography-Isotope Dilution Mass Spectrometry AU - Dai, Xinhua. *Analytical Letters*, 45(12), 1557–1565.
- Zheng, Y., Zhang, W., Li, Y., Chen, J., Yu, B., Wang, J., Zhang, L., & Zhang, J. (2017). Energy related CO₂ conversion and utilization: Advanced materials/nanomaterials, reaction mechanisms and technologies. *Nano Energy*, 40, 512–539.
- Zhong, J., Yang, X., Wu, Z., Liang, B., Huang, Y., & Zhang, T. (2020). State of the art and perspectives in heterogeneous catalysis of CO₂ hydrogenation to methanol. *Chemical Society Reviews*, 49(5), 1385–1413.

Chapter 8: Appendices

A. GC-MS CALIBRATION CURVES

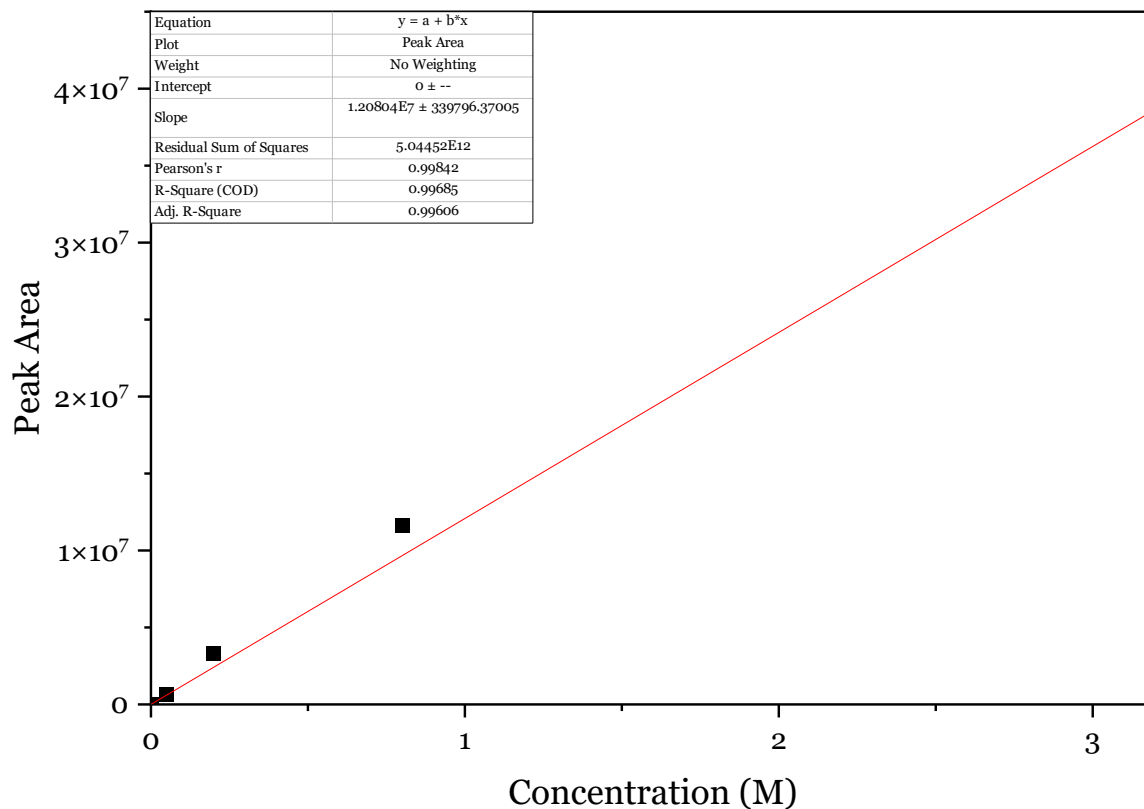


Figure 0.1 1,3 dibutylurea calibration curve used in Chapter 4, obtained by GC-MS analysis of standard solution prepared from commercial DBU

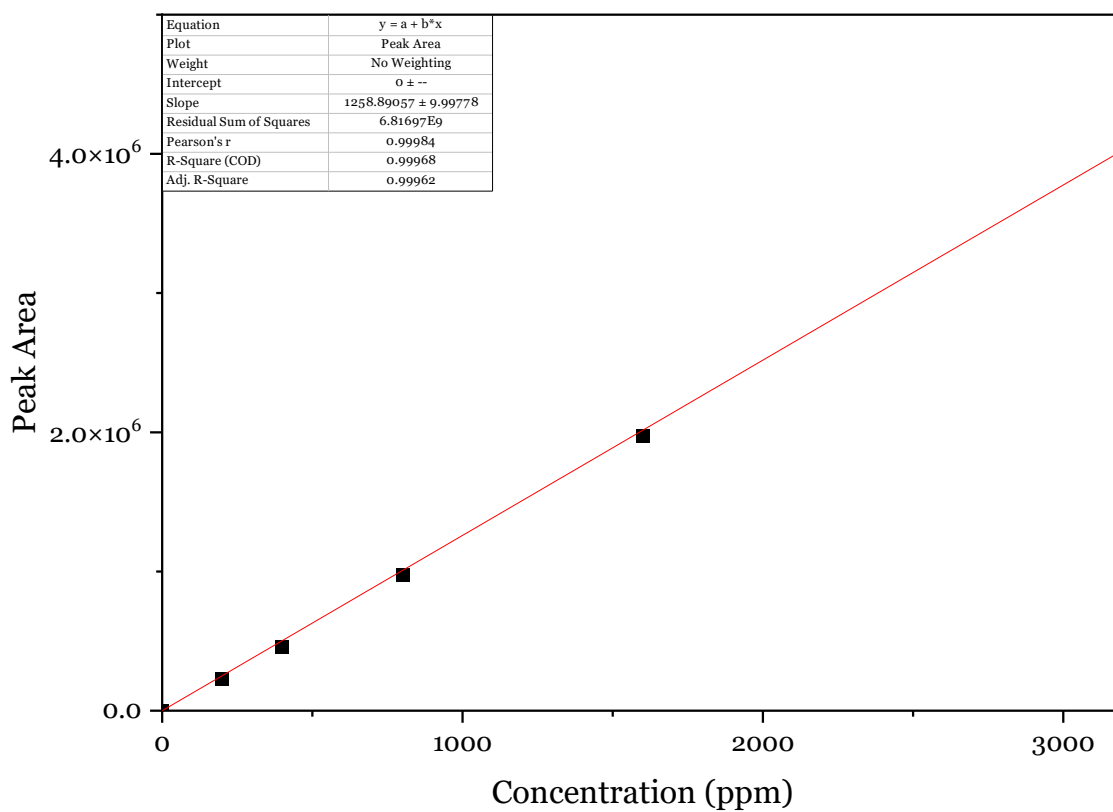


Figure 0.2 Butylamine calibration curve used in Chapter 4, obtained by GC-MS analysis of standard solution prepared from commercial butylamine

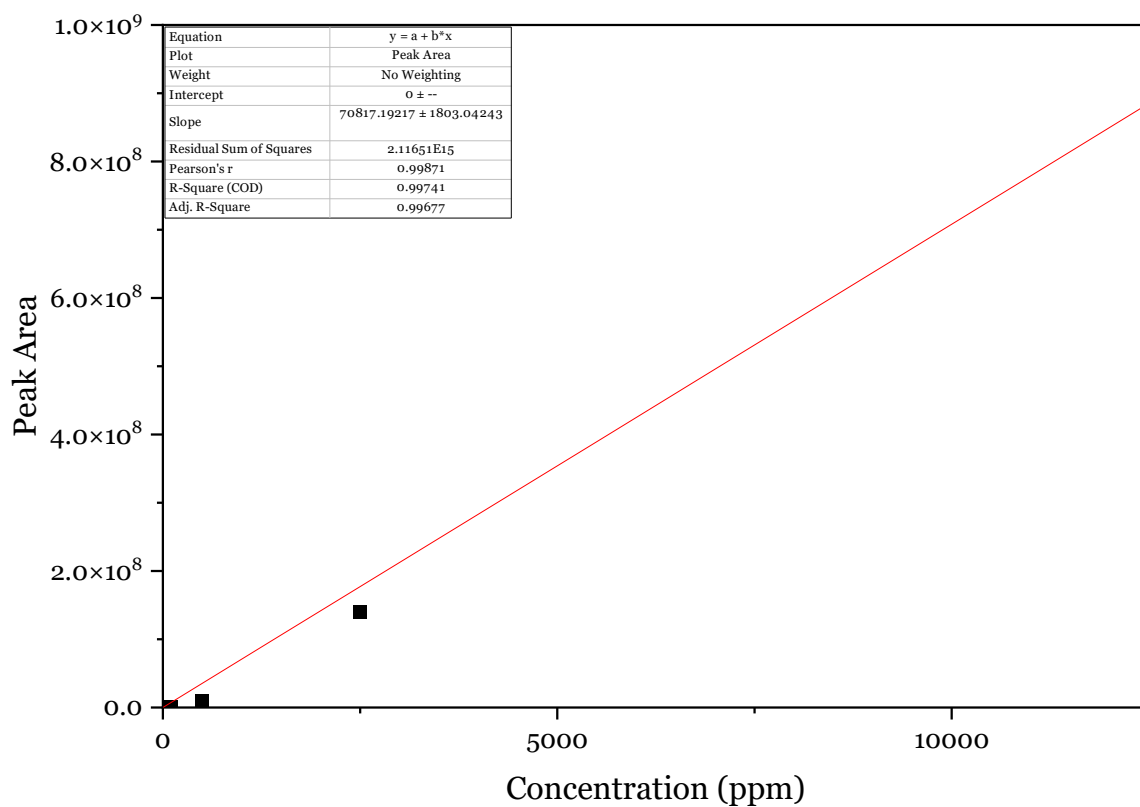


Figure 0.3 1,3 dibutylurea calibration curve used in Chapter 6, obtained by GC-MS analysis of standard solution prepared from commercial DBU

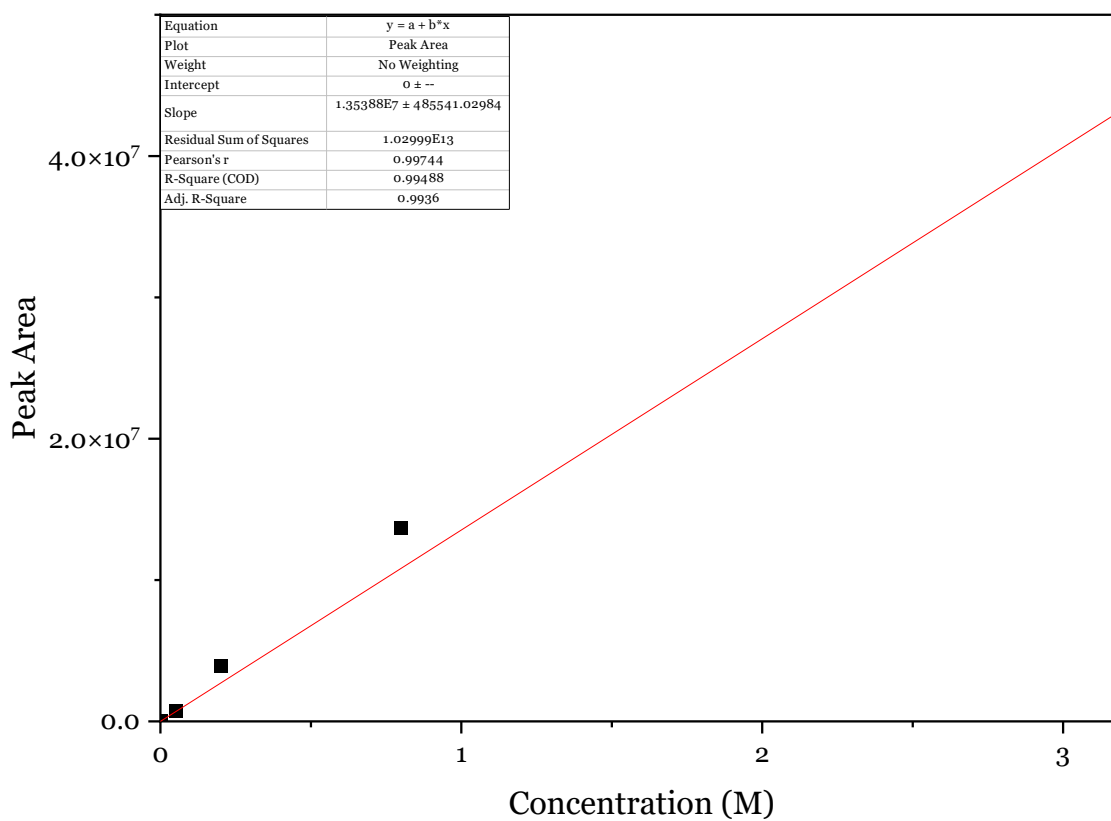


Figure 0.4 Butylamine calibration curve used in Chapter 6, obtained by GC-MS analysis of standard solution prepared from commercial butylamine

B. AAS CALIBRATION CURVES

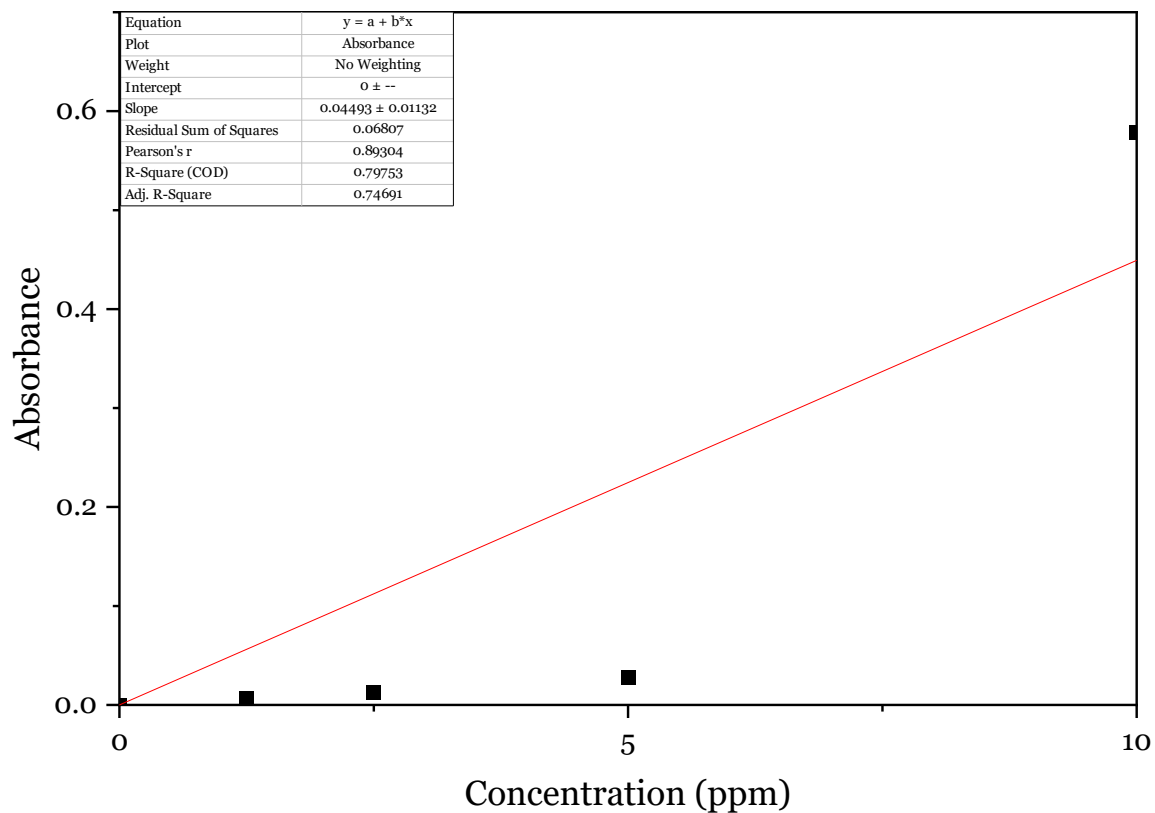


Figure 0.5 Calibration curves obtained by AAS using standard solutions prepared by commercial copper (II) nitrate dissolved in nitric acid

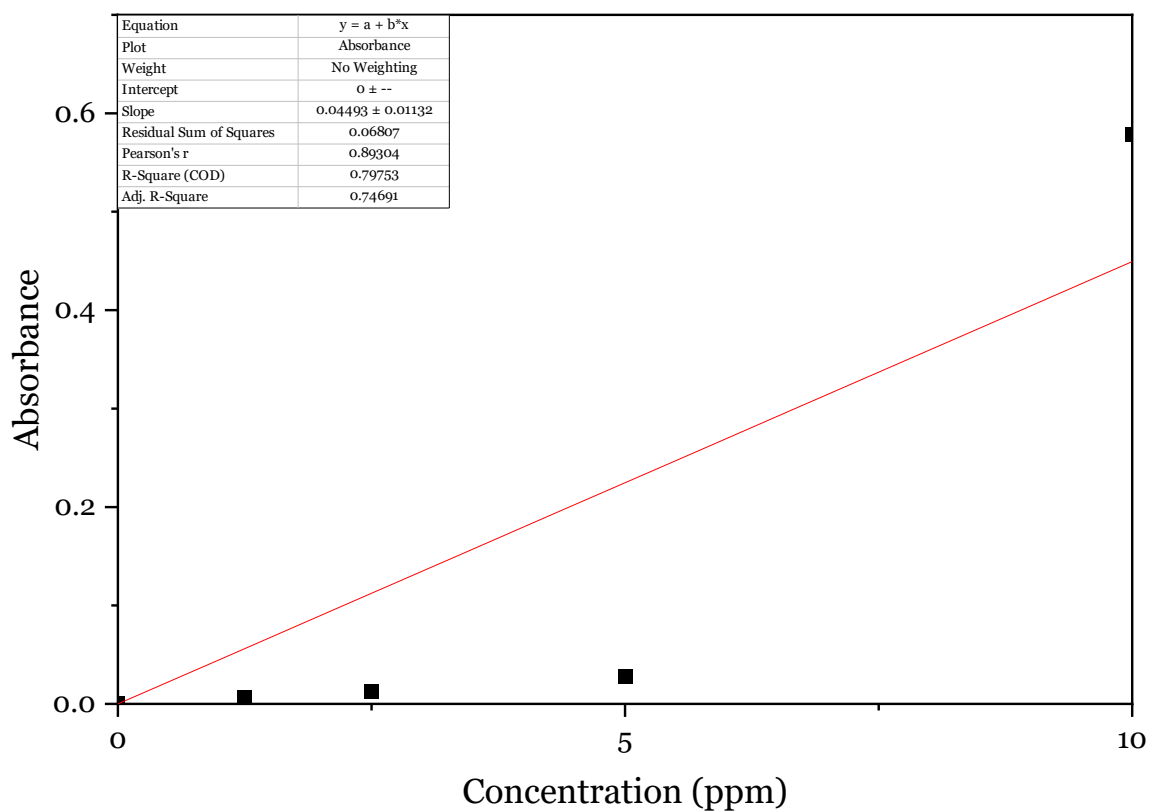


Figure 0.6 Calibration curves obtained by AAS using standard solutions prepared by commercial iron (III) nitrate dissolved in nitric acid

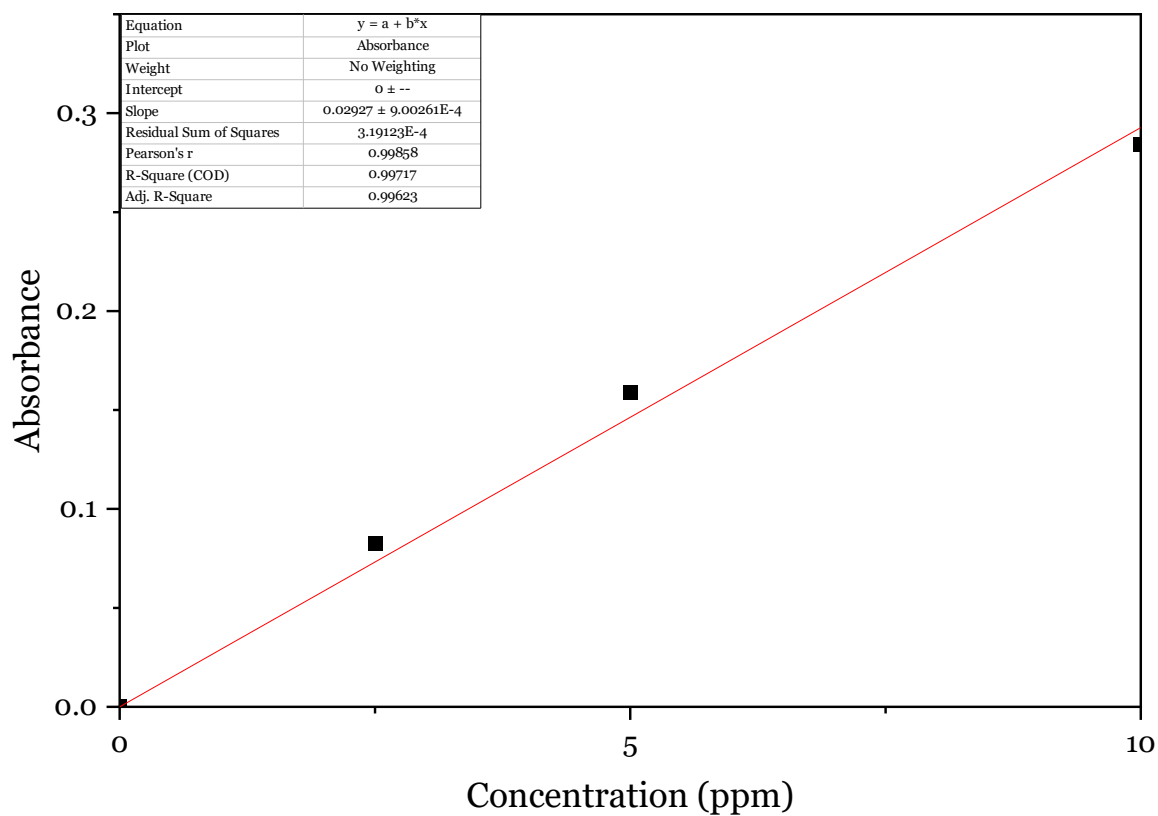


Figure 0.7 Calibration curves obtained by AAS using standard solutions prepared by commercial zinc (II) nitrate dissolved in nitric acid